

# Crack Arresting using Cutout Repair in Tubular Offshore Joints

by

Mostafa Atteya

Thesis submitted in fulfilment of  
the requirements for the degree of  
PHILOSOPHIAE DOCTOR  
(PhD)



---

University of  
Stavanger

Faculty of Science and Technology  
Department of Mechanical and Structural Engineering and Materials Science  
2023

University of Stavanger  
NO-4036 Stavanger  
NORWAY  
[www.uis.no](http://www.uis.no)

©2023 Mostafa Atteya

ISBN: 978-82-8439-191-5

ISSN: 1890-1387

PhD: Thesis UiS No. 723



## Abstract

Finding efficient repair methods for cracked tubular joints in offshore structures is important, both as a permanent or temporary repair solution. The exploration of such methods and techniques includes the use of hole drilling, possibly supplemented by techniques such as cold expansion, weld toe grinding and grooving. However, there is at present a lack of comprehensive understanding on the fatigue performance of tubular joints repaired by hole drilling and, even more so, on the use of crack deflecting holes. To address this knowledge gap, this research has experimentally investigated the fatigue performance of tubular joints repaired by crack deflecting holes. These experiments have been supported by detailed numerical analyses of the stress fields and the stress concentration factors around intact, cracked and repaired joints.

The study has revealed an unexpected location for fatigue crack initiation and further propagation after the hole drilling repair. This new fatigue crack initiation occurs at the weld toe behind the drilled hole, in contrast to the assumption in earlier work of crack initiation from the drilled hole. In addition, the work has observed a reverse coalescence of this new crack with the original crack. Such behaviour was observed both for crack-deflecting and crack-tip holes. This new insight also provides a reasonable explanation to the findings in earlier work on hole drilling as a repair method for tubular joints.

Furthermore, the experimental work indicate that crack-deflecting holes may be used to delay crack propagation in tubular joints, particularly for incipient through-thickness cracks. For fatigue in the high-cycle domain, this delay can be enhanced by weld-toe grinding in the area where the new crack is expected to initiate. The work also indicates that crack deflecting holes are more effective than crack-tip holes for tubular joints. In addition, the research has shown that cold expansion and grooving have limitations in tubular joints and may induce unfavourable stresses that could lead to premature crack initiation. These findings have been supported by finite element analysis that provides an explanation to the observed behaviour. The findings from this study provide valuable insights that can inform future repair designs for tubular joints in offshore structures.

## Acknowledgements

This thesis fulfils the requirements for the Doctor of Philosophy (PhD) degree at the University of Stavanger (UiS), Norway. The research was undertaken at the Department of Mechanical and Structural Engineering and Materials Science, Faculty of Science and Technology, UiS, spanning August 2018 to August 2023. This project was made possible through the financial support of the Ministry of Education and Research.

To my main supervisor, Associate Professor Ove Mikkelsen, I am profoundly grateful for your insights, dedication, efforts, and valuable feedback that greatly enhanced the quality and depth of my research. I am also thankful to my Co-supervisor, Professor Sudath C. Siriwardane, for the guidance, assistance, support, and critique throughout this work. Additionally, I appreciate all my colleagues for fostering a friendly and conducive working environment over these years.

Words often fall short when I try to express the gratitude I feel towards my co-supervisor, Professor Gerhard Ersdal. He has become more than just an academic advisor. His unwavering support, kindness, and understanding have been pivotal not only during this research but also in every aspect of my personal and professional growth. I am indebted for the wisdom he has shared, the patience he has demonstrated, and the encouragement he has given me throughout this challenging yet rewarding journey.

The norm for PhD students at the University of Stavanger is to spend at least 3 months as a visiting researcher at a foreign research institute. For this thesis, a stay was planned at TWI in Cambridge, UK. However, due to Covid restrictions and shutdowns, this stay could not be realized. In lieu of the visit and to ensure international research collaboration and input, Professor John Wintle of TWI graciously agreed to serve as an additional supervisor through video conferencing, that also included two in-person visits, spanning March 2020 to August 2022. I would like to take this opportunity to express my gratitude to John Wintle for his guidance, assistance, and motivation during this time.

I am privileged to have had the guidance of exceptional mentors, one of whom I am fortunate enough to count as part of my family.

Additionally, I'd like to extend my thanks to my fellow PhD students at the University of Stavanger's Institute of Mechanical, Structural, and Material Engineering. In particular, the discussions I had with Kristen Rege and Fredrik Bjørheim were invaluable to my work.

I'm also grateful for all the lab engineers for the help and support during the long and extensive testing period as they didn't save an effort to help getting the tests done as best as it could for their practical assistance in carrying out the fatigue tests.

Finally, I would like to thank my family for their consistent encouragement. A special acknowledgment goes to my wife, whose support has been invaluable throughout this journey. Her patience and understanding made all the difference. To her and our children, thank you for being my anchors.

# Nomenclature

## *Symbols*

All symbols are defined as they first appear in the text. The most common symbols are listed below.

### Roman letters

$c$	Half the surface crack length
$C$	Material dependent coefficients
$d$	Brace diameter
$D$	Chord diameter
$k$	Thickness exponent
$K$	Stress intensity factor
$\text{Log } A$	Intercept of the S-N curve
$m$	Slope of S-N curve
$N$	Number of cycles
$n$	Material dependent coefficients
$N_{1,..4}$	Number of cycles to endurance stages 1,..4
$OD$	Outer diameter
$P_{\max}$	Maximum load within a load cycle
$P_{\min}$	Minimum load within a load cycle
$R$	Load ratio
$Re$	remaining fatigue life beyond the occurrence of through-thickness cracking
$S$	Hot spot stress
$t$	Brace thickness
$T$	Chord thickness
$t_{ref}$	The reference thickness of tested joint
$eR$	Effectiveness of repair measure

### Greek letters

$\theta$	Angle between brace and chord
$\sigma_y$	Yield stress
$\rho$	Radius of drilled hole
$\beta$	Tubular joint diameter ratio, describe the compactness of the joint

$\tau$  Tubular joint wall thickness ratio, measure the likelihood that the chord wall will fail before the brace

#### Abbreviations

ACDP	Alternating current potential drop
API	American petroleum institute
AWS	American welding society
BEM	Boundary element method
BS	British standards
CoV	Coefficient of variation
CP	Cathodic protection
DNV	Det Norske Veritas
DoE	UK Department of Energy
DT	Double tee tubular joint
ECSC	European Coal and Steel Community
EPFM	Elastic plastic fracture mechanics
FMD	Flooded member detection
HAZ	Heat affected zone
HCF	High cycle fatigue
ISO	International standard organisation
LCF	Low cycle fatigue
LEFM	Linear elastic fracture mechanics
SCF	Stress concentration factors
SD	Standard deviation
SG	Strain gauge
TWI	The welding institute
UKSORP	United Kingdom offshore steels research project
XFEM	Extended finite element method

# Table of Contents

Abstract .....	i
Acknowledgements .....	ii
Nomenclature .....	iv
1 Introduction.....	1
1.1 Background .....	1
1.2 Problem statement and knowledge gaps .....	3
1.3 Research objectives .....	3
1.4 Thesis overview.....	4
1.5 Limitations .....	4
2 Fatigue life and repair methods for tubular joints .....	5
2.1 Introduction .....	5
2.2 Stress life approach .....	6
2.3 Tubular joints SCF .....	10
2.4 Remaining life of tubular joints .....	15
2.5 Repair methods.....	22
3 Fatigue testing of welded tubular joints as fabricated .....	33
3.1 General .....	33
3.2 Tubular joint design and material.....	33
3.3 Tubular joint fabrication.....	34
3.4 Fatigue testing rig.....	35
3.5 Instrumentation and measurement setup .....	37
3.6 Fatigue testing of tubular joints.....	40
4 Fatigue precracking of tubular joints .....	43
4.1 General .....	43
4.2 Fatigue testing of Specimen DT1 (control specimen).....	44
4.3 Precracking of Specimen DT2 .....	49
4.4 Precracking of Specimen DT3 .....	53
4.5 Precracking of Specimen DT4 .....	61
4.6 Results of specimens precracking .....	69
5 Stress concentration factors .....	79
5.1 General .....	79

5.2	Experimental Measurements .....	79
5.3	Existing parametric formulae .....	84
5.4	Finite Element Modelling.....	85
5.5	SCFs Comparison.....	95
5.6	Summary and Conclusions.....	98
6	Fatigue performance of repairs .....	101
6.1	Introduction .....	101
6.2	Fatigue performance of repairs to specimen DT2 .....	101
6.3	Fatigue performance of repairs to specimen DT3 .....	113
6.4	Fatigue performance of repairs to specimen DT4 .....	126
6.5	Reverse coalescence phenomenon .....	139
6.6	Summary .....	140
7	Evaluation of the effectiveness of repairs.....	141
7.1	General .....	141
7.2	Typical specimen behaviour (cracking) .....	142
7.3	Effectiveness of repairs .....	146
7.4	Crack deflecting holes .....	151
7.5	Cold expansion .....	158
7.6	Grinding .....	162
7.7	Remedial grinding (grooving).....	164
7.8	Crack tip holes.....	167
8	Repair evaluation methodology .....	168
9	Summary, conclusion and further work.....	172
9.1	Summary .....	172
9.2	Concluding remarks .....	173
9.3	Reflecting on Tubby’s research in hindsight of current findings.....	177
9.4	Scientific contribution .....	178
9.5	Suggestions for further work.....	178
	References .....	180
Appendix 1	Fatigue testing database of tubular joints .....	185
Appendix 2	Fabrication sheet.....	195
Appendix 3	Documentation of cracking events during testing .....	199
Appendix 4	Selected tubular joints .....	205
Appendix 5	List of publications .....	206

## Table of Figures

Figure 2-1: Definition of tubular joint stresses.....	11
Figure 2-2: Location of stress extraction points for linear interpolation to weld toe to determine stress concentration factors (courtesy of UK Department of Energy [11]).....	14
Figure 2-3. Database for surface crack development in tubular joint fatigue tests (left) database bounds (right) [23]. ....	19
Figure 2-4: Conventional FE approach for fatigue life estimation of cracked tubular joints [41].....	21
Figure 2-5: Hole drilling repair (Courtesy of the UK Department of Energy) [3] .....	27
Figure 2-6: crack treated by hole drilling and cold expansion process (Courtesy of the UK Department of Energy) [3].....	29
Figure 2-7: Remedial grinding of crack [58]. ....	31
Figure 3-1: DT Joint geometry .....	34
Figure 3-2: ultrasonic non-destructive testing examination. ....	35
Figure 3-3: Testing rig .....	36
Figure 3-4: Chord saddle strain gauge layout.....	38
Figure 3-5: Chord saddle strain gauge layout of specimen 2 .....	39
Figure 4-1: Strain measurements variation during precracking of quadrant Q4, specimen DT1. ....	45
Figure 4-2: Measured hot-spot stress range along the chord-brace intersection and chord side for the four quadrants on specimen DT1. ....	45
Figure 4-3: Change in hot-spot stress range during testing of specimen DT1, Q4.....	46
Figure 4-4: Strain evolution diagram during precracking of quadrant 4, specimen DT1. ....	47
Figure 4-5: Control specimen DT 1 – surface cracking at N4 with branching of crack close to the crown.....	48
Figure 4-6: Crack length evolution of quadrant 4 during fatigue testing of specimen DT1. ....	48
Figure 4-7: Strain measurements variation during precracking of quadrant 1, specimen DT2. ....	50



Figure 4-8: Measured stress range obtained from the first row of strain gauges, along the chord-brace intersection on chord side for the four quadrants on specimen DT2.....	50
Figure 4-9: Change in stress range during precracking of specimen DT2, Q1. ....	52
Figure 4-10: Strain evolution diagram during precracking of specimen DT2, Q1.....	52
Figure 4-11: Crack length evolution during precracking of specimen DT2, Q1. ....	53
Figure 4-12: Strain measurements variation during precracking of quadrant 2, specimen DT3. ....	54
Figure 4-13: Measured hot-spot stress range along the chord-brace intersection and chord side for the four quadrants on specimen DT3. ....	55
Figure 4-14: clamping induced hot-spot stresses at each quadrant of specimen DT3. ....	56
Figure 4-15: Change in hot-spot stress range during precracking of quadrant Q3, specimen DT3. ....	57
Figure 4-16: Strain evolution diagram during precracking of quadrant Q3, specimen DT3. ....	58
Figure 4-17: Crack length evolution during precracking of quadrant Q3, specimen DT3. ....	58
Figure 4-18: Change in hot-spot stress range during precracking of quadrant Q2, specimen DT3. ....	59
Figure 4-19: Strain evolution diagram during precracking of quadrant Q2, specimen DT3. ....	59
Figure 4-20: Change in hot-spot stress range during precracking of quadrant Q4, specimen DT3. ....	60
Figure 4-21: Strain evolution diagram during precracking of quadrant Q4, specimen DT3. ....	61
Figure 4-22: Strain gauge layout during precracking of quadrant 2, specimen DT4. ....	62
Figure 4-23: Measured hot-spot stress range along the chord-brace intersection and chord side for the four quadrants on specimen DT4. (Pmax = 60 kN, Pmin = 10 kN). ....	63

Figure 4-24: Measured hot-spot stress range along the chord-brace intersection and chord side for the four quadrants on specimen DT4. under the increased load ( $P_{max} = 72.5$ kN, $P_{min} = 12.5$ kN). .....	63
Figure 4-25: clamping induced hot-spot stresses at each quadrant of specimen DT4. ....	64
Figure 4-26: Change in hot-spot stress range during precracking of quadrant Q1, specimen DT4. ....	66
Figure 4-27: Strain evolution diagram during precracking of quadrant Q1, specimen DT4. ....	66
Figure 4-28: Change in hot-spot stress range during precracking of quadrant Q3, specimen DT4. ....	67
Figure 4-29: Strain evolution diagram during precracking of quadrant Q3, specimen DT4. ....	68
Figure 4-30: Crack length evolution during precracking of quadrants Q1 and Q3, specimen DT4. ....	68
Figure 4-31: Sample S-N curve from the experimental testing of specimens and standard S-N curve according to NORSOK N-004 [67]. ....	70
Figure 4-32: N1 and N3 S-N curves from the fatigue testing of specimens. The data include all the fatigue phases measured from all the quadrants on each specimen.....	71
Figure 4-33: Sample S-N curve from the experimental testing of specimens and standard S-N curve according to NORSOK N-004 [67]. ....	72
Figure 4-34: surface crack development in tubular joints fatigue tests.....	74
Figure 4-35: Brace/chord crack surface with rib marks, quadrant 1, Specimen DT1 .....	75
Figure 4-36: Brace/chord crack surface counterpart with rib marks, quadrant 1, Specimen DT1 .....	75
Figure 4-37: (a) Crack aspect ratio vs normalised endurance, (b) Normalised crack depth vs normalised endurance .....	76
Figure 5-1: Experimental hotspot SCF along the weld toe from the saddle ( $0^\circ$ ) to the crown ( $90^\circ$ ) .....	81
Figure 5-2: SCF at saddle from experimental work were plotted in a normal distribution paper, indicating a mean value of the SCF of 19.87 and a standard deviation of 2. ....	82
Figure 5-3: Experimentally measured SCFs sensitivity. ....	83

Figure 5-4: Axially loaded DT joints: chord SCF variation with $\beta$ for a set of joint parameters ( $\theta, \gamma, \tau$ ) .....	85
Figure 5-5: Axially loaded DT joints: chord SCF variation with $\tau$ for a set of joint parameters ( $\theta, \gamma, \beta$ ).....	85
Figure 5-6: Weld profile specifications as issued to the fabricator for these tests in line with appropriate standards, Section 3.3. ....	86
Figure 5-7: A 3D scanned of specimen to illustrate the weld between the brace and chord, brace and cone.....	87
Figure 5-8: Actual weld profile cut from one of the specimens. ....	87
Figure 5-9: Model and mesh idealisation. ....	89
Figure 5-10: Direct and linear extrapolation of SCF from first-order 8-node brick elements. ....	90
Figure 5-11: Direct and linear extrapolation of SCFs for first and second-order elements. ....	92
Figure 5-12: Experimental mean SCF with +/- N% bias values against FE SCF values. ....	94
Figure 5-13: Present experimental mean SCF values against parametric Efthymiou, previous experimental work and FE based SCF values. ....	96
Figure 5-14: SCF based FEA compared to SCF from specimen DT 1—quadrant 3.....	97
Figure 6-1: Strain measurements set up during precracking of quadrant 1, specimen 2. ....	102
Figure 6-2: Hole drilling by Magnetic-base drill, Crack-deflecting holes and crack-tip holes.....	103
Figure 6-3: Cold expansion process. ....	104
Figure 6-4: First repair attempt with two cold-expanded holes.....	105
Figure 6-5: Deflection of the crack trajectory towards crack deflecting holes. ....	106
Figure 6-6: New crack detected between SG 108 and the weld toe behind hole 1.....	107
Figure 6-7: Strain evolution diagram for two strain gauges around Hole 1 (SG 107 - red colour) between the drilled hole and the crack end and (SG 102 – red colour) the strain gauge beyond the hole.....	109
Figure 6-8: Strain evolution diagram for two strain gauges around Hole 2 (SG 103 - blue colour) between the drilled hole and the crack end	

and (SG 102 – red colour) the strain gauge beyond the hole. .....	109
Figure 6-9: Second repair attempt, new crack deflecting hole (hole 3) drilled at 70° .....	110
Figure 6-10: Strain evolution diagram for SG 108 between holes 1 and 3. The time-axis indicates, the time relative to the second repair attempt.....	112
Figure 6-11: Strain evolution diagram for two strain gauges: SG 102 (blue colour) located behind hole 2 to the left-hand side (Figure 6-9). SG 117 (green colour) behind hole 3 to the right-hand side (Figure 6-9). The time-axis indicates time relative to the second repair attempt. ....	112
Figure 6-12: Quadrant Q2 repair, crack-tip hole on the left-hand side and crack deflecting hole on the right-hand side.....	114
Figure 6-13: Quadrant Q3 repair, crack-tip hole on the left-hand side and crack deflecting hole on the right-hand side.....	115
Figure 6-14: Quadrant Q4 repair: crack removal by grinding at the centre of the saddle and weld toe improvement by grinding all the quadrant. .....	115
Figure 6-15: Stress range evolution diagram for the strain gauges around the crack deflecting hole on quadrant Q3. ....	117
Figure 6-16: Percentage change in strain range around the crack deflecting hole on quadrant Q3.....	118
Figure 6-17: Crack evolution at the crack deflecting hole on quadrant Q3, at 100,000 cycles.....	118
Figure 6-18: Stress range evolution diagram for the strain gauges around the crack-tip hole on quadrant Q3.....	119
Figure 6-19: Percentage change in strain range around the crack-tip hole on quadrant Q3.....	120
Figure 6-20: Final crack state at the crack-tip hole on quadrant Q3, at the end of the test.....	120
Figure 6-21: Stress range evolution diagram for the strain gauges around the crack deflecting hole on quadrant Q2. ....	121
Figure 6-22: Percentage change in strain range around the crack deflecting hole on quadrant Q2.....	122

Figure 6-23: Crack evolution at the crack deflecting hole on quadrant Q2 at the end of the test. ....	122
Figure 6-24: Stress range evolution diagram for the strain gauges around the crack-tip hole on quadrant Q2.....	123
Figure 6-25: Percentage change in strain range around the crack-tip hole on quadrant Q3.....	124
Figure 6-26: Crack evolution at the crack tip hole on quadrant Q2, at the end of the test. ....	124
Figure 6-27: Quadrant Q3 repair, crack removal by grinding, dye penetrant application. Specimen DT4.....	126
Figure 6-28: Quadrant Q3 repair by TIG welding after crack removal by grinding. Specimen DT4.....	127
Figure 6-29: Quadrant Q1 repair, material removal by grinding to achieve shorter crack length.....	128
Figure 6-30: Quadrant Q1 repair, crack deflecting holes centred at 30° from the chord saddle. Specimen DT4. ....	128
Figure 6-31: Percentage change in strain range around the left-hand side crack deflecting hole (H2) on quadrant Q1. ....	131
Figure 6-32: Stress range evolution diagram for the strain gauges around the left-hand side crack deflecting hole (H2) on quadrant Q1....	131
Figure 6-33: Stress range around the right-hand side crack deflecting hole (H1) on quadrant Q1.....	132
Figure 6-34: Percentage change in strain for the strain gauges around the right-hand side crack deflecting hole (H1) on quadrant Q1. ....	133
Figure 6-35: Quadrant Q1 second repair attempt, crack deflecting holes centred at 48° and 50° from the chord saddle. Specimen DT4. ....	134
Figure 6-36: Stress range evolution diagram for the strain gauges around the left-hand side crack deflecting hole (H3) on quadrant Q1. Second repair attempt. ....	135
Figure 6-37: Percentage change in strain range around the left-hand side crack deflecting hole (H3) on quadrant Q1. Second repair attempt. ....	136
Figure 6-38: Percentage change in strain range around the right-hand side crack deflecting hole (H4) on quadrant Q1. Second repair attempt. ....	137

Figure 6-39: Stress range evolution diagram for the strain gauges around the right-hand side crack deflecting hole (H4) on quadrant Q1. Second repair attempt. ....	137
Figure 6-40: Reverse crack coalescence behaviour. (a) crack condition at 115,00 cycles, (b) reverse crack coalescence with the lead crack. ....	139
Figure 7-1: Typical cracking pattern during fatigue testing. The top left-hand figure is indicating the original crack at position 1 and the crack deflecting hole repair. The top right-hand figure indicates the crack developing into the hole (stage a and later b). The bottom left-hand figure shows the formation of the new crack at position 3 beyond the crack arresting hole (stage c), instead of the expected crack development from the hole at position 2. Finally, the bottom right-hand figure shows the new crack entering the hole or coalescing with the original crack (stage d). ....	143
Figure 7-2: Re value against the estimated through-thickness crack length for the database provided in Appendix 2.....	149
Figure 7-3: Repair performance of crack deflecting holes. Based on $eR_{N1}$ measure (Remedial grinding specimen is not included in the curve fitting).....	150
Figure 7-4: Stress distribution of unrepaired specimens along the circumference of the chord for a nominal axial stress of 1 MPa in the brace. ....	152
Figure 7-5: Stress distribution of unrepaired specimens and repaired specimens with crack deflecting holes along the circumference of the chord for a nominal axial stress of 1 MPa in the brace.....	153
Figure 7-6: linearised stress distribution of unrepaired specimens and repaired specimens with crack deflecting holes along the circumference of the chord for a nominal axial stress of 1 MPa in the brace. ....	154
Figure 7-7: Maximum stresses for specimens repaired with crack deflecting holes and unrepaired specimen .....	155
Figure 7-8: fatigue measured fatigue life extension of tested repaired specimens ( $eR$ measured) compared to curve for estimate of life extension ( $eR$ estimate) according to Equation 7.12. ....	156

Figure 7-9: fatigue life extension of repaired specimens compared to life extension estimate curve, where $(N1^*-Ni2)$ is the dormant period of the crack in the hole before the initiating of the new crack and $N3$ is the mean fatigue life from the T-joint SN-curve. ....	157
Figure 7-10: Stress field around a cold expanded hole [55].....	159
Figure 7-11: Cold expansion of 0.1 mm performed on specimen DT2.....	160
Figure 7-12: the influence of cold expansion on crack-tip holes of 18.1 mm diameter (left, 0.5% diameter increase, right, 6% increase in the diameter). Upper figures in the weld toe are showing the tangential stresses while the lower ones show the radial direction of stresses. ....	161
Figure 7-13: Modification to design T curve for untreated weld resulting from weld toe dressing as per DNV RP C203 [6] and BS 7608 [60]. ....	163
Figure 7-14: Idealised model for a tubular member welded to a base plate..	165
Figure 7-15: Idealised model for a tubular member welded to a base plate of 8 mm thickness. ....	165
Figure 7-16: SCF increase as a function of remedial grinding profile. ....	166
Figure 8-1: Design methodology flowchart.....	170
Figure 9-1: Typical cracking pattern during fatigue testing. ....	176
Figure 9-2: crack treated by hole drilling and cold expansion process (Courtesy of the UK Department of Energy) [3].....	177
Figure 9-3: Crack propagation sequence as documented during testing. ....	200
Figure 9-4: Crack propagation sequence, quadrant Q2. ....	201
Figure 9-5: Crack propagation sequence, quadrant Q3. ....	202
Figure 9-6: Crack propagation sequence, quadrant Q1-a, Specimen DT4....	203
Figure 9-7: Crack propagation sequence, quadrant Q1-b, Specimen DT4....	204

## List of Tables

Table 1-1: Thesis overview .....	4
Table 2-1: SMR techniques to address fatigue crack defects [43] .....	22
Table 2-2: Fatigue testing results [3].....	28
Table 3-1: Specimen dimensions.....	33

Table 4-1: Key parameters for DT1 test. ....	44
Table 4-2: Fatigue testing results of precracking stage for specimen DT1 ....	47
Table 4-3: Key parameters for DT2 test. ....	49
Table 4-4: Fatigue testing results of precracking stage for specimen DT2 ....	51
Table 4-5: Key parameters for DT3 test. ....	54
Table 4-6: specimen DT3 precracking fatigue life .....	56
Table 4-7: Key parameters for DT4 test. ....	61
Table 4-8: specimen DT4 precracking fatigue life .....	65
Table 4-9: specimen's fatigue life .....	69
Table 4-10: Parameters of S-N curves developed from fatigue testing (N1 and N3) .....	71
Table 5-1: SCF correction factors from directional stresses to principal stresses .....	80
Table 5-3: SCFs from experimental work (present data) .....	81
Table 5-4: Chord side saddle SCFs based on Mises and principal stresses for first-order elements. ....	91
Table 5-5: Chord side saddle SCFs based on Mises and principal stresses for second-order elements. ....	91
Table 5-6: Circumferential variation of extracted SCF by direct and linear extrapolation methods for first and second-order elements. ...	93
Table 5-7: SCFs for different weld profiles based on unaveraged principal stresses. ....	95
Table 5-8: Correlation between FEA, present and previous experimental work and Efthymiou SCFs. ....	96
Table 5-9: SCF based FEA compared to SCF from specimen DT 1—Quadrant 3 (corrected for location of “a” and “b”). ....	97
Table 6-1: Summary of repair performed on specimen DT2. ....	104
Table 6-2: Sequence of events of the first repair attempt on specimen DT2. .....	108
Table 6-3: Sequence of events of the first repair attempt on specimen DT2. .....	111
Table 6-4: Repaired specimen DT2 fatigue life .....	113
Table 6-5: Summary of repair performed on specimen DT3. ....	116
Table 6-6: Sequence of the crack deflecting hole events on Q3 during the fatigue testing of the repaired specimen DT3. ....	117



Table 6-7: Sequence of the crack tip hole events on Q3 during the fatigue testing of the repaired specimen DT3.....	119
Table 6-8: Sequence of the crack deflecting hole events on Q2 during the fatigue testing of the repaired specimen DT3.....	121
Table 6-9: Sequence of the crack tip hole events on Q2 during the fatigue testing of the repaired specimen DT3.....	123
Table 6-10: Repaired specimen DT3 fatigue life .....	125
Table 6-11: Summary of repair performed on specimen DT4. ....	129
Table 6-12: Sequence of events of the crack deflecting hole H2 during the fatigue testing of the repaired specimen DT4.....	130
Table 6-13: Sequence of events of the crack deflecting hole H1 during the fatigue testing of the repaired specimen DT4.....	132
Table 6-14: Sequence of events of the crack deflecting hole H3 during the fatigue testing of the repaired specimen DT4.....	135
Table 6-15: Sequence of events of the crack deflecting hole H4 during the fatigue testing of the repaired specimen DT4.....	136
Table 6-16: Repaired specimen DT4 fatigue life .....	138
Table 6-17: Repaired specimen's fatigue life .....	140
Table 7-1: Summary of repairs performed. ....	142
Table 7-2: factors influencing the performance of location 2 and 3 on the chord side.....	145
Table 7-3: Repaired specimen's fatigue life .....	147
Table 7-4: Results of the study on grinding profile.....	166

# **1 Introduction**

## **1.1 Background**

Offshore structures are extensively used to support facilities for oil, gas and renewable energy production. Fixed steel offshore structures (jackets) are normally used in shallow waters (30-200 m), but have been used in water depths of up to 412 m [1]. Jacket type structures are fabricated from tubular steel members which are joined by welding. As for most offshore structures, jackets are commonly designed for a service life between 20-30 years. At present, many offshore structures in the oil and gas industry have exceeded their design life and are in need of a life extension.

Offshore structures may experience fatigue cracking due to the repeated cyclic actions of, for example, wind and waves. Designing and fabricating structures for fatigue endurance is, in general, an implicit part of standards and codes. In some cases, fatigue considerations may govern the design and fabrication of joints. However, experience has shown that despite all the efforts made during design and fabrication, fatigue cracks still initiate during the service life or life extension phase of an offshore structure.

Regular in-service inspections to detect any fatigue cracks often complement the initial design of offshore structures. When a fatigue crack is detected, it is essential to evaluate its impact on the integrity of the platform, including the strength of the joint or member and the remaining fatigue life. Different types of strengthening, modification and repair (SMR) may be required to continue operating the facility safely. The choice of the various SMR techniques should be carefully based on the root cause of the defects. When fatigue is the root cause for cracks, SMR techniques can be divided into:

- Permanent techniques that restore the joint fatigue strength and
- Temporary techniques that slow down the further fatigue crack growth and, hence, provide life extension compared to if the joint was left unattended.

Permanent repair techniques include dry welding, which is used to restore the fatigue strength of the joint. Dry welding is accepted to be a favourable repair

method from a technical standpoint. However, if dry welding is to be used as a repair method underwater it requires the construction of a hyperbaric room which is time-consuming and expensive. Clamp technology is an alternative permanent repair technique that changes the load path to the clamp structural element, ideally making the damaged element redundant. The use of composites in repairs is also an alternative. Composites are lightweight materials that does not require hot work. In addition, composite repairs add less additional wave forces into the structure compared to repair clamps which attracts significant hydrodynamic loads. However, the use of composites underwater is normally regarded as not proven [2]. These techniques are deemed as permanent repair techniques and can be used to repair significant anomalies. Such methods are used to both extend the fatigue life and regain the original strength of the joint. However, these all comes with relatively high costs and significant installation time [2].

In contrast, hole drilling and weld toe grinding are considered techniques to delay the fatigue damage and, hence, provide life extension to the component. The advantage of these techniques is that they are relatively easy to perform compared to the above-mentioned methods and that they do not require heavy equipment. In combination, this yields lower cost and more time efficiency compared to the above mentioned techniques [3].

Hole drilling is a common technique used extensively in plated structures by drilling through-thickness holes in the crack tip or in the vicinity of the crack tip to stop crack propagation. The holes are often cold expanded in order to induce a compressive residual stress field around the hole to delay crack initiation. Hole drilling and cold expansion are normally used as a repair method for through-thickness cracks, but is primarily intended as a temporary repair [4].

Weld toe grinding is used to excavate surface fatigue cracks and it has shown life extension of joints up to four times greater than the mean remaining fatigue life of unrepaired joints [3].

## **1.2 Problem statement and knowledge gaps**

While hole drilling can be employed at the crack-tip or in its vicinity (crack-deflecting holes), it is important to note the difference in the context of plated structures. Crack-tip holes have been extensively studied in base plates, but there are limited studies on welded details. For tubular joints, research on their effectiveness is also scarce. To the best of the author's knowledge, the only publicly available study on hole drilling for tubular joints is limited to two specimens that show mixed results. One specimen demonstrated a significant extension of the fatigue life, while the other exhibited no substantial improvement [3]. Hence, a comprehensive understanding of the fatigue performance of tubular joints repaired by hole drilling is lacking. Further, there is a particular knowledge gap concerning crack-deflecting holes and how they compare to the sparsely existing research on crack-tip holes.

## **1.3 Research objectives**

To address this knowledge gap, this thesis aims to evaluate the effectiveness of different hole drilling repair methods for tubular joints, including crack deflecting holes, and to explore the use of cold expansion, grinding and grooving as additional repair improvement techniques. Further, this research aims at improving the existing knowledge on this topic, including an increased understanding of:

- The stress field and stress concentration factors around intact tubular joints subjected to cyclic loading (chapter 5).
- The stress field and stress concentration factors around cracked and repaired tubular joint (chapter 7).
- Fatigue performance of intact tubular joints (chapter 4)
- Evaluation of the fatigue performance of tubular joints repaired by hole drilling supplemented by various methods (chapter 6 and 7)
- Repair evaluation methodology (Chapter 8)

Experimental testing of tubular test joints is conducted for hole drilling repair techniques, both crack deflecting holes and crack tip holes. In addition, the experimental testing included supplementary techniques to enhance the

performance of crack deflecting holes, such as cold expansion, weld toe grinding and grooving.

## **1.4 Thesis overview**

A graphical overview of the thesis is given in Table 1-1

<p><b>Chapter 2: Fatigue life of tubular joints</b>                  A state-of-the-art overview of fatigue analysis of tubular joints, remaining fatigue life of cracked tubular joints and repair method for cracked tubular joints</p>	
<p><b>Chapter 3: Fatigue testing of welded tubular joints</b>                  Presentation of the test setup, specimens, instrumentation and loading for the intact tubular joints and repaired cracked joints</p>	
<p><b>Intact joints</b></p>	<p><b>Repaired cracked joints</b></p>
<p><b>Chapter 4: Fatigue precracking of welded tubular joints</b>                  Description of the experimental work to test the fatigue life of tubular joints and measure stress concentration factors</p>	<p><b>Chapter 6: Fatigue performance of repaired tubular joints</b>                  Description of the experimental work to test the fatigue life of cracked tubular joints repaired by hole drilling</p>
<p><b>Chapter 5: Stress concentration factors</b>                  Interpretation of the measured stress concentration factors and numerical simulation of the stress concentration factors for intact tubular joints</p>	<p><b>Chapter 7: Evaluation of the effectiveness of the repairs</b>                  Interpretation of the results from the fatigue performance of the repaired cracked joints and numerical analysis to form a physical understanding of the observations</p>
<p><b>Chapter 8: Repair evaluation methodology</b>                  A methodology for evaluating the effectiveness of crack deflecting holes as a repair method.</p>	
<p><b>Chapter 9: Conclusion and further work</b></p>	

Table 1-1: Thesis overview

## **1.5 Limitations**

This thesis evaluates the fatigue life of axially loaded intact, cracked and hole-drilling repaired tubular joints for fixed offshore steel structures (jackets) of double T-type (DT). Other types of joints in jacket structures are not evaluated, nor other types of joints in other structures or other types of loads. The joints studied in this work are scaled down versions of the joints normally used in jacket structures.

## **2 Fatigue life and repair methods for tubular joints**

### **2.1 Introduction**

Tubular joints are critical components of offshore structures and they are subjected to cyclic loading due to wind, waves, and currents, which can cause fatigue damage over time. Fatigue failure of tubular joints can have severe consequences, including loss of life, environmental damage and financial loss. Therefore, understanding the fatigue life of tubular joints and developing reliable methods to assess their integrity are essential for the safety and sustainability of offshore structures. In this chapter, the state-of-the-art on the fatigue life of tubular joints is reviewed, exploring the different approaches used to estimate the remaining life of these joints and the practical implications of these methods for the design and maintenance of offshore structures.

There are several approaches to estimate the fatigue life of welded components, including:

- Hot spot stress approach: This approach involves identifying the critical location of the weld and calculating a representative stress at that location (weld) using analytical or finite element methods. The representative stress is normally called the hot-spot stress (HSS) and often described by a stress concentration factor (SCF). The hot-spot stress is then compared to the S-N curve to estimate the fatigue life of the weld.

Effective notch stress approach: This approach involves treating the weld as a notch and calculating the effective stress concentration factor at the weld using analytical or finite element methods. The effective stress is then compared to the S-N curve to estimate the fatigue life of the weld.

- Fracture mechanics approach: This approach involves calculating the critical crack size that would cause the weld to fail and the remaining life of the weld based on fracture mechanics principles.

The selection of the appropriate approach depends on various factors, including the geometry and loading conditions of the weld, the available data and

particularly the desired level of accuracy. Each approach has its strengths and limitations, and it requires careful consideration to ensure accurate and reliable estimation of the fatigue life of welds. For tubular offshore joints, the most common approach is the stress life approach which is dependent on the S-N relationship between the hot spot stress range and number of cycles until failure.

## **2.2 Stress life approach**

### **2.2.1 S-N relationship**

Fatigue in structures and materials became a concern in the 19th century as a result of the industrial revolution. It was observed as a fracture phenomenon that occurred after repeated load cycles, often seen in steam engines, locomotives and pumps. August Wöhler (1819-1914) conducted systematic fatigue tests and found and documented the maximum stress and number of repetitions before rupture in tables. Basquin (1910) plotted the test results in a log-log format and found the S-N relationship used in present standards [5].

$$S = CR^n \quad (1)$$

where S is the maximum stress used in each test and R is the number of repetitions of this stress required in rapture. C and n are material dependent coefficients.

The S-N curves in present day standards [6-8] are following similar relationship with some modifications.

$$N = AS^{-m} \quad (2)$$

Which can also be written in a log-log format as:

$$\log N = \log A - m \log S \quad (3)$$

where S is the stress range, N is the number of load cycles and failure, log A is the intercept of the curve while m is the slope of the S-N curve.

The fatigue life assessment of welded joints is typically based on S-N curves in combination with a damage rule. The assumption of linear cumulative damage using the Palmgren-Miner rule is widely applied [9].

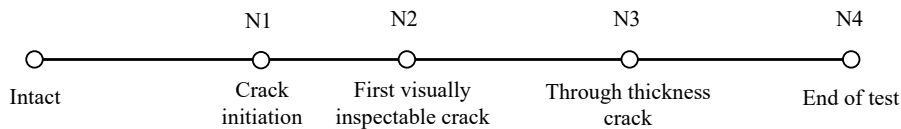


## 2.2.2 Tubular joints

Fatigue cracks will typically occur from discontinuities and defects in the material that are exposed to high cyclic stresses. Welded tubular joints is an example of this, as they normally contain high stress raisers and the welds are typically associated with defects. However, fatigue was not given high priority until the first incidents and accidents in the UK and Norwegian offshore oil and gas industry, such as the Alexander L. Kielland accident on the Norwegian continental shelf in 1980.

In the 1970s and 1980s, extensive testing of tubular joints was initiated to gather and establish reliable test data for use in design and certification purposes [10-12]. The majority of these tests were performed under constant amplitude loading, with a few tests conducted under variable amplitude loading. A variety of plate thicknesses, environmental conditions, and tubular joint geometries were evaluated, with different loading types, including axial, in-plane bending, and out-of-plane bending.

These tests in general characterised four different stages of the fatigue life of tubular joints [10-12]:



- N1 the first sign of cracking, for example indicated by a 15% strain drop measured in the strain gauge closest to the crack or first cracking detected by any method.
- N2 first visible surface cracking (visually).
- N3 first through-thickness cracking of the damaged member.
- N4 end of the test by either loss of load-carrying capacity or the testing rig inability to maintain the required conditions.

These tests were carried out at different laboratories and not all of them followed the above-mentioned stages. However, through-thickness crack was widely used and was decided to be the failure criterion for the current S-N

curves in codes and standards [6, 8, 9]. Below are the criteria used to define through-thickness cracking, N3, at different laboratories:

- UKOSRP-I, NEL [13]. Loss of internal air pressure or inferred from alternating current potential drop (ACPD) crack depth measurement.
- UKOSRP-I, TWI [13]. Observation of a maximum strain range on a strain gauge close to the centre of the fatigue crack. In some tests, this was correlated against the inference of through-thickness cracking by loss of internal chord pressurisation and good agreement was observed.
- UKOSRP-II, NEL [11] Two definitions were used, inference from ACPD. crack depth measurements and direct observation on the internal chord surface. The definitions generally differ by less than 5%.
- UKOSRP-II, Wimpey [11]. Inferred from ACPD. crack depth measurements.
- ECSC II, Dutch. Observation of a maximum strain range for a strain gauge close to the centre of the fatigue crack.
- UCL Inferred from ACPD. crack depth measurements.

A database of available tests is displayed in Appendix 1. Part of this database was used to create the current S-N curve for tubular joints, often called the T-curve (or the T'-curve). The data was preliminarily analysed with a linear regression between the mean  $\log(S)$  and  $\log(N)$ . The results showed that the slope line was close to 1/3 and to maintain consistency with previous guidance on welded plates, a fixed value of 3 was retained [14].

The design curves were selected as the curve corresponding to a 2.3% probability of failure. As fatigue endurance have been shown to follow a log-normal distribution [15], this corresponds to two standard deviations below the mean S-N curve. The design T curve for in air environment with a reference chord wall thickness of 16 mm and an endurance of less than  $10^7$  cycles is given by:

$$\log(N) = \log \bar{a} - m \log(S) \quad (4)$$

where N is the number of cycles,  $\log \bar{a}$  and m are material parameters and S is the hot-spot stress range at the weld toe. The hot-spot stress is defined as the nominal stress in the brace multiplied by the joint specific stress concentration factor (SCF), which is further described in section 2.3.

Member thickness has an impact on the fatigue life of tubular joints similar to other fatigue sensitive details. The experience is that thicker material has shorter fatigue life due to the higher concentration of defects and imperfections. These defects and imperfections increase the likelihood of crack initiation, ultimately leading to reduced fatigue lifespan [16].

The influence of the thicknesses larger than the references thickness on the S-N curve is included by applying a thickness correction factor to the stress range [6, 7, 16]

$$\log N = \log \bar{a} - m \log \left( S \left( \frac{t}{t_{ref}} \right)^k \right) \quad (5)$$

where  $t_{ref}$  is the reference thickness of the tested joints and  $k$  is a thickness exponent on the fatigue strength. Typical values for the T-curve used for tubular joints are  $t_{ref}$  of 16 mm and a  $k$  value of to 0.25.

It has also been observed that the corrosive environment has a high influence on the fatigue life of tubular joints. Seawater tends to create corrosion pits that acts as a local stress risers accelerating crack initiation. After crack initiation, it enhances the crack growth rates leading to shorter fatigue life compared to in air environment. Hence, different S-N curves are developed for structures in air, seawater and in seawater cathodically protected [11].

In addition, the mean stress in the detail has been shown to have an effect on the failure fatigue life. The main contributions to the mean stress are stress ratio and residual stresses from the welding process. However, the tests of tubular joints at different stress ratio in air, indicated that the stress ratio had little effect on the fatigue life. As stated in the [11]“*It is important to note that it is the presence of the residual welding stresses which diminishes the effect of the stress ratio on fatigue endurance*”. For as-welded tubular joints, it is recommended that the T curve is used directly for fatigue assessment, due to the presence of potentially high tensile residual stresses at the hot spots after fabrication [17].

## **2.3 Tubular joints SCF**

### **2.3.1 General**

Design S–N curves for various classes of welded joints have been established based on laboratory test specimens. A list of the tested specimen is provided in Appendix 1. Due to the geometry of welded tubular joints, high-stress gradients exist in the transition zone between the weld line and the base material. In linear stress analysis the geometric discontinuity of the weld toe defines a stress singularity.

In general, stresses in tubular joints arises from three main causes as shown in Figure 1. These are:

- The nominal stresses (member stress): stresses in the members under applied external loads without considering the detail of the joint intersection.
- Hot spot stress (deformation stresses): stresses close to the weld toe arising from the deformation of the tubular wall to maintain continuity at the intersection with the weld profile under the applied external loads.
- Notch stress: stresses introduced due to the geometrical discontinuity at the weld toe or root.

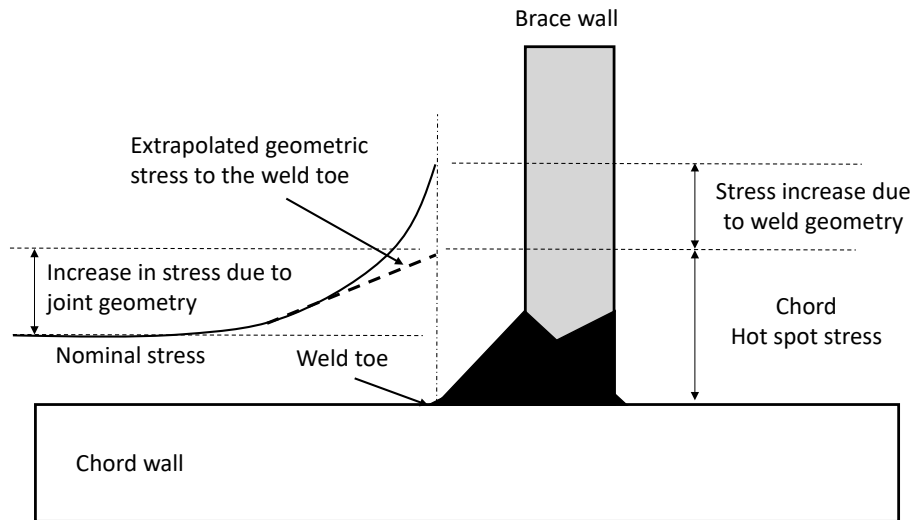


Figure 2-1: Definition of tubular joint stresses.

In the scope of stress analysis, the hot-spot stress serves as a representative value indicating the peak stress located as close as possible to the weld, specifically at the weld toe, while disregarding the influence of the weld toe notch. Typically, the ratio between the hot-spot stress and nominal stress is referred to as the stress concentration factor (SCF). As a result, one can estimate the hot-spot stress by adjusting the nominal cyclic stress according to the SCF. The precise determination of SCF at weld toes plays a crucial role in designing welded tubular joints to withstand fatigue failure in offshore structures, thus highlighting its significance in the engineering field.

Various parametric formulas have been developed for estimating SCFs, which are expressed using non-dimensional joint parameters adapted to accommodate distinct types of loading and boundary conditions. These formulas have been developed through both experimental and numerical methodologies, including:

- Beale and Toprac [5] developed empirical equation for SCFs of T-joints under tensile loading.
- Reber [6] and Visser [7] attempted to estimate the hot-spot stress of T, Y and K joints under compression loading using finite-element analysis.
- Marshall [8] adopted the Kellogg [9] formula to express SCF for brace and chord of K joints using classical solution methods.

- Kuang et al. [10] used finite element analysis to develop semi-empirical formulae to cover the SCF on brace and chord side for 138 T, Y, K and KT joints.
- Gibstein [11] carried out parametric analysis for seventeen T joints using FE analysis to investigate rigidly fixed chord ends.
- Wordsworth and Smedley [12] presented one of the first comprehensive parametric formulae for SCFs of T, Y, KT and DT joints. The parametric study was obtained from testing of acrylic model.
- Efthymiou [13] provided generalised influence functions developed for use in fatigue analysis. The SCFs are derived by establishing influence functions describing the ‘hot spot’ stress at a particular location of a specific member. It has been developed by performing finite element analyses using an in-house finite element program (PMBSHELL). The program uses thick shell elements for modelling the members and 3-D brick elements for the weld. The influence functions by Efthymiou are implemented in codes and standards and are the most widely used currently.

Smedley and Fisher [14] concluded that since Efthymiou SCFs are design formulae giving a mean fit to his FE database, it tends to underpredict in 20–40% of the cases compared to Lloyd’s Register experimental database consisting of steel and acrylic models. Hence, the first impression could be that Efthymiou formulae provide SCF values on the unsafe side of the database. However, ISO 19902 [1] indicates that Efthymiou’ parametric formulae have a bias of 19% to the safe side compared to the experimental values, with a coefficient of variation (CoV) of 19% (20% according to DNV-RP-C210 [15]). The formulae have been accepted as providing a reliable design basis for structures with tubular joints.

In practice, the tubular joint SCF is usually calculated from the parametric equations given in standards such as ISO 19902 [Ref], API RP2A [Ref] and DNV-RP-C203 [4]. The standard and code-based SCFs are expected to provide upper-bound values for use in design and life extension assessments.

Case by case finite element analysis is an alternative method to develop the SCFs. While the parametric equations have typically been developed from extrapolated experimental strain gauge measurements, finite element analysis uses linear extrapolation from the same points typically used for the strain

gauges. This approach does not include the weld profile tolerances captured in the tests. As a result, in some cases, the numerical finite element values could underestimate the SCF compared with those derived from parametric equations and experiments. Guidance on how to develop SCFs from finite element analysis is given in DNV RP C203.

### **2.3.2 SCF from finite element methods**

Standards and recommended practices provide two methodologies for SCF calculation. The first is the direct extraction of stresses for use in fatigue calculations, where stresses are measured from a strain gauge (grid length of 3 mm) placed perpendicular to the weld toe at a distance within 6 mm to  $0.1\sqrt{rt}$ . This method is adopted in API RP 2A [8] and AWS D1.1 [18]. The second method is the linear extrapolation of principal stresses. This method is recommended by ESCS and UKOSRP joint industry projects.

The second method is the linear extrapolation of principal stresses at measured or calculated at specific perpendicular distances from the weld toe as indicated by the A and B locations in Figure 2-2. This method was recommended by the UKOSRP [11] joint industry project. It was incorporated into the UK Department of Energy Design Guidance Notes and later adopted by the ISO standard [7]

$x = 0.2 \sqrt{rt}$  but not less than 4 mm

Range of linear stress distribution extends between A and B

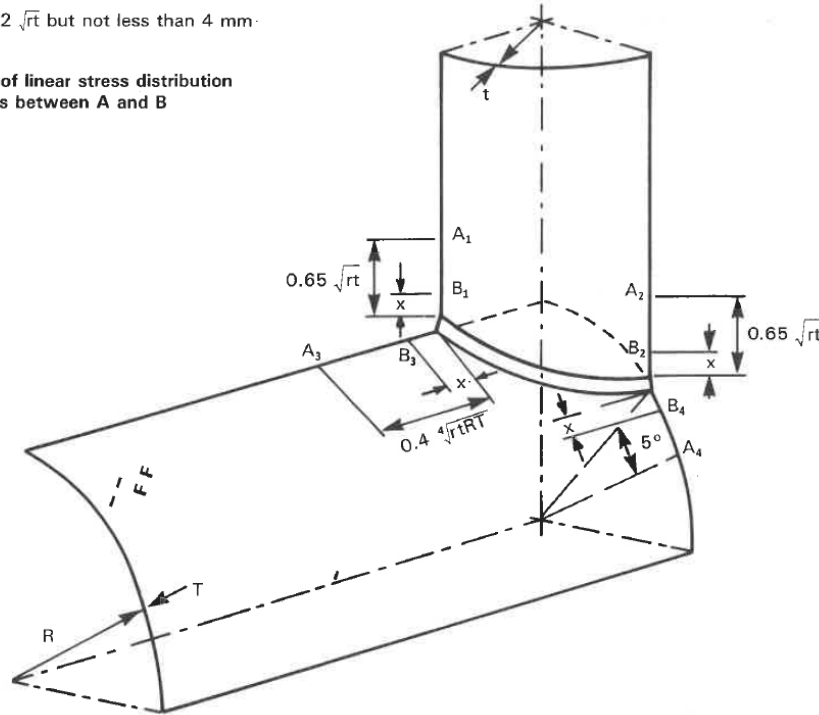


Figure 2-2: Location of stress extraction points for linear interpolation to weld toe to determine stress concentration factors (courtesy of UK Department of Energy [11]).

The purpose of using the FEA is to accurately compute the stresses at the points of interest. These points of interest need to be aligned with the elements' integration points, whether the direct extraction or the linear extrapolation method is selected. This could be done by using shell elements, but shell elements are not recommended for complex details and high local bending [19]. The alternative to shell elements is to use solid elements. However, conventional solid elements do not have integration points on the element surface, which is needed to extract the maximum stress. A possible mitigation for solid elements is the use of dummy membrane elements on the surface that share the same surface nodes. This allows for extraction of the stresses at the integration points in the aligned membrane elements, rather than extrapolating the stresses to the surface of the solid elements. However, it is rather impractical and cumbersome to use such dummy membrane elements and align the integration points' locations with the points of stress extraction, and a finer



mesh without such membrane elements are often a better solution. This will also result in nodal stresses closer to the stresses at the integration points.

## **2.4 Remaining life of tubular joints**

### **2.4.1 Introduction**

Assessment of the remaining life of tubular joints is of major importance for offshore structures for energy production. In most cases, initial fatigue design is complemented by regular inspection to detect fatigue cracks. If cracks are detected during inspection, the remaining life of the components may be assessed from any observed crack size to determine the significance of these defects. Depending on the assessment results, the defects may be tolerated with no additional actions, listed for more frequent inspections, investigated in further detail or repaired.

The assessment can be based on knowledge of the different stages of fatigue life ( $N_1$ ,  $N_2$ ,  $N_3$  and  $N_4$ ) or crack growth information. The different stages of fatigue life are presented and reviewed in the work of Zhang and Wintle [20], based on some of the data found in Appendix 1. The crack growth information can be obtained from a theoretical analysis based on fracture mechanics, from a series of in-service inspections [21-23].

### **2.4.2 S-N approach**

The S-N approach is the most common method for assessing the fatigue life of tubular joints. It is based on the relationship between the applied cyclic stress range ( $S$ ) and the number of cycles to failure ( $N$ ) of the material.

The fatigue life of tubular joints may be divided broadly into four stages from  $N_1$  to  $N_4$ , as previously mentioned (section 2.2.2).  $N_1$  is the point at which the crack is first noted by any inspection method,  $N_2$  denotes the first visual crack,  $N_3$  denotes through-thickness crack and  $N_4$  represents the actual failure of the joint.

The fatigue life calculated from the S-N approach is based on data for through-thickness cracks in the material ( $N_3$ ), while the available data from the fatigue

testing of tubular joints also exhibited recording of other endurance stages, for example, the fatigue life form N1 to N4.

The structural integrity management for offshore installations increasingly rely on flooded member detection (FMD) as the principal inspection method, as it can be routinely employed in a remotely operated vehicle and is more cost-effective than diver operated techniques. However, relying on FMD as an inspection tool requires that welded joints are able to retain sufficient fatigue life and static strength after through-thickness cracking.

A possible way of assessing the remaining fatigue life after through thickness cracking (N3) could be to study the N3 values versus the N4 values for the available specimens. Zhang and Stacey [20] reviewed and assessed the fatigue data of tubular joints used for offshore structures under fatigue loading. A comprehensive examination of published work containing data on fatigue lives beyond through-thickness cracking in offshore structures was carried out. This resulted in the development of a database of 281 relevant tests, most of which came from the United Kingdom Offshore Steels Research Project and large programs funded by the European Coal and Steel Community (ECSC). The database was used to perform a statistical assessment of the effects of different testing conditions and geometrical parameters on the remaining fatigue life beyond the occurrence of through-thickness cracking. The remaining fatigue life was represented by a parameter  $R_e$ .

The analysis indicated [20] that  $R_e$  depends strongly on chord thickness, loading mode, type of joint, and testing environment. In some cases, a significant amount of remaining life existed, often associated with T-type tubular joints with thin chord thickness under out-of-plane loading and a seawater (with CP) environment. The influence of the relevant parameters on  $R_e$  was discussed by Zhang and Stacey [20] and attributed to their effect on crack shape, stress distribution, cracking location and crack propagation path.

The review also examined available fatigue data on N3 and N4 of tubular structural members. The mean remaining life of a through-thickness cracked member relative to N3 was about 44%, but the remaining lives exhibited a large scatter. Statistical analysis was carried out on N3 and N4 endurance of all data

collected, and the mean and mean minus 2 standard deviations (SD) curves in terms of N3 and N4 were shown.

The development of cracks in tubular joints under fatigue loading is complex and can be influenced by many factors. The remaining life after through-thickness cracks was found to depend on specimen geometry and testing conditions. However, the experimental data examined had some dissimilarities with the actual situation in a structure regarding the remaining life of through-thickness cracks. Reduced stiffness due to cracking are argued to result in changing the load paths within the structure and possibly resulting in load shedding away from the damaged area. Such shedding can reduce the stress range and stress intensity factor  $K$ , which theoretically could drop below the threshold value and the crack might stop growing. There are several factors that can affect the accuracy of the S-N approach for assessing the remaining life of cracked tubular joints. Despite these challenges, the S-N approach remains a useful tool for assessing the remaining life of cracked tubular joints. The approach can be used to estimate the remaining life of a structure, and to develop maintenance and repair strategies to extend the life of the structure.

### **2.4.3 Crack growth information**

The UK Department of Energy proposes methods for the preliminary evaluation of defects in tubular joints [21-23]. These approaches rely on crack growth information derived from both surface crack expansion and crack depth progression. This review primarily focuses on surface crack length, as it is considered to be a more feasible inspection parameter compared to crack depth.

Initial crack detection in offshore structures typically employs techniques that provide a measure of surface crack length. It is essential to determine the significance of a defect with a particular surface length concerning the remaining life to failure of the tubular intersection. The study by UK Department of Energy [21-23] proposes a method for assessing the significance of defects discovered during the inspection of offshore tubular joints, based on observations of surface crack development in a sample of over 100 cracks noted during tubular joint fatigue tests. Failure is defined as the development of a fatigue crack through the full member thickness (N3). Experimental crack growth data are characterized by approximate bounds, with the lower bound

providing an initial estimate of remaining life for a joint with a specific surface crack length.

The proposed method by UK Department of Energy [21-23] not only permits initial assessment of the significance of specific defects, but also allows for predictions of the number of surface cracks of particular lengths expected within a specified population of joints. An example prediction is made for the number of cracks anticipated in a typical northern North Sea jacket structure, suggesting that few cracked joints would be expected within the design life of such a structure (e.g., fewer than ten joints with cracks longer than twice the member thickness). The sensitivity of this prediction to various factors is assessed, and the possibility of calibrating the structural design for a specific platform using in-service data from non-destructive examination of tubular joints for that structure is discussed. In cases where tubular joint characteristic lives are shorter than initially forecasted design lives, a greater number of fatigue cracks than predicted may be detected early in life, potentially providing an advance warning of a fatigue problem. The stage at which this can be detected depends on the sensitivity of surface crack detection and the sampling rate used.

The surface crack growth method is developed by collecting the crack growth behaviour of tubular joints from 105 fatigue test (ECSC, UKOSRP). The data are then presented by normalising surface crack length ( $2c$ ) and endurance ( $N$ ) by member thickness ( $t$ ) and fatigue life to through-thickness crack ( $N_3$ ) respectively, as shown in Figure 2-3 (left). A general curve fitting to the data was derived to show the lower (95%) and upper bound (2%) of the data. It should be noted that the scatter in the surface crack growth behaviour was broad, and this is a conservative approach. To reduce the conservatism, the remaining life is refined by noting that individual subsets of data have specific ranges within the overall scatter in surface crack development. This leads to proposed four categories with different bounds of the data as stated below and shown in Figure 2-3 (right).

- Category A, lower bound given by the 50% percentile of the database as a whole,
- Category B, lower bound given by the 80% percentile of the database as a whole,

- Category C, lower bound given by the 95% percentile of the database as a whole,
- Category D, lower bound below the 98% percentile of the database.

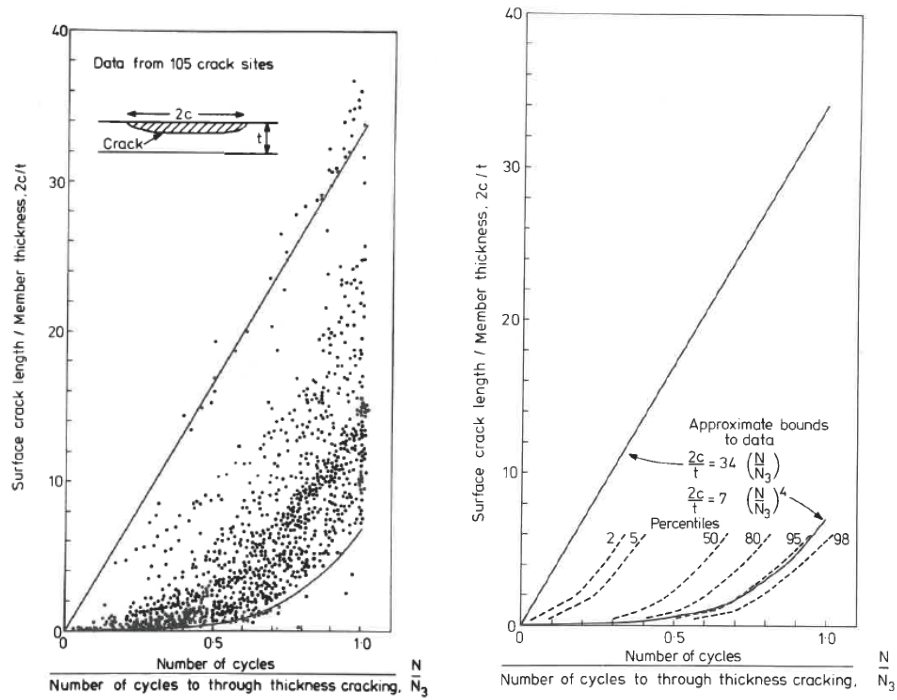


Figure 2-3. Database for surface crack development in tubular joint fatigue tests (left) database bounds (right) [23].

The method proposed by UK Department of Energy study enables initial estimates of remaining life to failure. The only required parameters are joint geometry details, the probable dominant loading type, an accurate measure of crack length obtained via an appropriate non-destructive testing method (e.g., magnetic particle method, such as magnetic particle inspection) and the life already elapsed. All of these parameters should be readily available. By leveraging these parameters, the proposed method offers a practical and efficient approach to evaluating the remaining life of tubular joints in offshore structures, which can ultimately contribute to the optimization of inspection schedules, maintenance plans, and structural designs. This, in turn, can enhance the safety, reliability, and cost-effectiveness of offshore structures, making them more sustainable and resilient in the long run.

#### **2.4.4 Fracture mechanics' approach**

The behaviour of cracked tubular joints can be studied using fracture mechanics [24]. The behaviour of each tubular joint is unique, as many variables can affect the joint behaviour. These variables includes the crack location, geometric dimensions, joint type, loading modes, stress ratio, weld profile and boundary conditions [25]. Full-scale laboratory testing of cracked tubular joints is expensive and time-consuming while numerical simulation of fracture process of tubular joints has been a major task in recent research. The advancement of numerical methods and computational power makes it possible to assess cracked tubular joints considering the uniqueness of each joint. Numerical methods such as finite element methods (FEM), extended finite element method (XFEM) and boundary element method (BEM) are typically used for fracture mechanics analysis. FEM is widely used for stress analysis and fatigue life estimation of cracked tubular joints [26-37], while applications for cracked tubular joints with the use of XFEM has not been identified. BEM was encountered only once by Borges et al. [38] for comparison between SIFs for cracked tubular joints estimated from FEM and BEM.

This section presents a review of the residual life estimation of cracked tubular joints using numerical methods. Based on the observations discussed above, this section focuses on the numerical modelling of fatigue life using FEM. In general, the numerical models are based on the assumptions of constant-amplitude fatigue loading with crack propagating from a given initial crack within the domain of linear elastic fracture mechanics (LEFM).

The assessment of structures using fracture mechanics approach requires sizing of a crack-like defect. The size of the crack is determined mainly by the inspection method used. If the crack cannot be observed, the crack size can be assumed as the largest undetectable crack size. Once the initial crack size is determined, fracture mechanics can be employed to evaluate the crack propagation until the onset of unstable crack extension, at which the structural element will lose its structural capacity. Fracture assessment of the component rely on the techniques of LEFM or elastic plastic fracture mechanics (EPFM) depending on material properties and plate thickness [16]. The fracture mechanics approach provides mathematical relationship between three critical variables, namely flaw size, stresses in the vicinity of the crack and toughness.

Fracture mechanics analysis of tubular joints is demanding. The tubular joint geometry with boundary conditions induce mixed-mode loading of the crack [39]. In this respect, the detailed analysis of stresses requires three-dimensional models of the joint[16, 40]. In the vicinity of the crack, the size of the finite elements must be comparable to the size of the crack increments, thus the meshing procedure becomes challenging.

Conventional FE approach can be divided into four main steps:

- a) development of numerical model with an initial crack-like defect,
- b) evaluation of fracture mechanics parameters,
- c) estimation of crack propagation rate, crack propagation direction and selecting crack increment size,
- d) updating the numerical model with the new crack front.

These steps are repeated for successive crack sizes until the structure loses its load carrying capacity as shown in Figure 2-4.

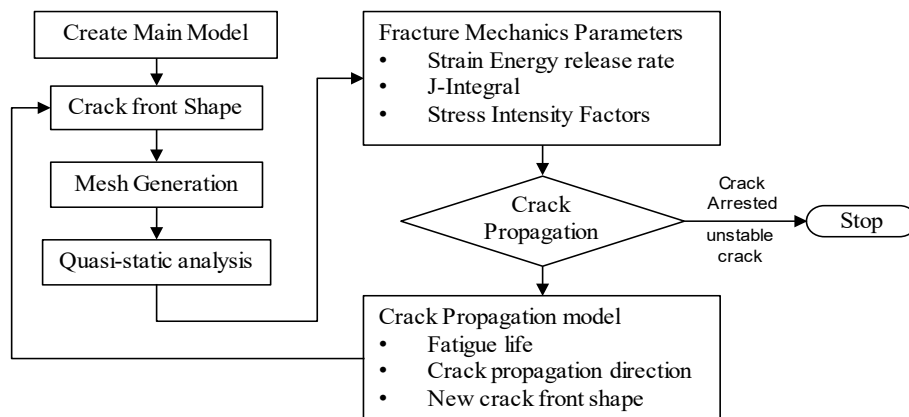


Figure 2-4: Conventional FE approach for fatigue life estimation of cracked tubular joints [41].

### **2.4.5 Practical use of these methods in assessment of cracks**

The practical use of the methods discussed in Sections 2.4.2 and 2.4.4 for assessing cracks has been discussed, and it has been shown that the S-N approach can provide a rough estimate of the remaining life in the case of the discovery of a through-thickness crack. Furthermore, this estimate can be refined using existing data to determine the remaining fatigue life in the case of a surface crack. The crack growth information approach is a reliable way to estimate the remaining life of a through-thickness crack, while the fracture mechanics approach is the most comprehensive and reliable approach to estimate the remaining life in the case of all types of cracks. These findings have practical implications for the design and maintenance of structures, where the use of appropriate methods for assessing cracks can improve safety and prolong the lifespan of critical components. Overall, the methods discussed in this chapter provide valuable tools for engineers and researchers to assess the integrity of structures and prevent catastrophic failures.

## **2.5 Repair methods**

### **2.5.1 Introduction**

The use of various strengthening, mitigation and repair (SMR) techniques should be based on the root cause of the defects. For fatigue cracks, SMR techniques such as dry welding, cutout repair, stressed mechanical clamps, unstressed/stressed grouted clamps and the use of composite materials are available [42]. For a given scenario, some techniques can be advantageous in terms of requirements for offshore equipment, timescales, costs and loading penalties [43], as indicated in Table 2-1.



Technique	Equipment Needs	Offshore Installation Timescale	Onshore Fabrication costs	Load Penalties	
				Weight	Wave Load
Dry Welding	Heavy	Very slow	High	None	None
Cutout repair (crack arresting)	Low	Moderate	None	None	None
Stressed mechanical clamp	Moderate	Quick	High	Moderate	High
Unstressed grouted clamp	Moderate	Moderate	Moderate	Moderate	Moderate
Stressed grouted clamp	Moderate	Slow	High	Moderate	High
Composites	Low	Quick	Moderate	Low	Low

Table 2-1: SMR techniques to address fatigue crack defects [43]

As mentioned in Chapter 1 Dry welding, despite being technically efficient, requires costly and time-consuming habitat construction. Clamp technology is another reliable repair method, which is useful for introducing a new load path through the clamp. Clamps are also useful in new members are needed to strengthen the structure. As previously mentioned, types of clamps include stressed mechanical clamps, un-stressed and stressed grouted clamps. The advantage of stressed mechanical clamps is that they show immediate gain in the joint strength capacity, but they are sensitive to the fabrication tolerances as they rely on the direct friction between the clamp and the existing structures. Hence, stressed mechanical clamps need to be fabricated and installed with strict tolerance acceptability. In addition, welds on the existing structures needs be ground flush before installation. Stressed as well as unstressed grouted clamps are less sensitive to tolerances, as the grout will fill the annulus between the clamp and the original members and transfer the loads when the grout is set. Stressed grouted clamps are often preferred, but since the grout needs to be cured prior to tensioning the stud bolts, these are more time consuming in the field than unstressed grouted clamps. Composites are lightweight and don't need hot work, but their underwater use isn't proven. These techniques, aimed at extending fatigue life and restoring joint strength, are considered permanent repair methods.[43]. These above-mentioned techniques can be used to extend fatigue life and regain original strength of the joint. All these techniques can be deemed as permanent repair techniques. Cutout repair technique is advantageous with respect to its simplicity and the need of light equipment. The technique can be used as a temporary repair until permanent repair can take

place. However, when removing material from the member, the capacity of the joint is reduced and the strength of the joint needs to be assessed. If the fatigue life extension from cutout repair and the joint/member strength both satisfy fitness for service requirements, then permanent repair may not be required.

In the context of this document, cutout repair is defined as any shape removed from the parent plate. These cut-outs may be drilled hole(s), dog-bone shape or two holes joined with a slit.

Crack arresting by cutout repair is typically used to extend the fatigue life of cracked structural components that cannot be repaired directly after crack discovery [44]. This method is relatively inexpensive, simple and fast to apply compared to other fatigue cracks repair techniques.

Despite the practical need and extended use of crack arresting by cutout repair, there is a lack of sufficient understanding and guidelines on crack arresting in tubular offshore structures [45]. The current practice is based on engineering judgement and Finite Element Analysis (FEA), which is not backed by experimental work. This has resulted in insufficient understanding of the benefits of the method and low confidence in implementing this technique.

### **2.5.2 Hole drilling**

Generally, hole drilling is a widely used repair to arrest fatigue cracks, primarily in plated structures. It is divided mainly into three categories:

- Crack-tip holes which are intentionally drilled to remove the stress singularity at the crack-tip [46-49].
- Crack flank holes by drilling two holes symmetrically relative to the crack plane, intended to reduce the stress intensity factor [50].
- Crack deflecting holes are drilled close to the crack tip to divert the crack path.

The latter can be used when crack-tip is not easily accessible or easily detectable. In addition, cold expansion is often used in combination with hole drilling to introduce compressive stresses in the hole wall and, hence, to slow the formation of a new crack at the wall of the hole [51, 52].

The most widely used hole drilling method for fatigue cracks is the crack-tip hole method. It is an obvious choice when the crack-tip is accessible and easy to detect. However, there is no widely accepted methodology for determining the hole size and hole treatment. In general, larger holes are assumed to be better for fatigue crack arresting, as long as the strength and stiffness of the structure are not jeopardised. From field experience hole diameter in the range of 2 to 4 inches (5-10 cm) have proven to be sufficient but in other occasions a 1 inch (2.5 cm) hole may be sufficient [53].

Widely used engineering equation [54] to determine the hole-size is expressed as follows:

$$\Delta K / \sqrt{\rho} \leq 10.5 \sqrt{\sigma_y}$$

where  $\Delta K$  is the stress intensity factor,  $\sigma_y$  is the yield stress of the material, and  $\rho$  is the radius of the hole. The equation computes the required crack tip curvature to arrest crack growth. It may be challenging to compute  $\Delta K$  in certain situations and a simplified approach based on the assumption of centre crack in an infinite plate under transverse loading can be used.

$$\Delta K = S_r \sqrt{\pi c}$$

where  $S_r$  is the nominal stress range while  $c$  is half the crack length. This expression can sometimes yield unconservative hole diameters when used with edge cracks.

As an alternative to crack tip holes, crack deflection holes have also been used for crack arresting in plated structures. Makabe et al [48, 51] studied the effect of crack deflecting holes on the crack-growth. Holes with pin inserts to produce compressive residual stress on the hole circumference were applied. The study was performed on aluminium alloy 2024-T3. It showed that crack propagation direction can be changed by drilling crack deflecting holes. The study concluded that this technique could improve the fatigue life and is suitable for crack arresting. Later, as part of this PhD work, Atteya et al [52] performed experimental and numerical work to study the effect of crack deflecting holes on the fatigue life of cracked plates. The work indicated that careful selection of the location of a drilled hole can increase the residual fatigue life by arresting the crack growth. Crack deflecting holes in plates affects the fatigue life of

cracked plates in two different ways. A crack growth acceleration will occur due to the effect of the stress concentration from the drilled hole and a crack growth retardation may occur due to the hole distributing the stresses away from the crack tip (shielding effect). Atteya et al [52] also provided a numerical study, and a model was provided and verified against two analytical solutions of two simple plates: a) prediction of SIF in the vicinity of the crack-tip of a finite width plate with a central notch. b) estimation of the stress concentration factor around a drilled hole in a finite width plate. The numerical model was successfully validated against the results of the experimental work. Two crack propagation criteria were investigated, namely the maximum energy release rate and the maximum tangential stress. The crack growth direction under mixed-mode I + II loading was accurately predicted by both criteria.

### **2.5.3 Hole drilling in tubular joints**

For tubular structural joints, the only publicly available study on hole drilling to arrest cracks were performed by The Welding Institute (TWI) for the UK Department of Energy in 1989 [3]. The project investigated different repair methods for a series of fatigue cracked tubular joints to establish a ranking for the repair methods in terms of remaining fatigue life after repair. The repair methods investigated were welding, grinding, hole drilling and combinations of repair methods. Two hole-drilling tests were included in the TWI project. Both these specimens included cold-expanded crack-tip holes as a method for crack arresting.

The T joints tested had a chord dimension of 457 mm outer diameter and 16 mm wall thickness and brace dimensions of 229 mm OD and 12 mm wall thickness. The specimens were fatigue tested under constant amplitude out of plane loading with approximately 350 MPa hot spot stress range with load ratio  $R = -1$ . One specimen was precracked with a through-thickness crack of the chord wall (specimen No. 7), and one precracked to 50% of the chord wall (specimen No. 8). The specimens were then repaired using 13.41 mm diameter holes accurately drilled at the crack-tips, as shown in Figure 2-6. The holes were then treated with a split sleeve cold expansion [55] process to produce compressive residual stress at the hole circumference.

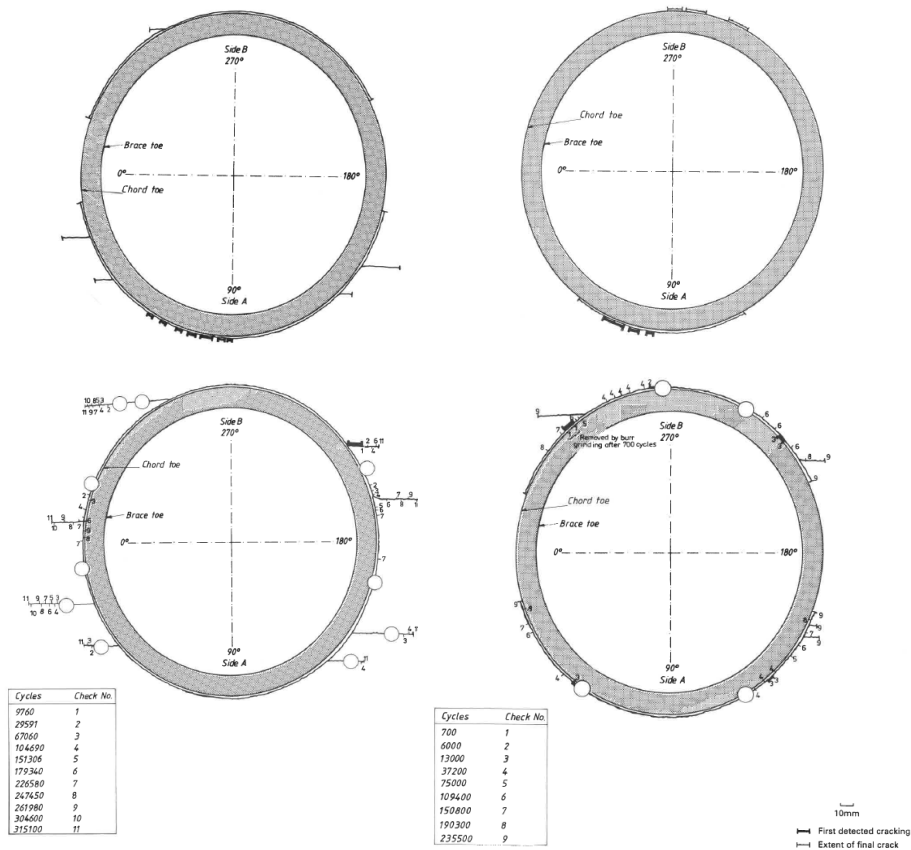


Figure 2-5: Hole drilling repair (Courtesy of the UK Department of Energy) [3]

The results for specimen No.7 showed a total fatigue life of  $6.2 \times 10^5$  cycles, including cycles during pre-cracking and after hole drilling, while specimen No.8 showed a total fatigue life of  $3.56 \times 10^5$  as shown in Table 2-2. Thus, specimen No.7 showed a total fatigue life of more than double the fatigue life to develop a through-thickness crack which resembles the mean S-N fatigue life of such a joint. On the other hand, specimen No. 8 did not show a significant extension in fatigue life after repair. Based on these findings, it was concluded that hole-drilling and cold expansion were not as effective means of delaying crack propagation as other studied repair methods. However, hole drilling and cold expansion repair method have some benefits in fatigue life extension,

which was noticeable in specimen No.7. The repair method is easy to execute with low cost and equipment requirements.

<i>Specimen</i>	<i>Precracking cycle count</i>	<i>After repair cycle count</i>	<i>Total fatigue life</i>	<i>Remarks</i>
7	$3.05 \times 10^5$	$3.15 \times 10^5$	$6.20 \times 10^5$	Through thickness crack precracking
8	$1.66 \times 10^5$	$1.90 \times 10^5$	$3.56 \times 10^5$	50% wall thickness precracking

Table 2-2: Fatigue testing results [3]

In terms of fatigue life performance, hole drilling at the crack-tip may have been thought to be a better method for fatigue life extension among the hole-drilling methods. The execution of hole drilling at the crack-tip results in a partial cut through the weld and full cut through the chord, as shown in Figure 2-7. Performing the cut at this location seems logical as it directly removes the sharp crack-tip and replaces it with a rounded polished surface. The magnitude of fluctuating tensile stresses and mean stresses for these types of repairs will be decisive for the crack re-initiation from the drilled hole. However, the inner hole surface, on the opposite side of the crack, suffers from the alignment of different contribution of tensile stresses. These contributions include stress concentrations from the load transfer path, the weld notch stresses and the inherent residual stresses from the welding process. The latter stress type is assumed to affect the mean stress rather than the fluctuating stresses.

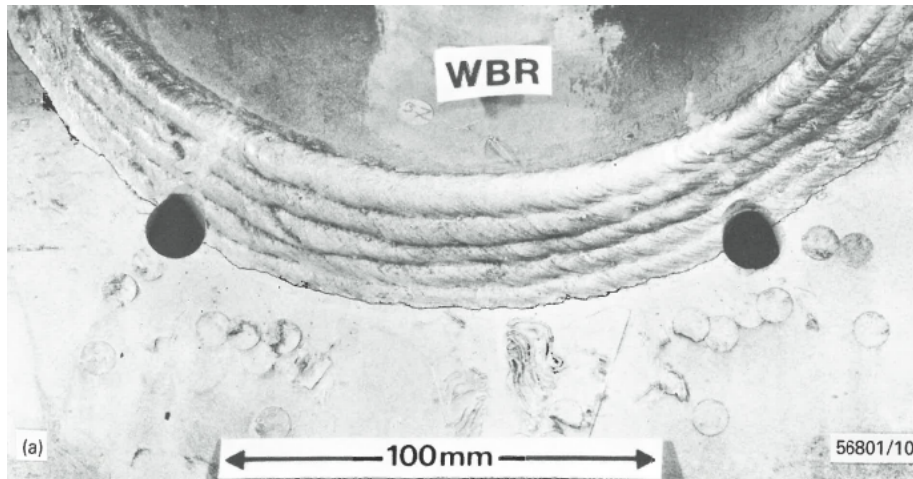


Figure 2-6: crack treated by hole drilling and cold expansion process (Courtesy of the UK Department of Energy) [3]

Crack deflecting holes are in contrast performed away from the weld toe to deflect the crack tip from the weld toe into the parent material. The benefit of crack deflecting holes is that it avoids the alignment of tensile notch stresses with the other determinantal stresses. However, there is no available research on the use any other hole drilling method than the crack-tip hole.

#### ***2.5.4 Treatment of drilled holes (Cold expansion)***

The objective of hole treatment is to induce a compressive residual circumferential stress around the periphery of the hole to enhance the fatigue performance of drilled holes. The result is a reduction of the effective tensile stresses at the hole edges. Hence, it could delay fatigue crack initiation and propagation. Such compressive residual stresses can be achieved by expanding the hole radially by cold expansion.

The most widely used cold expansion methods in practice are hole edge expansion, direct mandrel expansion, ball expansion and split sleeve expansion process. The first three methods are based on pushing a tapered indenter, mandrel or a ball through the hole. This equipment usually has a slightly bigger diameter than the hole.

The split sleeve expansion process is superior to other processes because it does not damage the hole surface at the interface during the cold expansion process. In this process, a solid tapered mandrel and a split sleeve are used. The mandrel and the sleeve are inserted into the drilled hole and then the sleeve is fixed into the hole by the aid of support then the mandrel with the larger diameter than the sleeve inner diameter is withdrawn from the sleeve.

The cold expansion process generates elastic and plastic deformations in the material. Some elastic recovery will take place after the cold expansion process is finalized, but the cold expansion process induces a permanent increase in the hole diameter. This permanent deformation is achieved, some compressive residual stresses is induced around the hole.

Tubby tested the use of cold expansion and concluded that cold expanded holes at the crack tips were ineffective as means of delaying the crack propagation [3].

### ***2.5.5 Grinding as weld improvement technique***

Improvement of weld toe profile and the removal of crack like defects can be achieved by grinding [56]. Grinding gives the weld a favourable shape that reduces the stress concentration at the joint, which can lead to delayed fatigue crack initiation [57]. Grinding can be achieved either by a rotary burr (burr grinding) or with a disc (disc grinding). To obtain the maximum benefits from grinding, it is important to remove all small undercuts and inclusions.

The degree of improvement achieved increase with the amount of machining carried out and care taken by the operator. Burr grinding is preferred over disc grinding as it provides a smoother machined surface. However, disc grinding is less time-consuming and less expensive [58].

The performance of weld-toe grinding, for joints adequately protected from corrosion, shows an increase in the fatigue life by a factor of 2.2 if controlled local machining or grinding of the weld toe is carried out [59]. To achieve this increase in fatigue life, the standards [60] requires that the treatment should produce a smooth concave profile at the weld toe with the depth of excavation into the surface to at least 0.5 mm below the bottom of any visible undercut. In



addition, the treatment should ensure that no exposed defects are remaining in the weld toe.

### **2.5.6 Remedial grinding**

As mentioned in section 2.5.5, grinding is a practical way to remove the surface crack and reintroduce the crack initiation stage. For welded joints with surface cracks, a significant extension of the fatigue life can be expected if grinded such that the crack initiation stage is reintroduced. However, grinding out the surface crack is critically dependent on the complete removal of the crack. If a part of the crack-tip is not removed, the crack will rapidly reinitiate and marginal to no improvement can be expected on the fatigue life of the joint. For deeper cracks, this requires the grinding of grooves at significant depth. Such repairs are often called remedial grinding [54].

Literature on plate specimens and tubular joints (Gibstein, Moe et al, 1987; Haagensen and Slind, 1993) has shown that a fatigue crack with depth of 50-60% of the plate thickness can be successfully repaired by remedial grinding. A remaining fatigue life similar to that of the as-welded joint can be achieved [12, 54, 56].

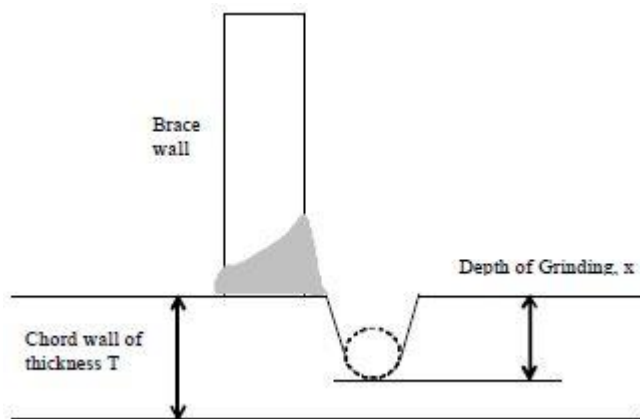


Figure 2-7: Remedial grinding of crack [58].

UK Department of Energy [3] tested 9 tubular joint specimens with part-wall flaws repaired by grinding. The specimens were pre-cracked by out of plane bending. Then repaired by burr grinding to a range of excavation depths and

profiles up to 60% of the chord wall thickness. The excavation shape was dictated by the profile of excavated crack without attempts to optimise the shape. This study concluded that the remaining fatigue life achieved could be up to four times greater than the mean fatigue life for unrepaired joints.

## **3 Fatigue testing of welded tubular joints as fabricated**

### **3.1 General**

The design and preparation of specimens used in the fatigue testing is presented in this chapter. This includes discussion on the principles guiding specimen design and the test setup, including specimen fabrication and testing rig. Further, the chapter describe the instrumentation used for data collection and measurement, ensuring precision and reliability. This chapter aims to provide a comprehensive understanding of the essential preparation steps for the testing campaign.

### **3.2 Tubular joint design and material**

Four DT joints were fabricated with dimensions as given in Table 3-1 with geometric factors of  $\beta = d/D \approx 0.5$ ,  $\tau = t/T = 1$ , and chord to brace angle  $\theta$  of  $90^\circ$ .

<b>Description</b>	<b>Symbol</b>	<b>value</b>	<b>Units</b>
Chord outer diameter	D	219	mm
Chord thickness	T	8.19	mm
Brace outer diameter	d	114	mm
Brace thickness	t	8.56	mm

Table 3-1: Specimen dimensions

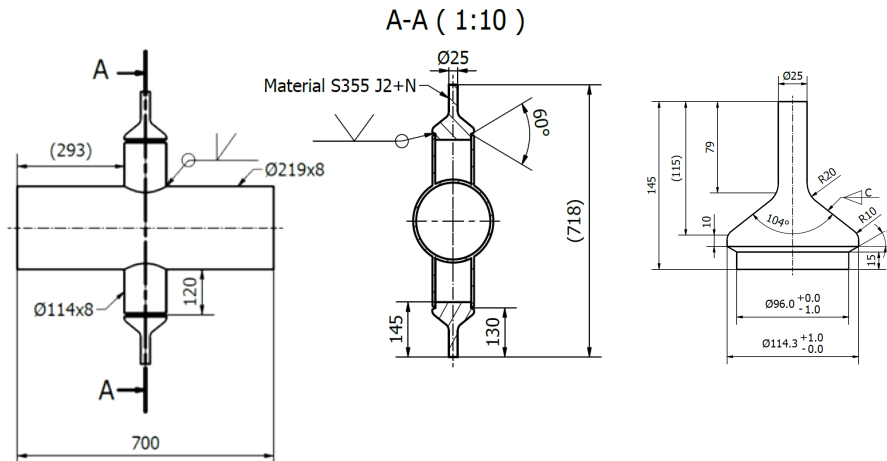


Figure 3-1: DT Joint geometry

Normalised weldable structural steel was used for both chord and brace members, satisfying the grade requirements of S355G15+N. The chord member had a yield strength of 444 MPa and tensile strength of 553 MPa, while brace members had a 387 MPa and tensile strength of 514 MPa. All material used was from a traceable supply with mill certificates being obtained for all tubular materials.

### 3.3 Tubular joint fabrication

The tubular joint specimens were fabricated at RPT Production in Norway, a specialised welding workshop and a leading offshore market fabricator. All steelwork fabrication, inspection and testing were conducted in line with DNV OS-C401 guidelines. The as-built drawings and welding specifications are provided in Appendix 2.

Each welded joint was subject to thorough dimensional and visual inspections to confirm that dimensions and welded details met specifications. Additionally, all around (100%) magnetic particle and ultrasonic non-destructive testing examination performed by a third party. Figure 3-2 shows UT examination of the tubular joint.



Figure 3-2: ultrasonic non-destructive testing examination.

The welding of the specimens was performed by certified welders. The welding process utilized tungsten inert gas arc welding (welding process 141) for the initial pass, followed by tubular cored metal arc welding with an active gas shield (welding process 136) for subsequent passes. The specimens were aligned and accurately positioned using a jig prior to welding. No post-weld treatments or weld improvement techniques were applied to the specimens before pre-cracking.

It should be noted that specimen DT3 was initially fabricated with a lateral misalignment exceeded the specified limits which required rework to achieve acceptable alignment. The misalignment was mitigated by adjusting the circumferential welds between the brace and cones.

### **3.4 Fatigue testing rig**

Tests were performed at the laboratory at the Mechanical and Structural engineering and Materials science department at the University of Stavanger, Norway. All tests were performed in a servo-controlled fatigue rig MTS 809 axial-torsional testing system at room temperature. The test rig is a self-reacting frame into which the specimen is vertically positioned.

The specimens were gripped from each brace end with the lower gripper connected to a dynamic actuator for load application while the top gripper is connected to a load cell and dead support as shown in Figure 3-3. The actuator-rated dynamic force is 250 kN axially and the maximum dynamic stroke of 150 mm.



Figure 3-3: Testing rig

### **3.5 Instrumentation and measurement setup**

#### **3.5.1 Strain gauges and thermocouples**

Electrical resistance strain gauges were glued to the chord and brace members. The strain gauges are attached to the specimen to measure the response under static and dynamic loading in the laboratory environment. Installation and data acquisition setup was carried out by trained personnel. The main strain gauge used throughout the experimental work is LY71 – 3/120. It has a linear geometry connected via solder tabs with a nominal resistance of 120 ohms. PT100 sensors monitored the temperature at strain gauge locations, and the deviation in strain readings due to temperature was compensated while post-processing the measurement data.

Strain gauges were mounted to the specimen to effectively measure strains at the joint and calculate the stress concentration factors (SCFs) at the weld toe throughout all stages of testing. Moreover, these strain gauges demonstrated high efficiency in detecting cracks and monitoring the crack trajectories, providing invaluable data for the analysis and understanding of the specimen's behaviour under stress.

#### **3.5.2 Strain gauge locations**

The strain gauges were glued to the chord and brace members to determine the stress distribution on the chord side from the saddle to the crown and nominal stresses in brace members. The chord saddle strain gauges layout is shown in Figure 3-4. The method of extrapolation used for each specimen tested is the linear extrapolation method. Strain gauge locations are placed based on the recommendation from the ECSC project. According to these recommendations, the first row of strain gauges is to be located at a distance from the weld toe defined by the greatest of  $0.2\sqrt{rt}$  and 4 mm, while the second row of strain gauges is to be located according to the position on the brace-to-chord intersection, as specified:

- At the chord saddle             $= 5^\circ$  arc
- At the chord crown            $= 0.4\sqrt[4]{rtRT}$
- At the brace side              $= 0.65\sqrt{rt}$

Based on the recommendations above, the first row of strain gauges on the chord side was glued with its centre located at 4.5 mm from the weld toe, while the second row of gauges was glued at varying distances; 9.5 mm from the weld toe at the chord saddle and 10.5 mm from the weld toe at the chord crown.

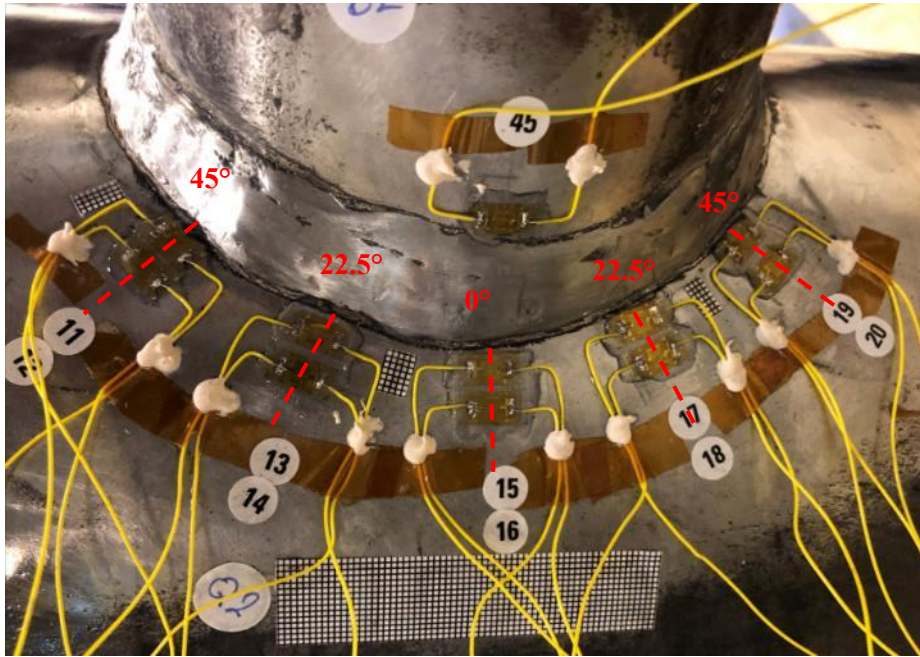


Figure 3-4: Chord saddle strain gauge layout

The number of instrumentation channels was limited to 52 channels; of that, 48 were used for strain gauges, 3 for thermocouples and one vacant channel. The general layout included 10 strain gauges at each chord saddle and 4 on each brace. On specimen two, the strain gauges layout was changed by adding 8 strain gauges to the chord crown and 4 strain gauges on each brace to measure the strains and, eventually, the stress concentration factors at the chord crowns at four locations and the brace saddle and crown locations. 4 strain gauges were then removed from each chord saddle due to the limitation on the number of channels. Specimen 2 strain gauge layout is shown in Figure 3-5



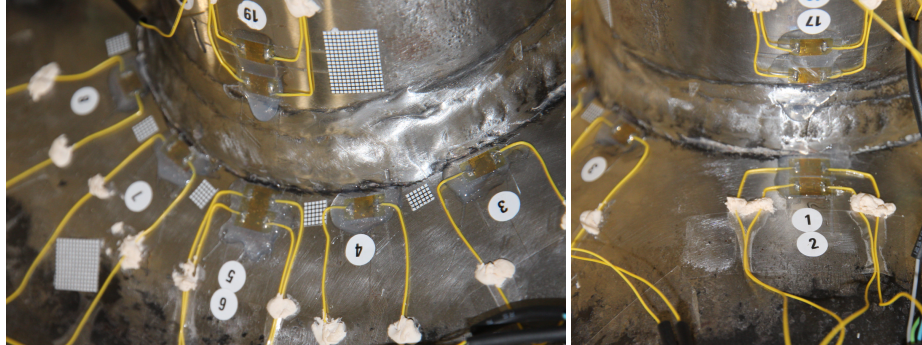


Figure 3-5: Chord saddle strain gauge layout of specimen 2

### **3.5.3 Data logging and processing**

Strain gauges were connected via a Wheatstone quarter bridge configuration to a computer-controlled data acquisition system. Four data logging modules were used during the project, three QuantumX bridge amplifiers with 16 channels each and one QuantumX universal amplifier with eight channels. The modules were synchronised via FireWire connections and an Ethernet switch.

It is recommended to use at least a sample rate of about ten times the test frequency. During testing, a sample rate of 200 Hz/channel was selected. Raw data generated during the test were processed using catmanAP version 5.3 software. The software was used to process the strain readings and temperature variation to:

- Compensate for strain reading due to temperature change.
- Extrapolate the stresses to the weld toe to estimate the hot spot stresses.
- Recording the hotspot stress change over time to correlate it to crack initiation, propagation and relief of residual stresses.

### **3.5.4 Hand-held digital microscope**

Throughout the testing process, a hand-held digital microscope proved to be a valuable tool for assisting with the visual inspection of cracks. With a magnification power of 220X, this enabled efficient observation of cracks and facilitated a more detailed analysis. Furthermore, the digital microscope was

employed to examine the crack surfaces after the specimens were cut, allowing for the detection of beach marks on the crack surfaces. The utilization of the hand-held digital microscope greatly enhanced the overall inspection and analysis process, providing valuable insights into the characteristics and behaviours of the cracks under investigation.

### **3.6 Fatigue testing of tubular joints**

#### **3.6.1 Differences in fatigue life between load and displacement control.**

Fatigue testing in this thesis was performed under load-controlled condition rather than displacement controlled (as further described in section 3.6.2). Steel offshore structures (jackets) are normally quite redundant. This implies that they have alternative load paths, should one joint or member lose its load-carrying capacity. Hence, the loads will be redistributed (load shedding) as a result of cracking or other damage causing loss of stiffness of the joint or member. In practice, this implies that the loading on a joint in a real structure is closer to deformation (displacement) controlled.

Nevertheless, most fatigue tests carried out in laboratories are load controlled. The difference in fatigue life between joints loaded in-service (displacement-controlled) and in laboratory (load-controlled) conditions does not give any effect until crack is well developed. However, once a crack is developed the geometry and load path through the joint may change. As the result, the joint becomes less stiff and the load and displacement-controlled tests will differ significantly. In this situation, load controlled testing will maintain the force on the joint resulting in higher stresses, in contrast to displacement control testing where stresses will decrease with decreasing stiffness. The definition of failure in both S-N curves and in this study is predicated upon the occurrence of through-thickness cracking. This criterion is deemed to be a safe failure threshold in relation to offshore structures possessing a degree of redundancy. The rationale behind this is that these criteria are predicated on test results derived under load-controlled circumstances, which are inherently more conservative when compared to displacement control conditions.

### **3.6.2 Loading of the specimens**

For each of the specimens, an initial tensile load was applied to create a mean tensile axial stress in the brace members. The load was then cycled around the mean stress such that the axial stresses in the braces remained in tension with a positive R ratio.

During testing strain gauge readings and loading measurements for determining SCFs, fatigue lives and crack propagation rate were obtained as follows:

- Strain readings were collected before and after clamping the specimens to estimate the clamping stresses and the system misalignment.
- The load was applied incrementally and all strain gauge readings were monitored to estimate the location of the highest stress concentration and approximate hotspot stress per unit load.
- Cyclic loading was used to 'shakedown' the strain gauges and reliably achieve stable strain readings. Strains were measured for 100 cycles of the axial tensile load causing 50% yield stress at the hotspot. The peaks of the cyclic loading were then analysed to obtain SCFs at saddles on the chord side.
- Start of fatigue testing under constant amplitude sinusoidal loading, with load ratio of 0.17 and frequency of 3 Hz. The test runs continuously until N1 fatigue life is obtained.

### **3.6.3 Monitoring during testing**

The strain gauges mounted to the chord saddle serve to monitor the deformation stresses experienced by the tubular joint. In addition to mapping the stress distribution on the chord side and eventually estimating the hot-spot stresses. In general, deviations in the strain gauge readings beyond the anticipated stress range typically signal changes in the joint's stiffness, which may be indicative of specimen cracking. As a result, the strain gauges are also an accurate way to measure crack initiation and propagation. To complement the strain gauge data, a hand-held digital microscope was employed for the detection and quantification of surface cracks (as described in 3.5.4).

An alternative technique for measuring the length and depth of cracks involves the following steps: Upon the detection of crack initiation, either by strain gauges or a handheld digital microscope, an interval of 200 cycles is applied at intervals ranging from 20,000 to 40,000 cycles. This approach uses a loading ratio of 0.8 and a frequency of 1 Hz to create a unique rib mark on the cracked surface. The marker load applied is set to reach a peak load equivalent to the maximum load experienced during fatigue testing, thereby ensuring similarity in the maximum crack opening for both loads. This methodology supports the inspection of cracked surfaces via fractographic analysis and facilitates the post testing assessment of crack depths with increased accuracy.

## **4 Fatigue precracking of tubular joints**

### **4.1 General**

The test program for tubular joint specimens aims to evaluate their fatigue life and the effectiveness of repair techniques. The program consists of three main stages:

1. the precracking stage, where cyclic loading is applied to the specimen to develop a crack around the weld toe until it penetrates the entire chord wall,
2. the repair stage, which employs hole drilling to alter the stress field and redirect or arrest crack growth, and
3. the post-repair stage, in which the repaired specimen is subjected to additional cyclic loading to identify new crack initiation and assess the repair performance concerning the joint's fatigue life.

This section focuses on the first stage of the testing program, featuring four axially loaded double tee (DT) joints. The initial specimen acted as a control specimen and was tested to failure without repair, while the remaining three specimens experienced precracking to create through-thickness cracks before undergoing repair and post-cracking tests. The fatigue testing of the control specimen (DT1) and the precracking process for the subsequent specimens (DT2, DT3, and DT4), which resulted in through-thickness cracks suitable for repair, are detailed in the following sections.

A summary of the fatigue life derived from the tests is presented, comparing the sample data with the standard S-N curve (T-curve). Furthermore, a study investigating the surface crack length and, where applicable, depth evolution in relation to fatigue life is introduced. This research provides a simplified method for estimating the remaining fatigue life of tubular joints with surface-breaking cracks but is limited to DT joints with geometric parameters similar to the tested samples.

Postprocessing of the first stage's results allowed for the determination of stress concentration factors, tubular joint fatigue life, and crack aspect ratios.

## 4.2 Fatigue testing of Specimen DT1 (control specimen)

### 4.2.1 Test loading

The first specimen to be tested, designated as the control specimen DT1, aimed to undergo testing until the development of a through-thickness crack and ultimately to final failure. Subjected to constant amplitude sinusoidal loading, the specimen experienced a load ratio  $R$  of 0.17 and a frequency of 3 Hz. The maximum load applied ( $P_{max}$ ) reached 60 kN, while the minimum load applied ( $P_{min}$ ) was 10 kN. Throughout the testing process, strain gauge readings and loading measurements were recorded to determine stress concentration factors (SCFs), fatigue lives and crack propagation rates. The key parameters of the test DT1 loading is presented in Table 4-1.

<b>Id</b>	<b>Pmax</b>	<b>Pmin</b>	<b>R</b>	<b><math>\Delta\sigma_{nom}</math> in brace</b>
DT1	60 kN	10 kN	0.17	17.65 MPa

Table 4-1: Key parameters for DT1 test.

### 4.2.2 Stress distribution in intact joint

As already explained in Chapter 3, strain gauges were glued to both the chord and brace members to determine the stress distribution on the chord side ranging from the saddle to the crown and nominal stresses in brace members. Figure 4-1 illustrates the layout of the strain gauges positioned on the chord saddle. The reported stresses are directly extracted from the strain gauges mounted on the first row adjacent to the weld toe.

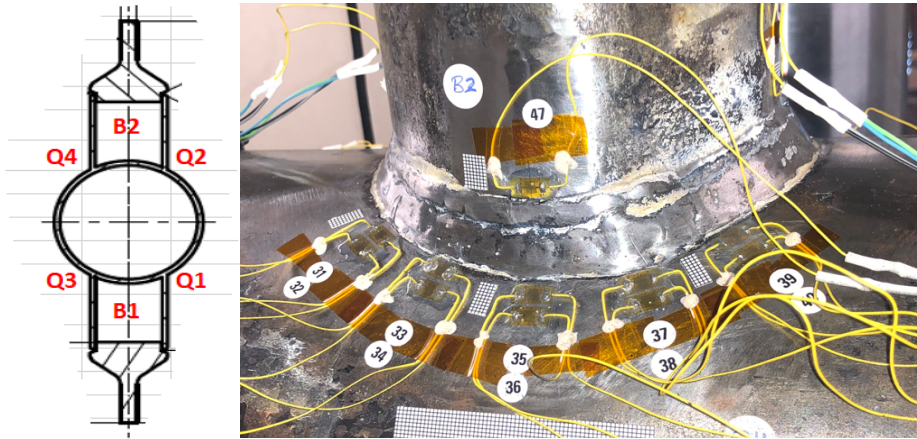


Figure 4-1: Strain measurements variation during precracking of quadrant Q4, specimen DT1.

As anticipated, section 2.3, for tubular joints subjected to axial loading, the maximum hot-spot strain in the chord is found in the saddle area along the centreline of the brace (at zero degrees). The stresses gradually diminish towards the crown. Figure 4-2 displays the hot-spot stress range variation along the chord-brace intersection, extrapolated from strain gauge measurements, for the chord side for all quadrants on specimen DT2. The maximum observed stress occurs in Q1, while the minimum stress is located in Q2.

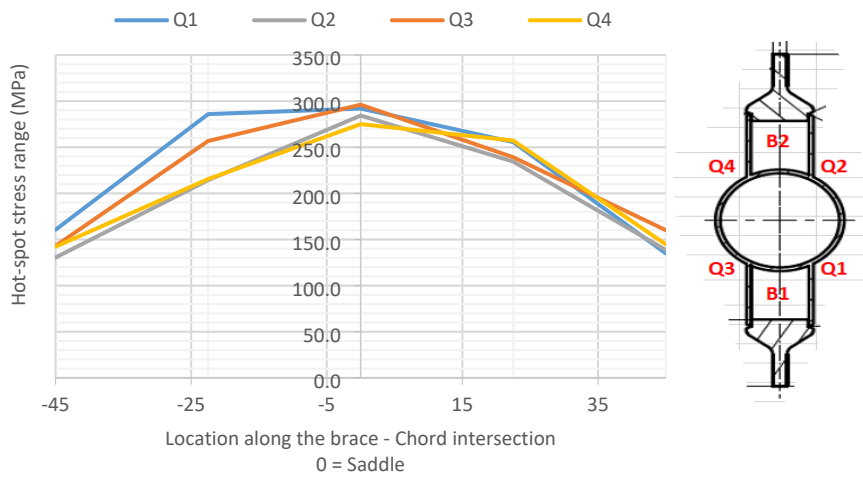


Figure 4-2: Measured hot-spot stress range along the chord-brace intersection and chord side for the four quadrants on specimen DT1.

### 4.2.3 Results of fatigue test

During fatigue testing, specimen DT1 developed a through-thickness crack in Q4 with a crack length spanning 74 mm. A 15% decrease in the measured hot-spot strain was observed at 316,000 cycles, marking the N1 fatigue life. The crack initiated at the saddle's centre (0°) and gradually expanded toward the positive and negative 22.5° sectors. A visually observable 7.5 mm (N2) crack in Q4 was detected at 380,000 cycles.

Upon reaching 632,000 loading cycles, a 100% drop in the hot-spot stress range was noted, and through-thickness cracking at Q4 was achieved. Fatigue testing continued until a surface crack measuring 1.5 times the brace's diameter developed at 820,000 cycles. The test was then stopped to prevent excessive bending of the specimen and potential damage to the fatigue rig. Figure 4-3 presents the variation of hot-spot stress range as a function of the number of cycles during specimen testing. A summary of the fatigue test results can be found in Table 4-2.

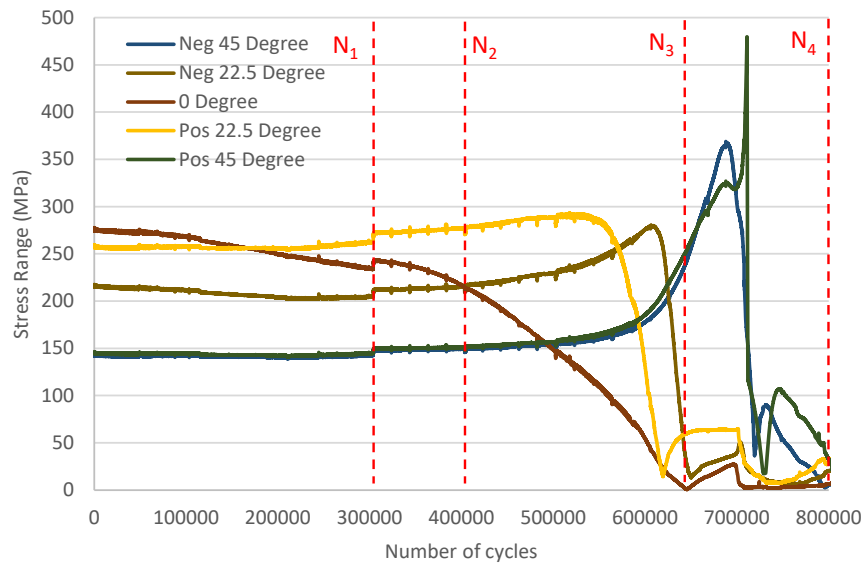


Figure 4-3: Change in hot-spot stress range during testing of specimen DT1, Q4.



Fatigue life	Number of cycles	Remark
N1	316,000	15% drop in the measured hot-spot strain*
N2	380,000	7.5 mm surface crack length
N3	632,000	observation of 100% loss in the hot-spot strain reading
N4	820,000	end of the test, crack length of 1.5 times the brace diameter.

\*The hot-spot strain is determined by linear extrapolation from the readings of the two strain gauges placed perpendicular to the weld toe

Table 4-2: Fatigue testing results of precracking stage for specimen DT1

At each measurement point on the chord side, strain evolution was documented and presented in the strain evolution diagram, as illustrated in Figure 4-4. Changes in strain gauge readings are presented as a function of the number of load cycles, with positive values representing a decrease and negative values indicating an increase in SG readings.

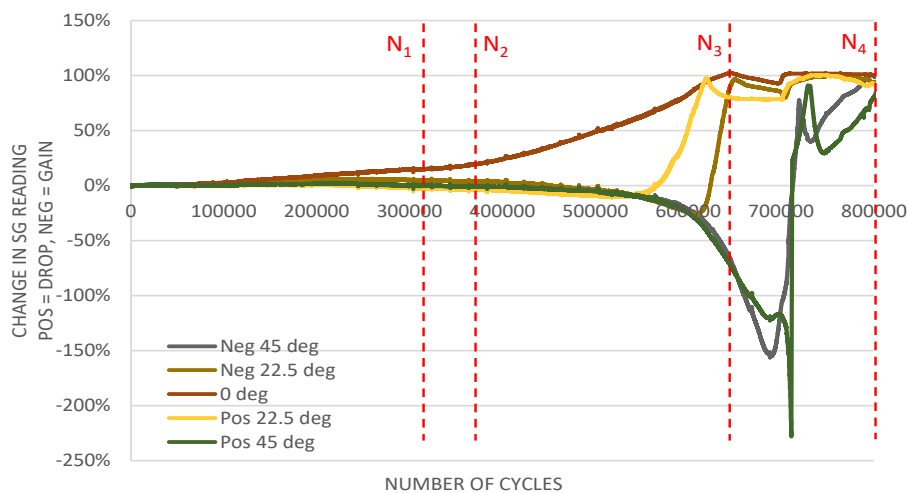


Figure 4-4: Strain evolution diagram during precracking of quadrant 4, specimen DT1.

In the case of DT1, the crack extended to the midpoint between the saddle and the crown before deviating from the weld toe into the parent material. As cyclic loading continued, the crack was arrested in the parent material and bifurcated at the weld toe, where the deviation had initially begun. This behaviour is commonly referred to as crack branching. Crack branching of DT1 is illustrated in Figure 4-5. Tubby [3] observed similar crack branching in several tests. This

report presents only the lead surface crack length, with the measured surface crack lengths plotted against the number of cycles in Figure 4-6.

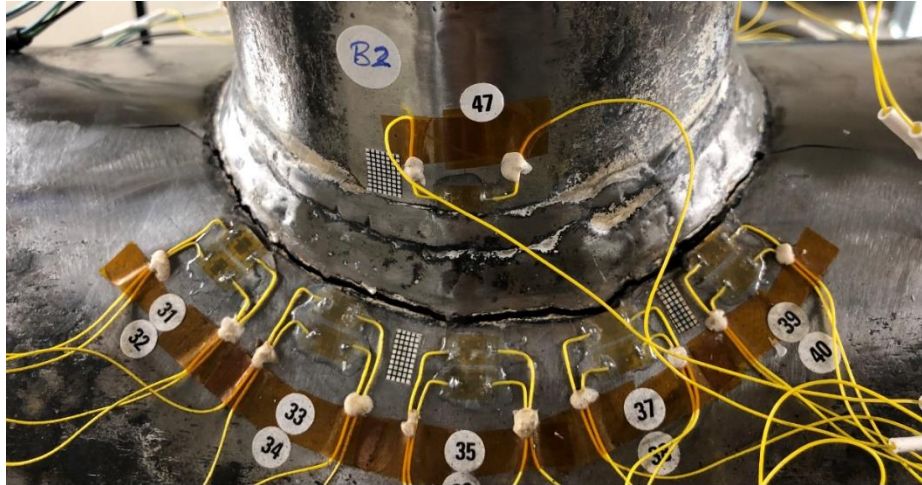


Figure 4-5: Control specimen DT 1 – surface cracking at N4 with branching of crack close to the crown.

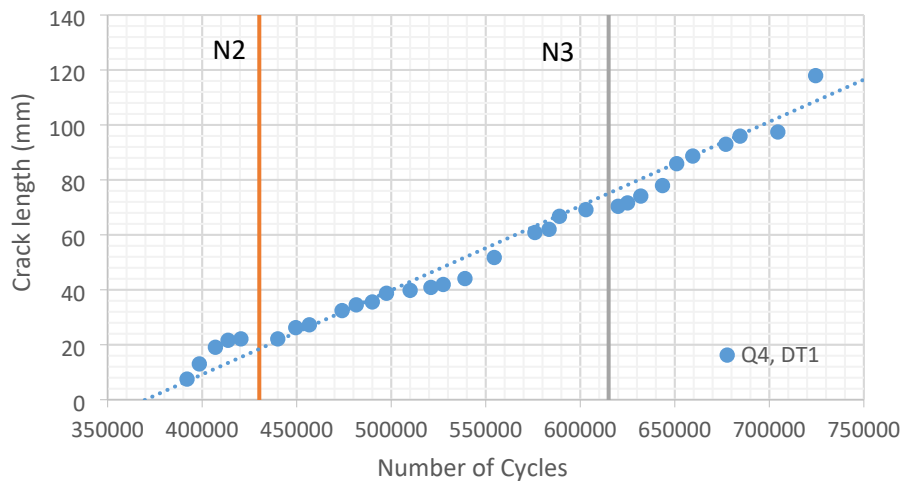


Figure 4-6: Crack length evolution of quadrant 4 during fatigue testing of specimen DT1.

### **4.3 Precracking of Specimen DT2**

#### **4.3.1 Test loading**

The DT2 specimen underwent precracking similar to specimen DT1 with a load ratio  $R$  of 0.17 and a frequency of 3 Hz. The maximum applied load,  $P_{max}$ , reached 60 kN, while the minimum applied load,  $P_{min}$ , was 10 kN. Throughout the testing process, strain gauge readings and loading measurements were recorded to determine SCFs, fatigue lives and crack propagation rates. The key parameters of the test DT1 loading is presented in Table 4-3.

<b>Id</b>	<b><math>P_{max}</math></b>	<b><math>P_{min}</math></b>	<b>R</b>	<b><math>\Delta\sigma_{nom}</math> in brace</b>
DT2	60 kN	10 kN	0.17	17.65 MPa

Table 4-3: Key parameters for DT2 test.

#### **4.3.2 Stress distribution in unrepaired joint**

The strain gauges were glued to the chord and brace members to determine the stress distribution on the chord side from the saddle to the crown and nominal stresses in brace members. The chord saddle strain gauges layout is shown in Figure 4-7. Contrasting with specimen DT1, the layout of strain gauges in specimen DT2 was particularly different. In locations other than the saddle centres, only a single row of strain gauges was glued. This modification in the layout was forced by instrumentation constraints and the requirement to incorporate additional strain gauges on other locations of the joint as the instrumentations was limited to 52 channels. Consequently, the reported stress values are extracted directly from the strain gauges located on the first row adjacent to the weld toe. They do not represent hot-spot stress or strain values, which would typically be derived from extrapolating data from two rows of strain gauges.

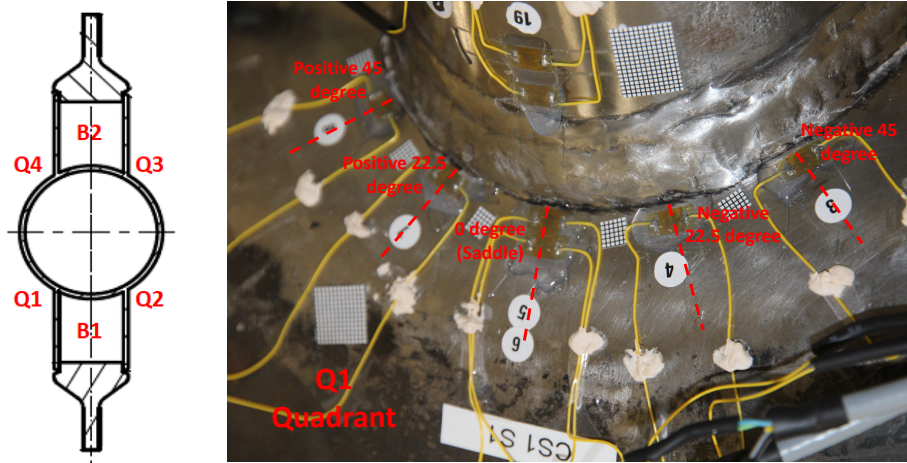


Figure 4-7: Strain measurements variation during precracking of quadrant 1, specimen DT2.

Figure 4-8 presents the fluctuation of the stress range, obtained from the first row of strain gauges, along the intersection of the chord-brace on the chord side, for all quadrants of specimen DT2. The highest observed stress occurs in Q4, whereas the lowest stress is located in Q3.

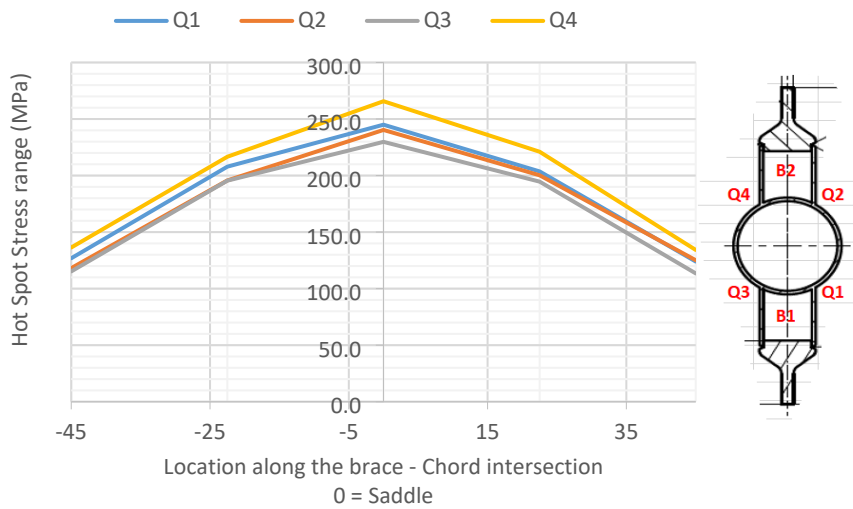


Figure 4-8: Measured stress range obtained from the first row of strain gauges, along the chord-brace intersection on chord side for the four quadrants on specimen DT2.

### 4.3.3 Results of fatigue test

At 430,000 cycles, a 7.5 mm surface crack length became visually apparent in the first quadrant, Q1, situated between the saddle centreline and the negative 22.5° measurement point. The crack length was determined using a digital handheld microscope. Concurrently, the measured tensile strains began to decrease at the saddle's centre. A 15% reduction in the measured hot-spot strain occurred at 466,000 cycles, suggesting that the crack had penetrated the chord's full thickness. As these strain reading drops were observed between the chord's centreline and negative 22.5°, neighbouring strain gauges at positive 22.5°, 45°, and negative 45° experienced strain increase, indicating strain redistribution during the precracking process. At 613,000 cycles, a total loss in the strain gauge measurement at the chord's centreline was noted, signalling the development of through-thickness cracking at Q1, as defined in Table 4-4. At this stage, the surface crack length was estimated to be 83 mm, spanning from -47° to 28°. The fatigue test results are consolidated in Table 4-4.

Figure 4-9 presents a typical variation of hot-spot stress range as a function of the number of cycles during specimen precracking. For each measurement point on the chord side, the strain evolution under axial cyclic loading was systematically recorded and depicted in the strain evolution diagram, as illustrated in Figure 4-10, with strain gain or loss in function of number of cycles. Furthermore, Figure 4-11 demonstrates the crack length evolution in quadrant Q1 during the precracking process, providing valuable insights into the specimen's response to cyclic loading throughout the test program.

<i>Fatigue life</i>	<i>Number of cycles</i>	<i>Remark</i>
N1	466,000	15% drop in the measured strain
N2	430,000	7.5 mm surface crack length
N3	613,000	observation of 100% loss in the hot-spot strain reading

Table 4-4: Fatigue testing results of precracking stage for specimen DT2

Fatigue precracking of tubular joints

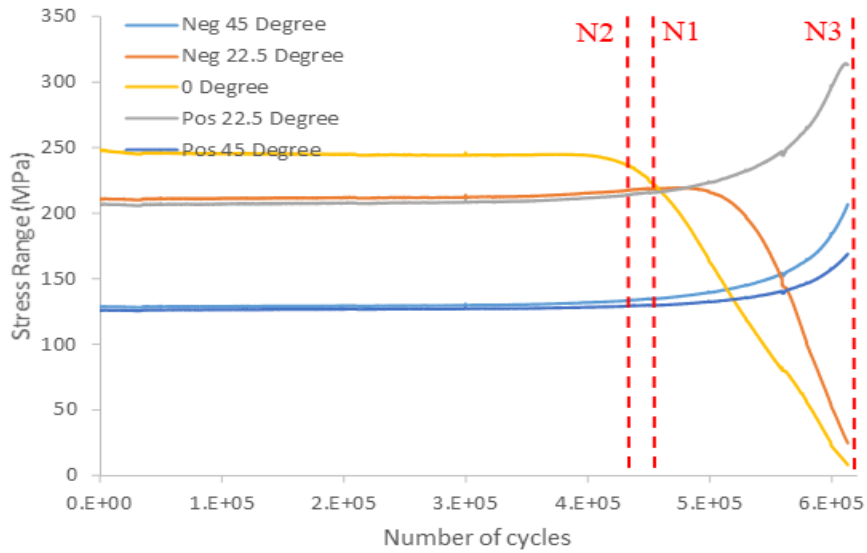


Figure 4-9: Change in stress range during precracking of specimen DT2, Q1.

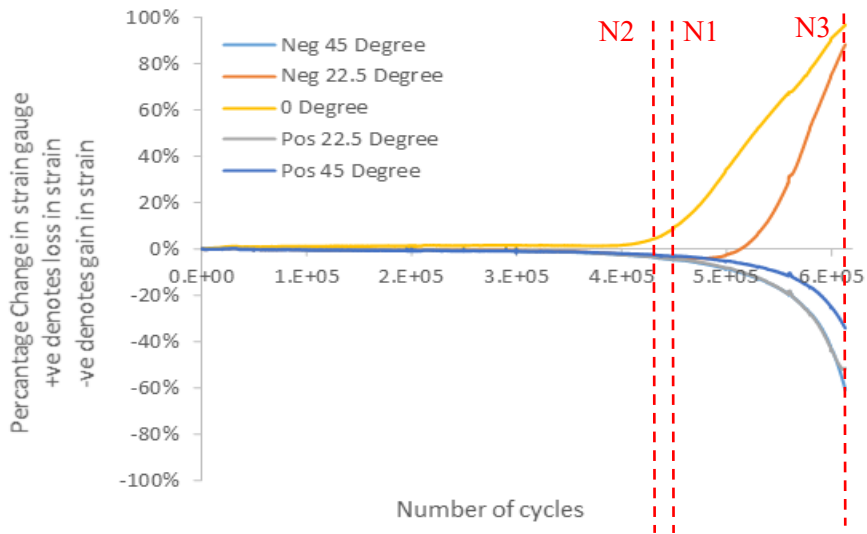


Figure 4-10: Strain evolution diagram during precracking of specimen DT2, Q1.

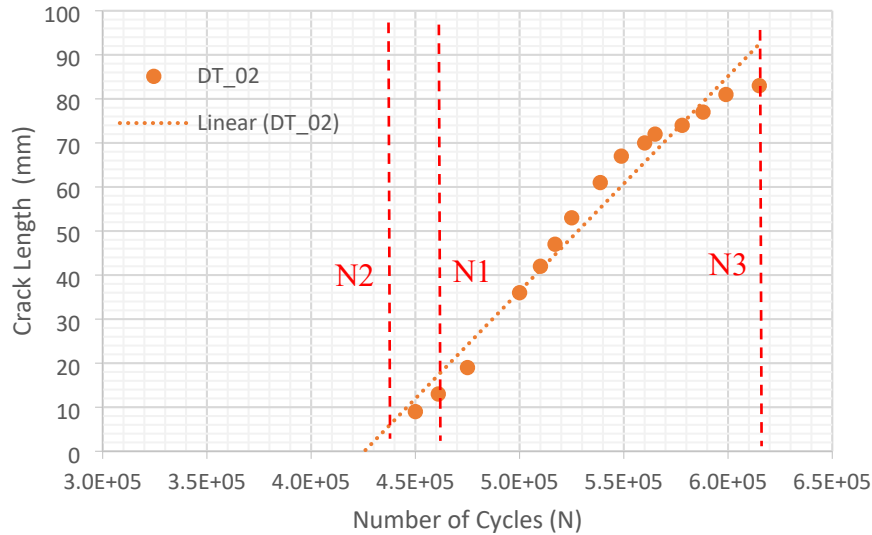


Figure 4-11: Crack length evolution during precracking of specimen DT2, Q1.

#### 4.4 Precracking of Specimen DT3

##### 4.4.1 Test loading

Specimen DT3 subjected to the predetermined precracking load of  $P_{max}$  60 kN and  $P_{min}$  10 kN, the specimen exhibited a 7 mm crack in quadrant Q3 at a cycle count of 504,000. Following this development, the crack became dormant, and no additional signs of cracking were observed. The test was interrupted at 1,140,017 cycles. Subsequently, a new precracking load was established, with a  $P_{max}$  of 85 kN and a  $P_{min}$  of 15 kN, while maintaining the same load ratio and a frequency of 3 Hz. The precracking results discussed in this section exclude the cycles applied before the precracking load change. Throughout the testing process, strain gauge readings and loading measurements were recorded to determine SCFs, fatigue lives and crack propagation rates, as elaborated in the following sections. The key parameters of the test DT1 loading is presented in Table 4-5.

<b>Id</b>	<b>Pmax</b>	<b>Pmin</b>	<b>R</b>	<b><math>\Delta\sigma_{nom}</math> in brace</b>
DT3 (runout)	60 kN	10 kN	0.17	17.65 MPa
DT3 extension	85 kN	15 kN	0.17	24.71 MPa

Table 4-5: Key parameters for DT3 test.

#### 4.4.2 Stress distribution in unrepaired joint

The strain gauges were glued to the chord and brace members to determine the stress distribution on the chord side and brace side saddles. The chord saddle strain gauges layout is shown in Figure 4-12. Hot-spot strain is measured by the linear extrapolation of SG readings at the weld toe from two existing strain gauges on the same row.

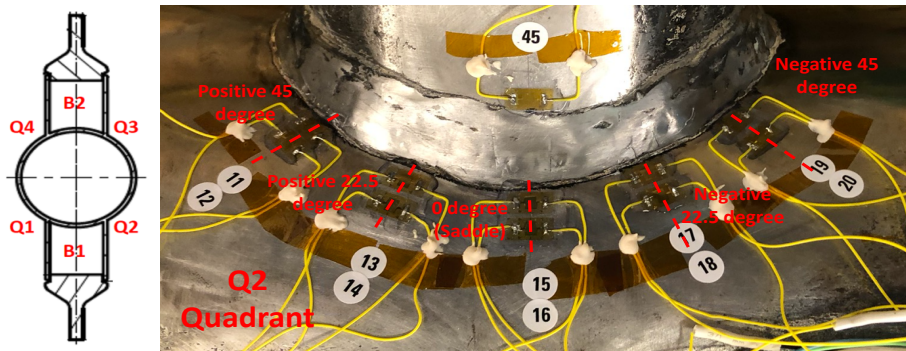


Figure 4-12: Strain measurements variation during precracking of quadrant 2, specimen DT3.

The maximum hot-spot strain occurred in the chord saddle on quadrant Q4, while the minimum hot-spot saddle strain occurred on quadrant Q1. Figure 4-13 shows the variation in hot-spot stress range along the Chord-brace intersection on the chord side for all the quadrants on specimen DT3. The maximum observed stress is in Q4, while the minimum is in Q3.



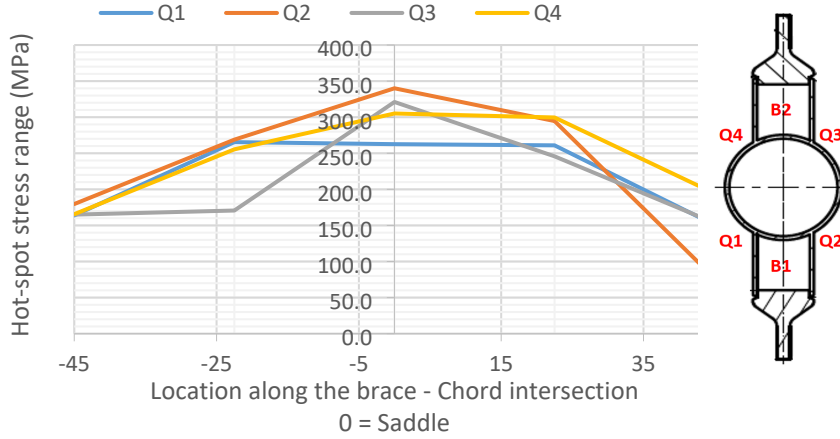


Figure 4-13: Measured hot-spot stress range along the chord-brace intersection and chord side for the four quadrants on specimen DT3.

Upon mounting the test specimen in the fatigue rig, an out of straightness between the brace and chord of specimen DT3 was identified. To rectify this misalignment, the specimen was forcibly realigned by clamping it within the rig grippers. The stress distribution induced from straightening the specimen in the testing rig is illustrated in Figure 4-14. A peak stress of 44 MPa, attributed to the clamping process, was detected in quadrant Q3. Although this stress level is deemed insignificant with respect to the overall test objectives, it is important to note that stress concentrations in Q3 could potentially intensify under subsequent loading, rendering this region susceptible to crack initiation.

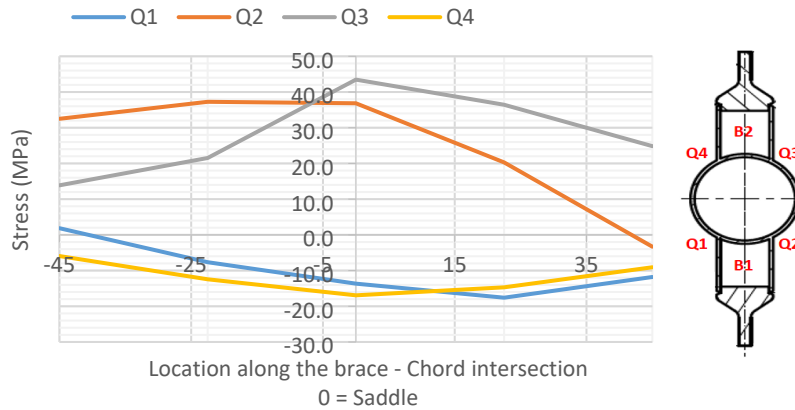


Figure 4-14: clamping induced hot-spot stresses at each quadrant of specimen DT3.

#### 4.4.3 Results of fatigue test

Throughout the precracking phase, cracks developed in three quadrants: Q2, Q3 and Q4. A through-thickness crack appeared in quadrant Q3, whereas quadrants Q2 and Q4 exhibited surface cracks. A summary of fatigue life outcomes for specimen DT3 can be found in Table 4-6.

Specimen	Quad.	HSS (MPa)	N1 x10 <sup>3</sup>	N2 x10 <sup>3</sup>	N3 x10 <sup>3</sup>
DT3	Q1	407	-	-	-
	Q2	516	50.9	-	-
	Q3	697	31.4	-	68.4
	Q4	462	61.7	-	-

- N1 denotes a 15% drop in the measured hot-spot strain by linear extrapolation from two strain gauges placed perpendicular to the weld toe,  
 - N2 denotes the formation of a 7.5 mm surface crack, and  
 - N3 denotes the observation of 100% loss in the hot-spot strain reading or direct crack observation on the chord's internal surface

Table 4-6: specimen DT3 precracking fatigue life

#### Quadrant Q3

The hot-spot stress at the saddle within quadrant Q3 reached the highest value observed on the specimen, measuring 697 MPa. Crack initiation took place

between the saddle's centre at 0° and the positive 22.5° position. At 31,400 cycles, a 15% decrease in the measured hot-spot strain was recorded, signifying the commencement of N1 fatigue life. Measuring N2 for quadrant Q3 was found unreasonable after elevating the precracking load, as a pre-existing 7 mm crack was already present in the same quadrant. At 68,400 cycles, the hot-spot strain experienced a complete reduction, leading to through-thickness cracking in Q3. As a result, the specimen precracking test was stopped.

The through-thickness crack length was estimated at 90 mm and was confined between the positive 45° and negative 22.5° sectors. Figure 4-15 illustrates the typical hot-spot stress range variation as a function of the number of cycles during the specimen precracking process. Figure 4-16 presents the hot-spot stress range evolution as a function of the number of load cycles at quadrant Q3. Lastly, for Q3, Figure 4-17 displays the evolution of crack length during precracking for the primary crack developed in quadrant Q3.

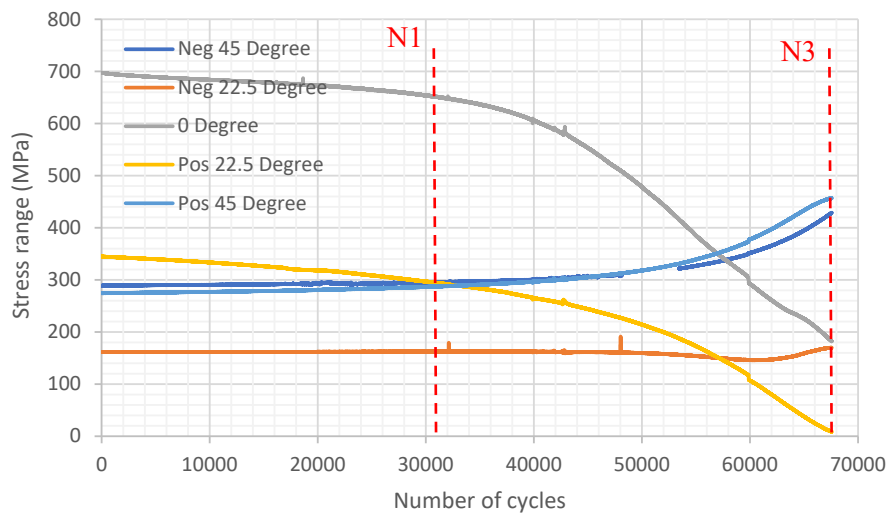


Figure 4-15: Change in hot-spot stress range during precracking of quadrant Q3, specimen DT3.

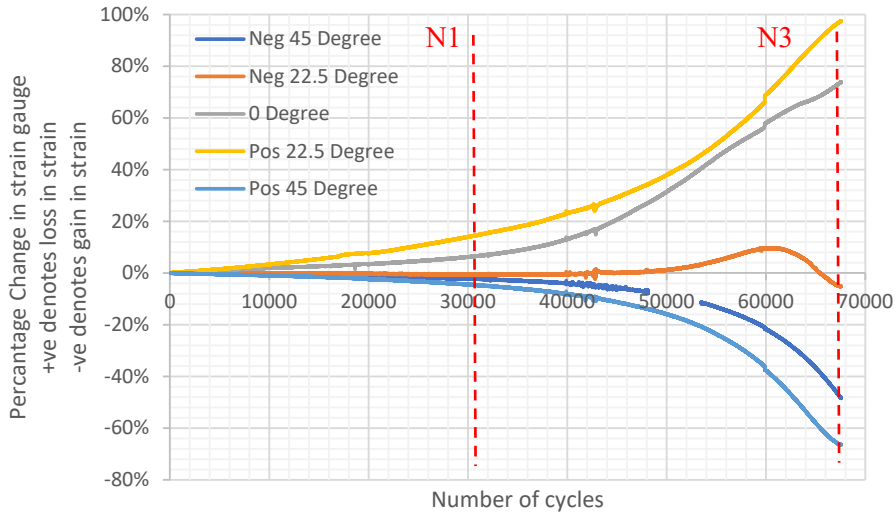


Figure 4-16: Strain evolution diagram during precracking of quadrant Q3, specimen DT3.

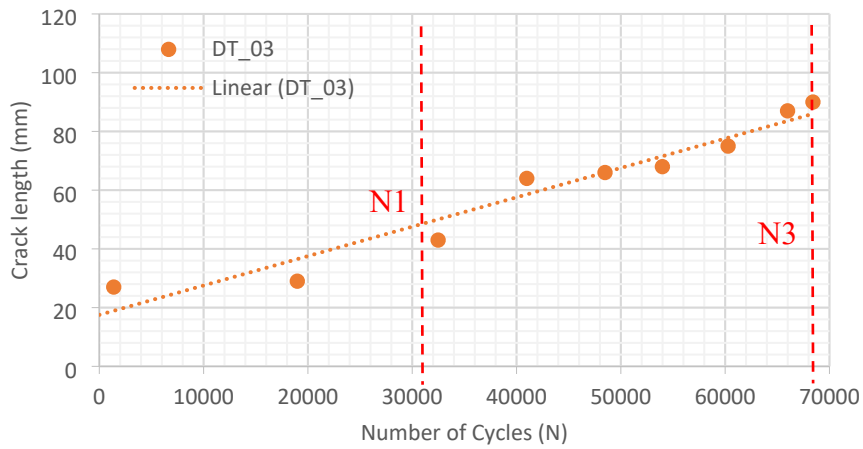


Figure 4-17: Crack length evolution during precracking of quadrant Q3, specimen DT3.

### Quadrant Q2

The hot-spot stress measured in quadrant Q2 was 516 MPa, ranking as the second-highest value across the specimen. The onset of N1 fatigue life was observed at 50,900 cycles. At the conclusion of the precracking stage, a 49 mm

crack was identified at 68,400 cycles, confined to the sector between positive 22.5° and negative 22.5°. This crack exhibited a partial penetration of 43% through the chord wall thickness. Figure 4-18 shows the typical hot-spot stress range variation as a function of the number of cycles during specimen precracking, while Figure 4-19 presents the Q2 strain evolution diagram.

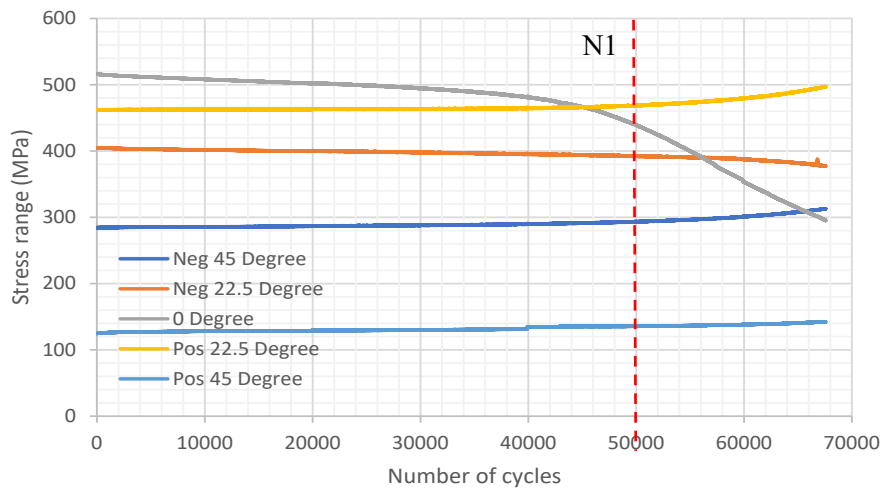


Figure 4-18: Change in hot-spot stress range during precracking of quadrant Q2, specimen DT3.

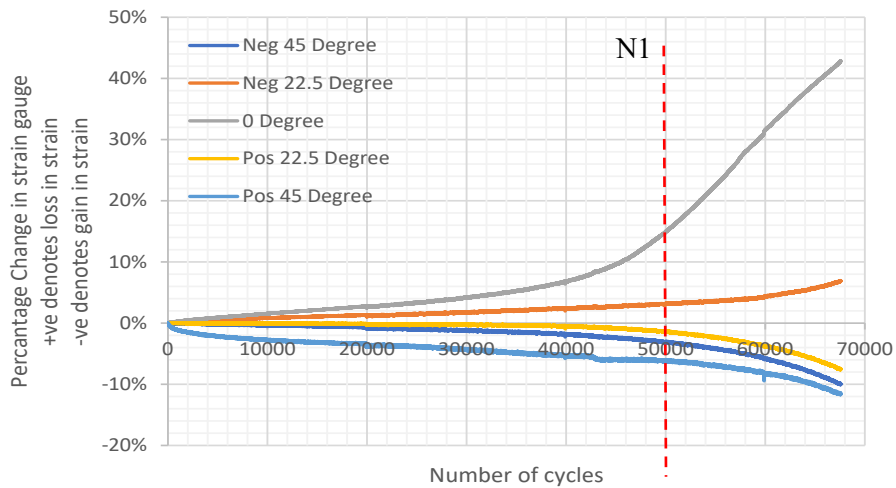


Figure 4-19: Strain evolution diagram during precracking of quadrant Q2, specimen DT3.

### Quadrant Q4

Quadrant Q4 exhibited a hot-spot stress of 462 MPa at the onset of testing. The N1 fatigue life was observed at 61,700 cycles. Upon completion of the precracking stage, at 68,400 cycles, a crack length of 50 mm was detected in Q4. This crack was confined to the sector between positive 22.5° and negative 45°, with a partial penetration of 24% through the chord wall thickness. Figure 4-20 displays the typical hot-spot stress range variation as a function of the number of cycles during specimen precracking. Meanwhile, Figure 4-21 presents the Q4 strain evolution diagram.

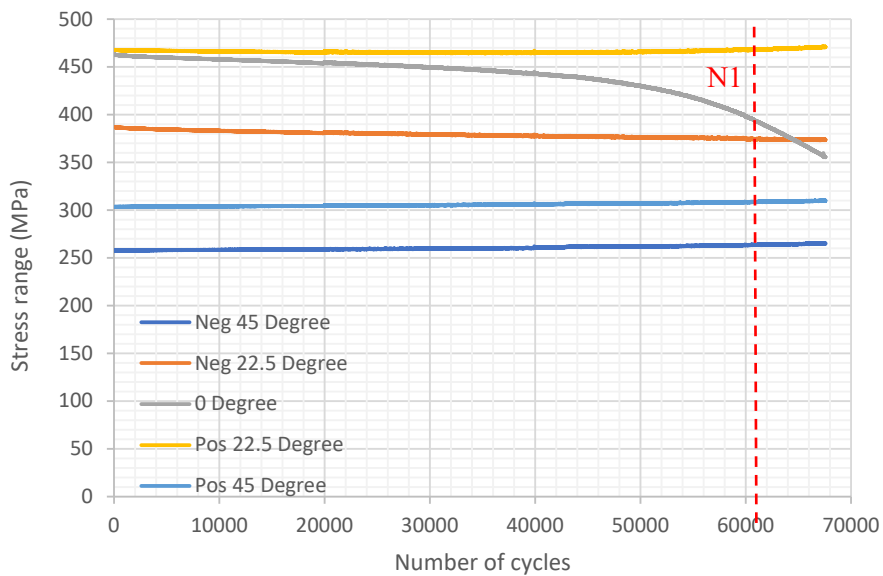


Figure 4-20: Change in hot-spot stress range during precracking of quadrant Q4, specimen DT3.

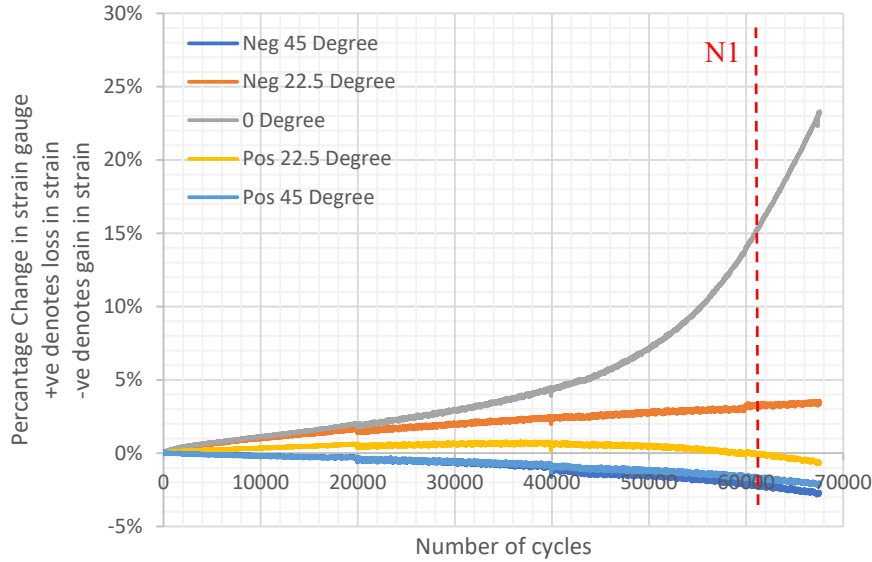


Figure 4-21: Strain evolution diagram during precracking of quadrant Q4, specimen DT3

## 4.5 Precracking of Specimen DT4

### 4.5.1 Test loading

Under the predetermined precracking load parameters of  $P_{max}$  at 60 kN and  $P_{min}$  at 10 kN, the specimen exhibited no indications of cracking up to 500,000 cycles, prompting the interruption of the test. To proceed with the precracking process, an increased precracking load was established, with a  $P_{max}$  of 72.5 kN and a  $P_{min}$  of 12.5 kN. The precracking results outlined in the following sections exclude the cycles endured before adjusting the precracking load. Throughout the testing phase, strain gauge readings and loading measurements were collected to determine SCFs, fatigue lives and crack propagation rates. The key parameters of the test DT1 loading is presented in Table 4-7.

Id	Pmax	Pmin	R	$\Delta\sigma_{nom}$ in brace
DT4 (runout)	60 kN	10 kN	0.17	17.65 MPa
DT4 extension	72.5 kN	12.5 kN	0.17	21.18 MPa

Table 4-7: Key parameters for DT4 test.

#### 4.5.2 Stress distribution in unrepaired joint

The strain gauges were glued to the chord and brace members to determine the stress distribution on the chord side and brace side saddles. The chord saddle strain gauges layout is shown in Figure 4-22.

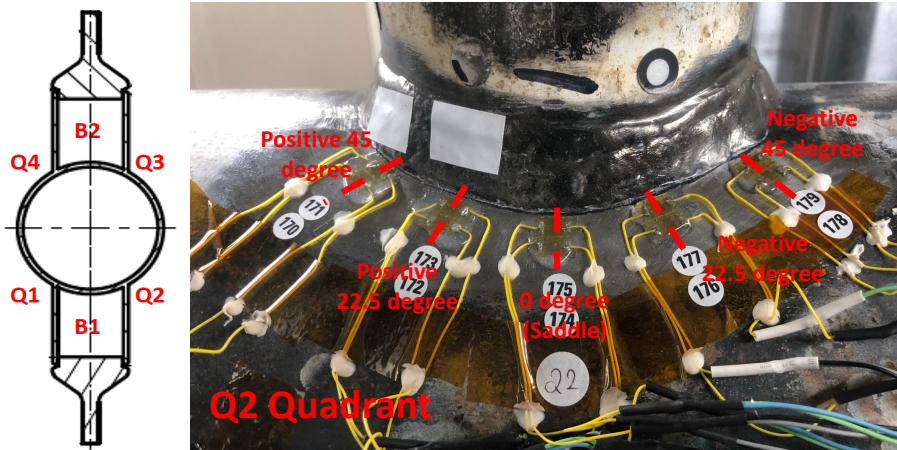


Figure 4-22: Strain gauge layout during precracking of quadrant 2, specimen DT4.

Under the first applied load cycles ( $P_{\max} = 60$  kN,  $P_{\min} = 10$  kN), the maximum hot-spot stress occurs in the chord saddle on quadrant Q2 while the minimum is on quadrant Q3. Figure 4-23 shows the hot-spot stress range variation along the Chord-brace intersection and chord side for all the quadrants on specimen DT4.



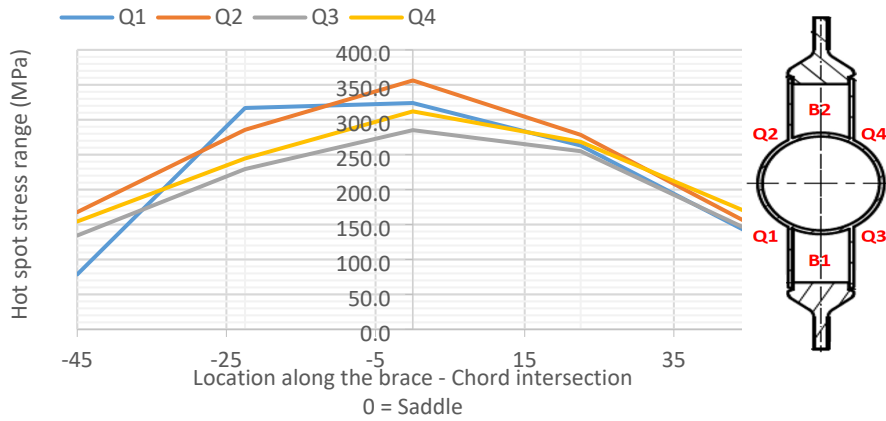


Figure 4-23: Measured hot-spot stress range along the chord-brace intersection and chord side for the four quadrants on specimen DT4. ( $P_{max} = 60$  kN,  $P_{min} = 10$  kN).

The adjusted precracking load parameters ( $P_{max} = 72.5$  kN,  $P_{min} = 12.5$  kN) and the hot-spot stress range variation along the chord-brace intersection on the chord side are illustrated in Figure 4-24. The peak hot-spot stress is observed in the chord saddle within quadrant Q2 (426.9 MPa), whereas the lowest value is found in quadrant Q3 (338.6 MPa).

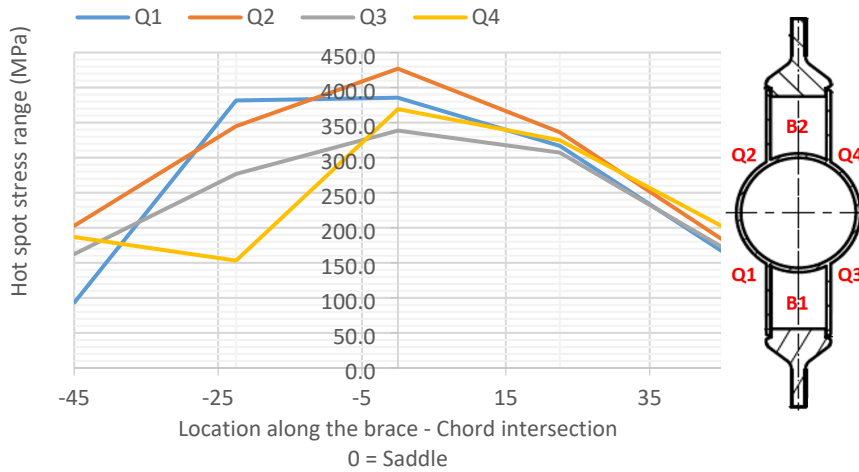


Figure 4-24: Measured hot-spot stress range along the chord-brace intersection and chord side for the four quadrants on specimen DT4 under the increased load ( $P_{max} = 72.5$  kN,  $P_{min} = 12.5$  kN).

Clamping the specimen in the fatigue rig reduces and eventually remove misalignment of the welded joint. Consequently a small bending moment is induced in the chord wall along the brace-chord intersection. The distribution of bending stress induced by clamping is shown in Figure 4-25. The maximum stress, amounting to 26 MPa, is attributable to clamping and occurs in quadrant Q3, while the minimum stress of -18 MPa is observed in quadrant Q1.

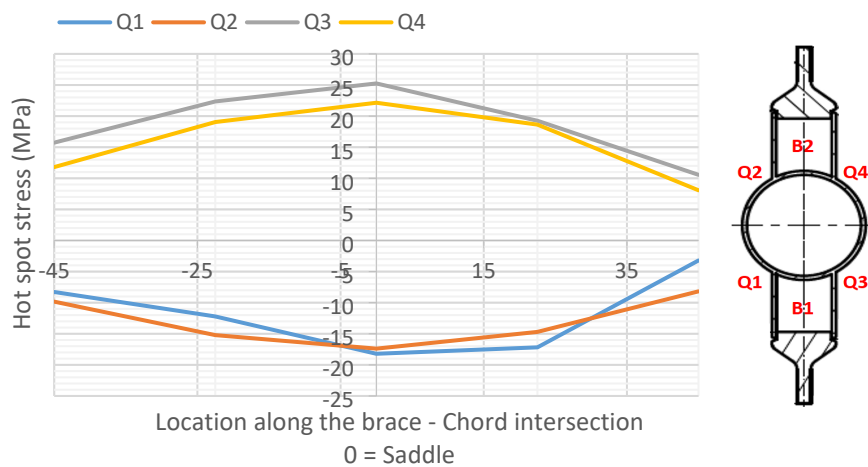


Figure 4-25: clamping induced hot-spot stresses at each quadrant of specimen DT4.

### 4.5.3 Results of fatigue test

Under the revised precracking load, specimen DT4 exhibited a through-thickness crack in quadrant Q1, with a crack length extending 80 mm. Additionally, a 40% through-thickness crack emerged in quadrant Q3, accompanied by a surface crack length of 75 mm. In contrast, quadrants Q2 and Q4 did not display any detectable crack development. Table 4-8 summarises the fatigue life of different stages during precracking for quadrants Q1 and Q3.

Specimen	Quad.	HSS range (MPa)	N1 x10 <sup>3</sup>	N2 x10 <sup>3</sup>	N3 x10 <sup>3</sup>
<b>DT4</b>	Q1	385	256	251*	443
	Q3	338	303	265*	-
<p>* N2 values are interpolated from crack propagation records.</p> <ul style="list-style-type: none"> <li>- N1 denotes a 15% drop in the measured hot-spot strain by linear extrapolation from two strain gauges placed perpendicular to the weld toe,</li> <li>- N2 denotes the formation of a 7.5 mm surface crack, and</li> <li>- N3 denotes the observation of 100% loss in the hot-spot stain reading or direct crack observation on the chord's internal surface</li> </ul>					

Table 4-8: specimen DT4 precracking fatigue life

### **Quadrant Q1**

The hot-spot stress range at the saddle within quadrant Q1 measured 385 MPa. At 256,000 cycles, a 15% reduction in the measured hot-spot strain was recorded, marking the beginning of N1 fatigue life. The crack initiated at the saddle's centre at 0° and progressively expanded towards both positive and negative 22.5° sectors.

The first visually detected crack on Q1 exhibited a surface length of 23 mm. Consequently, N2 fatigue life (corresponding to a 7.5 mm crack) was interpolated from the crack propagation records and estimated to occur at 251,000 cycles. At 443,000 cycles, the hot-spot stress range dropped completely, leading to through-thickness cracking in Q1. The specimen precracking was subsequently terminated.

The through-thickness crack length was estimated at 80 mm and was confined between the positive 45° and negative 45° sectors. Figure 4-26 illustrates the typical hot-spot stress range variation as a function of the number of cycles during specimen precracking, while Figure 4-27 presents the Q1 strain evolution diagram.

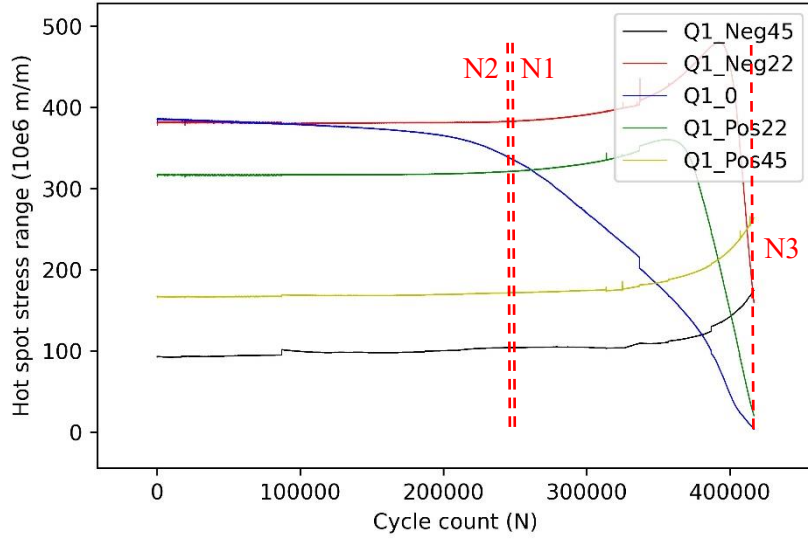


Figure 4-26: Change in hot-spot stress range during precracking of quadrant Q1, specimen DT4.

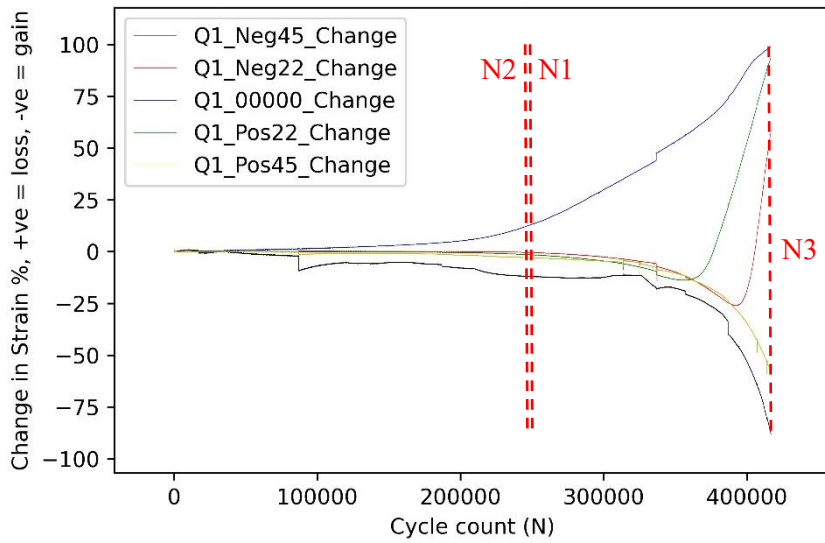


Figure 4-27: Strain evolution diagram during precracking of quadrant Q1, specimen DT4.

### Quadrant Q3

The hot-spot stress measured in quadrant Q1 was 338 MPa, representing the lowest stress at the centre of any saddle across the specimen. Nevertheless, quadrant Q3 exhibited the highest tensile stress due to misalignment. The N1 fatigue life was observed at 303,000 cycles, while the N2 fatigue life was interpolated to 265,000 cycles. Upon completion of the precracking stage at 443,000 cycles, a crack length of 75 mm was observed in Q3, confined between positive 45.0° and negative 45.0°. This crack demonstrated a partial penetration of 40% through the chord wall thickness. Figure 4-28 portrays the typical hot-spot stress range variation as a function of the number of cycles during specimen precracking, with the Q3 strain evolution diagram shown in Figure 4-29 The longitudinal progression of the leading crack in quadrant Q3 is presented in Figure 4-30 which also illustrates the crack length evolution during precracking of the primary crack developed in quadrant Q3.

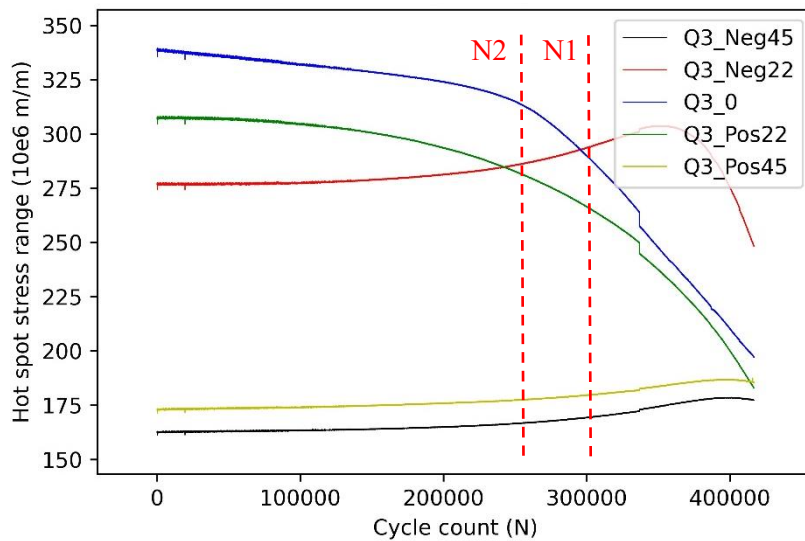


Figure 4-28: Change in hot-spot stress range during precracking of quadrant Q3, specimen DT4.

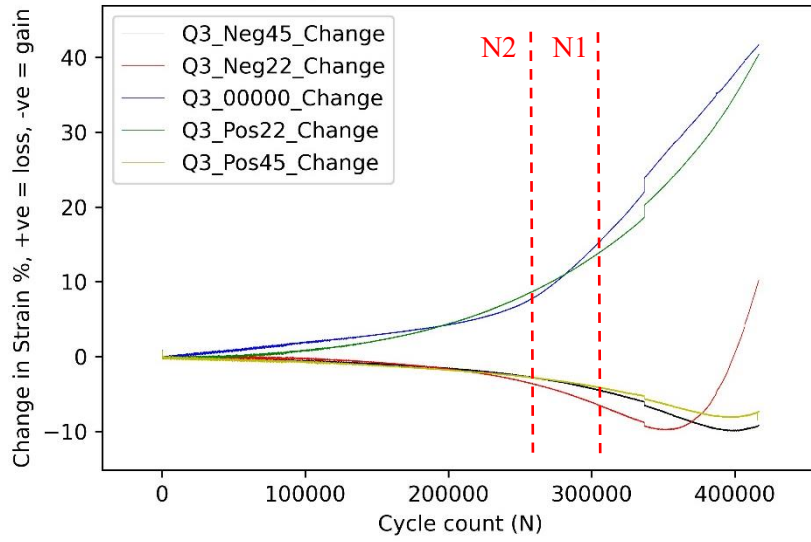


Figure 4-29: Strain evolution diagram during precracking of quadrant Q3, specimen DT4.

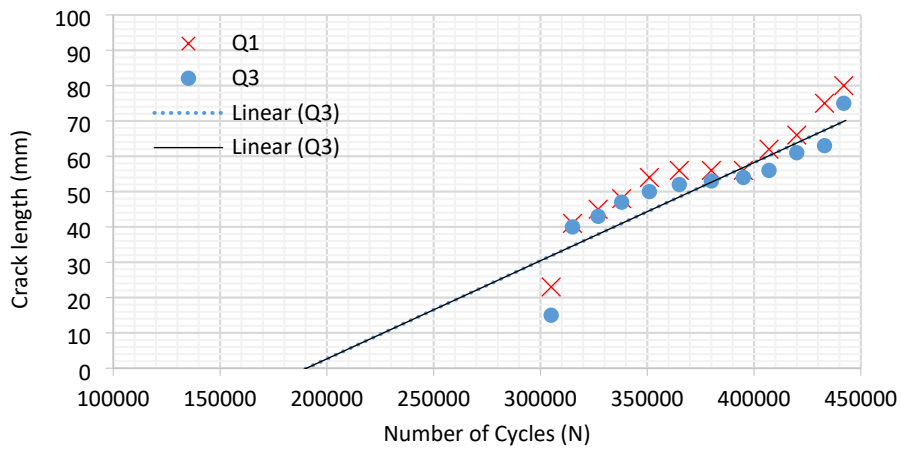


Figure 4-30: Crack length evolution during precracking of quadrants Q1 and Q3, specimen DT4.

## **4.6 Results of specimens precracking**

### **4.6.1 The fatigue life of control and precracking specimens**

The fatigue cracking behaviour exhibited by the four specimens discussed in this chapter demonstrated considerable similarities. Cracks typically initiated at or near one of the saddle points of the specimen, occasionally occurring simultaneously in two locations. Following crack initiation, surface cracks propagated circumferentially along the weld toe towards the crown.

As the surface crack extended a significant distance around the weld toe, crack depth at the centre increased, maintaining a ratio of 0.1 – 0.2 relative to the surface crack length. Upon penetration through the thickness, crack branching emerged in the control specimen DT1. Simultaneously, the surface crack propagation rate accelerated, potentially leading to rapid joint failure without repair. For specimens DT2-DT4 the test stopped at once the development of through-thickness crack.

Table 4-9 summarizes the fatigue life in terms of cycles from the control specimen and the pre-cracked ones. The hot-spot stress range is measured as the variation between HSS at  $P_{max}$  and HSS at  $P_{min}$ . Results are tabulated for three fatigue phases N1 to N3, while for the control specimen N4 is included.

No.	HSS (MPa)	N1 ( $\times 10^3$ )	N2 ( $\times 10^3$ )	N3 ( $\times 10^3$ )	N4 ( $\times 10^3$ )
1	275	316	380	632	820
2	248	466	430	613	-
3	697	31	-	68	-
4	385	256	235	443	-

Table 4-9: specimen's fatigue life

The fatigue testing and precracking performed within this work have an HSS range that falls within the HCF as well as the LCF regime of tubular joints. The fatigue life for the four specimens is indicated in Figure 4-31 together with the S-N curve from NORSOK N-006 [68] Figure 4-30 which covers the fatigue life of tubular joints in the LCF and HCF regimes.

The low cycle S-N curve in NORSOK N-006 [68] only provides a design curve. In order to establish an estimate of the mean curve, it was assumed that the standard deviation on the logA from the high cycle fatigue is applicable in the low cycle fatigue domain. The log A standard deviation considered as defined in OTH 92 390 [15].

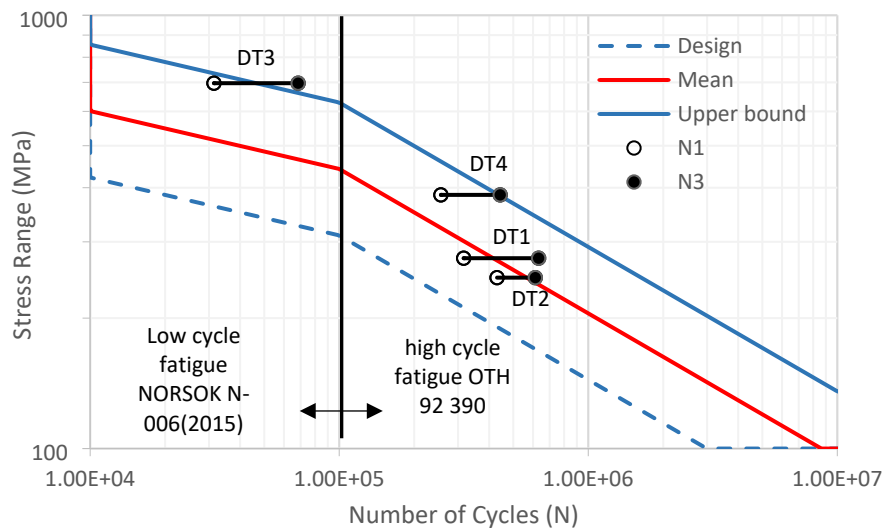


Figure 4-31: Sample S-N curve from the experimental testing of specimens and standard S-N curve according to NORSOK N-004 [67].

The fatigue life of the tested tubular joints is plotted against the hot-spot stress range, and an S-N curve is constructed following the same methodology as the OTH 92 390 [15] recommendations, as illustrated in Figure 4-32. The S-N curve parameters are provided in Table 4-10. S-N curves have been developed for N1 and N3 phases, with both curves exhibiting an inverse slope of  $m = 3$ . The N1 and N3 curves have intercept logA values of 12.93 and 13.30, respectively, along with standard deviations of 0.15 and 0.21.



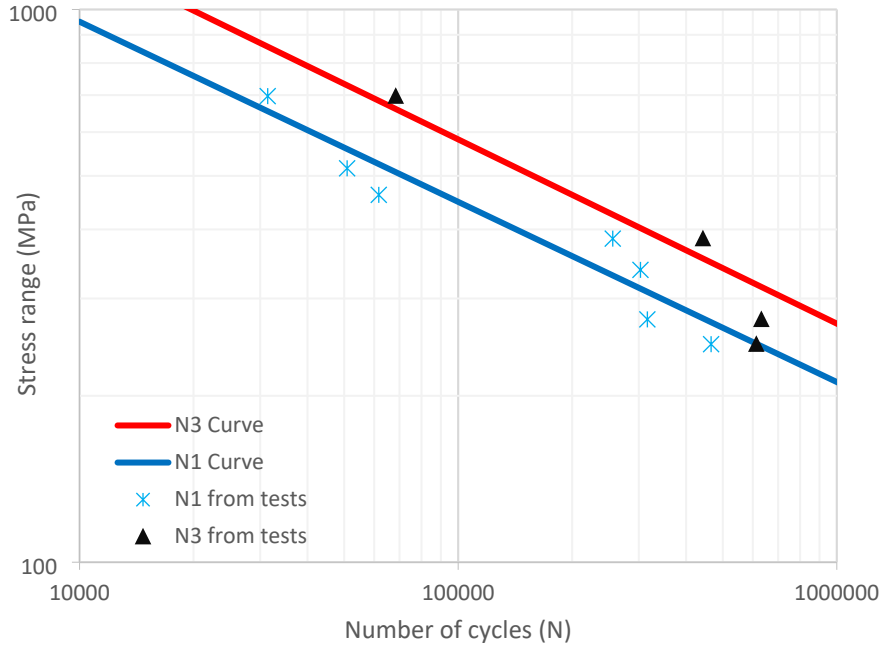


Figure 4-32: N1 and N3 S-N curves from the fatigue testing of specimens. The data include all the fatigue phases measured from all the quadrants on each specimen.

	Log A	m	SD
N1	12.93	3	0.147
N3	13.30	3	0.205

Table 4-10: Parameters of S-N curves developed from fatigue testing (N1 and N3)

The S-N curve estimated from the test sample (through-thickness cracking N3) is compared to the standard S-N curve of T-joint in Figure 4-33 for both mean and design strength. By comparing the SN curve estimated from the test sample to the standard SN curve, it is evident that the tested samples exhibit higher endurance for the same stress range. This discrepancy may be attributed to the significant data scatter present in the standard SN curves, as they represent multiple types of tubular joints and loading conditions.

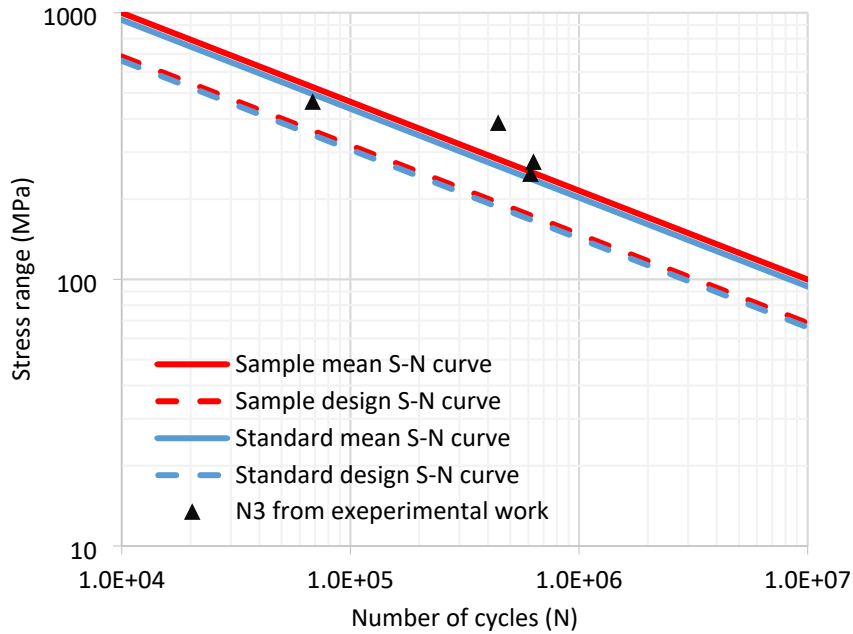


Figure 4-33: Sample S-N curve from the experimental testing of specimens and standard S-N curve according to NORSOK N-004 [67].

The fatigue cracking behaviour observed in the four specimens aligns well with expectations derived from earlier tests and the established SN curves. The consistency in crack initiation points, crack propagation rates, and the maintained ratio of crack depth to surface crack length across the specimens further validate these findings. By comparing the SN curve estimated from the test sample to the standard SN curve, it is evident that the tested samples exhibit higher endurance for the same stress range. This discrepancy may be attributed to the significant data scatter present in the standard SN curves, as they represent a variety of tubular joint types and loading conditions. Overall, the results of this study are in good agreement with prior testing and the SN curve models, setting the basis for these specimens to be used for further repair and post repair testing.

#### 4.6.2 Surface crack growth

In addition to the fatigue life measured during testing, surface crack lengths and, in some cases, depths were measured as cracking progressed. In general, cracks initiated at the weld toe on the chord side saddle (the location with the highest stress gradient) then grew around the brace/chord intersection following the weld toe.

Fatigue crack lengths and depths information for tubular joints has been published by Clayton [61] within the first phase of the UKOSRP joint-industry project, while Tweed later presented and discussed the crack length and depth information in the second phase of the UKOSRP [21-23]. Previous studies developed methods for estimating the remaining fatigue life of cracked tubular joints based on the surface crack length and crack depth. The work presented in this thesis is intended to be supplementary to the already existing database.

For specimen DT1, crack branching was observed close to the end of the test. For simplification, only the length of the lead crack has been presented in the data for the surface crack length ( $2c$ ) as a function of fatigue life ( $N$ ).

The surface crack length ( $2c$ ) and the number of cycles ( $N$ ) were normalised with respect to the cracked member thickness ( $t$ ) and the number of cycles to through-thickness cracking ( $N_3$ ), respectively. The data gathered from this work is presented in Figure 4-31 in normalised form. It is evident that there is a structure within the scatter. The upper and lower bounds to the majority of the data have been drawn in Figure 4-31.

- Upper bound  $\frac{2c}{t} = 12\left(\frac{N}{N_3}\right)^{-0.5}$

- Lower bound  $\frac{2c}{t} = 7\left(\frac{N}{N_3}\right)^4$

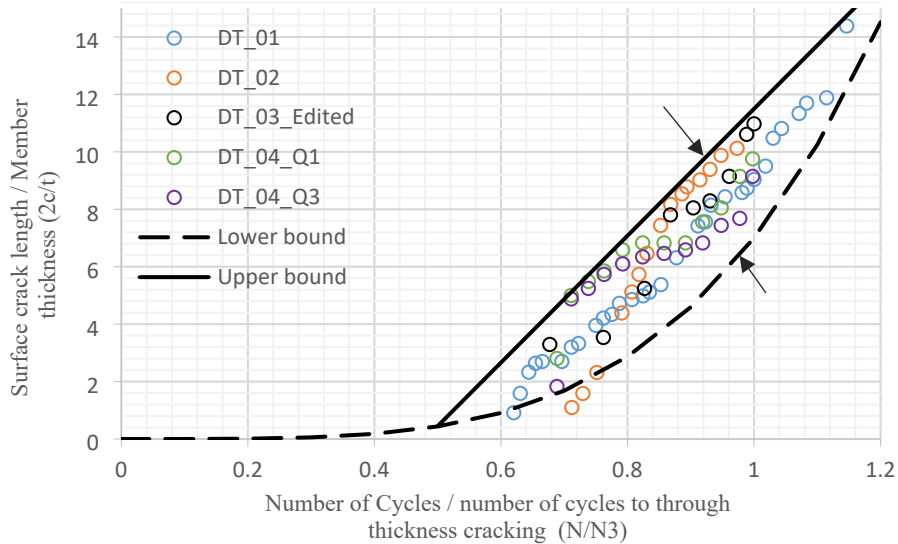


Figure 4-34: surface crack development in tubular joints fatigue tests

The data gathered from the tested samples with these drawn bounds permits a simplified estimate of the remaining life of tubular joints with a surface-breaking crack. For example: for a given tubular joint with known geometry and stress range,

1.  $N_3$  can be estimated from the S-N curve provided in Figure 4-31.
2. Substituting the crack length in the lower and upper bound drawn above provides a lower and upper bound elapsed fatigue life.
3. The percentage of the remaining fatigue life to through-thickness cracking with respect to  $N_3$  equals  $100\left(1 - \frac{N}{N_3}\right)$

### 4.6.3 Crack aspect ratio

The depth of the crack was monitored by applying a marker load of 200 cycles every 20,000 to 40,000 cycles during the fatigue testing of DT1, after reaching the first fatigue life  $N_1$ . The marker load had a peak load the same as the peak of the fatigue testing to ensure that the maximum crack opening was the same from both loads. A load ratio of 0.8 and a frequency of 1 Hz were applied to create a rib mark on the crack surface.

The rib marks were used during specimen fractography for estimating fatigue crack depth at each marker load cycle. Figure 4-35 and Figure 4-36 show the crack surface and its counterpart.

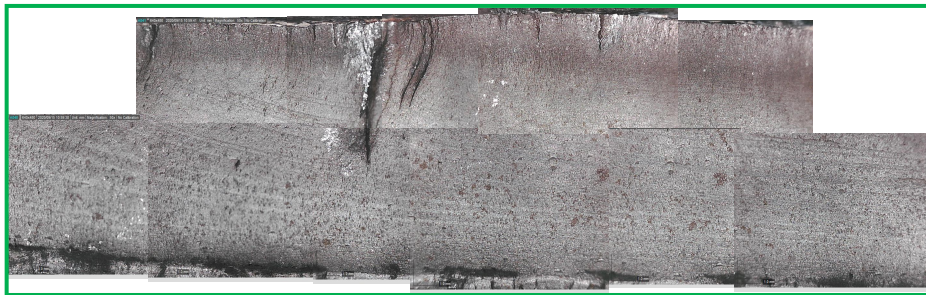
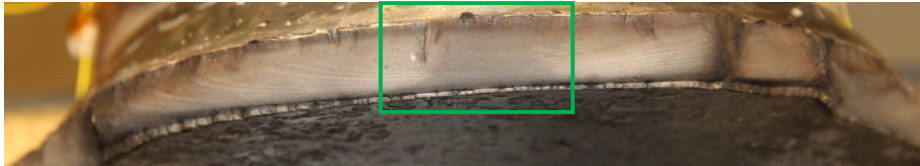


Figure 4-35: Brace/chord crack surface with rib marks, quadrant 1, Specimen DT1

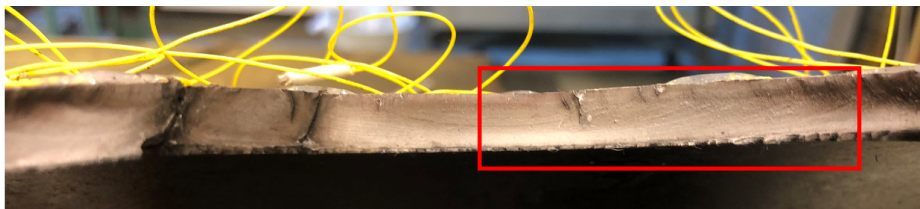


Figure 4-36: Brace/chord crack surface counterpart with rib marks, quadrant 1, Specimen DT1

The remaining life of cracked tubular joints may be estimated by assuming a linear relationship between the crack depth growth relative to the fatigue life.

Crack shape development gathered from the reference specimen DT1 show a good trend between the crack aspect ratio ( $a/2c$ ) and normalised fatigue life ( $N/N_3$ ), as shown in Figure 4-37 (a). The crack aspect ratio ( $a/2c$ ) was found to be approximately 1:5 at  $N/N_3 \sim 65\%$  while a ratio of 1:10 for  $N/N_3 = 100\%$ .

Additionally, normalised crack depth ( $a/t$ ) against fatigue life showed a linear relationship with zero intercepts, as shown in Figure 4-37 (b). It is clear that within the region of stable crack growth, a reasonable estimate of the remaining life of the tubular joint can be performed given the crack depth.

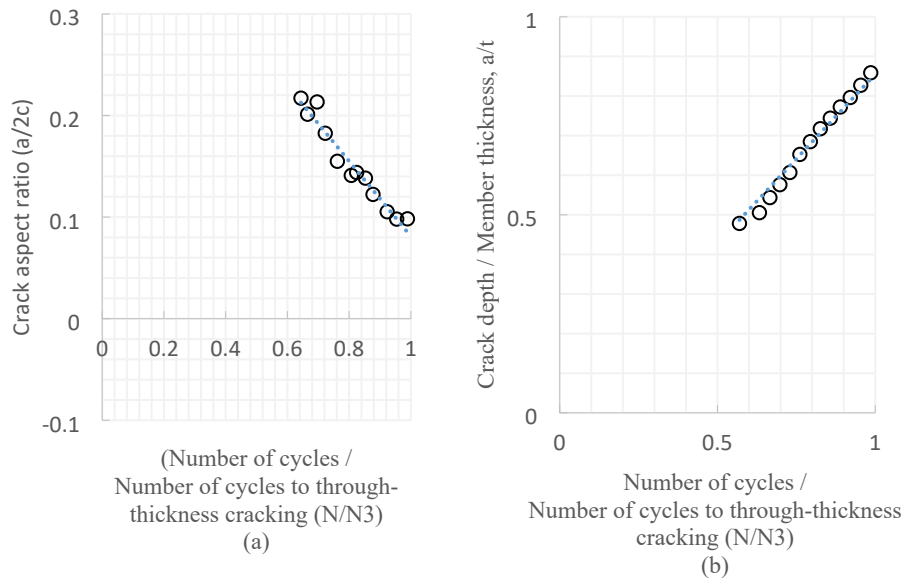


Figure 4-37: (a) Crack aspect ratio vs normalised endurance, (b) Normalised crack depth vs normalised endurance

In conclusion, the study conducted on the fatigue life of tubular joints, alongside the analysis of surface crack lengths and depths, has provided valuable insights that supplement the existing database on cracked tubular joint fatigue life and set the basis for specimen repair. The upper and lower bounds for the normalised surface crack length and the number of cycles has been established, allowing for a simplified estimation of the remaining life of tubular

joints with surface-breaking cracks. The standard crack aspect ratio used in many situations is 0.15 [62], which falls within the range of values observed in this study. The relationship between crack aspect ratio and normalised fatigue life, along with the normalised crack depth and fatigue life, demonstrates a clear structure within the scatter, which is promising for future analyses. Incorporating the crack aspect ratio as a function of  $N/N_3$  in a probabilistic analysis could be a feasible approach, and the curve developed in this work could be used as a guide. Overall, the findings from this research contribute to a better understanding of crack development in tubular joints and offer a simplified approach for estimating the remaining life of cracked tubular joints, which is crucial for the assessment, maintenance, and repair of these structures.





## **5 Stress concentration factors**

### **5.1 General**

Before commencing the fatigue testing of the tubular joints, stress concentration factors (SCFs) were determined under static loading conditions. The clamping stresses are carefully measured for each test to confirm the absence of substantial misalignments. Subsequently, the instrumentation measurements are reset to establish a baseline datum to isolate the stresses induced from the misalignment and SCFs measurement (deformation stresses), as described in Chapter 4.

This chapter explains the experimental quantification of SCFs and subsequently compares these findings with high-fidelity finite element analysis to validate the computational work against the experimental and empirical SCFs available in the literature. Additionally, the examination encompasses the investigation of statistical variations and uncertainties inherent in both experimental and finite element analysis (FEA) approaches. Factors such as the finite element modelling of the weld profile, mesh size, element type and the methodology employed for deriving the SCF are scrutinized.

### **5.2 Experimental Measurements**

#### **5.2.1 Results**

The experimental work presented herein followed second method as described in Section 2.3.2, for the SCF extrapolation from strain gauges. Due to the space limitation on the chord saddle, only linear strain gauges perpendicular to the weld toe were glued, and lateral strain gauges were omitted. The strains measured as-is from this layout is not sufficient to calculate the maximum principal stresses. A study by Lloyd's Register tested three ways of calculating the SCF from strain gauge results [63]:

- Extrapolation of maximum principal stresses.
- Extrapolation of the strains perpendicular to the weld toe.
- Conversion of the SNCF in method (b) to biaxial stress.

The study found that for 90° joints, the maximum principal stress estimated with method a) was approximately 15% larger than the directional stresses based on method b).

This study applies experimental strain measurements combined with FE analysis to estimate the principal stresses. The measured strains perpendicular to the weld toe are used to validate the FE analysis. Then, the FE analysis is used to determine the ratio between the principal stresses and the stresses perpendicular to the weld toe at all the measurement locations.

The FE analysis showed that the principal stresses at the saddle are 14.5% higher than the perpendicular stresses and increase slightly towards the crown, reaching 17.6% as shown in Table 5-1. The results are in line with the study by Lloyd's register, and hence this technique is used for estimating the principal stresses at all the strain gauge measurement locations. Details of the FE analysis are presented in Section 5.4.

<b>Location</b>	<b>0° - Saddle</b>	<b>22.5°</b>	<b>45°</b>	<b>90° - Crown</b>
Correction factor	14.7%	14.8%	15.2%	17.6%

Table 5-1: SCF correction factors from directional stresses to principal stresses

The SCFs from the experimental work were modified by correction factors as per Table 5-1 to be compatible with the parametric code equations (Efthymiou formulae [13]) and the SCFs extracted from FE models.

The distribution of hot spot SCFs along the circumference of the brace to chord intersection as measured by linear extrapolation of principal stresses for all the specimen tested is presented in Figure 5-1 where the distribution of estimated SCFs is presented with reference to each specimen at the respective angular positions while Table 5-2 present key statistics with mean values and standard deviation reported for each specimen with sample statistics for the complete measurements of hotspot SCFs. The distribution was plotted along the intersection with reference to an angular position from the saddle at 0° to the crown at 90°.

*Stress concentration factors*

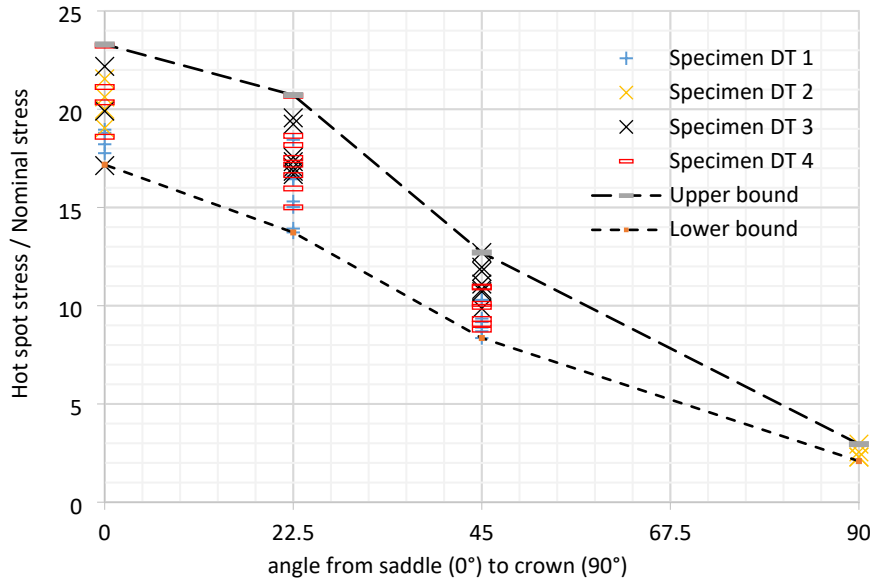


Figure 5-1: Experimental hotspot SCF along the weld toe from the saddle (0°) to the crown (90°)

Specimen	Location	Saddle	* 22.5°	45°	Crown
DT 1	Number of points	4	8	8	-
	SCF (mean)	18.43	15.74	9.27	-
	Std. dev.	0.55	1.57	0.69	-
DT 2	Number of points	4	-	-	4
	SCF (mean)	20.36	-	-	2.53
	Std. dev.	1.06	-	-	0.31
DT 3	Number of points	3	7	7	-
	SCF (mean)	19.79	17.78	11.27	-
	Standard deviation	2.54	1.17	0.94	-
DT 4	Number of points	4	8	7	-
	SCF (mean)	20.88	17.50	9.87	-
	Std. dev.	1.93	1.89	0.87	-
Entire sample (DT 1, DT 2, DT 3 and DT 4)	Number of points	15	23	22	4
	SCF (mean)	19.87	16.98	10.10	2.53
	Std. dev.	1.72	1.73	1.17	0.31
	Coeff. of variation	8.7%	10.2%	11.6%	12.2%

\* Angle measured from the chord saddle centre.

Table 5-2: SCFs from experimental work (present data)

The distribution of the SCF's at the saddle point from the experimental work fit reasonably well the normal distribution, as shown in Figure 5-2. By bootstrapping the data, it is indicated that the 90% confidence interval for the mean value of the SCF was [19.3, 20.6] and for the standard deviation [1.2, 2.1], providing a CoV in the range of 5–10%.

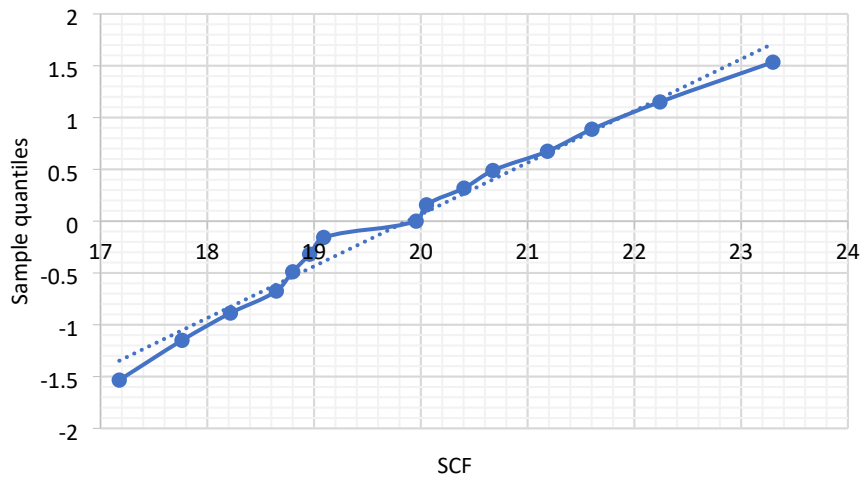


Figure 5-2: SCF at saddle from experimental work were plotted in a normal distribution paper, indicating a mean value of the SCF of 19.87 and a standard deviation of 2.

### 5.2.2 Review of the Accuracy of Experimental SCFs

The precision in the individual positions of the strain gauge's locations was studied at eight locations of the chord side saddle from two randomly selected specimens of a total of four. The variation between actual position and average strain gauge location is a useful indicator of the overall accuracy of the SCF for the specimen. The distance normal to the weld toe to the strain gauge's locations were measured to an accuracy of  $\pm 0.1$  mm, and then the measured points and their strain readings were used to extrapolate for the SCFs linearly.

The results show that the strain gauges at point "a" location were scattered without evidence of any systematic error. However, for the strain gauges at point "b", there is a scatter around a mean shift of 1.1 mm from the intended "b" location. The shift in mean value can be explained by the length of the strain

gauge carriers. The carrier's length was 5 mm, while the difference between points "a" and "b" was only 5.1 mm, making it challenging to position the strain gauges manually.

Table 5-4 shows the distribution of strain gauges along the weld toe's intended "a" and "b" locations and the extrapolation lines to the SCF value for each pair of points. After strain gauge installation, the average distance between "a" and "b" was approximately 6.3 mm.

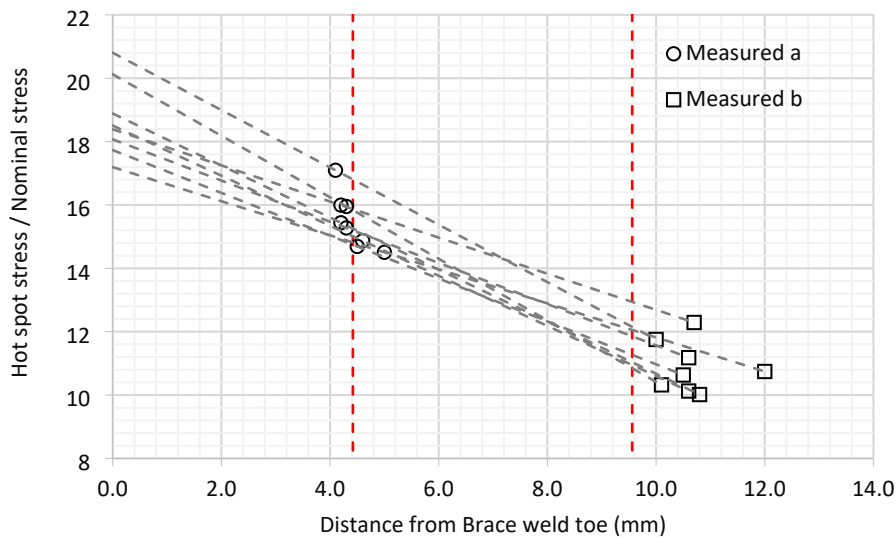


Figure 5-3: Experimentally measured SCFs sensitivity.

The average SCF measured at the chord saddle from these eight points was 18.71 with a standard deviation of 1.21, providing a CoV of 6.5%, while the uncorrected average for the same two specimens provides a mean SCF of 19.4 with a CoV of 8.4%. The difference between the mean value between these two samples can be assumed to be due to inaccuracy in the strain gauge locations, while the variation between the results from the eight points was a combination of other inherent uncertainty (geometry, material, measurement, etc.).

This implies that the shift in strain gauge location introduces a bias of 3.7% to the safe side, which can also easily be seen to be reasonable by a geometric evaluation. For the entire sample, the average SCF was found to be 19.87 with a standard deviation of 1.72 and CoV of 8.7%. To adjust for the strain gauge

location, assuming the same trend for the two remaining specimens as for the two tested, the mean value of the SCF should be set to  $19.87/1.037 = 19.16$  and a CoV of 8.4%.

In summary, it can be concluded from the obtained statistical coefficients that the average test values were in good agreement with the accurately measured values and the data can be treated as valid. The test data was further verified by correlation with the finite elements and available parametric formulae.

Subsequently, fatigue tests were carried out on the specimens used for the SCF estimation. The objective is to get the fatigue behaviour through joint life and to record the crack development. The specimens are tested in the air under constant amplitude axial cyclic loading.

### **5.3 Existing parametric formulae**

This section presents a set of formulae found in existing literature that offer estimations of SCF distributions along the brace-to-chord intersection. These formulae, derived from design SCFs and prior experimental work on DT joints, will be utilized for comparison with the experimental and finite element analyses conducted in this study.

Two parametric equations do exist to estimate the chord saddle SCFs of DT joints, namely, Wordsworth/Smedley (6) and Efthymiou (7).

$$SCF_{c(saddle)} = 1.7\beta\gamma\tau(2.42 - 2.28\beta^{2.2})\sin^{\beta^2(15-14.4\beta)}\theta \quad (6)$$

$$SCF_{c(saddle)} = 3.87\gamma\tau\beta(1.1 - \beta^{1.8})(\sin\theta)^{1.7} \quad (7)$$

Where  $\alpha = 2L/D$ ,  $\beta = d/D$ ,  $\gamma = D/2T$ , and  $\tau = t/T$ .

A comparison of the variation in the chord saddle SCF for  $\beta$  and  $\tau$  between the two sets of formulae are given in Figure and Figure . The expression of chord saddle from Efthymiou and Wordsworth/Smedley showed that both expressions have slight to no difference. Under constant  $\tau$ , Wordsworth and Smedley's expression show higher SCF by some 2% than Efthymiou for midrange  $\beta$  values while Efthymiou shows higher values than Wordsworth and

Smedley at  $\beta$  higher than 0.9. Under constant  $\beta$ , Wordsworth show higher values than Efthymiou by 3% for any  $\tau$  value.

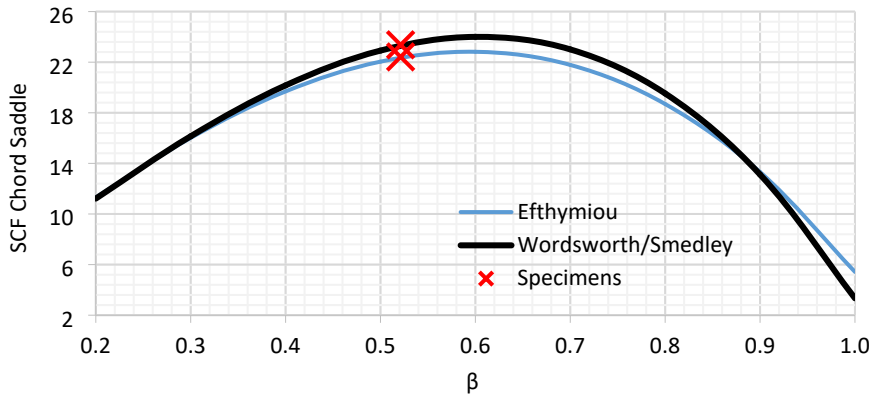


Figure 5-4: Axially loaded DT joints: chord SCF variation with  $\beta$  for a set of joint parameters ( $\theta, \gamma, \tau$ )

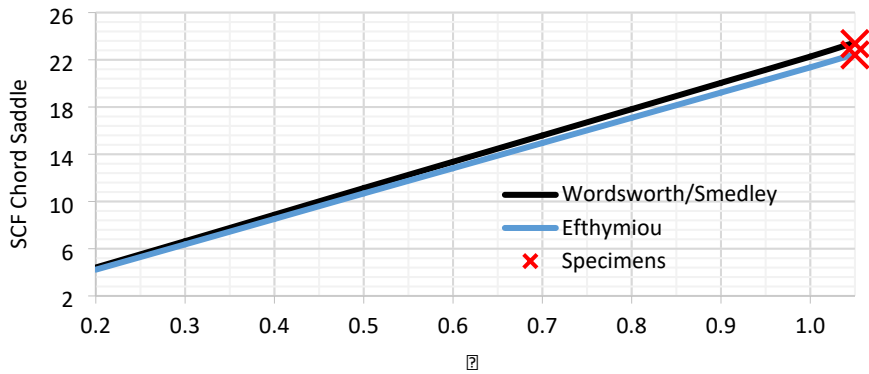


Figure 5-5: Axially loaded DT joints: chord SCF variation with  $\tau$  for a set of joint parameters ( $\theta, \gamma, \beta$ )

## 5.4 Finite Element Modelling

### 5.4.1 Specimen configuration and weld profile

The DT joint consists of a chord member of 219.1 mm diameter and 8.2 mm thickness with a brace on each side of 114.3 mm diameter and an 8.5 mm

thickness. The braces are connected to the chord through single-sided full penetration welds as shown in Figure 3-1.

The weld profile instructions specified to the fabricator were as shown in the weld details drawing below, Figure 5-6. The weld profile at the saddle was specified to be that of weld location 2, and the weld profile at the crown was specified to be that of weld location 1.

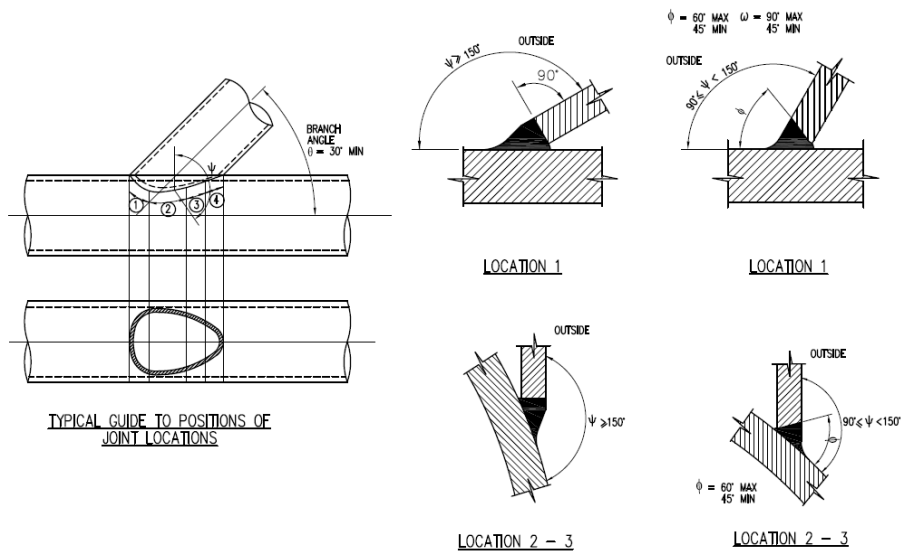


Figure 5-6: Weld profile specifications as issued to the fabricator for these tests in line with appropriate standards, Section 3.3.

A 3D scan of specimen DT1 is performed to be used as guidance of the as-built weld geometry. Furthermore, specimen DT1 was after the test cut into segments every  $20^\circ$  from the saddle to the crown so as to measure accurately the weld profile of each cross-section as shown in Figure 5-8. At the saddle, the brace was cut back to normal to the axis of the brace cylinder. At the crown, the parent material was assumed to be cut back to approximately  $45^\circ$  and then filled so that the intersection between the weld and the brace was at a right angle.





Figure 5-7: A 3D scanned of specimen to illustrate the weld between the brace and chord, brace and cone.

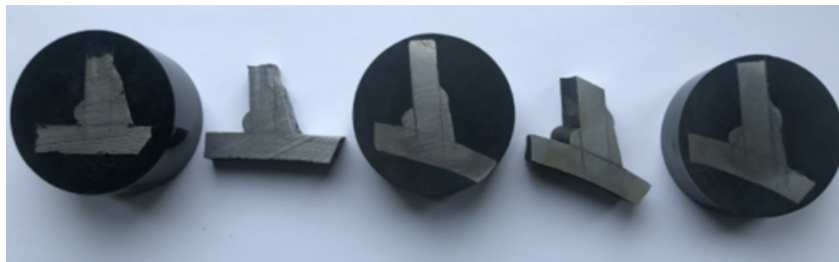


Figure 5-8: Actual weld profile cut from one of the specimens.

These measured weld profiles were used as the basis for the finite element modelling of the weld. The weld was modelled as a smooth transition interpolating elliptically from the profiles of the cut segments and those at the saddle and crown. The interpolation process was executed utilizing the loft function within the Abaqus software. This function shares a degree of similarity with the sweep function, which carries an object along a predetermined path without altering its original geometric attributes. Unlike the sweep function, the loft operation propels the object along a path whilst simultaneously adjusting its geometric configuration. This transformation initiates with one geometric form at the commencement of the path, and systematically morphs to a distinct geometry by the time the object reaches the end of the path.

In the FE models, the radii at the weld toe and weld root were omitted for simplicity. These radii were unlikely to affect the hot spot stress at the weld toe as this was derived by extrapolating the chord stresses from points sufficiently away from the weld toe.

#### **5.4.2 Finite element model description**

The 3D finite element model was developed using Dassault Systems Abaqus Version 2020. The DT tubular joint was modelled using first order C3D8R and second order C3D20R hexahedron elements for the joint stubs with a characteristic element size of 1 mm at the chord to brace intersection. This mesh size provided nine elements through-thickness of the chord at the weld toe.

The purpose of the FEA was to accurately compute the stresses at specific points of interest. These points of interest needed to be aligned with the elements' integration points, whether the direct extraction or the linear extrapolation method is selected. While this could have been done by using shell elements, shell elements are not recommended for complex geometries of varying thickness and where high local bending loads are applied to the surface of thick sections.

The alternative to shell elements is to use 3D solid elements. However, these do not have integration points on the element surface. A possible mitigation for solid elements is the use of dummy membrane elements on the surface that share the same surface nodes. This allows for extraction of the stresses at the integration points in the aligned membrane elements, rather than extrapolating the stresses to the surface of the solid elements. However, it is rather impractical and cumbersome to use such dummy membrane elements and align the integration points' locations with the points of stress extraction, and a finer mesh without such membrane elements is often a better solution. This will also result in nodal stresses closer to the stresses at the integration points.

A coarser representation of the outer extents of the tubular members was created using the same elements to a distance of approximately 40 mm from the weld (Figure 5-9). The cone and rod at the brace ends were modelled to ensure the loading applied represented that on the specimen as accurately as possible.

As the DT tubular joint was symmetric about each of the three principal planes, only one-eighth of the actual joint was modelled. Zero displacement boundary conditions were applied normal to the planes of symmetry to replicate the 3D behaviour. In the polar co-ordinate system about the axis of the braces, the saddles were at  $0^\circ$  and the crowns at  $90^\circ$ .

All materials (parent and weld) were assumed to behave linear elastically and to have a Young's modulus of 207 GPa and Poisson's ratio of 0.3. In order to generate the required SCFs, an axial tensile force was applied at the end of the rod extension to the cone model. This force was reacted by the zero-displacement boundary condition on the horizontal plane through the chord.

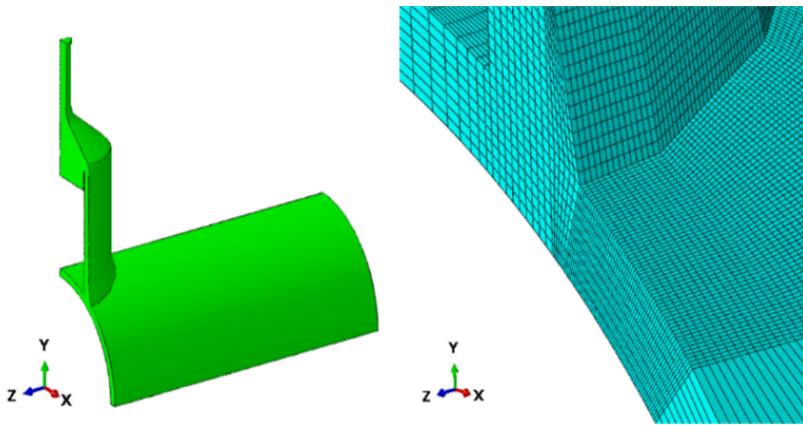


Figure 5-9: Model and mesh idealisation.

### 5.4.3 SCF Calculation Methodology

In the finite element analysis, the first method described in Section 2.3.2 would imply reading the von Mises stress at the Gaussian integration points within a perpendicular distance of between 2.2 mm and 6 mm from the weld toe. The second method would imply reading the maximum principal stresses at both 4.4 mm and 9.6 mm from the weld toe and using these to extrapolate to the weld toe.

In this work, the hot spot stress at weld toe was primarily determined using the second method (linear extrapolation) method. This was equivalent to the hot spot stress derived experimentally using strain gauge measurements. Hot spot

stresses determined from using the direct extraction method were also determined.

In the linear extrapolation method, the maximum principal stresses at each node on the path perpendicular to the weld toe were extrapolated from the unaveraged stresses at the integration points of the elements. These were used to interpolate to the stresses at point “a” and “b” (the points of interest). As an example, the extrapolation from the stresses at these two points to the hot spot stress at the weld toe at the saddle is shown in Figure 5-10.

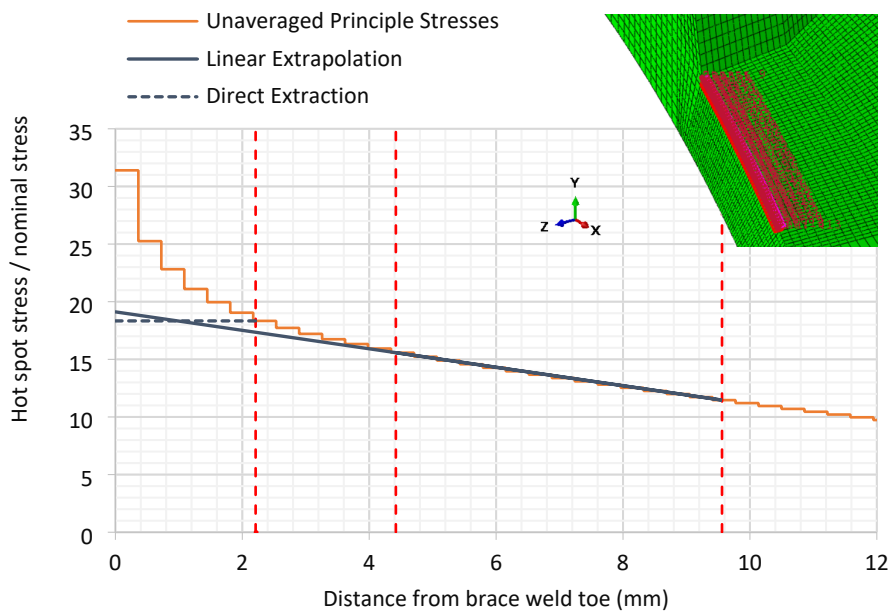


Figure 5-10: Direct and linear extrapolation of SCF from first-order 8-node brick elements.

The SCF at the weld toe was taken as the maximum absolute value of the linearly extrapolated maximum principal stresses divided by the nominal stress at this position without the stress concentration created by the weld toe. The SCFs at the weld toe were calculated at the saddle, 22.5° from the saddle, 45° from the saddle and at the crown positions. The SCFs at these positions determined using both the direct extraction and linear extrapolation methods were plotted as a function of the angle from the saddle.

#### 5.4.4 FE Verification and Validation

##### Mesh Convergence

The weld toe area is a mesh sensitive area as meshing with few elements will result in rapidly varying stresses. Hence, a fine mesh is required. A mesh convergence study was performed first to find the optimum number of elements required to provide reasonable numerical accuracy. The relative convergence method is the only way to confirm that the proper mesh is achieved. The method compares the results from subsequent models where the mesh is systematically refined. Two parameters of mesh refinement were considered in this analysis. The first is the characteristic element length and the second is the number of elements through-thickness. The study was performed for both first-order elements and second-order elements Table 5-3 and Table 5-4.

Description	Direct Extraction from $0.1\sqrt{rt}$				Linear Extrapolation			
	Location							
Element length	1.50	0.90	0.56	0.36	1.50	0.90	0.56	0.36
Elements through-thickness	4	4	6	9	4	4	6	9
Principal (unaveraged)	16.55	16.91	17.74	18.33	19.11	18.16	18.73	19.12

Table 5-3: Chord side saddle SCFs based on Mises and principal stresses for first-order elements.

Description	Direct Extraction from $0.1\sqrt{rt}$				Linear Extrapolation			
	Location							
Element length	1.50	0.90	0.56	0.36	1.50	0.90	0.56	0.36
Elements through-thickness	4	4	6	9	4	4	6	9
Principal (unaveraged)	20.55	20.58	20.55	20.30	21.14	21.17	21.17	21.03

Table 5-4: Chord side saddle SCFs based on Mises and principal stresses for second-order elements.

For the first-order elements using linear extrapolation 2% relative convergence was achieved in the SCF estimation from the unaveraged principal stresses at an element length of 0.36 mm with nine elements through-thickness. While for the second-order elements, 1.5 mm element length and four elements through-thickness were enough to achieve less than 1% relative convergence.

Reference points for extrapolation can be used as the averaged or unaveraged stress between element nodes. The finer the mesh, the closer the results from both averaged and unaveraged stresses will be. First-order elements with reduced integration points (1 point) at the most refined mesh showed a difference in the linearly extrapolated SCFs of 1.0% between the averaged and unaveraged principal stresses and 1.6% for the direct extraction method. While for second-order elements with reduced integration (8 points), the average and unaveraged stresses for both direct extraction and linear extrapolation showed less than 1% variation.

### **Results Verification and Validation**

Two types of elements were tested, first-order 8-node brick and second-order 20-node hexahedron elements. For the same mesh density of 0.36 mm element length, nine elements through-thickness in the vicinity of the weld toe, the circumferential variation of the calculated SCFs along the chord-side and the two SCF calculation methods are provided below in Figure 5-11 and Table 5-5. It can be shown that second-order elements consistently provided higher SCF than linear elements by 10% at the saddle location, then decreased circumferentially until there was no noticeable difference at the crown location. The direct extraction method fairly represented the linear extrapolation method for the SCF extraction. It was only short to the linear extrapolation method by 4% at the saddle location while higher by 4% at the crown location.

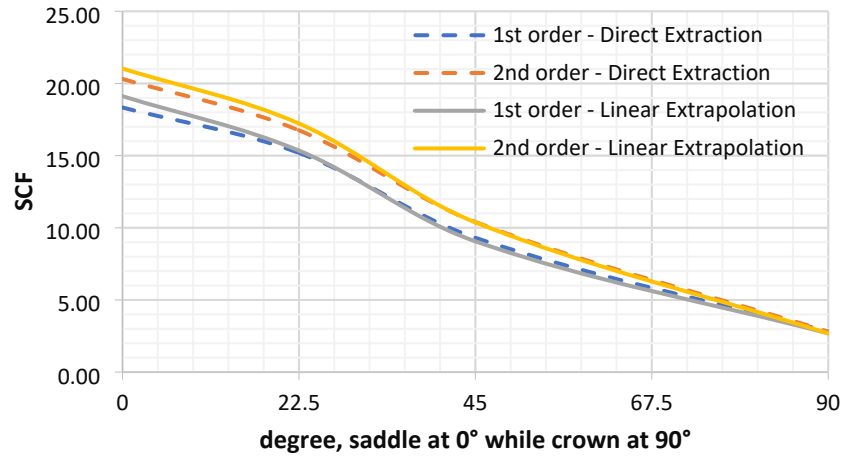


Figure 5-11: Direct and linear extrapolation of SCFs for first and second-order elements.

Location	FEA Direct Extraction from $0.1\sqrt{rt}$ Location		FEA Linear Extrapolation	
	First-order Element	Second-order Element	First-order Element	Second-order Element
0°—Saddle	18.33	20.31	19.12	21.03
22.5°	15.19	16.75	15.35	17.22
45°	9.31	10.4	9.06	10.38
90°—Crown	2.8	2.8	2.68	2.68

Table 5-5: Circumferential variation of extracted SCF by direct and linear extrapolation methods for first and second-order elements.

The results displayed can fairly represent the SCFs obtained from the experimental work, elaborated further in Table 5.8. The spectrum of recorded values ranged from a minimum of 18.3, procured from direct extraction from first-order elements to a maximum of 21.03, discerned through the employment of linear extrapolation on the stresses obtained from second-order elements. Figure 5-12 provides a comparative analysis between the experimentally measured SCFs and those derived from FE methods along the connection. The analysis spans from the saddle to the crown for both first order and second order (quadratic) elements, incorporating two considered methods, namely, direct extraction and linear extrapolation. Observations indicate that the first-order elements produced conservative results at the saddle points, only when

applying linear extrapolation, though with a slight underestimation when compared with the experimental results attained through the direct extrapolation method. Conversely, the second-order elements exhibited conservative results using both methods in comparison to the experimental data.

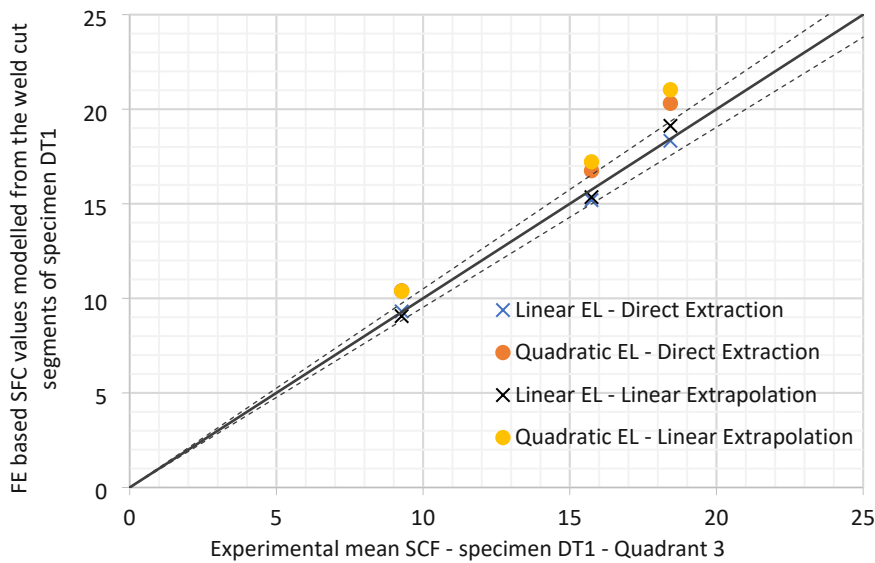


Figure 5-12: Experimental mean SCF with +/- N% bias values against FE SCF values.

### 5.4.5 Influence of Weld Profile Geometry

The variation in the SCF due to the weld profile modelling was investigated by modelling the tubular joints with an idealised “smallest” and “largest” accepted weld profiles and without the weld profile. The “smallest” accepted weld profile was the shortest acceptable weld leg length as per fabrication specifications and the “largest” was the most extended acceptable weld leg length as per fabrication specifications [18]. For the model without the weld profile, the stresses at “a” and “b” were measured from a fictitious weld toe location similar to the lower bound condition.

The weld profile can affect the local stresses in the joints in two ways. The first way is by the angle between the weld profile and chord surface as it affects the



notch stresses. The second is by changing the local stiffness of the intersection. The direct extraction method was affected by both the weld angle and weld size. In contrast, the linear extrapolation method should, in theory, not be affected by the weld profile angle, as the purpose of the methodology is to omit the notch stresses and capture only the deformation stresses.

It is not recommended to calculate the SCF using the direct extraction method for the FE model without the weld profile, as the effect of weld angle was missed. This model provides the highest SCF estimates using the linear extrapolation method since the sudden change in the angle between the brace and the chord formed a stress singularity.

The variation in the estimated SCF due to weld size (from lower bound to upper bound) was found to be less than 3.2% except for the direct extraction method from the first-order element where a variation of 9.8% was found.

The variation of the SCFs for models with different weld profiles was within the range of variation between different modelling techniques (18.3–21), Table 5-5 and Table 5-6. Only the model with no weld profile pushes the maximum estimated SCF at the saddle outside these values to an SCF of 22.2. Hence, it seems more reasonable to model the weld and it is recommended to model both the lower bound and the upper bound of the weld profile, as the weld could end up as any of these and use the highest SCF of these.

Weld profile	Direct Extraction from 0.1 $\sqrt{rt}$ Location		Linear Extrapolation	
	1st Order	2nd Order	1st Order	2nd Order
No Weld	-	-	20.2	22.2
Idealised smallest accepted weld profile	20.1	19.8	18.5	20.4
Idealised largest accepted weld profile	18.3	20.3	19.1	21.0

Table 5-6: SCFs for different weld profiles based on unaveraged principal stresses.

## 5.5 SCFs Comparison

A comparison between the estimated SCFs is given in Table 5-7 and Figure 5-13. These methods include:

1. Present experimental work.
2. Previous experimental work shown in section 2.3
3. Range of valid finite element analyses.
4. Efthymiou parametric formulae [64].

There is a good agreement between all the methods used to estimate the SCFs, where the Efthymiou equations form an upper bound.

Location	Present Experimental Work	Finite Element Analysis	Efthymiou	Previous Experimental Work
0° Saddle	19.9	18.3–21.0	22.4	18.9
22.5°	17.0	15.9–17.2	17.6	14.8
45°	10.1	9.1–10.4	12.8	10.8
90° Crown	2.5	2.7–2.8	3.2	2.7

Table 5-7: Correlation between FEA, present and previous experimental work and Efthymiou SCFs.

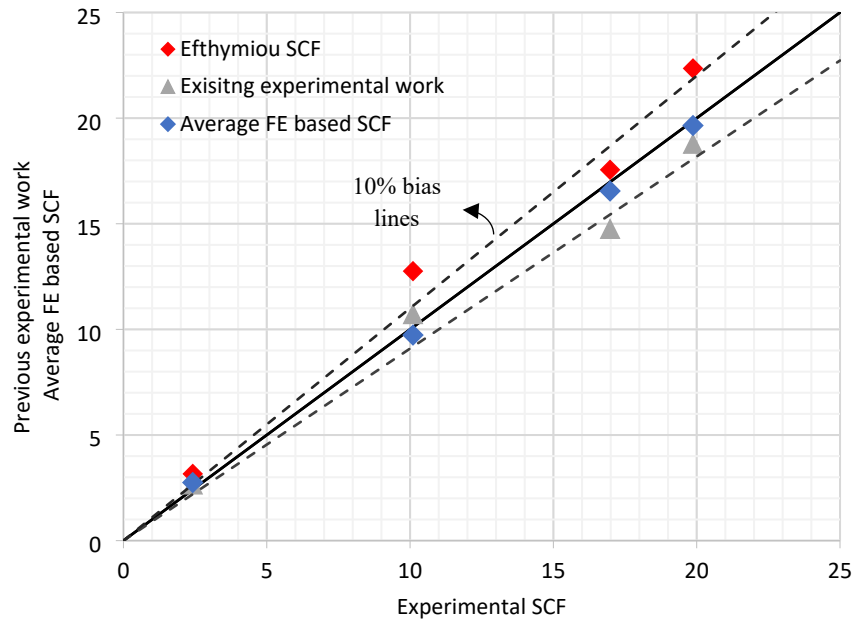


Figure 5-13: Present experimental mean SCF values against parametric Efthymiou, previous experimental work and FE based SCF values.

The FE based SCFs were from a model whose geometry matched the profile of the weld cut segments taken from the third quadrant of the first specimen. As shown in Table 5-5, the results varied with the modelling techniques. A comparison between the finite element based SCF and the experimental SCF of the same quadrant of same specimen is shown in Table 5-8 and

Figure 5-14. The experimental findings closely approached the lower bound SCF values for the finite element models across all measurements taken along the joint's circumference.

SCF	Saddle	22.5°	45°
Experimental mean	18.5	15.7	9.3
Finite Element analysis	18.3–21.0	15.9–17.2	9.1–10.4

Table 5-8: SCF based FEA compared to SCF from specimen DT 1—Quadrant 3 (corrected for location of “a” and “b”).

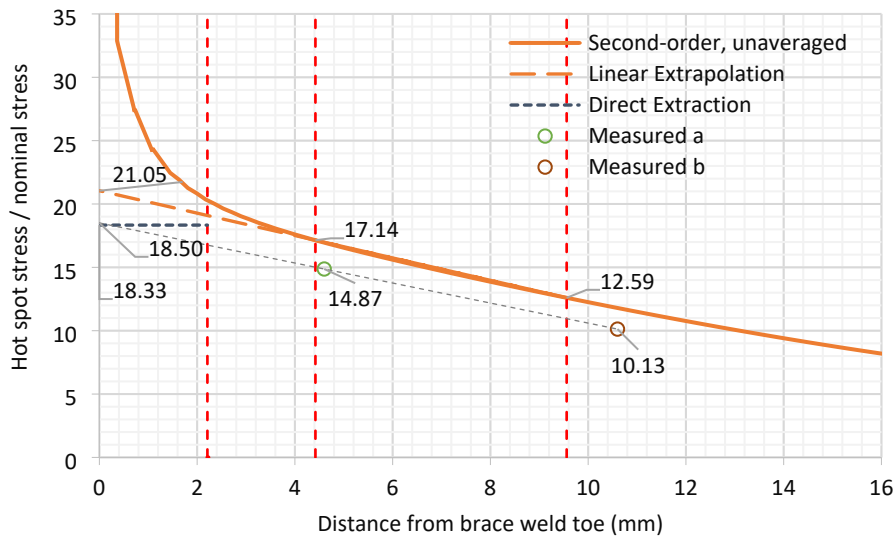


Figure 5-14: SCF based FEA compared to SCF from specimen DT 1—quadrant 3.

Estimation of SCFs by the aid of FEA was highly dependent on the user judgement. The SCFs values can change depending on the type of elements selected, mesh density and SCF extrapolation method. Four different SCF

estimation methods from the FEA are shown in this paper. It should be highlighted that all these models were valid as per codes and recommendations.

Even though all meshes provide reasonable convergence levels, a variation in the SCF estimation of 15% was found between these different methods. Such a variation in the SCF when applied to the S–N curve with an inverse slope of three will yield a variation in the fatigue life of 52%, even though all these methods are valid.

## **5.6 Summary and Conclusions**

Stress concentration factors for cruciform tubular joints of a chord and brace intersection (also called double T or X joints) were determined at different positions along the weld toe of the chord using detailed finite element analysis and from strain gauge measurements made during experimental testing of four representative joints. These SCFs were compared with SCFs determined from published parametric equations, including those by Wordsworth and Smedley and Efthymiou, the latter being the basis of those in the design codes ISO 19902 [7], API RP2A [8] and DNV-RP-C203 [6]. The intention of this study was to provide insight about the variations between SCFs from different methods so that users may take these into account when determining the fatigue life of the joint.

Detailed finite element analysis was undertaken to investigate the sensitivity of the SCF to:

1. The mesh density,
2. The choice of element type (1st order linear or 2nd order quadratic),
3. The method for deriving SCF, either using direct extraction at the  $0.1\sqrt{rt}$  location or from linear extrapolation of stresses to the weld toe,
4. The range of weld profiles allowed by standards such as API RP2A [8] and AWS D1.1 [18].

The results showed a variation of the SCF with mesh size with the SCF tending to increase with the fineness of the mesh down to an element size of 0.36 mm. The analyses of different weld profiles showed that the SCF based on the maximum weld profile (according to API RP2A [8]) was higher than that for

the minimum allowable weld profile, as the extra weld metal concentrates the loading of the chord at the weld toe. Using the finest mesh, the SCF at the saddle varied between:

1. 18.3 using 1st order linear elements, direct extraction and the idealised largest accepted weld profile and,
2. 21.0 using 2nd order quadratic elements, linear extrapolation and the idealised largest accepted weld profile.

The SCFs determined from strain gauge measurements at positions around the weld toes of the four nominally identical DT joints tested allowed the experimental variation of up to 16 nominally identical locations to be determined (i.e., four saddle points per joint). This database increased when SCFs at the crowns and two intermediate positions were calculated. From this the mean SCF, standard deviation and coefficient of variation (CoV) were determined at different positions of each joint and for the sample of four joints.

The mean experimental SCF at the saddle positions varied from 18.43 from specimen DT1 to 20.88 from specimen DT3, with an average SCF of 19.87 with a standard deviation of 1.72 and CoV of 8.7%. The variation can be seen to be small and enables a statistical bias for design purposes. Although not directly related, these CoV values are within the range (5–10%) that probabilistic codes, such as DNV-RP-C210 [6], assumes for SCFs derived from a detailed FE analysis.

For two randomly selected specimens, the locations of the strain gauges were measured with an accuracy of 0.1 mm, reducing the average SCF at the chord saddle from 19.4 to 18.71 (bias of 3.7%) and reducing the CoV from 8.4% to 6.5%. If the inaccuracy in the location of the strain gauges can be assumed to be systematic also for the remaining two specimens, the average SCF of these experiments can be assumed to be 19.16 with a CoV of 8.4%.

In a further development, when specimen DT1 was sectioned, it was found to correspond with the largest weld profile allowed by API RP2A [8]. This enabled a comparison to be made with the detailed finite element analysis of this profile. Here reasonable agreement was obtained between the SCF found using 2nd order quadratic elements with a fine mesh and linear extrapolation

(21.0) and the mean experimental SCF (19.9), providing a useful validation of the detailed finite element approach.

The SCF results of this study were then benchmarked against the standard empirical parametric equations used to calculate SCFs of tubular joints, including those by Wordsworth and Smedley and Efthymiou. These equations were themselves derived from experimental studies and finite element models and implemented in design codes such as ISO 19902 [7] and DNV-RP-C203 [6]. The use of the parametric equations was found to be well on the safe side and more detailed analysis could be beneficial if conducted using a fine mesh (e.g., 0.36 mm element) and 2nd order quadratic elements.

The following conclusions are therefore drawn from the study:

- SCFs determined using detailed finite element analysis were subject to variations depending on the mesh size, the choice of element type (linear or quadratic), the method for deriving the SCF (directly extracted or linearly extrapolated) and the weld profile modelled. In general, a higher SCF was obtained with a finer mesh, quadratic elements, linear extrapolation and a larger weld profile.
- The experimentally determined SCFs also show variations caused by the strain gauge positions and other inherent uncertainties. Comparison of the experimental SCFs with the SCF from detailed finite element analysis for a matching weld profile showed good agreement thereby validating the finite element approach.
- SCFs obtained from the parametric equations of Efthymiou [64] given in design codes ISO 19902 [7] and DNV-RP-C203 [6] were a reasonable upper bound to the variations in the values obtained by a detailed finite element analysis and experimentally in this study. These results provide continued support for the use of these equations in design. A detailed finite element analysis could be beneficial if small gains in the fatigue life need to be justified.

## **6 Fatigue performance of repairs**

### **6.1 Introduction**

A novel temporary repair method on tubular joints has been examined, where holes are drilled in the vicinity of the crack to deflect the crack away from the weld and then arrest the crack. Additional repair improvement methods to supplement the repair method has been used. These include drilled hole treatment by cold expansion, weld toe grinding and grooving. The fatigue performance of these repairs is presented in this section.

This chapter describes the fatigue testing of welded tubular joints in which fatigue cracks were repaired by hole drilling supplemented by drilled hole improvement by cold expansion, weld grinding and grooving. The principal objective is to study the performance of crack deflecting holes as a repair method.

### **6.2 Fatigue performance of repairs to specimen DT2**

#### **6.2.1 General**

As described in Chapter 4, specimen DT2 was pre-cracked to a through-thickness crack at quadrant 1 (Q1) while the other three quadrants remained intact. The surface crack extended unsymmetrically on Q1 from the centreline of the chord saddle, to 47° towards one side of the saddle and 28° towards the other side. The crack measured 83 mm in total. Crack tips were located by strain gauge readings during pre-cracking and confirmed with a hand-held digital microscope. Figure 4-7 shows the strain measurements set-up during precracking of Q1, specimen DT2.

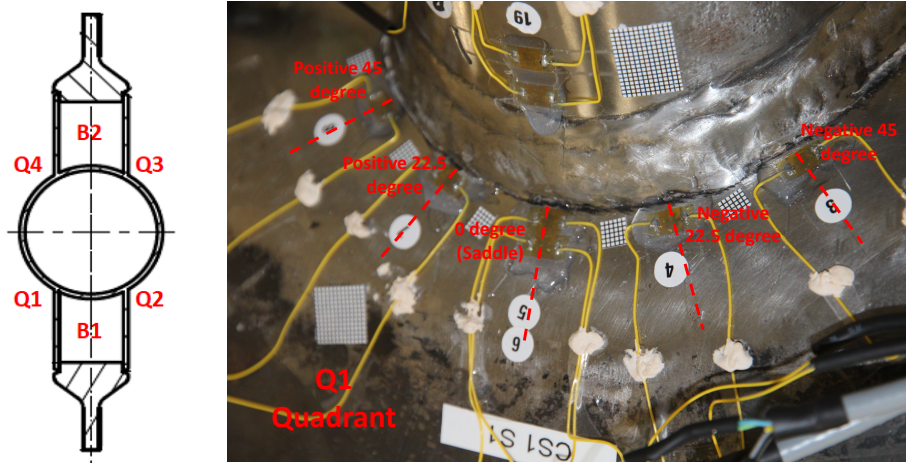


Figure 6-1: Strain measurements set up during precracking of quadrant 1, specimen 2.

After the precracking, the specimen was repaired by drilling crack deflecting holes treated by cold expansion and the fatigue test was continued, as shown in the following sections.

### 6.2.2 Specimen Repair

The specimen repair was performed by drilling two holes in the vicinity of the crack tips. The hole was centred at  $60^\circ$  on the side of the  $47^\circ$  crack-tip and at  $40^\circ$  towards the side of the  $28^\circ$  crack-tip. The drilled holes were shifted perpendicular to the weld-toe by 15 mm.

The holes were drilled using the magnetic-base drill shown in Figure 6-2. and the carbide twist bits of 18.1 mm diameter were used together with coolant mixed with oil to avoid overheating the hole surface during drilling. All hole edges were ground smooth to remove the burrs in the hole surface from the drill bit.



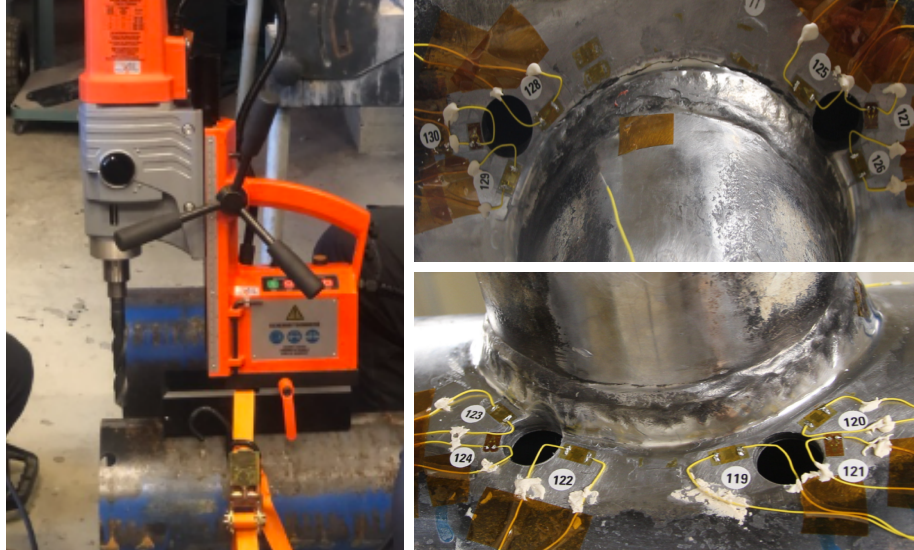


Figure 6-2: Hole drilling by Magnetic-base drill, Crack-deflecting holes and crack-tip holes.

The drilled holes were treated by cold expansion using the split sleeve process. The process is used to improve the fatigue life of drilled holes by inducing compressive residual stress at the hole circumference. An in-house tool was fabricated to perform the cold expansion treatment of the 18 mm diameter drilled hole. The tool consists of a mandril, split sleeve, support and helix nut, as shown in Figure 6-3. The split sleeve was placed over the mandrel, and the assembly was inserted into the hole. The mandrel with the larger diameter was then withdrawn through the split sleeve generating plastic deformations while retracted. Some elastic recovery takes place after the removal of the mandrel. The split sleeve was removed after the expansion process was complete.

The process successfully induced a compressive residual stress field around the holes. Both holes were plastically deformed with a permanent cold expansion of 0.1 mm increase in diameter. A summary of the repair performed on specimen DT2 is shown in Table 6-1.



Figure 6-3: Cold expansion process.

The specimen was re-gauged after repair. The strain gauges were used to measure the strains around the holes. Two strain gauges and a rosette were positioned around each hole, as shown in Figure 6-4.

- One of the strain gauges was positioned between the crack end and the hole. The first strain gauge (SG-103 and SG-107) aims to measure the strain change due to the cracking of the ligament between the crack tip and the drilled holes.
- The second strain gauge (SG-102 and SG-108) was placed on the crack-free side and used to detect if the original crack should continue past the drilled hole along the weld toe.
- The rosette (R1 and R2) was placed to detect any crack initiating at the backside of the hole.

Repair identification code	Crack deflecting hole	Crack-tip hole	Hole location from saddle	Cold Expansion
DT2_Q1_H1_D_L40_C	√	-	40°	√
DT2_Q1_H2_D_L60_C	√	-	60°	√
DT2_Q1_H3_D_L70	√	-	70°	
The repair methods investigated for specimen DT2: <ol style="list-style-type: none"> <li>1. Crack-deflecting holes, in addition to hole treatment by cold expansion</li> <li>2. Crack-deflecting holes without hole treatment by cold expansion</li> </ol>				

Table 6-1: Summary of repair performed on specimen DT2.

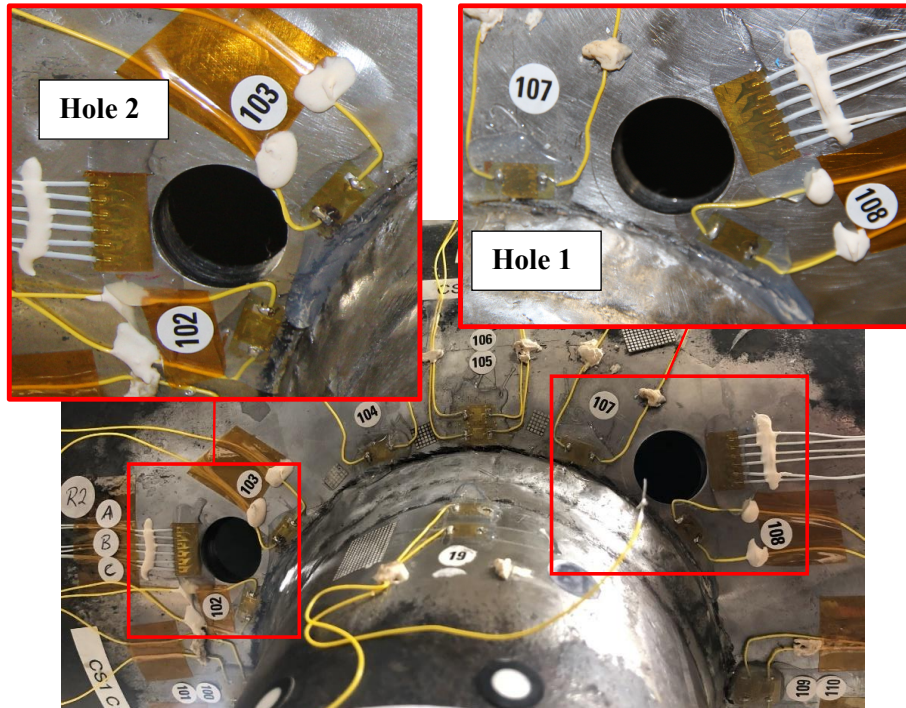


Figure 6-4: First repair attempt with two cold-expanded holes

### 6.2.3 Repair Performance

#### First repair attempt

The specimen was reloaded axially under constant amplitude loading with an R ratio of 0.17, a frequency of 3 Hz and a load range of 50 kN, the same loading recipe as with pre-cracking.

Upon reloading, the original crack started propagating towards the drilled deflecting hole, reaching hole 1 before hole 2. The path of the crack propagation indicated clear evidence that the deflecting holes altered the crack trajectory away from the weld toe, into the parent material and further into the deflecting holes, as shown in Figure 6-5.

A total of 16500 cycles were required for the crack to turn from a surface crack into a full through-thickness crack. The material was severed through the thickness from the outer surface to the inner surface of the chord.

An additional 47,500 cycles elapsed between the developed through-thickness crack into hole 1 and the formation of a *new crack*. Figure 6-6 shows the crack initiated at the weld-toe behind the drilled hole rather than initiating from the "backside".

A total of 64,000 cycles elapsed between the crack advancement into hole 1 and the appearance of the new crack.

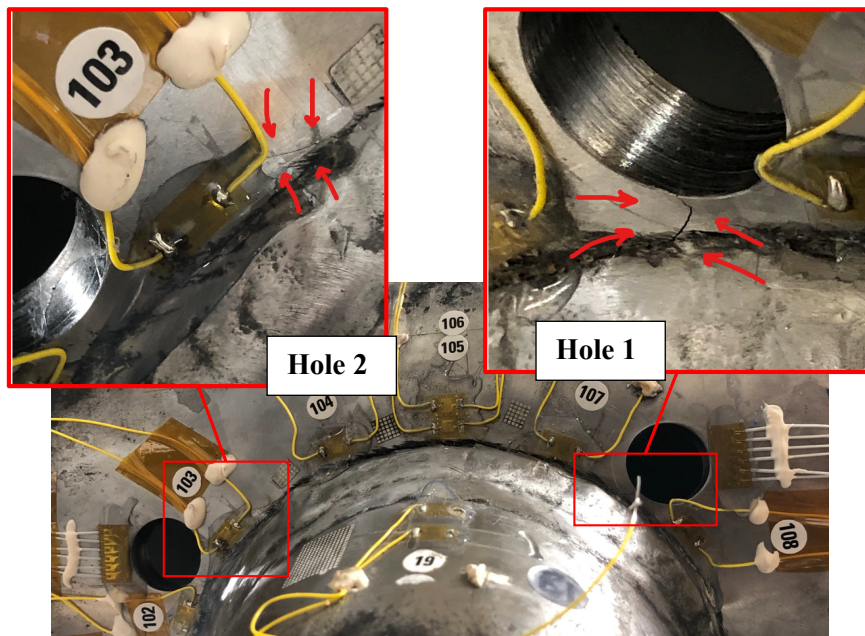


Figure 6-5: Deflection of the crack trajectory towards crack deflecting holes.

The crack was investigated further by polishing the area between the weld toe and hole 1 to aid in detecting whether this newly discovered crack and the original through-thickness crack were connected or not. A hand-held digital microscope was used, and it was found that the new crack was an isolated crack and not connected to the main crack or Hole 2. Testing was stopped at 101,524



cycles for further mitigation and a second repair attempt was performed, as shown in the next section.

A detailed sequence of events during the first repair attempt of DT2 is shown in Table 6-2 and the subsequent figures (Figure 6-7 and Figure 6-8).

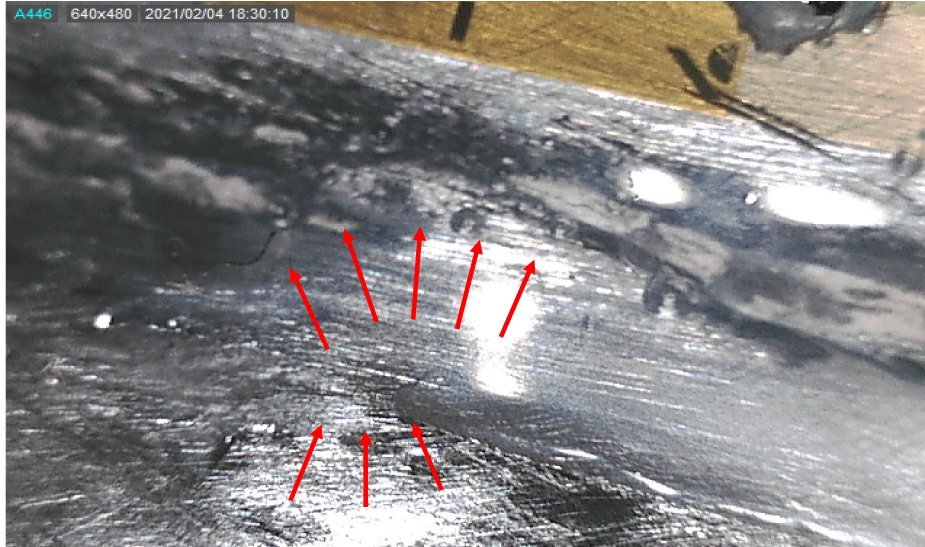


Figure 6-6: New crack detected between SG 108 and the weld toe behind hole 1

*Fatigue performance of repairs*

<b>Cycle count</b>	<b>Location</b>	<b>Remarks</b>
At the start of reloading	Ligaments between the crack-tip and drilled holes	SG 107 and SG 103 were the most strained areas showing a strain range of 1658 $\mu m/m$ and 938 $\mu m/m$ , equivalent to a stress range of 343 MPa and 194 MPa, respectively.
Early cycles	Hole 1	A steep drop in SG 107 readings was observed due to material severance in front of the strain gauge.
33,000	Hole 1	The crack propagated past SG 107 and advanced into hole 1. Complete severance of the material in front of SG 107 was visually observed and it was also evident because of the total loss of strain range reading. (at 11,000 seconds in Figure 6-7)
37,500 - 49,500	Hole 1	A steep increase in mean stress at SG 108. This clearly indicates the development of a through-thickness crack in hole 1.
50,000	Hole 2	The strain range reading kept increasing at SG 103 (Figure 6-8) and reached its peak of 1730 $\mu m/m$ (352 MPa)  A steep drop in strain readings was observed on SG 103 as a consequence of the crack advancing into hole 2 and the material between the precrack and hole 2 was severed, as shown in Figure 6-5 and Figure 6-8.
76,500	Hole 2	Through-thickness crack development (Figure 6-8)
90,000	Hole 1	SG 108 started to show a drop in the strain range as an indication of material degradation between SG 108 and the weld toe (Figure 6-7).
97,000	Hole 1	A drop of 15% in the strain range at SG 108 is observed compared to the highest accumulated strain range during the crack. This clearly indicates a new crack initiated between SG 108 and the weld toe beyond Hole 1 (Figure 6-7) and Figure (6)  Testing stopped for further mitigation of the specimen due to the unexpected crack initiation beyond the hole.

Table 6-2: Sequence of events of the first repair attempt on specimen DT2.

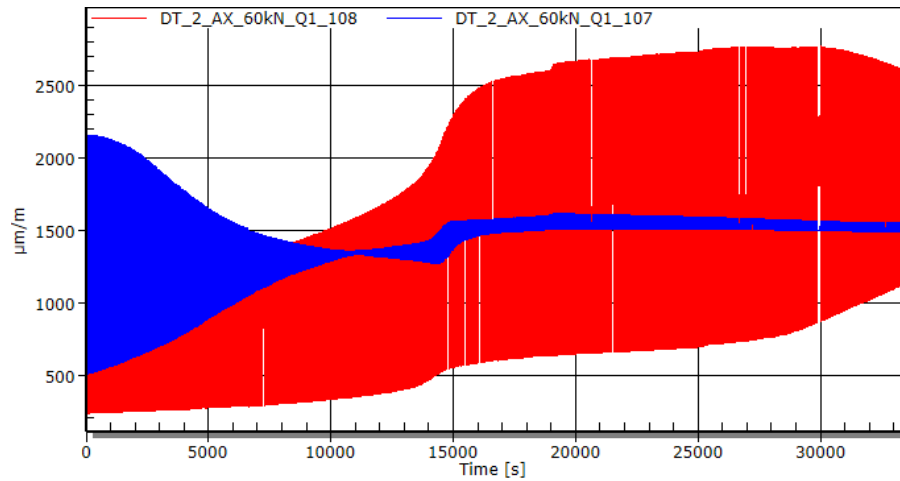


Figure 6-7: Strain evolution diagram for two strain gauges around Hole 1 (SG 107 - red colour) between the drilled hole and the crack end and (SG 102 – red colour) the strain gauge beyond the hole.

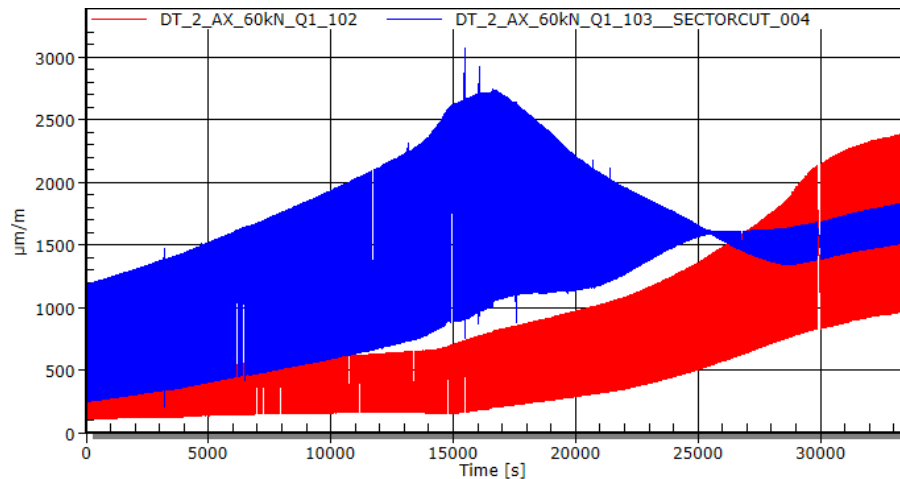


Figure 6-8: Strain evolution diagram for two strain gauges around Hole 2 (SG 103 - blue colour) between the drilled hole and the crack end and (SG 102 – red colour) the strain gauge beyond the hole.

### Second repair attempt

After discovering the new crack behind hole 1, another repair attempt was performed to investigate whether this behaviour was a coincidence or the behaviour would be repeated (it should be noted that the crack at this stage had not reached hole 2 yet). A new crack deflecting hole (hole 3) was drilled at  $70^\circ$

from the centre line of the chord saddle. The hole was left untreated (without cold expansion). A strain gauge SG 107 was placed behind Hole 3 to detect if any crack would initiate behind the newly drilled hole. The general arrangement of the second repair is shown in Figure 6-9.

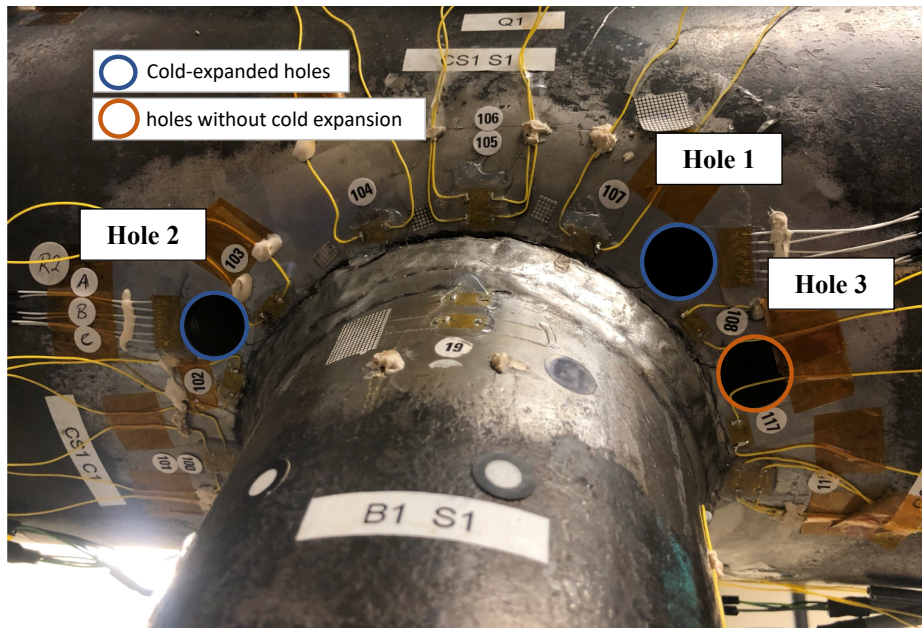


Figure 6-9: Second repair attempt, new crack deflecting hole (hole 3) drilled at 70°.

The specimen was reloaded again under the same loading condition as of precracking and the first repair attempt. The lives quoted after the second repair exclude the cycles applied during precracking but include the cycles elapsed during the first repair attempt unless noticed otherwise.

The crack propagated towards Hole 2, showing a similar behaviour as compared to the behaviour at Hole 1. After further cycling, both Hole 2 and Hole 3 showed crack initiation behind the holes, similar to the unexpected crack initiation behind Hole 1. This behaviour will be referred to as "reverse coalescence" in further discussion.

The specimen is then fatigue tested until complete failure by the formation of crack length equivalent to 1.5 the brace diameter. A detailed sequence of events during the second repair attempt of DT2 is shown in Table 6-2 and the



subsequent figures, Figure 6-7 and Figure 6-8. Finally, a summary of specimen DT2 fatigue stages after the repair is provided in Table 6-4.

<b>Cycle count</b>	<b>Location</b>	<b>Remarks</b>
Start	Hole 3	SG 108 was the most strained gauge, showing a strain range of 1647 $\mu m/m$ (341 MPa).
	Hole 3	The crack started propagating towards hole 3 and backwards towards hole 2. A steep drop in SG 108 readings was observed (Figure 6-10)
112,000	Hole 3	the crack propagated into hole 3
130,000	Hole 2	the crack propagated towards hole 2
135,000	Hole 3	SG 117 (Figure 6-11) showed a sudden increase in the mean stress. This clearly indicates that the crack developed from a surface crack to a through-thickness crack at hole 3.
144,000	Hole 2	SG 102 (Figure 6-11) showed a 15% drop in strain range, which is evidence of a new crack initiating behind hole 1.
153,000	Hole 3	A new crack was initiated behind hole 3, between SG 117 (Figure 6-11) and the weld toe. The drop in strain range observed is 15%.
160,000	Hole 2 and hole 3	The newly initiated cracks behind the holes entered the holes reversely.
181,000		The crack length reached 1.5 the brace diameter marking the end of fatigue testing of specimen DT2.

Table 6-3: Sequence of events of the first repair attempt on specimen DT2.

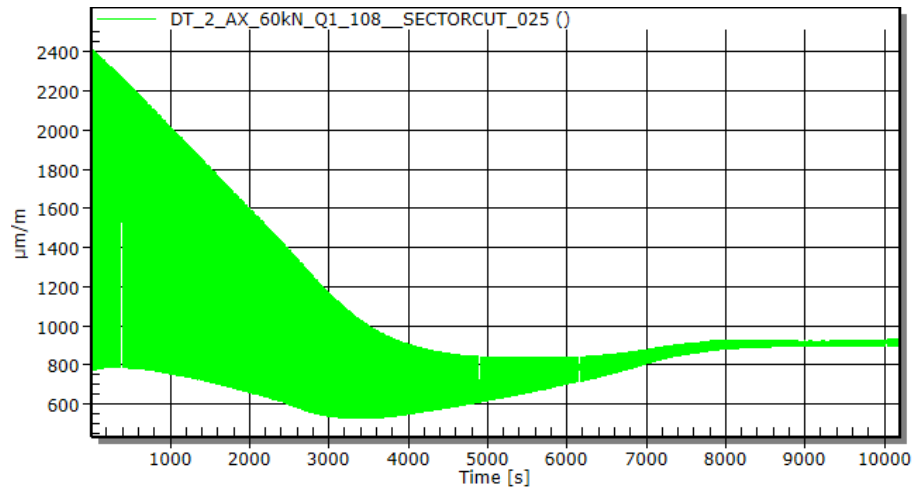


Figure 6-10: Strain evolution diagram for SG 108 between holes 1 and 3. The time-axis indicates, the time relative to the second repair attempt.

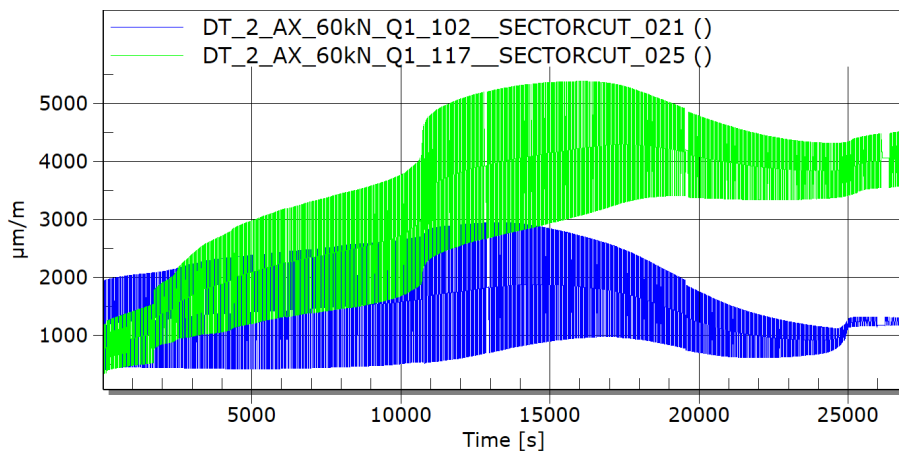
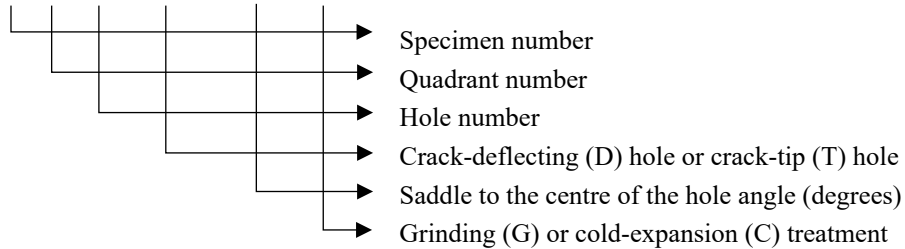


Figure 6-11: Strain evolution diagram for two strain gauges: SG 102 (blue colour) located behind hole 2 to the left-hand side (Figure 6-9). SG 117 (green colour) behind hole 3 to the right-hand side (Figure 6-9). The time-axis indicates time relative to the second repair attempt.

X#\_Q#\_H#\_(D\_or\_T)\_L#\_(G\_or\_C)



Quad.	Ni1 (x10 <sup>3</sup> )	Ni2 (x10 <sup>3</sup> )	N1* (x10 <sup>3</sup> )	N1* - Ni2 (x10 <sup>3</sup> )	N2* (x10 <sup>3</sup> )	N4* (x10 <sup>3</sup> )
DT2_Q1_H1_D_L40_C		33	97	64	130	181
DT2_Q1_H2_D_L60_C	50	76.5	151	38	160	181
DT2_Q1_H3_D_L70	112	135	153	18	160	181

fatigue stages definitions:  
 Ni1 when the lead crack enters the hole.  
 Ni2 when the lead crack is a through-thickness crack into the hole.  
 N1\* when a new crack is detected.  
 N2\* when the new crack enters the hole (reversely)  
 N4\* Stop of test.  
 \*\* end of the test

Table 6-4: Repaired specimen DT2 fatigue life

### 6.3 Fatigue performance of repairs to specimen DT3

#### 6.3.1 General

The tubular joint under investigation is specimen DT3 with the main features described in chapter 3. The specimen is fatigue tested up to precracking a through-thickness crack, as described in chapter 4. The specimen is then repaired using crack deflecting holes and crack tip holes, as described in the coming sections. The purpose is to compare the fatigue performance of the test-model with repairs using two different types of holes.

### 6.3.2 Specimen Repair

During the precracking of Specimen DT3, the specimen cracked at three quadrants Q2, Q3, and Q4. Quadrant Q3 developed a through-thickness crack with a surface crack length of 90 mm, while Q2 and Q4 developed crack lengths of 49 mm and 50 mm, respectively. Quadrants Q2 and Q3 were then repaired by two types of hole drilling with a fixed hole size of 18.1 mm. Crack-deflecting hole is performed on one side of the crack and a crack-tip hole on the other side of the crack. The two holes were drilled symmetric (mirrored) to the saddle centre. The areas behind the drilled holes are then ground to remove undetected surface cracks at the weld toe and enhance the weld profile behind the holes. Figure 6-12 and Figure 6-13 show the repair arrangement on quadrants Q2 and Q3, respectively.

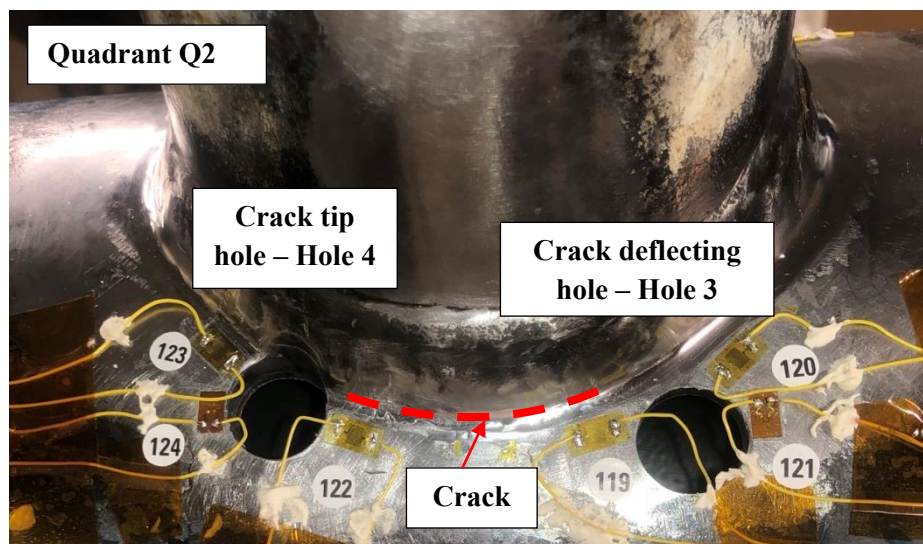


Figure 6-12: Quadrant Q2 repair, crack-tip hole on the left-hand side and crack deflecting hole on the right-hand side.

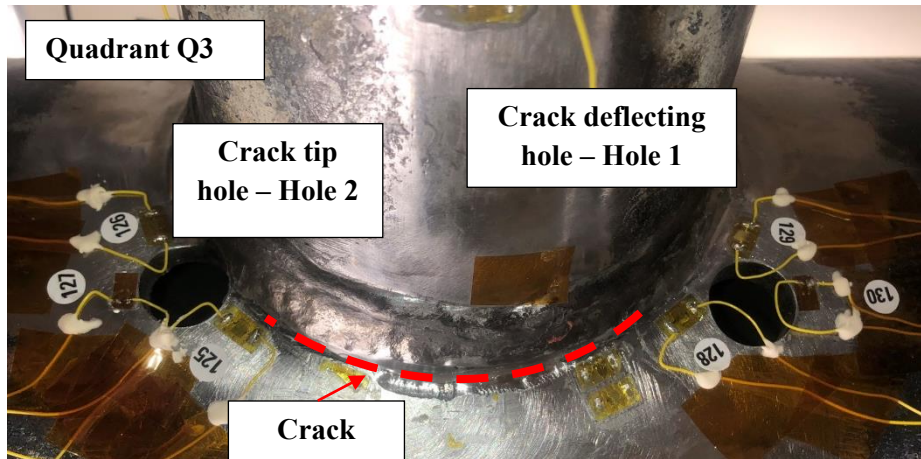


Figure 6-13: Quadrant Q3 repair, crack-tip hole on the left-hand side and crack deflecting hole on the right-hand side.

Quadrant Q4 was ground to remove the existing crack. The crack was 24% through the thickness of the chord. The weld toe of the Q4 quadrant was improved by grinding to avoid any premature specimen failure. Figure 6-14 shows the repair of Q4.



Figure 6-14: Quadrant Q4 repair: crack removal by grinding at the centre of the saddle and weld toe improvement by grinding all the quadrant.

The specimen was instrumented by strain gauges located before and after each drilled hole to monitor the crack propagation and any crack initiating from the hole or the weld toe. Another strain gauge is mounted close to the area with the highest SCF around the hole. A summary of the repair performed on specimen DT3 is shown in Table 6-5.

Repair identification code	Crack deflecting hole	Crack tip hole	Hole location from the saddle	Weld toe grinding	Comments
DT3_Q3_H3_D_L53_G	√		53°	√	Main crack
DT3_Q3_H4_T_L53_G		√	53°	√	Main crack
DT3_Q2_H1_D_L20_G	√		20°	√	Secondary crack
DT3_Q2_H2_T_L20_G		√	20°	√	Secondary crack
DT3_Q4_G				√	Secondary crack
The repair methods investigated for specimen DT3: 3. Crack-deflecting holes in addition to weld improvement by grinding behind the hole. 4. Crack-tip holes, in addition to weld improvement by grinding behind the hole.					

Table 6-5: Summary of repair performed on specimen DT3.

### 6.3.3 Repair Performance

The specimen was reloaded axially under constant amplitude loading with an  $R = 0.17$ , a frequency of 3 Hz and a load range of 50 kN. The maximum load is  $P_{\max} = 60$  kN and the minimum is  $P_{\min} = 10$  kN. The sequence of events while testing the repaired specimen is summarised as shown in the following sections. The cycle count quoted after repair excludes the cycles applied during precracking.

#### *Fatigue performance of crack deflecting hole on quadrant Q3*

A detailed sequence of events of the fatigue performance of the crack deflecting hole on quadrant Q3 is shown in Table 6-6. Figure 6-15 and Figure 6-16 summarize the evolution of stress range and change in strain gauge readings.

*Fatigue performance of repairs*

Cycle count	Location	Remarks
start		As the crack propagated toward the hole, the stress range increased for all the strain gauges mounted around the deflecting hole.
0 - 47,100	Hole 1	Increase in the stress range of SG 128 The crack started propagating gradually along the weld toe towards the crack deflecting hole.
47,100	Hole 1	A drop in stress range level at SG 128 indicates that the crack is propagating between the strain gauge and weld toe penetrating the hole.
55,000	Hole 1	Massive drop in stress range reading at SG 128 indicating complete severance of the material between the strain gauge and weld toe because of the development of the crack through thickness and complete break out of the hole.
92,000	Hole 1	15% drop in strain gauge SG129 reading indicating crack initiation beyond the hole.
154,000		End of fatigue testing of specimen DT3

Table 6-6: Sequence of the crack deflecting hole events on Q3 during the fatigue testing of the repaired specimen DT3.

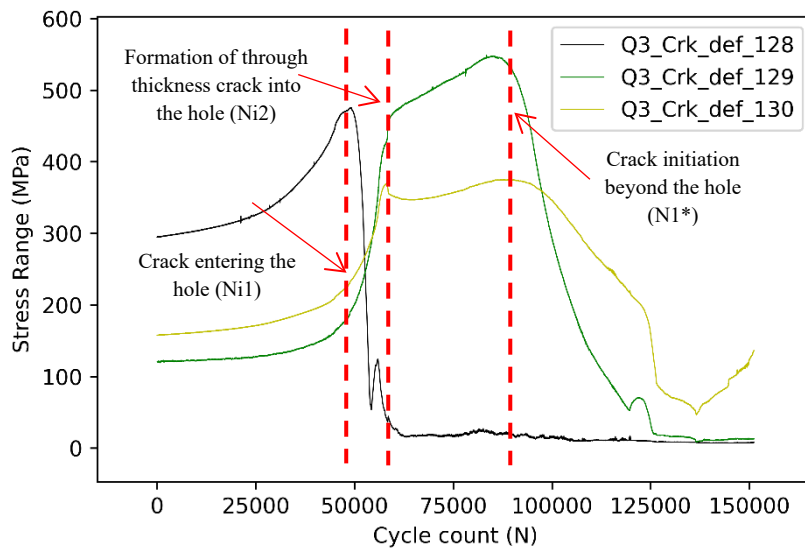


Figure 6-15: Stress range evolution diagram for the strain gauges around the crack deflecting hole on quadrant Q3.

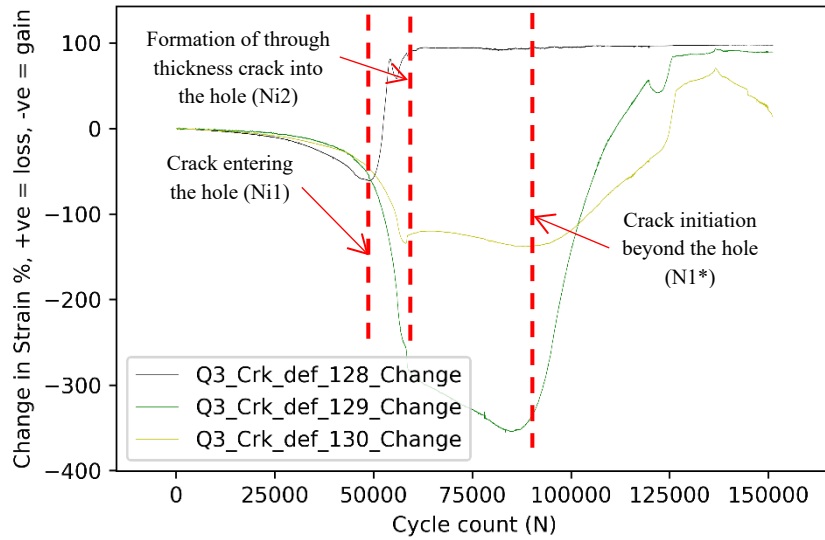


Figure 6-16: Percentage change in strain range around the crack deflecting hole on quadrant Q3.

Figure 6-17 shows the crack development into the hole with the formation of a new crack beyond the hole. Similar behaviour to the "reverse coalescence" was discovered beyond the crack deflecting holes from specimen DT2.

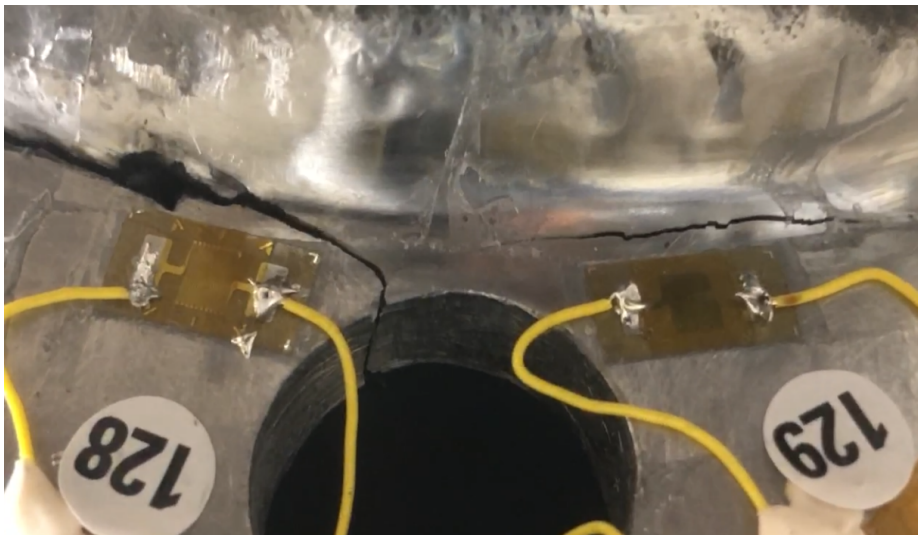


Figure 6-17: Crack evolution at the crack deflecting hole on quadrant Q3, at 100,000 cycles.



*Fatigue performance of crack tip hole on quadrant Q3*

The sequence of events of the fatigue performance of the crack tip hole on quadrant Q3 is shown in Table 6-6, while Figure 6-18 and Figure 6-19 summarize the evolution of stress range and change in strain gauge readings around the crack tip hole on quadrant Q3. Figure 6-20 shows the crack development into the hole and then the crack breaking out.

Cycle count	Location	Remarks
start		The stress range increased for all the strain gauges mounted around the crack tip hole.
33,300	Hole 2	Complete loss of strain reading on SG125, indicating a severance of the material between SG 125 and the weld toe and the formation of a through-thickness crack into the crack tip hole.
61,500	Hole 2	15% drop in strain gauge reading of SG126 indicating crack initiation beyond the hole.
154,000	Hole 2	End of fatigue testing of specimen DT3

Table 6-7: Sequence of the crack tip hole events on Q3 during the fatigue testing of the repaired specimen DT3.

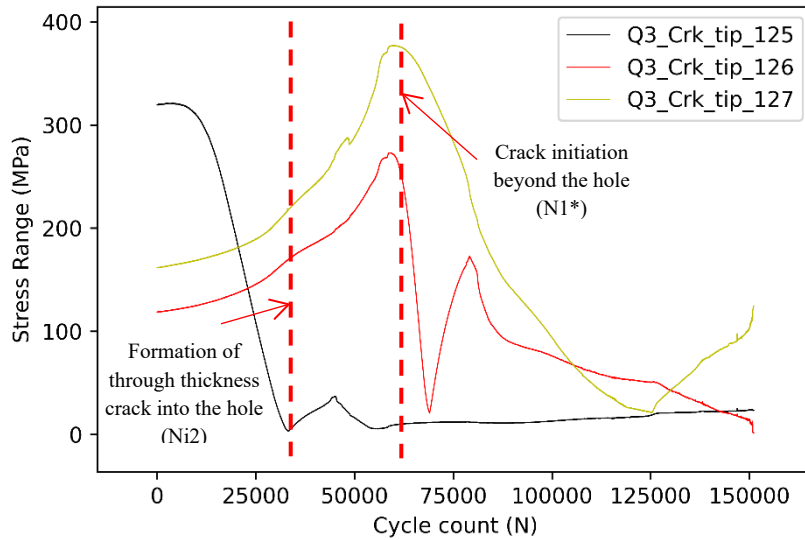


Figure 6-18: Stress range evolution diagram for the strain gauges around the crack-tip hole on quadrant Q3.

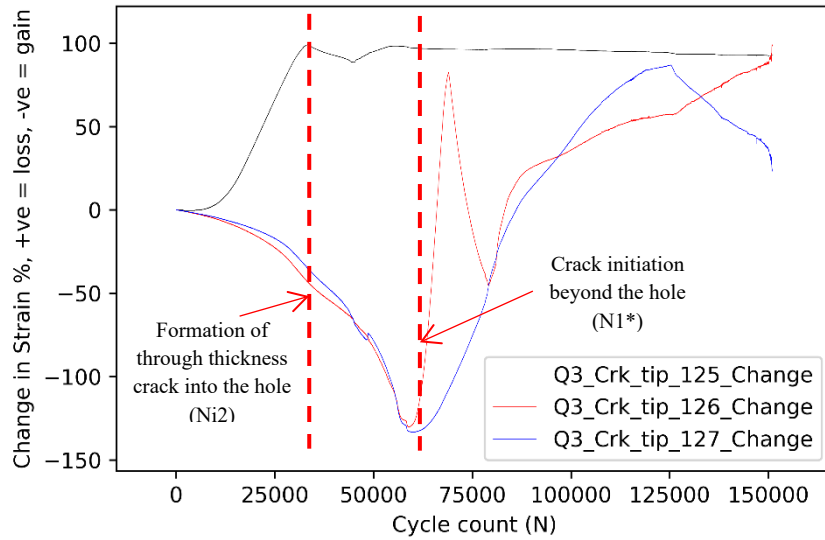


Figure 6-19: Percentage change in strain range around the crack-tip hole on quadrant Q3.



Figure 6-20: Final crack state at the crack-tip hole on quadrant Q3, at the end of the test.

### *Fatigue performance of crack deflecting hole on quadrant Q2*

A detailed sequence of events of the fatigue performance of the crack deflecting hole on quadrant Q2 is shown in Table 6-10, while Figure 6-21 and Figure 6-22 summarize the evolution of stress range and change in strain gauge readings. Figure 6-23 shows the crack development into the hole and then the formation of

a new crack beyond the hole. Similar behaviour to the "reverse coalescence" was discovered beyond the crack deflecting holes from specimen DT2.

Cycle count	Location	Remarks
Start of testing		The stress range increased for all the strain gauges mounted around the crack deflecting hole as the crack propagated towards the hole
96,000	Hole 3	drop in stress range level of SG119, indicating that the crack propagates between the strain gauge and weld toe penetrating the hole.
122,000	Hole 3	A significant drop in the stress range reading of SG119 indicates complete severance of the material between the strain gauge and weld toe, marking the crack's development through thickness into the hole.
147,300	Hole 3	15% drop in strain gauge SG120 reading indicating crack initiation beyond the hole.
154,000		End of fatigue testing of specimen DT3

Table 6-8: Sequence of the crack deflecting hole events on Q2 during the fatigue testing of the repaired specimen DT3.

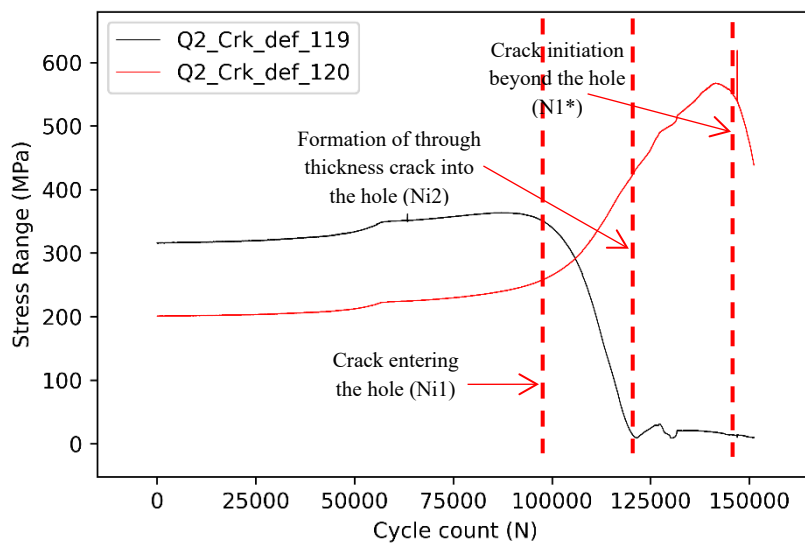


Figure 6-21: Stress range evolution diagram for the strain gauges around the crack deflecting hole on quadrant Q2.

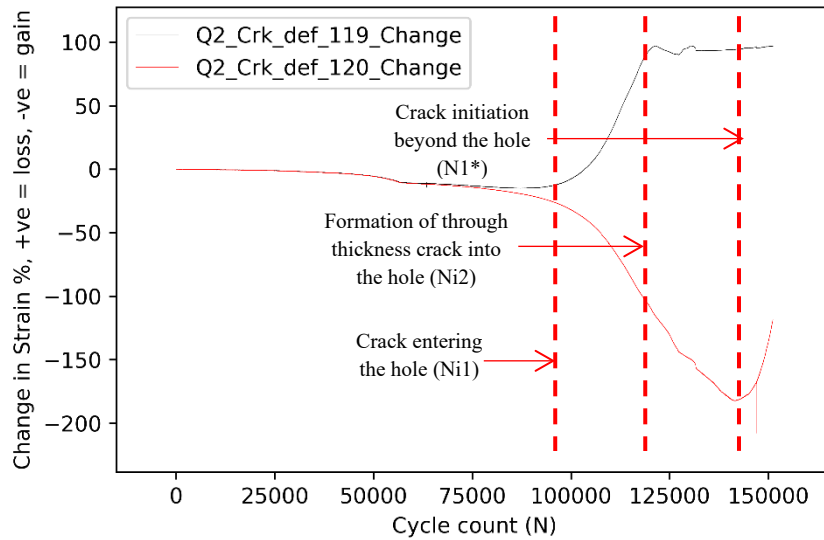


Figure 6-22: Percentage change in strain range around the crack deflecting hole on quadrant Q2.

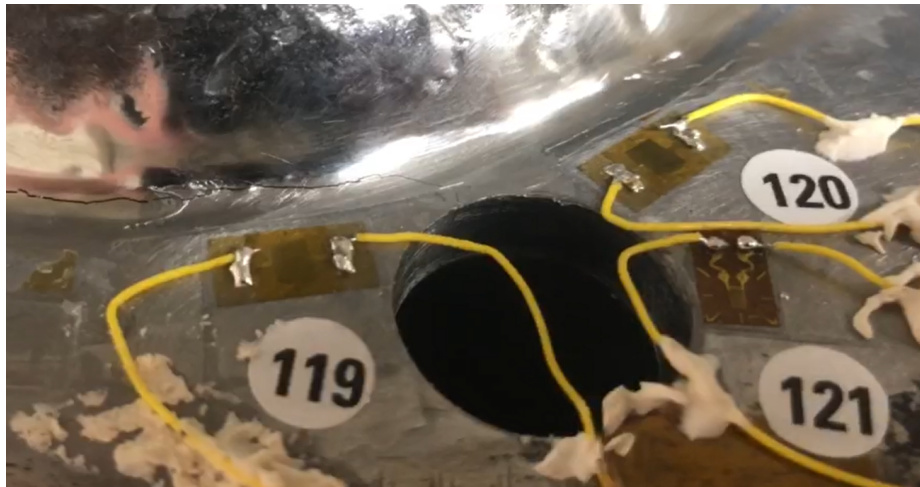


Figure 6-23: Crack evolution at the crack deflecting hole on quadrant Q2 at the end of the test.

### Fatigue performance of crack tip hole on quadrant Q2

The sequence of events of the fatigue performance of the crack tip hole on quadrant Q3 is shown in Table 6-9, while Figure 6-24 and Figure 6-25 summarize the evolution of stress range and change in strain gauge readings

around the crack tip hole on quadrant Q2. Figure 6-26 shows the crack development into the hole with the crack breaking out.

Cycle count	Location	Remarks
start		The stress range increased for all the strain gauges mounted around the crack tip hole.
89,400	Hole 4	drop in stress range level on SG 122, indicating that the crack is propagating between the strain gauge and weld toe, penetrating the hole
118,200	Hole 4	considerable drop in stress range at SG 122 reading indicates complete severance of the material between the strain gauge and weld toe, marking the crack's development through thickness into the hole.
122,400	Hole 4	A 15% drop in strain gauge SG 123 reading indicates crack initiation beyond the hole.
154,000		End of fatigue testing of specimen DT3

Table 6-9: Sequence of the crack tip hole events on Q2 during the fatigue testing of the repaired specimen DT3.

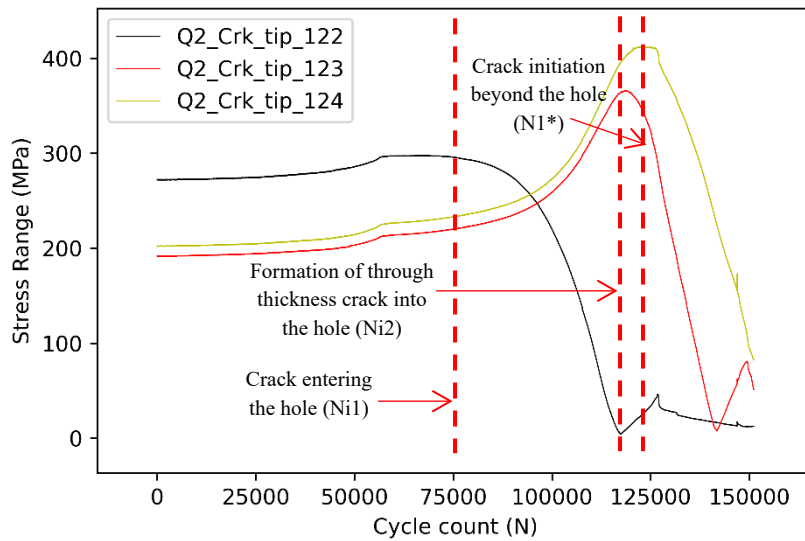


Figure 6-24: Stress range evolution diagram for the strain gauges around the crack-tip hole on quadrant Q2.

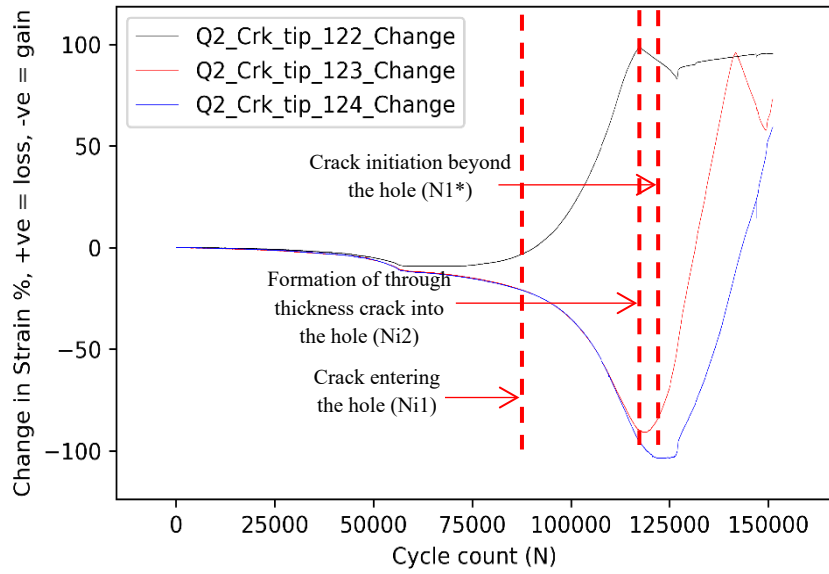


Figure 6-25: Percentage change in strain range around the crack-tip hole on quadrant Q3.

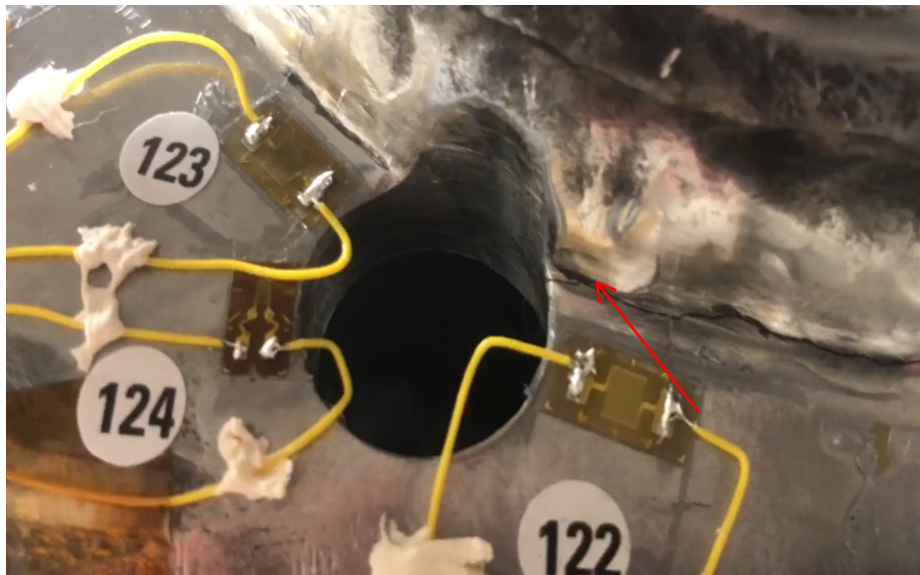


Figure 6-26: Crack evolution at the crack tip hole on quadrant Q2, at the end of the test.

*Fatigue performance of repairs*

---

*Fatigue performance of grinding on quadrant Q4*

The crack removal repair by grinding on quadrant Q4 was successful and no cracks developed on the quadrant during testing. A summary of specimen DT3 fatigue stages after the repair is provided in Table 6-2.

Quad.	Ni1 (x10 <sup>3</sup> )	Ni2 (x10 <sup>3</sup> )	N1* (x10 <sup>3</sup> )	N1* - Ni2 (x10 <sup>3</sup> )	N2* (x10 <sup>3</sup> )	N4* (x10 <sup>3</sup> )
DT3_Q2_H1_D_L20_G	96	122	147.3	25.3		-
DT3_Q2_H2_T_L20_G	89.4	118.2	122.4	4.2		-
DT3_Q3_H3_D_L53_G	47	55	92	37	125	154
DT3_Q3_H4_T_L53_G	0	33.3	61.5	28.2	125	154

Table 6-10: Repaired specimen DT3 fatigue life

## **6.4 Fatigue performance of repairs to specimen DT4**

### **6.4.1 General**

The tubular joint under investigation is specimen DT4 with the main features described in chapter 3. The specimen is fatigue tested up to precracking a through-thickness crack, as described in chapter 5. The specimen is then repaired using crack deflecting holes and crack removal by grinding, as described in the coming sections. The purpose is to compare the fatigue performance of crack deflecting holes.

### **6.4.2 Repair methodology**

#### ***Q3 Repair***

Q1 and Q3 fall on the same chord side, and both developed relatively large cracks. Q1 with the through-thickness crack was selected to test repair using crack deflecting holes to avoid Q3 crack interference with the repair on Q1. The fatigue strength of Q3 was reinstated by grinding the surface crack and then filling it with TIG welding, as shown in Figure 6-27 and Figure 6-28. A strain gauge rosette was installed to help in detecting any cracks emanating from quadrant Q3.



Figure 6-27: Quadrant Q3 repair, crack removal by grinding, dye penetrant application. Specimen DT4.



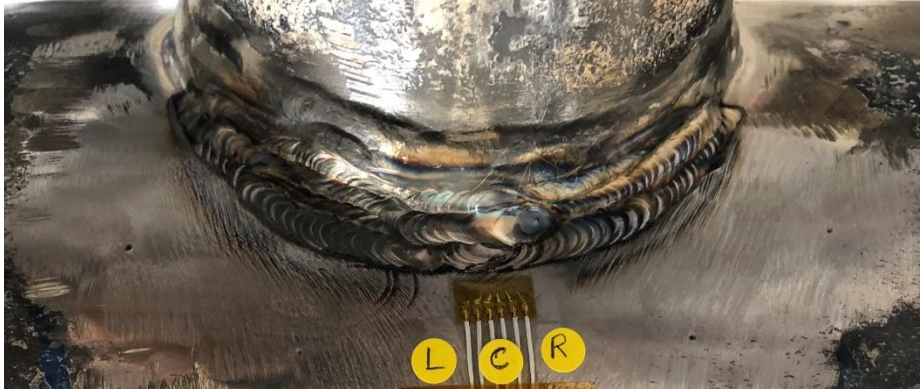


Figure 6-28: Quadrant Q3 repair by TIG welding after crack removal by grinding. Specimen DT4.

### ***Q1 Repair***

From the experience of testing specimen DT2, it was noticed that the closer the holes to the centre of the saddle, the longer the fatigue life of a crack to initiate beyond the hole. Detailed hole locations and fatigue lives are shown in Figure 6-30. It was decided for specimen DT4 to repeat 30° crack deflecting holes to the centre of the saddle.

The through-thickness crack length was estimated to be 80 mm and confined between positive 45° and negative 45° sectors. To drill two holes at 30° requires that the crack be shortened. A trial to shorten the crack length was done by partially grinding into the chord thickness. The crack length was measured using a dye penetrant, as shown in Figure 6-29.



Figure 6-29: Quadrant Q1 repair, material removal by grinding to achieve shorter crack length.

This process led to a shorter crack length. However, it decreased the chord thickness to 5 mm. Two crack deflecting holes were then drilled on Q1 at 30° from each side of the saddle centre, as shown in Figure 6-30. The sensitive areas beyond the hole were ground as a weld improvement technique to avoid crack initiation. A summary of the repair performed on specimen DT4 is shown in Table 6-11.

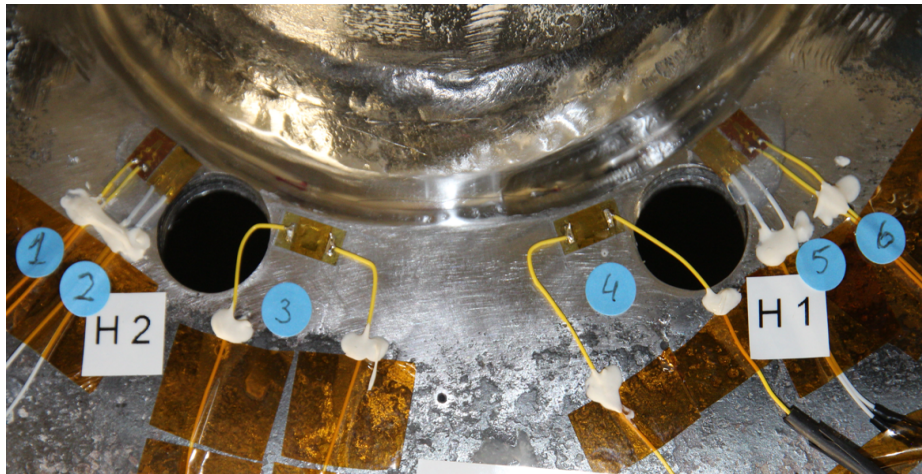


Figure 6-30: Quadrant Q1 repair, crack deflecting holes centred at 30° from the chord saddle. Specimen DT4.

*Fatigue performance of repairs*

Repair identification code	Crack deflecting hole	Hole location from saddle	Cold Expansion	Weld improvement (Grinding)	Crack removal (Grinding)	Tig weld
DT4_Q1_H1_D_L30_G	√	30°		√		
DT4_Q1_H2_D_L30_G	√	30°		√		
DT4_Q1_H3_D_L48_G	√	48°			√	
DT4_Q1_H4_D_L50_GC	√	50°	√		√	
DT4_Q3_W				√		√

The repair methods investigated for specimen DT4:

1. Crack-deflecting holes and weld-toe grinding
2. Crack-deflecting holes treated with cold expansion in addition to weld toe grinding.
3. Crack removal by grinding.

Table 6-11: Summary of repair performed on specimen DT4.

### 6.4.3 Repair Performance

The specimen was reloaded axially under constant amplitude loading with a load ratio of  $R = 0.17$ , a frequency of 3 Hz, a maximum load of  $P_{\max} = 60$  kN, and a minimum load is  $P_{\min} = 10$  kN. The sequence of events while testing the repaired specimen is summarised in the following sections. The cycle count quoted after repair excludes the number of cycles until precracking

#### *Fatigue performance of the left-hand side hole (H2) on quadrant Q1*

A detailed sequence of events of the fatigue performance of the left-hand side crack deflecting hole, Hole 2 on quadrant Q1, is shown in Table 6-12, while Figure 6-31 and Figure 6-32 summarize the evolution of stress range and change in strain gauge readings.

*Fatigue performance of repairs*

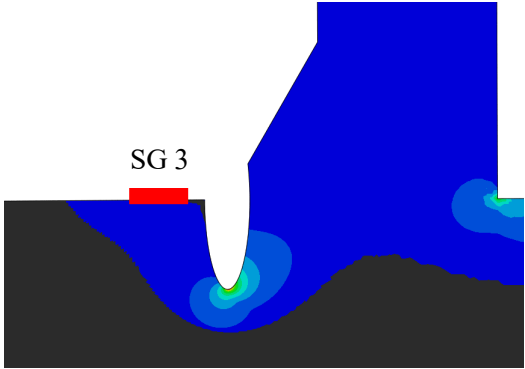
Cycle count	Location	Remarks
Start of testing		<p>The highest stresses at the joint do exist at the groove formed by grinding.</p> <p>The stress flow from the brace to the weld through the remaining ligament from the grinding process. As illustrated below, SG 3 was ineffectively placed at a spot insensitive to the load path. Hence, the results from SG 3 were unreliable, evident from the SG behaviour shown in Figure 6-31 and Figure 6-32.</p> 
23,100	Hole 2	<p>SG 1 and 2 showed a 15% drop in strain gauge reading, indicating a crack initiation beyond hole 2. Crack initiation was observed before the lead cracks penetrated the hole, resulting from amplified stresses due to the thickness loss from grinding and the ground profile.</p>
26,000		<p>Testing stopped for further mitigation of the specimen due to the unexpected crack initiation beyond the hole.</p>

Table 6-12: Sequence of events of the crack deflecting hole H2 during the fatigue testing of the repaired specimen DT4.

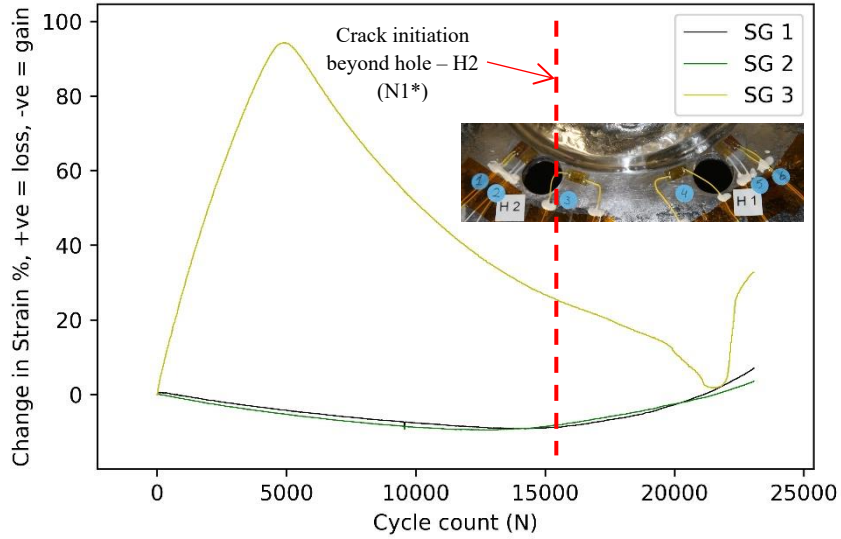


Figure 6-31: Percentage change in strain range around the left-hand side crack deflecting hole (H2) on quadrant Q1.

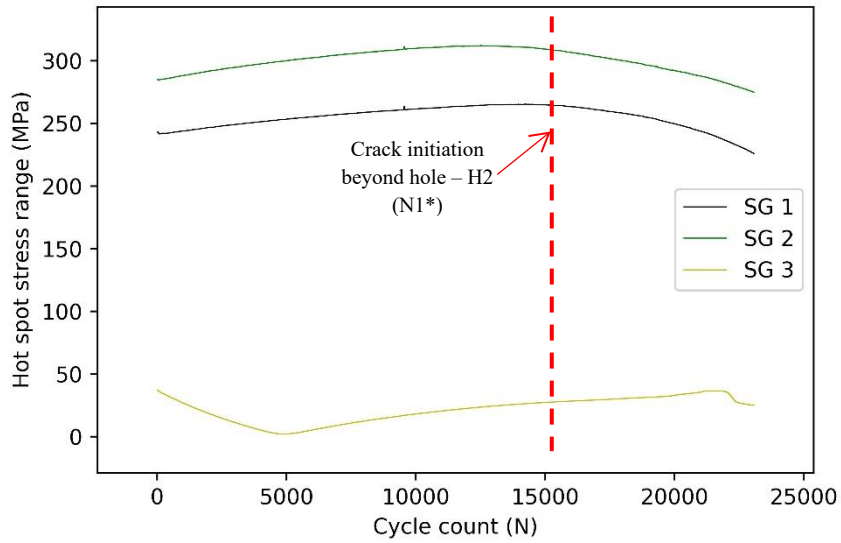


Figure 6-32: Stress range evolution diagram for the strain gauges around the left-hand side crack deflecting hole (H2) on quadrant Q1.

*Fatigue performance of the right-hand side hole (H1) on quadrant Q1*

The sequence of events of the fatigue performance of the right-hand side crack deflecting hole, Hole 1 on quadrant Q1, is shown in Table 6-13, while Figure 6-34 and Figure 6-35 summarize the evolution of stress range and change in strain gauges readings.

Cycle count	Location	Remarks
Start of testing	Hole 1	Similar to SG3, SG4 was ineffective because of its location away from the stress flow.
26,000	Hole 1	SG 5 and 6 showed a 15% drop in strain gauge reading, indicating a crack initiation beyond hole 1. The crack propagated along the weld toe without being deflected towards the hole as a result of amplified stresses due to the thickness loss from grinding.
26,000	Hole 1	Testing stopped for further mitigation

Table 6-13: Sequence of events of the crack deflecting hole H1 during the fatigue testing of the repaired specimen DT4.

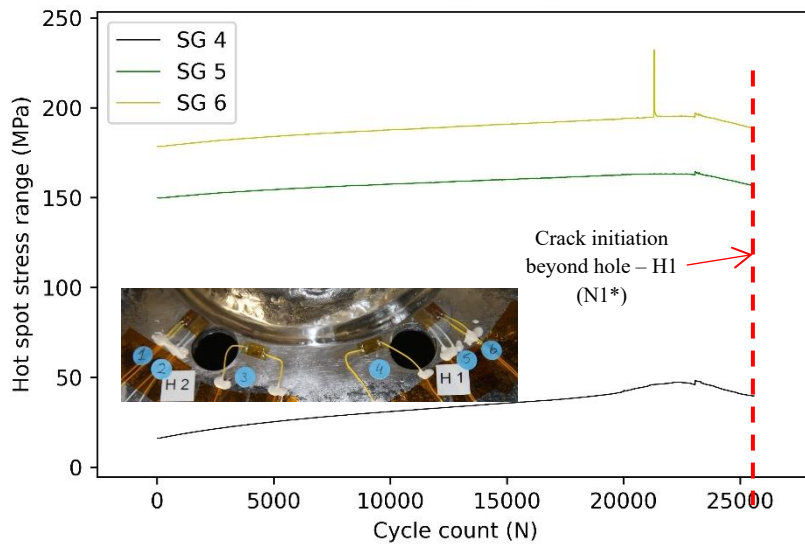


Figure 6-33: Stress range around the right-hand side crack deflecting hole (H1) on quadrant Q1.

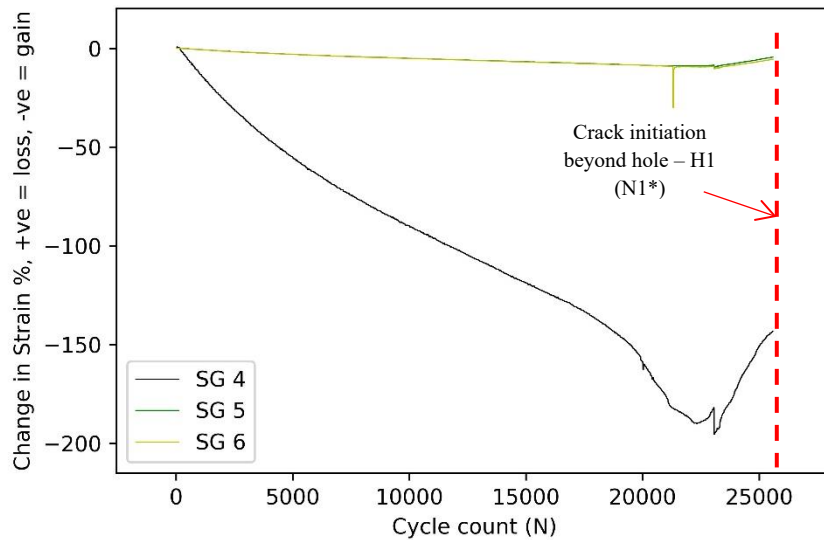


Figure 6-34: Percentage change in strain for the strain gauges around the right-hand side crack deflecting hole (H1) on quadrant Q1.

### Second repair attempt

The initial repair attempt proved unsuccessful, as the specimen experienced premature failure beyond both holes upon reloading. Cracks emerged before the lead crack could form a through-thickness crack within the holes. A second repair attempt was undertaken, involving the drilling of two new crack-deflecting holes. The left-hand side hole (H3) was drilled at a 48° angle from the chord saddle's centreline, while the right-hand side hole (H4) was drilled at a 50° angle. Additionally, Hole 4 underwent cold expansion treatment, increasing the hole diameter from 18.1 mm to 18.25 mm. Subsequently, a set of strain gauges was installed beyond the holes to monitor any crack initiation occurring at these locations. Figure 6-35 presents the general arrangement of the second repair attempt.



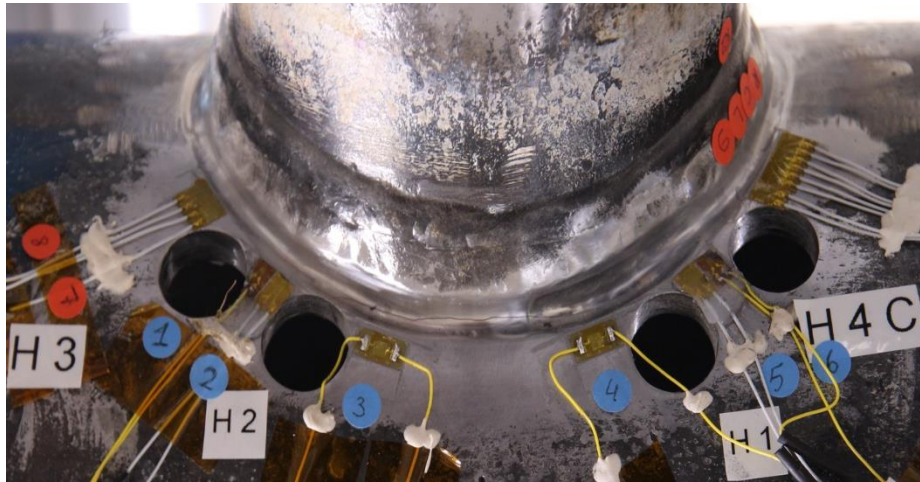


Figure 6-35: Quadrant Q1 second repair attempt, crack deflecting holes centred at 48° and 50° from the chord saddle. Specimen DT4.

### **Second repair performance**

The specimen was reloaded again under the same condition of precracking and the first repair attempt. The number of cycles quoted during the fatigue testing of the second repair attempt exclude the cycles applied during precracking but include the cycles that elapsed during the first repair attempt unless noticed otherwise.

#### *Fatigue performance of the left-hand side hole (H3) on quadrant Q1*

The sequence of events of the fatigue performance of the left-hand side crack deflecting hole, Hole 3 on quadrant Q1, is shown in Table 6-14, while Figure 6-36 and Figure 6-37 summarize the evolution of stress range and change in strain gauges readings.



*Fatigue performance of repairs*

Cycle count	Location	Remarks
0 – 48,300	Hole 3	A decrease in the stress range of SG 2 indicates the gradual propagation of a crack along the weld toe towards the crack deflecting hole.
47,100	Hole 3	complete loss of SG 2 stress range, indicating the development of a through-thickness crack in the wall of the hole (H3).
53,5000	Hole 3	A 15% drop in strain gauge SG8 reading indicates crack initiation beyond the hole
58,800	Hole 3	The lead crack developed into a through-thickness crack.
70,000		End of fatigue testing of specimen DT4

Table 6-14: Sequence of events of the crack deflecting hole H3 during the fatigue testing of the repaired specimen DT4.

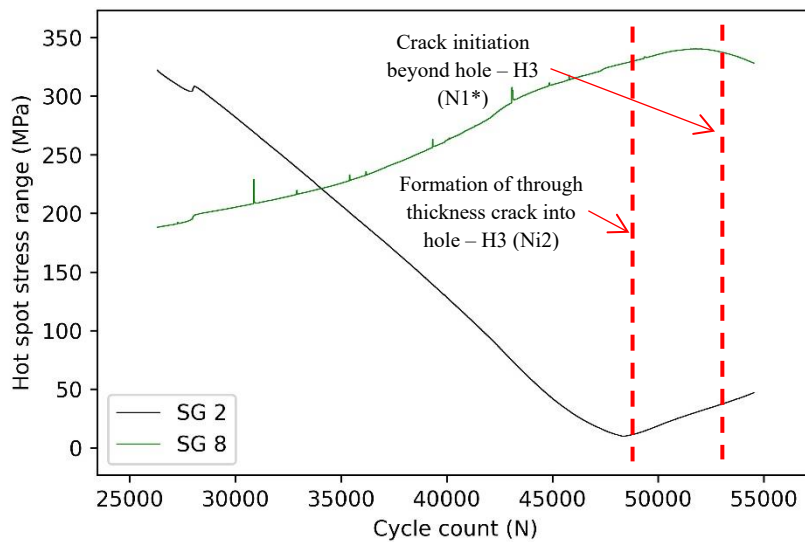


Figure 6-36: Stress range evolution diagram for the strain gauges around the left-hand side crack deflecting hole (H3) on quadrant Q1. Second repair attempt.

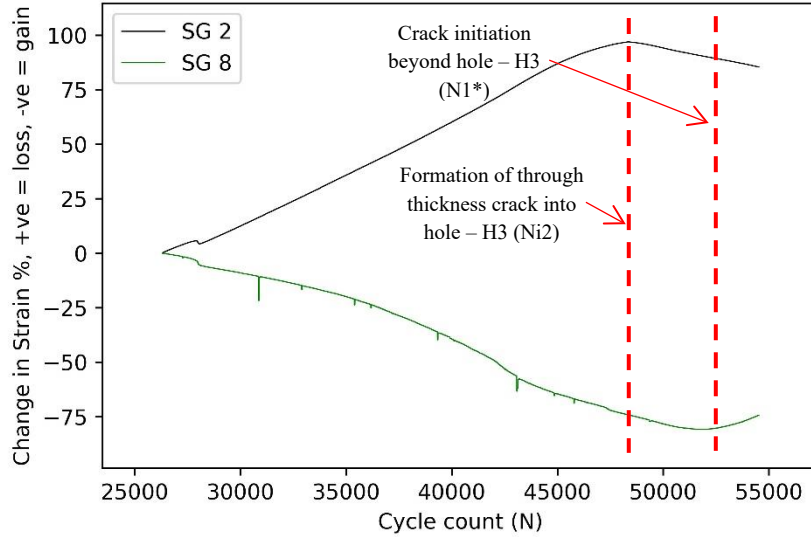


Figure 6-37: Percentage change in strain range around the left-hand side crack deflecting hole (H3) on quadrant Q1. Second repair attempt.

*Fatigue performance of the right-hand side hole (H4) on quadrant Q1*

The sequence of events of the fatigue performance of the right-hand side crack deflecting hole, Hole 4 on quadrant Q1, is shown in Table 6-15, while Figure 6-38 and Figure 6-39 summarize the evolution of stress range and change in strain gauges readings.

Cycle count	Location	Remarks
40,000	Hole 4	A complete loss in strain gauge SG 6 reading, indicating material severance between SG 6 and the weld toe.
69,500	Hole 4	New crack initiated beyond Hole 4
70,000		End of fatigue testing of specimen DT4

Table 6-15: Sequence of events of the crack deflecting hole H4 during the fatigue testing of the repaired specimen DT4.

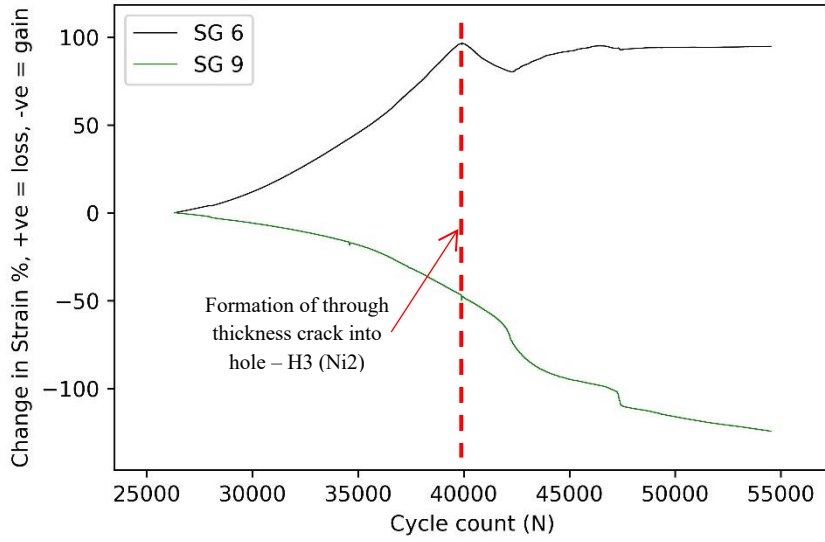


Figure 6-38: Percentage change in strain range around the right-hand side crack deflecting hole (H4) on quadrant Q1. Second repair attempt.

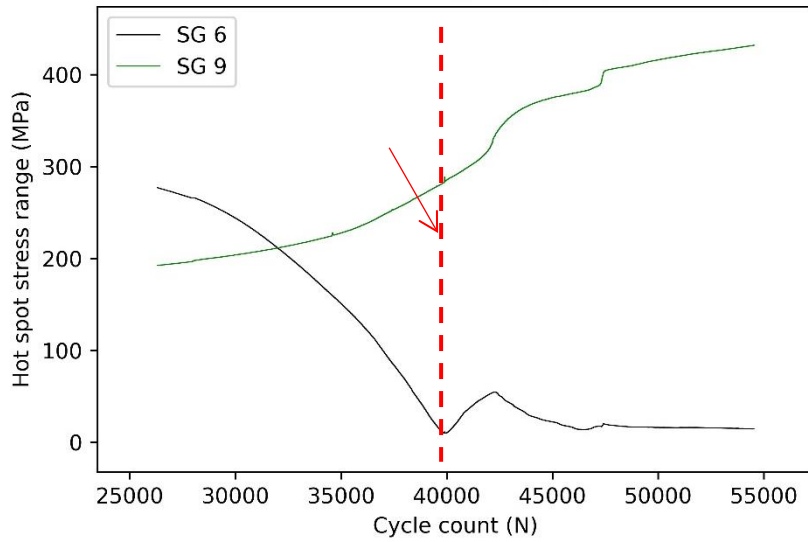


Figure 6-39: Stress range evolution diagram for the strain gauges around the right-hand side crack deflecting hole (H4) on quadrant Q1. Second repair attempt.

*Fatigue performance of crack removal by grinding and TIG welding on quadrant Q3*

The crack removal by grinding and TIG welding on quadrant Q3 succeeded, and no further cracks developed during fatigue testing.

***Summary of specimen DT4 fatigue stages after repair***

A summary of specimen DT4 fatigue stages after the repair is provided in Table 6-16.

<b>Quad.</b>	<b>Ni1 (x10<sup>3</sup>)</b>	<b>Ni2 (x10<sup>3</sup>)</b>	<b>N1* (x10<sup>3</sup>)</b>	<b>N1* - Ni2 (x10<sup>3</sup>)</b>	<b>N2* (x10<sup>3</sup>)</b>	<b>N4* (x10<sup>3</sup>)</b>
DT4_Q1_H1_D_L30_G			26			-
DT4_Q1_H2_D_L30_G			23.1			-
DT4_Q1_H3_D_L48_GR	47.1	58.8	53.5	-5.3	65	70
DT4_Q1_H4_D_L50_GC		40	69.5	29.5		70

Table 6-16: Repaired specimen DT4 fatigue life

## **6.5 Reverse coalescence phenomenon**

After the original crack grew into the crack deflecting hole, a new crack did not initiate from the hole. Rather, the new crack initiated from the weld toe a short distance beyond the hole. The crack then grew back towards the hole and coalesced with the original crack. This phenomenon was observed for all the repairs done by crack deflecting holes and is referred to as "reverse coalescence".

An example of this behaviour is shown in Figure 7-15 for specimen DT2, where a crack initiated beyond the hole at cycle count of 115,000 and then reverse coalesced at 130,000 cycles.

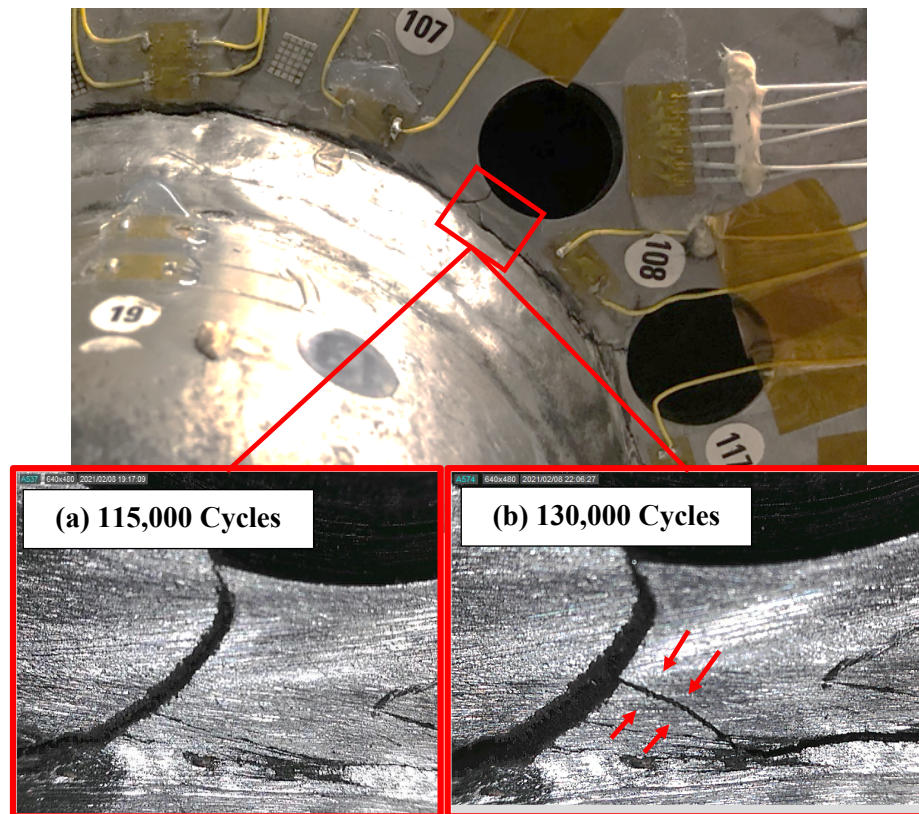
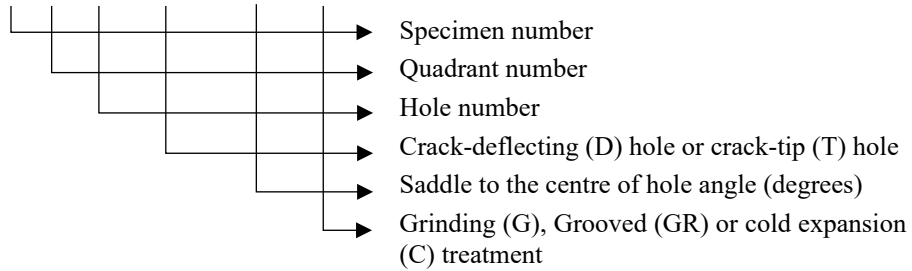


Figure 6-40: Reverse crack coalescence behaviour. (a) crack condition at 115,000 cycles, (b) reverse crack coalescence with the lead crack.

## 6.6 Summary

A summary of fatigue results of the repaired specimens is provided in Table 6-4.

X#\_Q#\_H#\_(D\_or\_T)\_L#\_(G\_or\_C)



Quadrant.	Ni1 (x10 <sup>3</sup> )	Ni2 (x10 <sup>3</sup> )	N1* (x10 <sup>3</sup> )	N1* - Ni2 (x10 <sup>3</sup> )	N2* (x10 <sup>3</sup> )	N4* (x10 <sup>3</sup> )
DT2_Q1_H1_D_L40_C		33	97	64	130	181
DT2_Q1_H2_D_L60_C	50	76.5	151	38	160	181
DT2_Q1_H3_D_L70	112	135	153	18	160	181
DT3_Q2_H1_D_L20_G	96	122	147.3	25.3		**
DT3_Q2_H2_T_L20_G	89.4	118.2	122.4	4.2		**
DT3_Q3_H3_D_L53_G	47	55	92	37	125	154
DT3_Q3_H4_T_L53_G	0	33.3	61.5	28.2	125	154
DT4_Q1_H1_D_L30_G			26			**
DT4_Q1_H2_D_L30_G			23.1			**
DT4_Q1_H3_D_L48_GR	47.1	58.8	53.5	-5.3	65	70
DT4_Q1_H4_D_L50_GC		40	69.5	29.5		70

Ni1 is the lead crack entering the hole  
 Ni2 is the lead crack is a through-thickness crack into the hole  
 N1\* is the formation of a new crack  
 N2\* is the new crack entering the hole (reversely)  
 N4\* Stop of test  
 \*\* runout, test ended before cracking

Table 6-17: Repaired specimen's fatigue life

## **7 Evaluation of the effectiveness of repairs**

### **7.1 General**

The experimental work presented in previous chapters has investigated the behaviour of tubular joints with fatigue cracks repaired by hole drilling in the vicinity of the crack. In addition, multiple techniques to improve the effectiveness of the repair have been investigated. The repair methods investigated were as follows:

- **Crack deflecting holes "As-is".**  
Drilling of crack deflecting holes close to the crack tip to divert the crack path out of the weld toe into the parent material.
- **Crack deflecting holes and cold expansion**  
Treating the drilled hole by inducing a compressive residual circumferential stress around the periphery of the hole to enhance the fatigue performance of drilled holes.
- **Crack deflecting holes and weld toe grinding**  
Improving the weld toe profile and removes any crack-like defects by grinding.
- **Crack-deflecting holes and grooving**  
Grooving the crack ends with the aim to shorten the crack, then drilling crack deflecting holes.
- **Crack tip holes and weld toe grinding**  
Drilling a hole at the crack tip to remove the stress singularity at the crack tip.

Table 7-1 summarises the combinations of repair methods and improvement techniques performed during the fatigue testing of cracked tubular joints.

Repair identification code	Crack deflecting hole	Crack-tip hole	Hole location from saddle	Cold Expansion	Crack removal (Grinding)	Weld improvement (Grinding)
DT2 Q1 H1 D L40 C	√		40°	√		
DT2 Q1 H2 D L60 C	√		60°	√		
DT2 Q1 H3 D L70	√		70°			
DT3 Q3 H3 D L53 G	√		53°			√
DT3 Q3 H4 T L53 G		√	53°			√
DT4 Q1 H3 D L48 GR	√		48°			√
DT4 Q1 H4 D L50 GC	√		50°	√		√

Table 7-1: Summary of repairs performed.

## 7.2 Typical specimen behaviour (cracking)

The typical cracking pattern for the specimens (precracked to through-thickness crack and repaired by the use of crack deflecting holes) comprised of the following stages, illustrated in Figure 7-1 :

- a. Crack propagation of the main crack towards the hole, deviating away from the weld toe and then entering into the hole.
- b. The crack develops further and becomes through thickness into the hole.
- c. Under further cyclic loading, a new crack re-initiates from the weld toe beyond the drilled hole. This new crack extends in two directions, one towards the joint crown and the other towards the crack-deflecting hole or the original crack.
- d. The new crack enters the crack-deflecting hole or coalesce with the original crack.
- e. The lead crack has extended to be one and half times the brace diameter which is defined as testing stopping criteria for the safety of facilities and personnel.



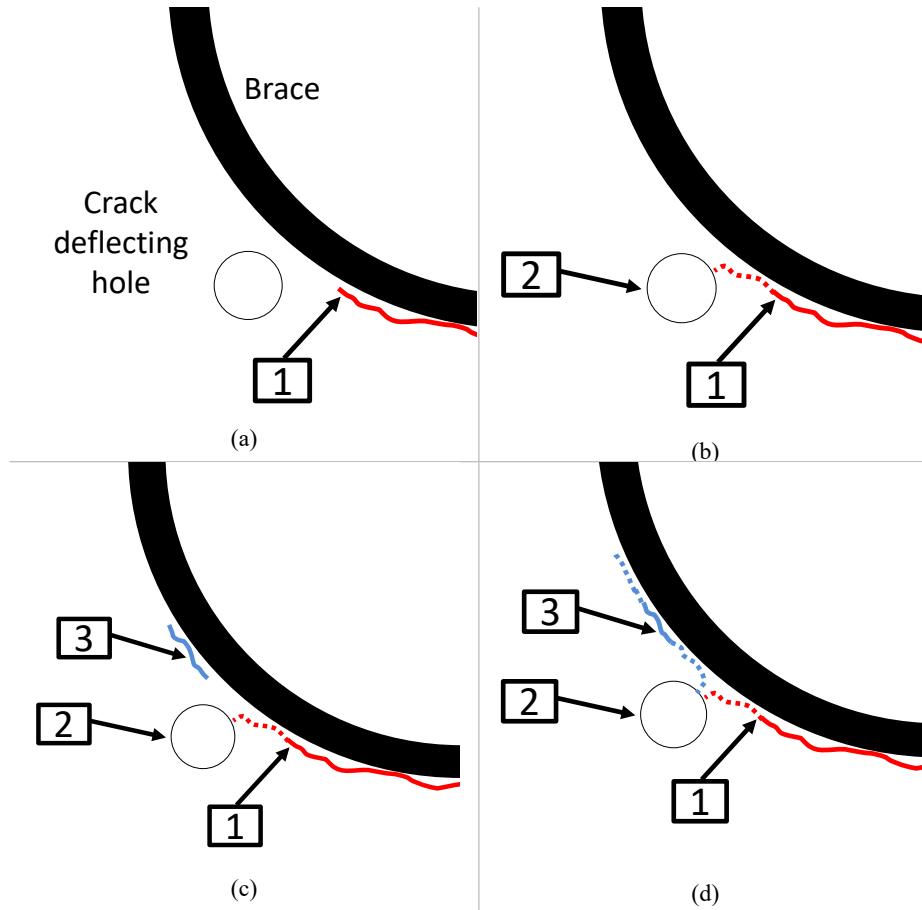


Figure 7-1: Typical cracking pattern during fatigue testing. The top left-hand figure is indicating the original crack at position 1 and the crack deflecting hole repair. The top right-hand figure indicates the crack developing into the hole (stage a and later b). The bottom left-hand figure shows the formation of the new crack at position 3 beyond the crack arresting hole (stage c), instead of the expected crack development from the hole at position 2. Finally, the bottom right-hand figure shows the new crack entering the hole or coalescing with the original crack (stage d).

These stages have in this thesis been associated with the following nomenclature:

- Stage a is denoted as  $Ni1$  where the lead crack is entering the hole.
- Stage b is denoted as  $Ni2$  where the lead crack is becoming a through-thickness crack into the hole.
- Stage c is denoted as  $N1^*$  where the new crack is initiated.
- Stage d is denoted as  $N2^*$  where the new crack entering the hole (reversely)
- Stage e is denoted as  $N4^*$  which is the stop of test.

The idea of repair by a crack deflecting hole is that the crack will propagate towards the hole and get arrested for a significant time before a likely crack re-initiation from the drilled hole. That has been shown in the work presented in [51, 52] by drilling crack deflecting holes in plates where the increase in the fatigue life was significant. To enhance the delay of the new crack development from the crack deflecting hole, cold expansion has also been used as shown with good results in [55]. The same type of results was attempted to be achieved by Tubby by the use of treated (cold expanded) crack-tip holes for tubular joints. However, it did not provide significant delay in the fatigue life of the specimen. The reason can be related to a new crack initiated beyond the hole reversely coalesce into the hole while propagating towards the chord crown.

The drilled hole location and size influence the stress field at the crack vicinity. It has two primary effects on the performance of the repaired joints. Firstly, it affects the stress intensity factor at the crack tip, which controls the trajectory of the crack propagation. Secondly, it affects the stress field at the weld toe region beyond the hole. During testing, a typical crack pattern was observed as stated in section 7.2 where the crack re-initiates at location 3 beyond the hole instead of location 2, as shown in Figure 7-1. It would have been beneficial if the repair would have led to the crack re-initiating from the drilled hole, as the crack would then have grown in the parent material. In hindsight, it is clear that to achieve this, the hole size and location would have needed to be tuned to provide significantly higher stresses around the hole (position 2 in Figure 7-1) than what is found at the weld toe beyond the hole (position 3 in Figure 1).

Table 7-2 provides a comparison between location 2 and 3 in terms of the stress fields and the material resistance to fatigue loading.

	<b>Location 2</b>	<b>Location 3</b>
Factors influencing the stress field	<ul style="list-style-type: none"> <li>- Global deformation stresses</li> <li>- Stress concentrations due to the proximity of the drilled hole</li> </ul>	<ul style="list-style-type: none"> <li>- Global deformation stresses</li> <li>- Notch stresses from the weld toe</li> <li>- Stress concentrations due to the proximity of drilled hole</li> </ul>
Factors influencing the material resistance	<ul style="list-style-type: none"> <li>- Cracking would initiate in the parent material (significantly better than the S-N curve for the weld toe)</li> <li>- Compressive residual stress field due to cold expansion if the holes are treated.</li> </ul>	<ul style="list-style-type: none"> <li>- Cracking would initiate in the HAZ.</li> <li>- Welding residual stresses</li> </ul>

Table 7-2: factors influencing the performance of location 2 and 3 on the chord side.

As a result of the observations mentioned in Table 7-2, it can be indicated that the new crack initiated at the weld toe beyond the crack arresting hole. Further optimisations to force the crack to start from the hole (position 2) instead of at the weld toe beyond the hole (position 3) could be done. This would have included increasing the distance between the weld toe to the drilled hole, which would reduce the influence of the drilled hole on the stresses at the weld toe. However, increasing the distance between the weld to the drilled could result in the crack not propagating to the hole. Hence, the crack propagation towards the hole should be studied carefully, ensuring that the crack will still propagate into the hole.

An alternative would be to improve the weld toe (position 3) by grinding to remove notch stresses or hammer peening to remove the residual stresses. Grinding was used in specimen DT3 with the aim of studying this effect, which is further discussed in section 7.7.

### 7.3 Effectiveness of repairs

Several ways of evaluating the effectiveness of the repair are possible. An intuitive way would be to assess the fatigue life of the repaired joint versus an unrepaired joint. In this context, the effectiveness of repair could be measured by comparing the number of cycles for which there is no crack growth after the repair (the period where the crack could be said to be arrested or dormant) to the number of cycles to crack initiation ( $N1$ ) or through-thickness crack development ( $N3$ ) for the intact specimen. Comparing the dormant phase to the crack initiation phase of an intact specimen may be the most relevant measure as it compares like by like (i.e., the crack initiation of the intact joint to the crack initiation of the repaired joint). However, it may not be easy to find  $N1$  for T joints<sup>1</sup> and, hence, comparing the dormant phase to  $N3$  can be more easily used in practical situations, as  $N3$  is known. Hence, the dormant period can be estimated based on the experienced fatigue life when the crack is found.

The effectiveness measures, defined here as  $eR$  can be written as:

$$eR_{N1} = \frac{N1^* - Ni2}{N1} \% \quad (7.8)$$

$$eR_{N3} = \frac{N1^* - Ni2}{N3} \% \quad (7.9)$$

where  $N1^*$  is the number of cycles to a new crack initiation while  $Ni2$  is the number of cycles for the lead crack to become a through-thickness crack into the hole.

$N1$  is the number of cycles to crack initiation, while  $N3$  is the number of cycles to the through-thickness crack of the original specimen.  $N1$  and  $N3$  will be estimated as shown in chapter 5, where the fatigue life of tested tubular joints is plotted against the hot spot stress range and S-N curve constructed on the same basis as OTH 92 360 recommendations [15]. As shown in Table 4-10, S-N curves have been developed for  $N1$  and  $N3$ , where both S-N curves have an inverse slope of  $m = 3$  while the  $N1$  and  $N3$  curves have intercept  $\log A$  of

---

<sup>1</sup> Chapter 4, Table 4.6 provides a suggestion for an  $N1$  curve for T joints developed from the same basis as the universal T curve.

12.93 and 13.3 with a standard deviation of 0.15 and 0.21 as per Table 4-10, respectively.

To exemplify this  $eR$  factor:

- An  $eR$  of zero would mean that no dormant period was seen.
- An  $eR$  of 100% would mean that crack re-initiation took the same number of cycles as the initiation of the original crack.
- A negative  $eR$  would mean that a new crack would be initiated ( $N1^*$ ) before the lead crack entered the hole ( $Ni2$ ) and became through the thickness. Essentially, the repair had a negative effect.

A summary of fatigue test results of the repaired specimens, as presented in Chapter 6, including the repair effectiveness measures  $eR$ , is provided in Table 6-4.

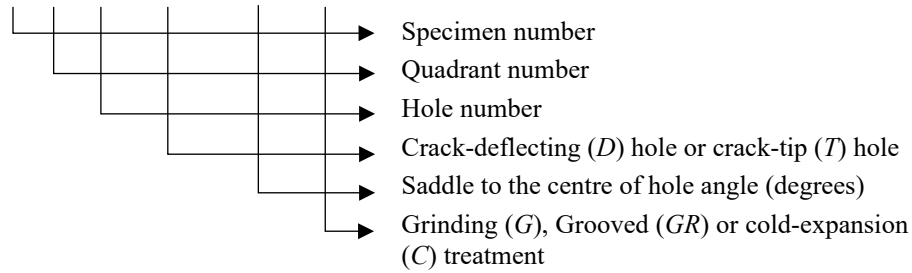
Quadrant.	$Ni1$ (x10 <sup>3</sup> )	$Ni2$ (x10 <sup>3</sup> )	$N1^*$ (x10 <sup>3</sup> )	$N1^*-Ni2$ (x10 <sup>3</sup> )	$N4^*$ (x10 <sup>3</sup> )	$eR_{N1}$ (%)	$eR_{N3}$ (%)
DT2_Q1_H1_D_L40_C		33	97	64	181	14	10
DT2_Q1_H2_D_L60_C	50	76.5	151	38	181	8	6
DT2_Q1_H3_D_L70	112	135	153	18	181	4	3
DT3_Q3_H3_D_L53_G	47	55	92	37	154	8	6
DT3_Q3_H4_T_L53_G	0	33.3	61.5	28.2	154	6	5
DT4_Q1_H3_D_L48_GR	47.1	58.8	53.5	-5.3	70	-1	-1
DT4_Q1_H4_D_L50_GC		40	69.5	29.5	70	6	5

$Ni1$  is the lead crack entering the hole  
 $Ni2$  is the lead crack through-thickness into the hole  
 $N1^*$  is the formation of a new crack  
 $N2^*$  is the new crack entering the hole (reversely)  
 $N4^*$  Stop of test  
 $eR_{N1}$  Effectiveness of the repair, based on  $N1$  mean values  
 $eR_{N3}$  Effectiveness of the repair, based on  $N3$  mean values  
\*\* runout, test ended before cracking

Table 7-3: Repaired specimen's fatigue life

The naming of the specimens, as previously described in section NN, is according to the following convention:

*DT#\_Q#\_H#\_(D\_or\_T)\_L#\_(G\_or\_C)*



Several observations can be drawn from the results shown in Table 6-4. The most striking observation is that none of the repaired specimens achieved the same number of cycles after through thickness crack until final failure ( $N4-N3$ ) as the test specimen (*DT1*) did, where  $N4-N3=188 \times 10^3$ . This could be construed to be a proof that the repair method is ineffective. However, the *DT1* specimen seems to give a statistically high  $RE=(N4-N3)/N3$  value compared to the database of similar specimens provided in 0. While for *DT1*, the  $RE$  value is 0.3, the database for axially loaded specimens with a similar load ratio  $R$  value (0-0.1) gives an  $RE$  value of approximately 0.22, with maximum value of 0.66. Further, it can be found that the  $RE$  changes with the through-thickness crack length as shown in Figure 7-2 (where the boxes are indicating the median, upper and lower quartile while the whiskers indicate upper and lower extremes)

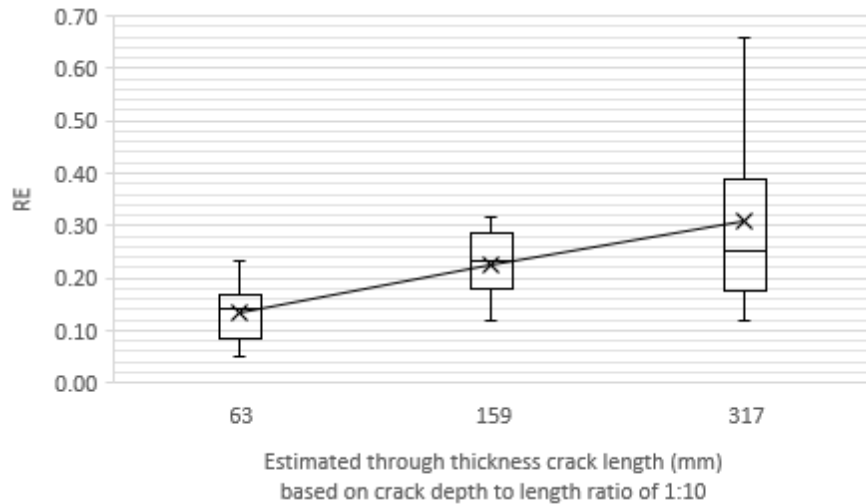


Figure 7-2: Re value against the estimated through-thickness crack length for the database provided in Appendix 2

From the tested specimens, the through-thickness crack lengths measured from precracking (chapter 5) were found to be in the range of 75 – 90 mm. That range of crack length would indicate an RE value between 0.15 and 0.17. Hence, DT1 may not be a fair comparison and some of the specimens do indeed achieve a comparable RE value higher than 0.15.

Further, particularly the effect of the position of the crack deflecting hole relative to the saddle centre is obviously an important factor in the effectiveness of the repair, as shown in Figure 7-3. This dependence of the angle will be further studied and explained in section 7.3.

In Figure 7-3, the two cold expanded and the as-is drilled specimens are from DT2, while the grinded specimens are from DT3, and the grinded and cold expanded specimen and the remedial grinding specimen are from DT4.

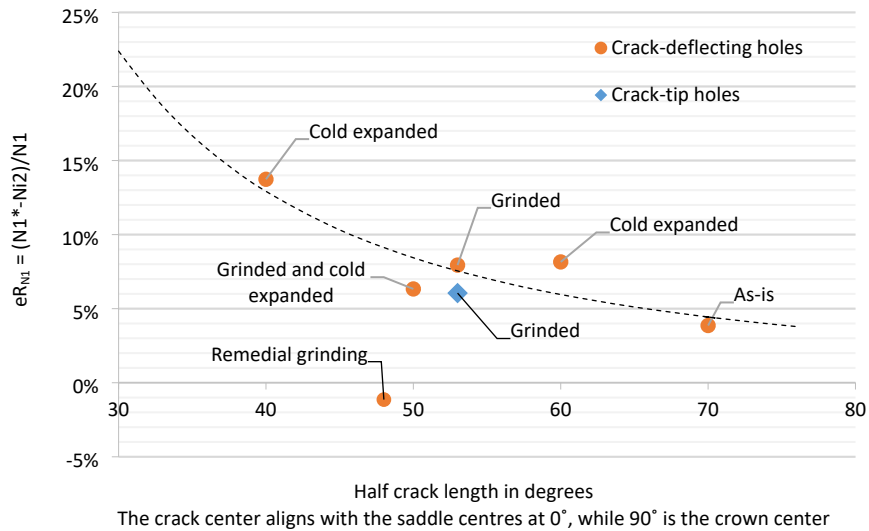


Figure 7-3: Repair performance of crack deflecting holes. Based on  $eR_{N1}$  measure (Remedial grinding specimen is not included in the curve fitting)

From Table 7-3 and Figure 7-3 it can be seen that cold expansion and grinding does not provide a significant improvement. An explanation for the lack of effect from cold expansion will be further described in section 7.5 and grinding in section 7.6.

Specimen DT4 was repaired by remedial grinding (grooving) in addition to the crack deflection hole. The idea of this additional grooving was to shorten the length of the crack and, as a result take benefit of the observed improved behaviour of smaller angles between the hole and the saddle point. However, as shown in Table 7-3 and Figure 7-3 it did not show any improvement of the fatigue life of the joint. In contrast, it showed a negative effect. This unfavourable behaviour can be related to the stresses resulting from the excessive grooving needed to remove the crack. This grooving led to slimmer chord thickness and substantially higher stress concentration factor at the bottom of the groove. This resulted in the crack bypassing the hole on one side as shown in Figure 6-35. Grooving is investigated further in section 7.7.



Crack tip holes were for optimal comparison tested on a specimen at the same angle as a crack deflection hole. As expected, the test indicate that the crack deflection hole is performing better than the crack-tip hole.

The effectiveness of repair factor explained above will be used to assess the repair performance in the next sections and will be used to predict the effect of drilling crack deflection hole as a repair method.

#### **7.4 Crack deflecting holes**

This section further investigates the impact of the crack length and as a result the position of the crack deflecting holes on delaying the further crack growth.

As indicated in Table 7-3, crack deflecting holes at 40°, 50°, 60°, and 70° crack lengths were investigated, and the results of the tests showed eR factors of 13.7%, 7.1% (average of 7.9% and 6.3%), 8.2% and 3.9% respectively as shown in Figure 7-3. A reasonable correlation between the eR factor and the location of the drilled hole relative to the saddle centre is found where the eR is a power function of the angle between the drilled hole and the saddle. The benefit of a crack-deflecting hole in extending the life of the joint is, therefore, highly dependent on the angle from the saddle to the centre of the drilled hole.

The benefit from the repair becomes less as the crack length increases. This trend for the tested tubular joints is consistent with the conclusion of earlier work on a crack in a finite width plate repaired with crack-deflecting holes [52]. Here, the cracked and repaired tubular joints are idealised as a plate with a centre crack perpendicular to the direction of loading with two drilled holes at the crack-tips. For force-controlled loading (Constant force), the net cross sectional area decreases upon crack development, leading to higher stresses in the remaining section. Hence, the decrease in eR value with the increased angle between drilled hole and saddle centre.

To investigate and further explain this behaviour for the tubular joints, an FE model was developed to numerically assess the influence of a crack on the stress distribution from the chord saddle to crown. In addition, an FE model was developed to investigate the effect of the subsequent repair by drilling a crack deflection hole.

Figure 7-4 show the resulting stress distribution along the joint circumference in the presence of a crack for multiple crack length as function of angle. It should be mentioned that the estimated stress at the crack-tip is not actually a stress measurement, as it ignores the singularity at the crack-tip. The hot-spot stress distribution on the chord side from Figure 7-4 is estimated on the same basis as the hot-spot stress method by measuring stresses at two points slightly away from stress raisers and linearly extrapolate to the point of interest.

The stresses used in this study are derived from the principal stresses which should be inline with the currently used SN curves. It is essential to note that these are not necessarily equivalent to the uniaxial stresses extrapolated from the strain measurements in the experimental work.

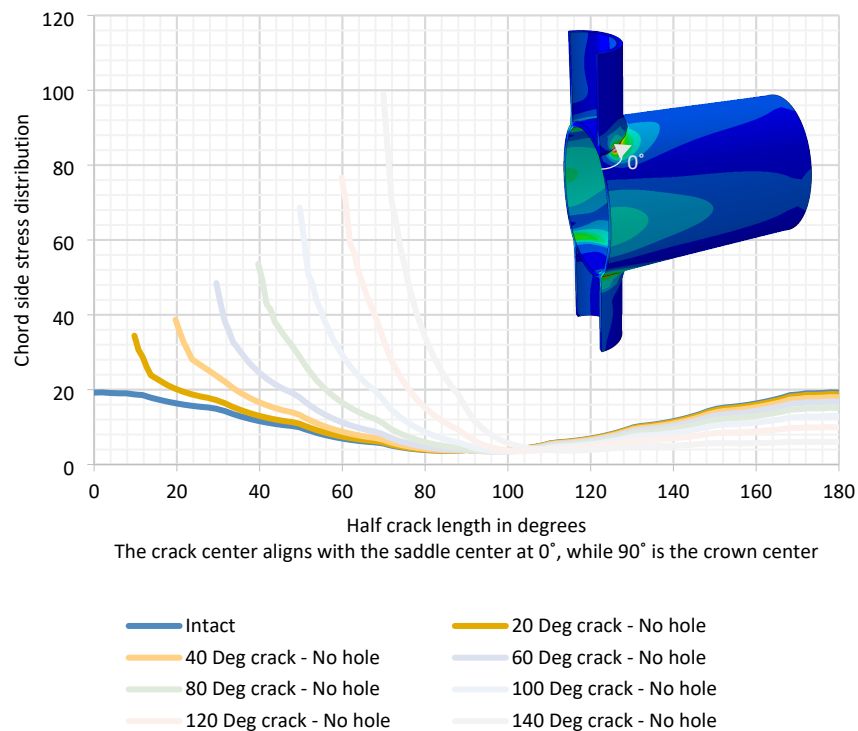


Figure 7-4: Stress distribution of unrepaired specimens along the circumference of the chord for a nominal axial stress of 1 MPa in the brace.

Figure 7-5 includes the stress distribution around the chord circumference for multiple crack lengths with crack deflecting holes. The shielding effect behind

the hole can clearly be seen, but particularly for the larger angles (60-140) the increase in stress beyond the drilled hole is clearly visible. This increase is obviously the result of the crack forming beyond the hole as observed in the experimental tests.

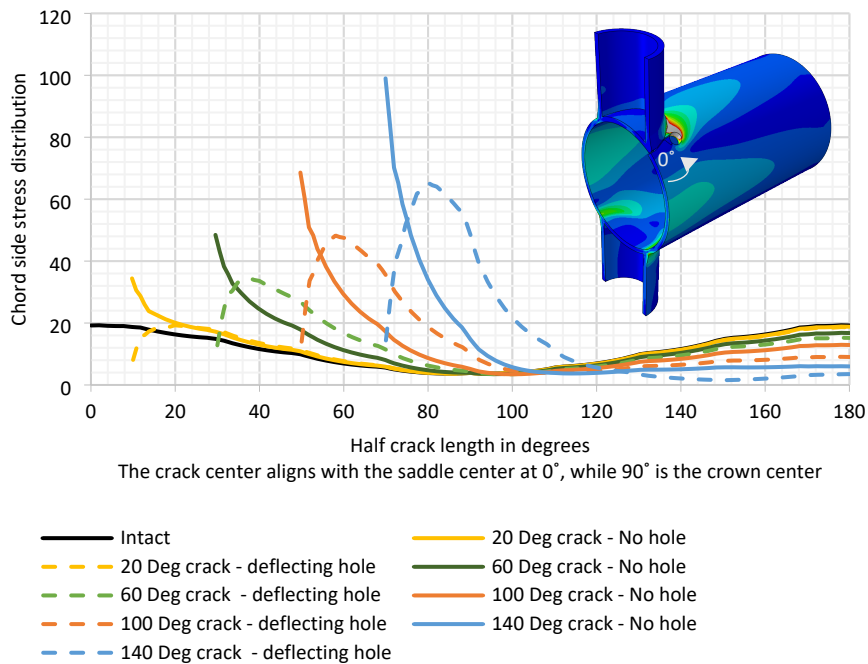


Figure 7-5: Stress distribution of unrepaired specimens and repaired specimens with crack deflecting holes along the circumference of the chord for a nominal axial stress of 1 MPa in the brace.

Figure 7-6 shows a normalised version of Figure 7-5 where these stress distributions are divided by the maximum stress in the chord saddle for the intact joint. These normalised curves give a relative stress concentration factor for the situation with and without holes. Without holes, the highest relative SCF is for obviously reasons at the crack tip and the crack will continue to grow from the crack tip. However, where the crack has been repaired by a hole, the dashed curves indicates the location of the maximum stress and hence the likely location of a new crack.

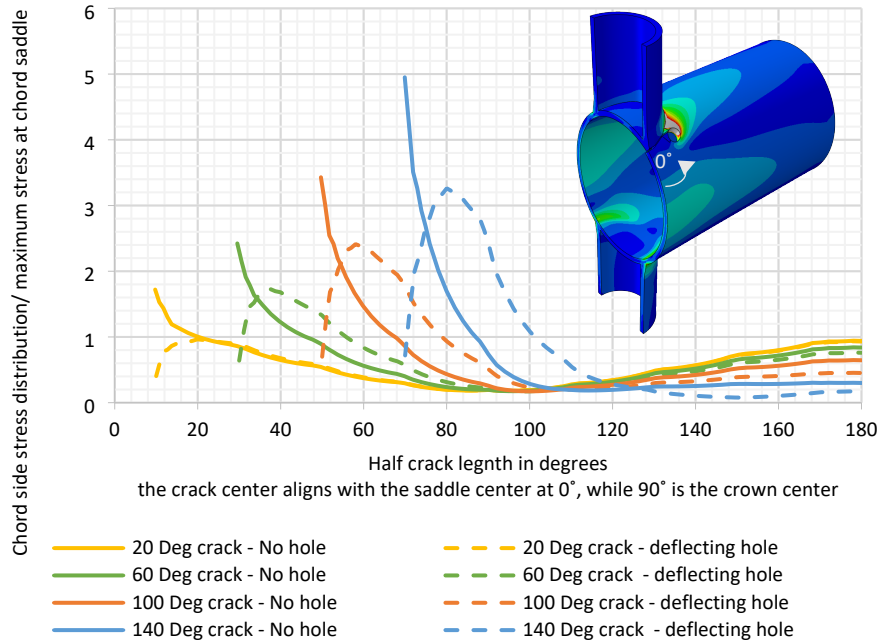


Figure 7-6: linearised stress distribution of unrepaired specimens and repaired specimens with crack deflecting holes along the circumference of the chord for a nominal axial stress of 1 MPa in the brace.

As shown in Figure 7-6, there is a close to linear increase in stress at the weld toe beyond the hole (position 3) for increasing angles, while a slightly non-linear increase is seen for the hot-spot stress for increasing angle for the unrepaired joint. An illustration of these maxima is shown in Figure 7-7.



Figure 7-7: Maximum stresses for specimens repaired with crack deflecting holes and unrepaired specimen.

These curves can be used to estimate the remaining fatigue life of a specimen repaired by a crack deflection hole using the hot-spot stress method. For example, in the precracking stage of specimen DT2, 466,000 cycles elapsed until crack initiation (*NI*). The specimen is then repaired by drilling a crack deflecting hole at 40° from the saddle's centre. From Figure 7-7, it can be found that the SCF beyond a crack deflecting hole at 40° is 2.09 that of the SCF at the centre of an intact saddle. A 2.09 of the SCF for an in-air S-N curve with a slope of  $m = 3$ , would reduce the fatigue life by 10.9%; hence, an estimate of the  $eR$  would be 10.9 as shown in equation 4 and rough estimate of the number of cycles to a crack re-initiation would then be 51,100 cycles as shown in equation 3. From the actual test, the crack initiation beyond the crack deflecting hole drilled at 40° on specimen DT was found to be 64,000 cycles, which is 25% on the safe side compared to 51100 cycles.

$$eR_{estimate} = \frac{1}{SCF_{increase}^m} = 10.9\% \quad (7.10)$$

$$(N1 * -Ni2)_{estimate} = \frac{N1_{DT2}}{SCF_{increase}^m} = 51,100 \text{ cycles} \quad (7.11)$$

Similarly, an estimate of the time of crack re-initiation could be estimated by the SCF increase.

$$eR_{measured} = \frac{N1 * -Ni2}{N1_{DT2}} = \frac{64,000}{466,000} = 13.7\% \quad (7.12)$$

when dividing the above expression for the tested specimens by  $N1$ , a simple expression of one divided by the increase in SCF in the power of  $m$  would be comparable to the above equation 7.12. Figure 7-8 show the  $eR$  measured for tested specimens normalised by  $N1$  in comparison to the  $eR$  estimate.

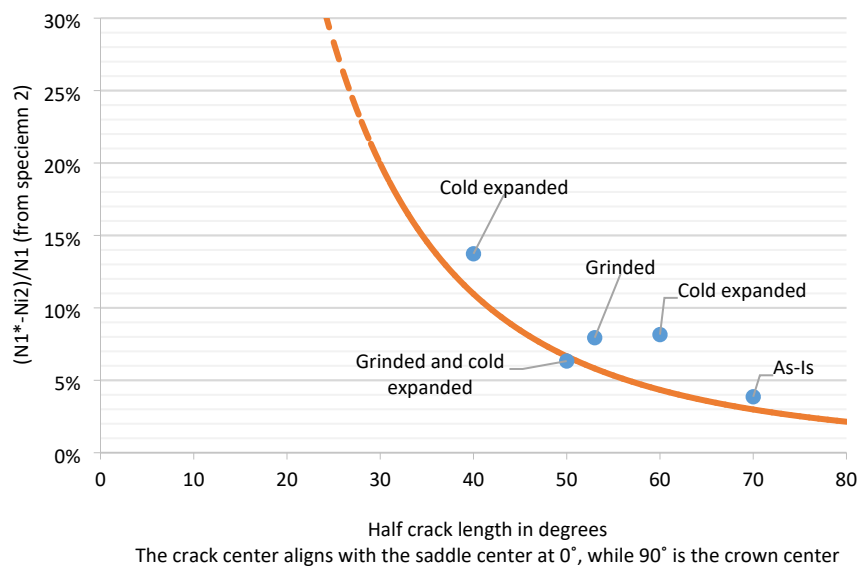


Figure 7-8: fatigue measured fatigue life extension of tested repaired specimens ( $eR$  measured) compared to curve for estimate of life extension ( $eR$  estimate) according to Equation 7.12.

Since  $N1$  will not be available without fatigue testing or access to the original data used to construct the T-joint S-N curve,  $N3$ , through thickness crack, will be a better reference as it is known from the available standards. In further comparisons, the mean values of  $N3$  will be used. For example, for specimen

DT2, the tested  $N_3$  was 613,000 cycles. Hence, the measured additional fatigue life of repaired specimen until crack re-initiation could be expressed as follows.

$$eR_{measured} = \frac{N1 * -Ni2}{N3_{DT2}} = \frac{64,000}{613,000} = 10.4\% \quad (7.13)$$

In comparison, the predicted additional fatigue life by the method described above is 10.9% as shown in equation 7.13. Similarly, an estimate of the time of crack re-initiation could be estimated by the SCF increase.

All the specimens are shown in Figure 7-9 by a similar calculation, indicating the drop in the effectiveness of the repair with increasing angle.

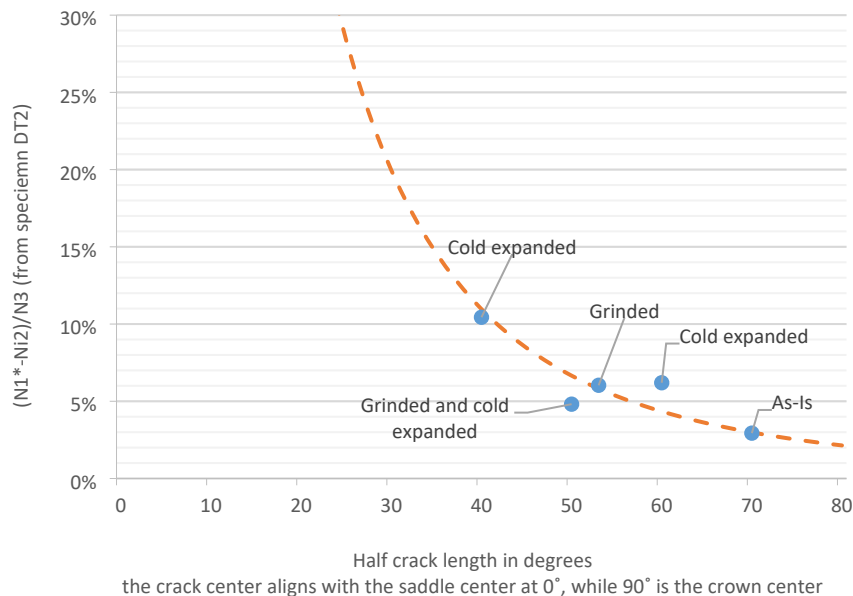


Figure 7-9: fatigue life extension of repaired specimens compared to life extension estimate curve, where  $(N1^*-Ni2)$  is the dormant period of the crack in the hole before the initiating of the new crack and  $N_3$  is the mean fatigue life from the T-joint SN-curve.

It is shown in Figure 7-9 that, the predicted  $eR$  by these simple estimates are in good agreement with most of the measured  $eR$  for the specimens. However, it should be noted that the specimen treated with cold expansion and grinding (DT4\_Q1\_H4\_D\_L50\_GC) falls on the unsafe side. Nevertheless, since  $N1^*$  is

a measure of the formation of a new crack rather than the new crack being through thickness, this method is considered a low estimate of the remaining fatigue life. In addition, the N3 used in Figure 7-9 is the observed N3 from specimen DT2 which is higher than the design N3 value from design S-N curves. Hence, if the calculation of the remaining fatigue life utilises the design S-N curves, this should bring all point to the safe side.

To conclude, it was believed that repair improvement techniques such as cold expansion and weld toe grinding would improve on the experienced life extension. However, as shown in Figure 7-9, no significant improvement from the predicted life can be concluded. It should be noted that the number of specimens do not satisfy the minimum acceptable statistical spread. Hence, the experimental work will be supplemented by additional evaluations in the following sections, 7.5 for the cold expansion, section 7.6 for grinding, section 7.7 for the remedial grinding (grooving) and section 7.8 for a comparison between crack-tip holes and crack deflection holes.

## **7.5 Cold expansion**

As described in section 2.5.4, in most cases where hole drilling is used as a repair method, these are combined with cold expansion of the holes. This cold expansion induces a compressive residual stress field around the hole circumference, reducing the effective tensile stresses at the hole edges. Hence, for cracks that re-initiate from the hole, the method delays fatigue crack initiation and propagation.

As a result, cold expansion is frequently used to delay crack initiation from the hole, particularly in plated structures, but also for tubular joints as shown in Tubby [3].

However, the cold expansion process in the vicinity of welds has some drawbacks. Figure 7-10 shows the stress field around a drilled hole treated with cold expansion in an infinite plate and it can be seen that tensile stresses (10-15% of the yield strength) arise in the neighbour material [55].



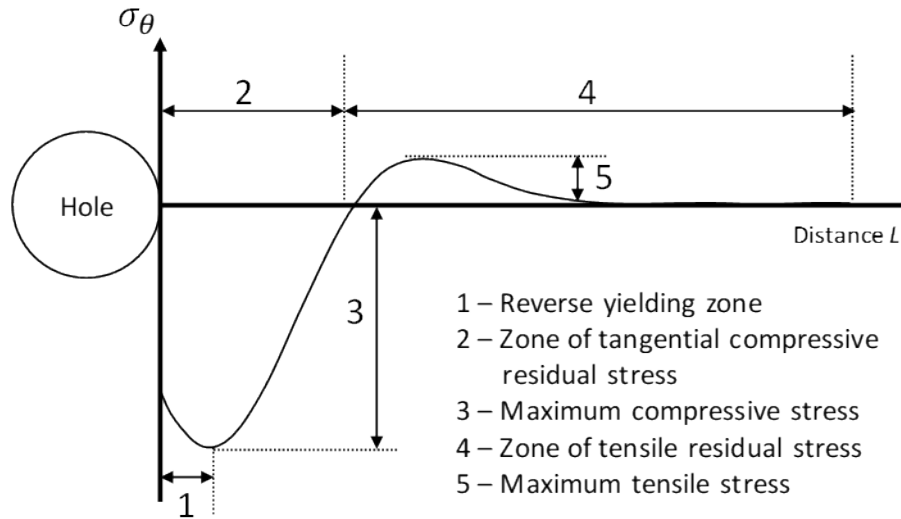


Figure 7-10: Stress field around a cold expanded hole [55]

Hence, although cold expansion helps delay crack re-initiating from the hole, it will generate tensile stresses that act transversely to the weld toe in the direction of the undesired tensile stresses (i.e., residual stresses, notch stresses, deformation stresses). This overlooked aspect of the cold expansion process will as a result accelerate the crack re-initiation beyond the treated holes if this stress increase coincides with the weld toe.

To study this effect for the more complex geometry of a tubular joint, an FE model was created to replicate the stresses introduced by the cold expansion. In the tests (Chapter 6), the amount of cold expansion to the holes did not exceed 0.5% of the hole diameter. However, as shown in Figure 7-11 this resulted in an induced  $\sim 175$  MPa tensile stresses at the weld toe where the crack re-initiated in the experiments.

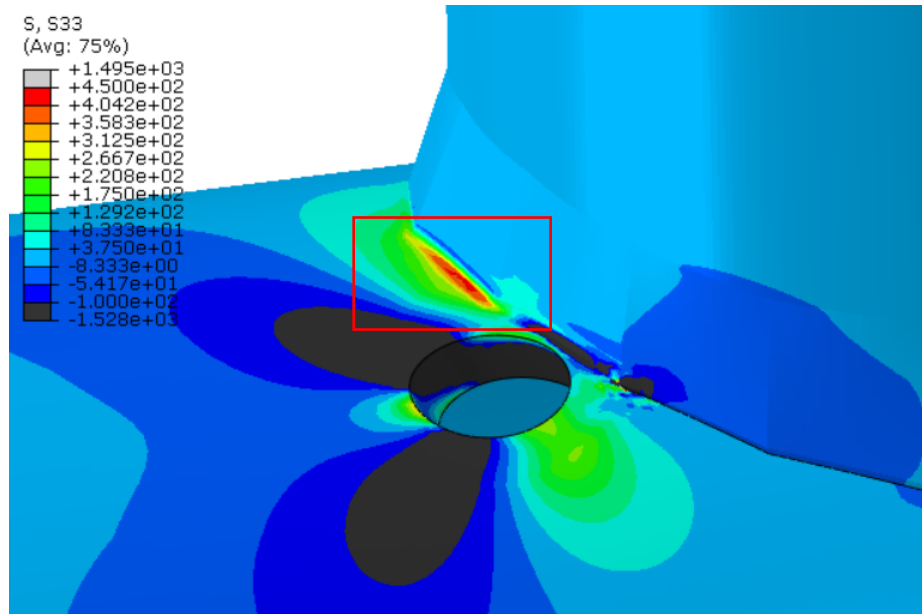


Figure 7-11: Cold expansion of 0.1 mm performed on specimen DT2 (Stresses are shown in MPa).

In hindsight, with the information about where the crack initiated, it can be concluded that cold expansion did not necessarily improve the fatigue life of the repaired detail. Such an increase of stresses would be regarded as a change in mean stress at the weld toe, the mean stresses in normally ignored for tubular joints as it is assumed that the weld toe mean stresses already equal to the yield stress and any additional stresses will shake down the existing one and maintain a mean stress equal to the yield stress. However, it is believed that the mean stress of already cracked and repaired tubular joints has an influence on the remaining fatigue life.

In OTH 89 307 [3], crack-tip holes were used to arrest through-thickness cracks on tubular joints, followed by cold expansion that increased the holes' diameter by approximately 6%. In order to understand the effect this had on the results reported by Tubby [3], a similar FE model was made also for these joints. This FE analysis indicated as shown in Figure 10, that a 6% increase in the diameter by cold expansion generated 400 MPa tensile stresses (three times higher than the 0.5% increase in diameter) at the weld toe beyond the crack-tip holes. As a result, the cracks in the study by Tubby [3] could possibly have re-initiated beyond the hole as in the experimental work presented in chapter 6. However,

it can be debated whether this would in principle have occurred with or without cold expansion.

In the experiments presented in chapter 6, two specimens were repaired with crack-tip holes without cold expansion. In both cases, the tests showed crack re-initiation at the weld toe slightly away from the drilled hole then back coalesce into the hole. That can be due to one or more of the following reasons.

- The difference of mean stress field at the hole circumference and the weld toe,
- the weld has already accumulated damage from the precracking stage, but the drilled hole circumference has a reinstated fatigue strength.

As a result, it is believed that in the work of Tubby [3] the crack re-initiated beyond the hole where the maximum tensile stresses at the weld toe from the cold expansion occurs, as shown in Figure 10.

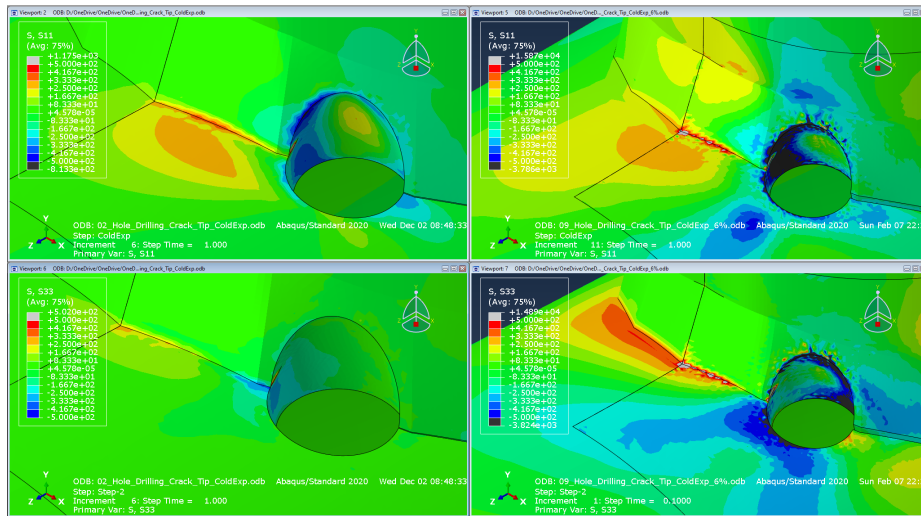


Figure 7-12: the influence of cold expansion on crack-tip holes of 18.1 mm diameter (left, 0.5% diameter increase, right, 6% increase in the diameter). Upper figures in the weld toe are showing the tangential stresses (MPa) while the lower ones show the radial direction of stresses (MPa).

## **7.6 Grinding**

As described in section 2.5.5, weld toe grinding using rotary burr is an efficient and widely acknowledged technique to improve the fatigue life of welds. In the present work, grinding has been performed for the following specimens:

- DT3\_Q3\_H3\_D\_L53\_G, crack deflecting hole drilled at 53°
- DT3\_Q3\_H4\_T\_L53\_G, crack tip hole drilled at 53°
- DT4\_Q1\_H4\_D\_L50\_GC, cold expanded crack deflecting hole at 50°

From these, only specimen DT3\_Q3\_H3\_D\_L53\_G is relevant to assess weld toe grinding in combination with crack deflecting hole. From Figure 7-8, weld toe grinding for this specimen did not significantly improve the fatigue life of the repaired joint.

As previously described in section 2.5.5, DNV RP C203 [6] provides a simplified method to account for weld toe grinding by increasing the fatigue life by a factor of 0.01fy for specified yield strength less than 350 MPa and 3.5 for specified yield strength higher than 350 MPa. In MSL [42], a single factor on the fatigue life of 2.2 is considered, which has been an often used "rule of thumb" for the effect of grinding. These improvements are applicable on long term stress range distribution that corresponds to service life of 20 years or more. In addition, DNV RP C203 [6] provides an improved set of S-N curves for weld that are toe grinded .

BS 7608 [60] also provide an improved S-N curves for weld toe grinding where the fatigue strength at  $10^7$  cycles is enhanced by a factor of 1.5 and the curve is rotated by a slope of  $m = 3.5$  compared to universal SN curve.

Both the modified SN curves in DNV RP C203 [6] and BS 7608 [60] to account for grinding are based on the universal S-N curves, as shown in Figure 7-13. These primarily indicate an improvement of the S-N curve for  $N > 10^5$ . It is also stated in DNV RP C203 [6] and the improvement on the fatigue life shown above does not apply for low cycle fatigue in the region  $N < 10^5$ .

The curves by BS 7608 [60] show slightly better fatigue performance than the ones from DNV RP C203 [6]. Applied to the universal T-curve, the first has a  $\log(a_1)$  intercept of 14.00 while the latter has a  $\log(a_1)$  of 13.91 which results

in BS 7608 [60] has a higher fatigue life by 6.5% for a given stress compared to DNV RP C203 [6].

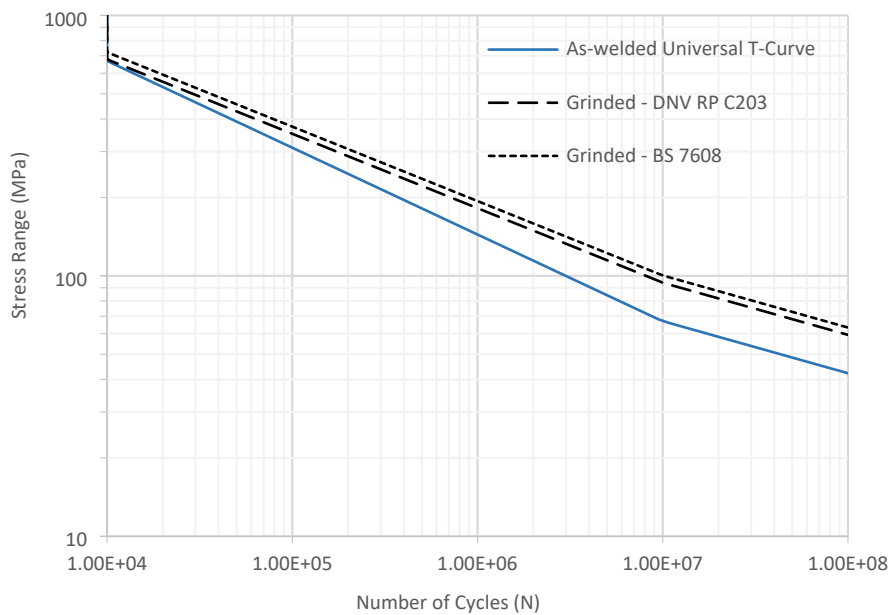


Figure 7-13: Modification to design T curve for untreated weld resulting from weld toe dressing as per DNV RP C203 [6] and BS 7608 [60].

The tested specimen showed a fatigue life for crack re-initiation after repair ( $N_1 * -Ni2$ ) of 37,000 cycles, which falls in the low cycle fatigue region. Comparing the as-welded universal T curve with the improved curves from DNV RP C203 [6] and BS 7608 [60] (extrapolated into the LCF region) in Figure 7-13, it is shown that for specimens with an estimated fatigue life below  $N < 10^5$ , there is no significant improvement expected in the fatigue life from weld toe grinding.

The improvement due to grinding on the SN curves from DNV RP C203 [6] and BS 7608 [60] is not believed to be applicable in the LCF region, as supported by the findings of for example Haagenen [56]. Hence, the results seen for this specimen is as expected.

However, in the LCF region, strain-life approach is known to be a better estimate of the fatigue life performance of welded specimens than the stress-life approach.

### **7.7 Remedial grinding (grooving)**

As described in chapter 2, remedial grinding (also often called grooving) is also used as a repair method, particularly for deeper cracks, to remove the crack and achieve a smooth excavation profile without abrupt variations in depth. However, it is normally required that a proper analysis of stresses and fatigue capacity is performed for the repaired specimen, e.g., to study the increased stress in the groove [65].

In the present work, remedial grinding was used for the specimen DT4\_Q1\_H3\_D\_L48\_GR. The purpose of using remedial grinding was to shorten the crack prior to drilling the crack deflection holes due to the findings that crack deflection holes at smaller angles were beneficial. However, Table 7-3 and Figure 7-3 show that, remedial grinding to shorten the crack length was unsuccessful.

As shown in chapter 6, upon reloading the specimen after repair with remedial grinding, a new crack re-initiated beyond the hole before developing a through-thickness crack leading to  $N_i^*$  higher than  $N_i^2$ . Hence, the negative  $eR$ .

To study the effect of grooves by remedial grinding, an FE analysis was performed on a tubular member welded to a plate with an added groove, as shown in Figure 7-14. The main purpose of this study was to identify the magnification of the local stress at the groove, due to burr grinding, compared to the hot-spot stress at the weld toe. The analysis considered the effect of the grinding depth and width on the stress field. The load applied as a tensile unit load on the tubular member. The model is idealised as a 2D axisymmetric solid of revolution with elastic material.

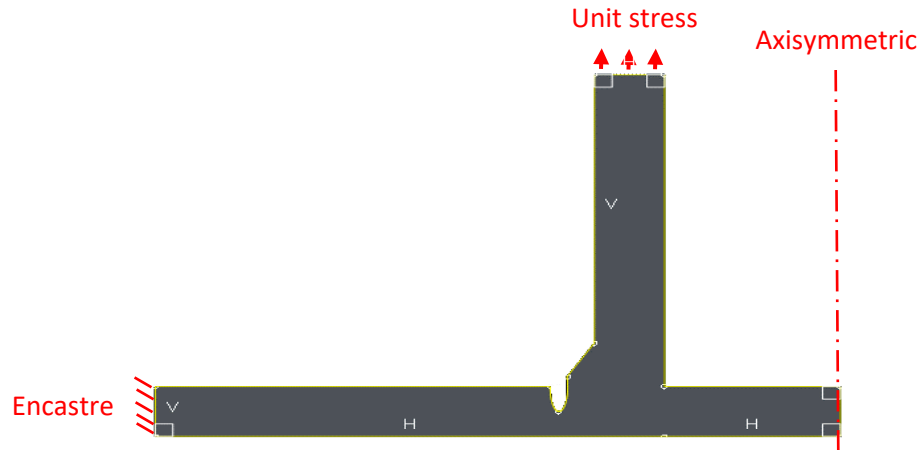


Figure 7-14: Idealised model for a tubular member welded to a base plate.

A parametric study was performed on remedial grinding for a range of excavation width and depth. The grinding profile is considered as a half ellipse with depth 'a' and width '2c' as shown in Figure 7-15. Details of the grinding profiles can be found in Table 7-4.

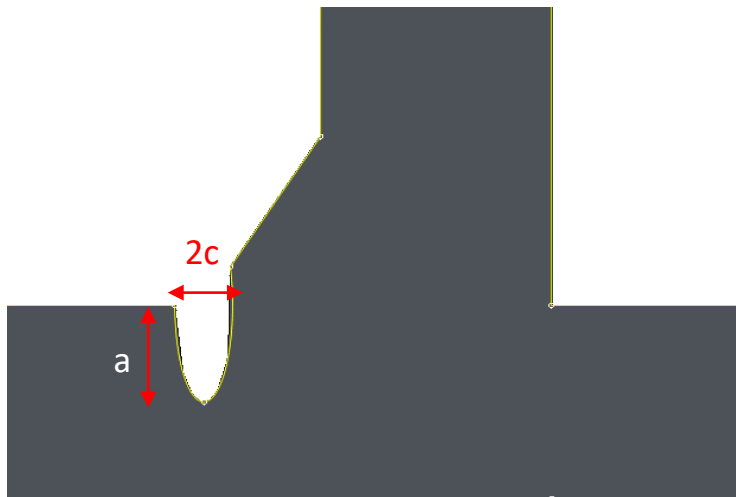


Figure 7-15: Idealised model for a tubular member welded to a base plate of 8 mm thickness.

In Table 7-4 and Figure 7-16 the different grinding grooves are presented along with the stress concentration increase seen. In the as-is case (no groove grinded)

the SCF was found to be 8.74. The added magnification of this stress is illustrated for each groove configuration evaluated.

Model	2c (mm)	A (mm)	Groove Stress (MPa)	SCF	Notch Stress/SCF (MPa)	a/2c	a/t
As-Is	-	-	-	8.74	-	-	-
1	2	2	39.3	-	4.49	1.00	0.25
2	2	4	59.0	-	6.75	2.00	0.5
3	2	6	41.3	-	4.72	3.00	0.75
4	4	2	24.3	-	2.78	0.50	0.25
5	4	4	33.1	-	3.79	1.00	0.5
6	4	6	27.3	-	3.12	1.50	0.75
7	6	2	20.7	-	2.37	0.33	0.25
8	6	4	25.6	-	2.93	0.67	0.5
9	6	6	24.9	-	2.85	1.00	0.75

Table 7-4: Results of the study on grinding profile.

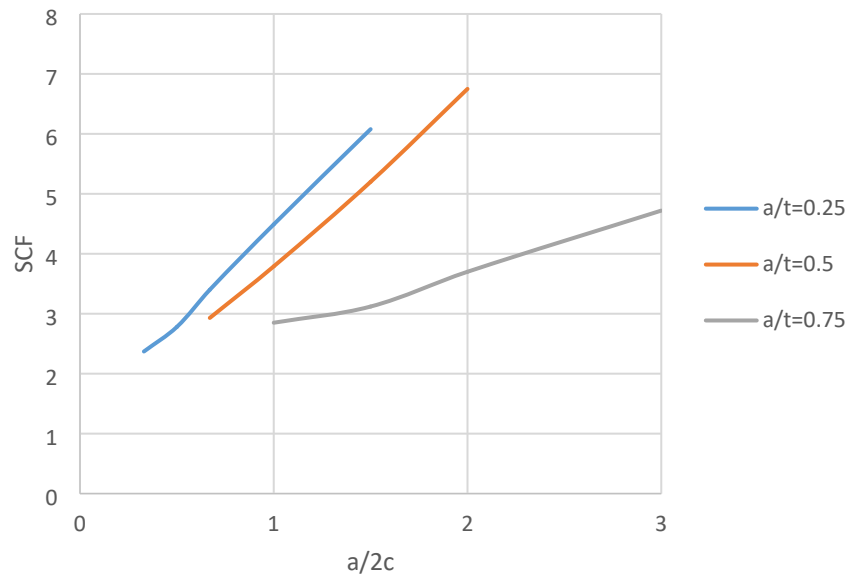


Figure 7-16: SCF increase as a function of remedial grinding profile.



This analysis shows that for an excavation of 35% in the plate thickness (approximately used in this specimen), the stress at the notch increased by three times for a  $a/2c$  around 0.67, compared to a specimen without remedial grinding. Hence, the partial grinding in the chord thickness induced high stress concentrations at the bottom of the groove. This was combined with the deformation stresses and resulted in a fast crack initiation from the groove without any significant benefit to the fatigue life.

Further work is required to establish an optimum excavation shape to minimise stress and hence provide the maximum remaining life.

## **7.8 Crack tip holes**

A common way of repair of hole drilling is by crack tip holes. The use of crack tip holes for repair of fatigue cracked tubular joints was studied by Tubby [3], as further described in Chapter 2. The conclusion in this study was essentially that hole drilling was not very effective compared to grinding, but not without effect. It should be noted that in the study by Tubby [3] the cracks studied were not through thickness and grinding was an option. At present, the inspection of jacket structures is normally performed by flooded member detection (FMD) and cracks are not discovered before they are through thickness. Hence, grinding is less relevant as a repair method, particularly the only repair method.

In the present work, crack-tip hole was used for the specimen DT3\_Q3\_H4\_T\_L53\_G. The specimen had the crack repaired on one side with crack-tip hole and the other with crack deflecting hole. Both were mirrored around the saddle centre at an angle of  $53^\circ$ . The purpose of using crack-tip hole was to compare its performance to crack-deflecting hole.

Based on Table 7-3 it can be seen that, as expected crack deflection holes performed better than crack-tip holes, with  $N_1-N_2$  of 37,000 cycles compared to 28,200 cycles, respectively. The Crack-tip hole showed an  $eR$  of 7.9%, while the crack deflecting hole showed an  $eR$  of 6.1%.

As a result, it is indicated that crack deflecting hole and performing better than crack-tip holes given that the crack deflects into the hole.

## **8 Repair evaluation methodology**

In this chapter a methodology for evaluating the usefulness of crack deflecting holes as a repair method is described. Based on the findings of this work, a preliminary recommendation for a crack evaluation process is suggested as shown in Figure 8-1. It needs to be mentioned that these recommendations are based on a limited number of joints and loading conditions tested, and further research is expected to improve and possibly change these findings.

Upon identifying a crack within a tubular joint of an offshore installation, an immediate assessment of the overall structural integrity is essential. This is to evaluate whether the structure can sustain its specified load-bearing capacity, considering the presence of the crack and its current size. In extreme loading conditions associated with the Ultimate Limit State (ULS), the potential for both the development of a brittle fracture and a ductile overload of the reduced section area are a significant threat.

Brittle fracture, characterized by the sudden propagation of a crack with minimal plastic deformation, can be particularly catastrophic due to its rapid and unexpected nature. The potential consequences of such a fracture increases when the crack expands to its critical length under ULS loading conditions. This is attributed to the fact that, under these extreme load conditions, the stress intensity factor at the crack tip may meet or exceed the material's fracture toughness. The result would be the initiation of a rapid, brittle fracture without prior plastic deformation or warning. Detailed assessment of the ultimate strength of cracked tubular joints can be found in references [69-70].

If the load-bearing capacity of the cracked joint is deemed insufficient, the affected detail must be addressed and repaired using a method that restores the structure's load-bearing capacity. Various strategies can be deployed to enhance the load-bearing capacity under such circumstances, ensuring the structural integrity and safety of the offshore installation. Although repairing the joint with crack-deflecting holes may have the potential to reduce the chance of brittle fracture, as it removes the sharp crack-tip and diminishes the stress intensity factor, it may not be the most suitable repair method.

Nevertheless, if the structure is deemed capable of retaining its load-bearing capacity despite the crack, then introducing crack-deflecting holes could be a viable option to enhance the Fatigue Limit State (FLS) of the cracked joint, as illustrated in Figure 8-1. Based on the work presented in this thesis, crack deflecting holes can be used to delay additional cracking of the joint and may particularly be an attractive alternative. There are multiple factors that influence the effectiveness of crack deflecting holes in this respect. These include, but are not limited to, the crack length; the ratio of the crack length to the circumference of the brace-to-chord intersection (crack angle) and the level of applied load.

The flow chart in Figure 8-1 illustrates a potential process for determining the effectiveness of the crack deflection holes repair. In the initial assessment, the chart indicates that repair by crack deflection holes is primarily relevant when the crack is through-thickness. This aligns with earlier findings that remedial grinding is a preferred repair method when the crack is not through-thickness (Tubby 1987) [3]. The crack angle, as mentioned earlier, serves as a measure of the crack length. As shown in Figure 7-5, the efficacy of a crack deflection repair decreases with an increasing crack angle (i.e., crack length). The subsequent decision box addresses the scenario of crack arrest, questioning whether the fatigue damage is within the high-cycle or low-cycle fatigue domain. As shown earlier in this thesis, the stresses increase in front of the crack tip as the crack grows in length. Although, the crack deflection hole reduces this stress, the stresses can increase to a level where low-cycle fatigue occurs. In such instances, the crack deflection repair is anticipated to be less effective. Moreover, the burr grinding, recommended alongside the crack deflection repair, also exhibits reduced efficiency for low-cycle fatigue.

With the crack deflecting hole drilling process, it is anticipated that the crack will propagate towards the drilled holes and subsequently get arrested. Consequently, the region enduring the maximum stress within the joint is located behind these holes, as illustrated at location 3 in Figure 7-1/c. This zone then becomes susceptible to new crack initiation. The time span required for this new crack initiation at location 3 serves as a benchmark for evaluating the effectiveness of the repair technique. If this period just surpasses the residual fatigue life of the joint in its cracked, yet unrepaired state, the repair method can be deemed beneficial (better than not repairing). However, if the duration leading up to a new crack initiation mirrors that of the original crack initiation

of the intact joint, the repair technique can be acclaimed as highly effective. It's worthy to note that, under identical nominal stresses applied to both the intact and the repaired joints, the latter is expected to exhibit a lower fatigue life. This reduction is attributed to the stress increase due to the stiffness loss resulting from the crack and the drilled hole—a theory that holds true.

To prolong the onset of new crack initiation, a technique involving weld toe improvement, specifically burr grinding, should be employed to enhance the joint's endurance. The performance of the weld toe grinding is dependent upon the magnitude of the stress level and its classification within the high or low-cycle fatigue domains. Optimal outcomes are anticipated when the joint's repaired state operates within the high-cycle fatigue domain, while the converse holds true in the context of the low-cycle fatigue domain.

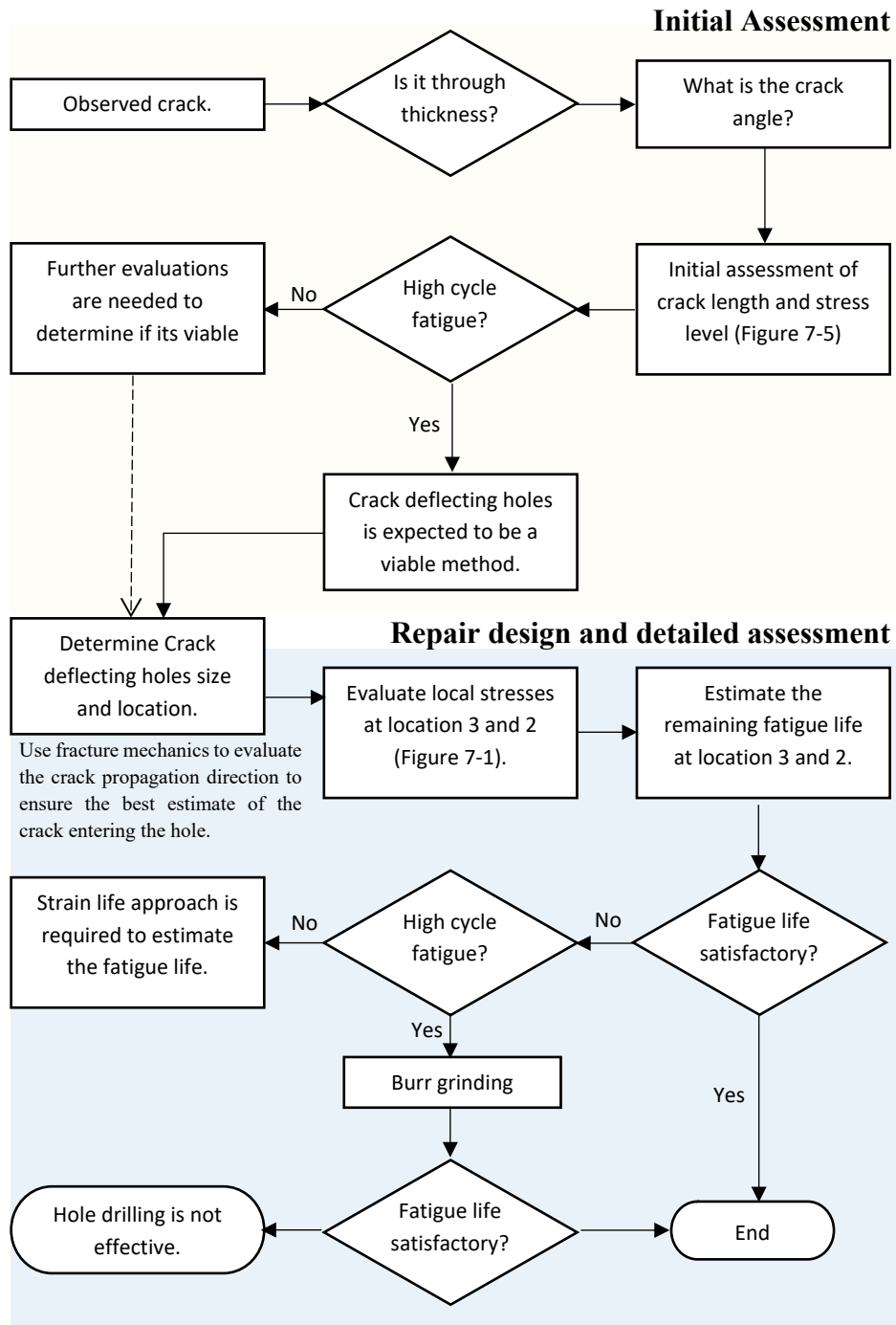


Figure 8-1: Design methodology flowchart

The flow diagram in Figure 7-14 indicates that the crack deflection repair method primarily is expected to be efficient if the stresses at location 3 is in a region leading to high-cycle fatigue. The effectiveness of crack deflection repair was further investigated by Riise (2023) [66], in a master thesis work supervised as part of this work. The indication from the work of Riise (2023) [66] is that crack deflection repair possibly reinstates the original fatigue life if the stresses are in the high-cycle fatigue region. However, it needs to be mentioned that the work of Riise (2023) consisted of one singular test joint, and more tests are needed to confirm these results. In addition, as also indicated, strain life analysis may be performed to further evaluate the efficiency of the repair method, which is particularly relevant if stresses are in the low-cycle fatigue domain.

In the performance of the repair, it is crucial to accurately determine the crack-tip location using the most accurate and reasonably practical inspection techniques available. This ensures the minimised risk of missing the crack-tip by the drilled hole. While the initial phase of repair design involves determining the hole diameter and its position in relation to the crack-tip, this specific aspect is not addressed in this thesis. Nevertheless, preliminary research, as cited in Atteya et al. [52], offers valuable insights for determining optimal hole locations. The fundamental principle guiding the selection of hole diameter and position is to strategically position the holes in proximity to, yet sufficiently distant from, the weld toe. This strategy aims to alter the crack propagation trajectory, redirecting it towards the drilled hole. The significant advantage of this approach is the redirection of the crack away from the weld toe, ensuring its arrest within the drilled hole in the base material of the chord. To accommodate uncertainties in pinpointing the most accurate crack-tip location, the drilled holes can be set with a margin ahead of the anticipated crack-tip.

## **9 Summary, conclusion and further work**

### **9.1 Summary**

The pursuit of an efficient temporary repair solution for cracked tubular joints in offshore structures has led to the exploration of various methods and techniques. The focus in this work has been on the use of crack deflecting holes as a crack arrestor, while also considering crack tip holes. Supplementary techniques to enhance the performance of crack deflecting holes, such as cold expansion, weld toe grinding and grooving has also been included in this work. The primary objective was to assess the effectiveness of crack deflecting holes in arresting weld cracks and compare their performance to conventional crack tip holes, aiming to provide a comprehensive understanding of the fatigue performance of crack deflecting holes.

To achieve these goals, this research has experimentally investigated the fatigue life of cracked tubular joints repaired by hole drilling. In addition, numerical evaluations of the stress field and stress concentration factors around intact, cracked and repaired joints have been performed using finite element analysis. This research has offered valuable insights into the factors influencing the effectiveness of the repair method, including;

- Revealing unexpected fatigue crack initiation after hole drilling and reverse coalescence at the weld toe behind the drilled hole for both crack-deflecting and crack-tip holes.
- Improved physical understanding of the local stresses in the vicinity of the repaired area and its influence on the fatigue performance of the repaired joint including a novel method to present stresses in cracked and hole drilled specimens (Figure 7-5).
- Indications that crack deflecting holes maybe an effective repair method for tubular joints under certain circumstances and developed a methodology to evaluate the repair performance of hole drilling in tubular joints.
- A statistical evaluation of the measured SCF from 15 hot-spot locations and improved understanding of the uncertainty on the SCF

estimation and its influence on the requirements for determining the SCFs using FE.

- Using fatigue test data to find a relationship between crack aspect ratio against number of cycles which will be useful in estimating the remaining of cracked tubular joint and fracture mechanics analysis of tubular joints to determine the transition from a surface crack to through-thickness crack.

Fatigue testing was conducted for hole drilling repair techniques (crack deflecting holes and crack tip holes) with various additional repair improvement techniques (cold expansion of the holes, weld toe improvement by grinding and remedial grinding). Additionally, each repair method was evaluated based on the findings from finite element analyses, enabling the identification of the most promising techniques for the repair of cracked tubular joints in offshore structures.

## **9.2 Concluding remarks**

The following remarks present the conclusions drawn from the findings of this work, related to factors influencing the SCFs, fatigue strength of unrepaired joints, performance of crack deflecting holes and the impact of supplementary repair techniques. All these findings could have impact on future design and repair methods for tubular joints in offshore structures.

- SCFs determined using detailed finite element analysis were subject to variations depending on the mesh size, the choice of element type (linear or quadratic), the method for deriving the SCF (directly extracted or linearly extrapolated) and the modelling of the weld profile. In general, a higher SCF was obtained with a finer mesh, quadratic elements, linear extrapolation and a larger weld profile.
- The experimentally determined SCFs also show variations caused by the weld profile, strain gauge positions and other inherent uncertainties. Comparison of the experimental SCFs with the SCF from detailed finite element analysis for a matching weld profile showed good agreement thereby validating the finite element approach.



- SCFs obtained from the parametric equations of Efthymiou [13] given in design codes ISO 19902 [1] and DNV-RP-C203 [4] were a reasonable upper bound to the variations in the values obtained experimentally and by a detailed finite element analysis. Hence, these results provide continued support for the use of these equations in design.

Based on the work of Tubby [3] as described in Section 2.5.3, it was assumed that a through thickness crack in a tubular joint repaired with crack-tip holes would propagate into the crack deflecting hole. The crack will then stay dormant in the hole for a period, until the crack start to grow from the hole. In order to slow the crack re-initiation from the hole, cold expansion should be used. This was assumed as the initial hypothesis for this work also for crack deflection holes. Based on the experimental work of this thesis, the following improvements to this hypothesis was identified:

- When the original crack propagated into the crack deflecting hole, a new crack did not originate from the hole itself. Instead, the new crack initiation occurred at the weld toe, just a short distance away from the hole. Subsequently, the crack grew back towards the hole, eventually merging with the original crack. This phenomenon, observed in all repairs involving crack deflecting holes, has been termed "reverse coalescence."
- The fatigue performance of crack deflecting hole repair is highly dependent on the crack length around the weld toe. The shorter the crack length with respect to the joint size, yet a through-thickness crack, the better the effectiveness of crack-deflecting holes.
- The fatigue performance of crack deflecting holes for the specimens investigated are better than crack tip holes given that the crack deflects into the hole.
- Cold expansion process for tubular joints is a double edge technique. It helps in delaying cracks reinitiating from the hole. However, it induces tangential tensile stresses at the neighbour material, possibly leading to earlier crack initiation from stress risers in the neighbour material.

- Weld toe improvement using grinding did not improve the fatigue life of the repaired joints. However, this is assumed to be due to the high cycle stress range (low cycle fatigue) applied to the ground weld toe of the specimens in this work. In contrast, for high cycle fatigue grinding is expected to improve the fatigue life, which has been shown by Riise (2023) in work supervised as a part of this project.
- Grooving to shorten the crack length was unsuccessful as partial removal of material in the chord thickness induced high stress concentrations at the bottom of the grooves.

As mentioned above, the findings from this research required a revision of our initial hypothesis, based on a better understanding of crack behaviour and repair techniques. The discovery of "reverse coalescence" (a new crack originating from the weld toe and growing back towards the hole) revises our expectations about crack propagation. Further, it has been shown that the effectiveness of crack-deflecting holes is highly dependent on the crack length. Additionally, the understanding of the local stress fields and cracking pattern have refined our assumptions about crack arresting and the potential for increased fatigue life. Moreover, the uncertain effects of the cold expansion process and the limited success of weld toe grinding and grooving required a reassessment of the efficacy of these techniques. Collectively, these findings serve as the basis for an updated hypothesis, providing a more comprehensive understanding of the mechanisms involved. The updated hypothesis is provided in the following points:

- The existing crack is predicted to grow and propagate into the crack deflecting hole.
- There is an expected period of latency in this stage, during which the crack will remain dormant. This period can be indicated as the actual gain in the fatigue life by this repair method.
- New crack(s) are anticipated to originate beyond the hole (as indicated at location 3 in Figure 9-1) and eventually this new crack will merge either with the original crack or the drilled hole (reverse coalescence)
- The angle  $\alpha$  is identified as the key parameter influencing the efficiency of the repair. Efforts should be undertaken to minimise this angle as

much as practical (for example by early detection of through thickness cracks).

- Cold expansion is not considered advantageous, given that it fails to induce compressive residual stresses where they are most required.
- Remedial grinding, also known as grooving, is not deemed beneficial due to two main reasons:
  - The groove introduces an increase in stress, thereby reducing the crack initiation fatigue life beyond the hole.
  - The crack is likely to follow the stress increase presents in the groove, preventing it from entering the crack deflection hole.
- Grinding of location 3 might prove beneficial under lower levels of stress ranges than those observed in these experiments.

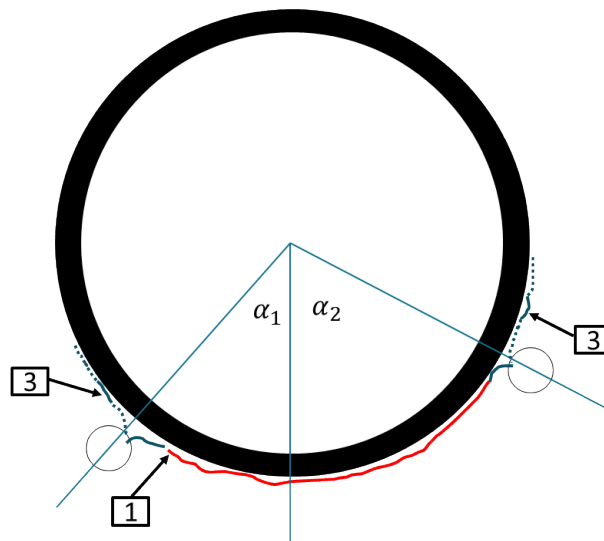


Figure 9-1: Typical cracking pattern during fatigue testing.

### 9.3 Reflecting on Tubby's research in hindsight of current findings

Given the insights from the current experimental tests, it is interesting to re-examine Tubby's research (1989). There are indications suggesting that Tubby also noted the occurrence of new crack formation, although it appears that the significance of this observation was not fully recognized, as per his report. He noted, "there was also a tendency for cracks to initiate at the chord toe ahead of those spreading from the holes", which implies that while the new cracks were observed, the prevailing belief was that the new cracks originated from the hole. However, this phenomenon could equally be an instance of reverse coalescence. As depicted in Figure 9-2 from Tubby's work, it is evident that new cracks developed around two of the holes in a manner similar to what has been found in the current study.

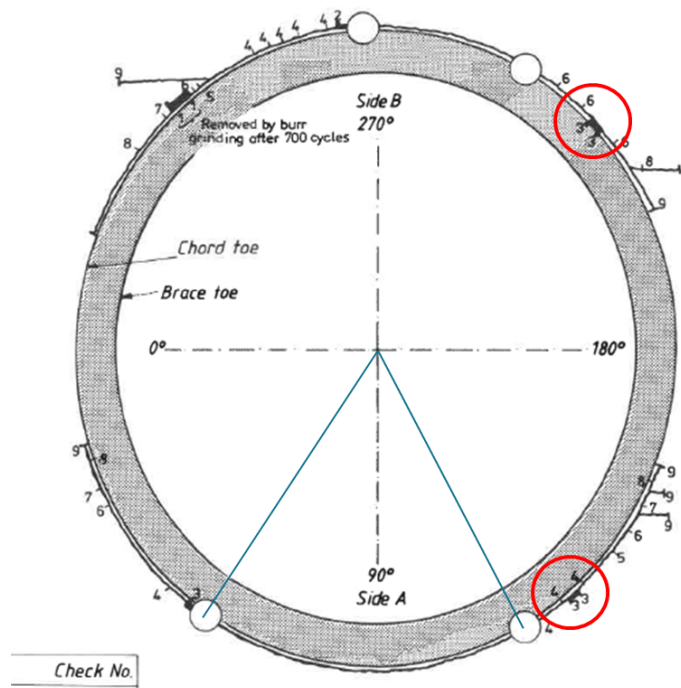


Figure 9-2: crack treated by hole drilling and cold expansion process (Courtesy of the UK Department of Energy) [3]

Further, the crack-tip holes in Tubby's work were cold expanded increasing the hole diameter by approximately 6%. In order to understand the effect this had on the results reported by Tubby [3], a FE model was made also for these joints indicating that this level of cold expansion generated a 400 MPa tensile stress at location 3 at the weld toe, as shown in Figure 7-11. As a result, it is believed that in the work of Tubby [3] the crack re-initiated at the weld toe beyond the hole at the location of the maximum tensile stresses from the cold expansion, as shown in Figure 7-11. However, it can be debated whether this would in principle have occurred with or without cold expansion.

#### **9.4 Scientific contribution**

This work has shown that crack-deflecting holes could be a way of arresting and delaying crack growth in welded tubular joints, which would primarily be effective for incipient through-thickness cracks. It also has been shown experimentally that crack-deflecting holes are more effective than crack-tip holes. In addition, it has been shown experimentally that cold expansion of drilled holes in the vicinity of the weld toe does not provide an improvement to the hole drilling repair method. Furthermore, it has been shown numerically that cold expansion may induce unfavourable tangential tensile stresses at the weld-toe, that could explain the premature crack initiation behind the hole.

The work in this PhD thesis has revealed and explained an unexpected fatigue crack behaviour for cracked tubular joints repaired by crack-deflection and crack-tip holes. This unexpected fatigue crack behaviour included crack initiation at the weld toe behind the drilled hole and reverse coalescence back to the hole or the lead crack, in contrast to crack initiation from the drilled holes as assumed in earlier work. Reverse coalescence has been explained by determination of the SCFs and fatigue resistance associated with the repair configuration.

#### **9.5 Suggestions for further work**

Future research should focus on optimizing the shape, size and position of the crack-deflecting holes in order to promote crack initiation from the hole itself, rather than the weld-toe. This optimization should take into consideration the stress state in the vicinity of the drilled hole and fatigue resistance in order to

maximize the effectiveness of the crack-deflecting holes for various joint configurations.

Investigating different joint types and geometry ranges is another area worth exploring, as it would provide insights into the applicability of crack-deflecting holes and other repair techniques across a wider range of joint configurations. Producing new life extension curves as a power function, similar to Figure 7-9 would be beneficial for understanding the behaviour of these joint types under various repair scenarios.

Additionally, it is crucial to study the impact of different loading types on the performance of crack-deflecting holes and other repair techniques. By examining various loading conditions, researchers can better understand the fatigue behaviour of repaired joints and tailor repair methods to suit specific loading requirements, ultimately contributing to more effective repair strategies for cracked tubular joints.

## References

1. Clauss, G., E. Lehmann, and C. Östergaard, *Offshore Structures*. 1992.
2. Limited, M.E., *Strengthening, modification and repair of offshore installations*. 1995.
3. Tubby, P.J., *Fatigue performance of repaired tubular joints*, D.o. Energy, Editor. 1989, Department of Energy: Her Majesty's Stationery Office.
4. John V. Sharp, G.E., *Underwater inspection and repair of offshore structures*. First ed. 2021: Wiley.
5. Basquin, O.H. *The exponential law of the endurance tests*. in *American Society for Testing and Materials (ASTM)*. 1910.
6. DNV, *DNV-RP-C203 Fatigue design of offshore steel structures*. 2021.
7. Standard, I., *Petroleum and natural gas industries - Fixed steel offshore structures*. 2020.
8. Institute, A.P., *Planning, Designing and Constructing Fixed Offshore Platforms*. 2020.
9. ISO, *ISO 19902 Petroleum and natural gas industries — Fixed steel offshore structures*. 2020.
10. UEG, *Design of tubular joints for offshore structures*. Vol. 2. 1985: UEG Offshore Research. 868.
11. Committee, U.-I.S., *United Kingdom Offshore Steels Research Project - Phase II, Final Summary Report*. 1987, The Department of Energy: London. p. 133.
12. Gibstein, M.B., *Parametric stress analysis of T joints*, in *European offshore steels research seminar*. 1978: Cambridge, UK.
13. R S Peckover, R.A.W.F., H G Crisp, D Long, E A Chadwick, T W Thorpe, *United Kingdom Offshore Steels Research Project - Phase 1, Final Report*. 1988, Department of Energy: London.
14. C R A Schneider and S J Maddox, T., *Best practice guide on statistical analysis of fatigue data*. 2003, International institute of welding.
15. MaTSU, F.C.L.a., *Background to new fatigue guidance for steel joints and connections offshore structures*. 1992, Health and Safety Executive: London.
16. Group, C.U.E., *Design of tubular joints for offshore structures*. 1985: UEG.
17. Lotsberg, I., *Fatigue design of marine structures*, ed. C.u. press. 2016.
18. Society, A.W., *AWS D1.1/D1.1M Structural Welding Code - Steel*. 2020.

19. Fricke, W. *Recommended Hot Spot Analysis Procedure For Structural Details of FPSOs And Ships Based On Round-Robin FE Analyses*. in *The Eleventh International Offshore and Polar Engineering Conference*. 2001.
20. Zhang, Y.H. and A. Stacey. *Review and assessment of fatigue data for offshore structural components containing through-thickness cracks*. in *International Conference on Offshore Mechanics and Arctic Engineering OMAE2008*. 2008. Estoril, Portugal.
21. Tweed, J.H., *Remainin life of defective tubular joints - An assessment based on surface crack growth in tubular joint fatigue tests* 1987, Department of Energy: London.
22. Tweed, J.H., *Remaining life of defective tubular joints: Depth of crack growth in UKOSRP II and implications*. 1987, Department of Energy: London.
23. Tweed, J.H., *Surface crack growth behaviour of UKOSRP-II joints and implications for prediction of remaining life of defective tubular joints*, in *Steel in marine structures*, C. Noordhoek and J.d. Back, Editors. 1987, Elsevier: Delft, The Netherlands.
24. Rhee, H.C. and M.F. Kanninen, *Opportunities for Application of Fracture Mechanics for Offshore Structures*. *Applied Mechanics Reviews*, 1988. **41**(2): p. 23-35.
25. Haswell, J. and P. Hopkins, *A Review of Fracture Mechanics Models of Tubular Joints*. *Fatigue & Fracture of Engineering Materials & Structures*, 1991. **14**: p. 15.
26. Rhee, H.C., *Fatigue crack growth analyses of offshore structural tubular joints*. *Engineering Fracture Mechanics*, 1989. **34**(5-6): p. 1231-1239.
27. Laham, S. and B. FM, *The Ultimate Strength of Cracked Tubular K-Joints*. 1997.
28. Cao, J.J., et al., *Crack modeling in FE analysis of circular tubular joints*. *Engineering Fracture Mechanics*, 1998. **61**: p. 537-553.
29. Bowness, D. and M.M.K. Lee, *Fracture Mechanics Assessment of Fatigue Cracks in Offshore Tubular Structures*. 2002: HSE Books.
30. Lee, M.M.K. and D. Bowness, *Estimation of stress intensity factor solutions for weld toe cracks in offshore tubular joints*. *International Journal of Fatigue*, 2002. **24**: p. 861–875.
31. Chiew, S.P., et al. *Parametric equations for stress intensity factors of cracked tubular T&Y-joints*. in *The Thirteenth International Offshore and Polar Engineering Conference*. 2003. Honolulu, Hawaii, USA.



32. Lie, S.T., C.K. Lee, and S.M. Wong, *Model and mesh generation of cracked tubular Y-joints*. Engineering Fracture Mechanics, 2003. **70**: p. 161–184.
33. YongBo, S. and L.S. Tjhen, *Parametric equation of stress intensity factor for tubular K-joint under balanced axial loads*. International Journal of Fatigue, 2005. **27**(6): p. 666-679.
34. Lie, S.T., T. Li, and Y.B. Shao, *Stress intensity factors of tubular T/Y-joints subjected to three basic loading*. Advanced Steel Construction, 2016. **12**: p. 109-123.
35. Yagi, K., et al., *Evaluation of crack propagation behaviors in a T-shaped tubular joint employing tetrahedral FE modeling*. International Journal of Fatigue, 2017. **96**: p. 270-282.
36. Chiew, S.P., et al. *Parametric Equations for Stress Intensity Factors of Cracked Tubular T&Y-Joints*. in *International Offshore and Polar Engineering Conference*. 2003. Honolulu, Hawaii, USA.
37. Lie, S.T., T. Li, and Y.B. Shao, *Stress Intensity Factors of Tubular T/Y-Joints Subjected to Three Basic Loading*. Advanced Steel Construction, 2016. **12**: p. 109-133.
38. Borges, L., et al., *Advanced Numerical Modeling of Cracked Tubular K Joints: BEM and FEM Comparison*. Journal of Bridge Engineering, 2012. **17**(3): p. 432-442.
39. Rhee, H.C., *The behavior of stress intensity factors of weld toe surface flaw of tubular X-joint*, in *Offshore technology conference*. 1986: Houston, Texas.
40. Zhang, Y.H. and A. Stacey. *Review and assessment of fatigue data for offshore structural components containing through-thickness cracks*. in *International Conference on Offshore Mechanics and Arctic Engineering*. 2008. Estoril, Portugal.
41. Branco, R., F.V. Antunes, and J.D. Costa, *A review on 3D-FE adaptive remeshing techniques for crack growth modelling*. Engineering Fracture Mechanics, 2015. **141**: p. 170-195.
42. Limited, M.E., *Strengthening, modification and repair of offshore installations*. 1995.
43. Limited, M.E., *Assessment of repair techniques for ageing or damaged structures*. 2004.
44. Wu, H., et al., *On the prediction of the residual fatigue life of cracked structures repaired by the stop-hole method*. International Journal of Fatigue, 2010. **32**: p. 670-677.

45. Chen, N.-Z., *A stop-hole method for marine and offshore structures*. International Journal of Fatigue, 2016. **88**: p. 49-57.
46. Ayatollahi, M.R., S.M.J. Razavi, and H.R. Chamani, *Fatigue Life Extension by Crack Repair Using Stop-hole Technique under Pure Mode-I and Pure mode-II Loading Conditions*. Procedia Engineering, 2014. **74**: p. 18-21.
47. Wu, H., et al., *On the prediction of the residual fatigue life of cracked structures repaired by the stop-hole method*. International Journal of Fatigue, 2010. **32**(4): p. 670-677.
48. Murdani, A., et al., *Stress concentration at stop-drilled holes and additional holes*. Engineering Failure Analysis, 2008. **15**(7): p. 810-819.
49. Song, P.S. and Y.L. Shieh, *Stop drilling procedure for fatigue life improvement*. International Journal of Fatigue, 2004. **26**(12): p. 1333-1339.
50. Shin C. S. , Wang C. M. , and S.P. S., *Fatigue damage repair: a comparison of some possible methods*. International Journal of Fatigue, 1996. **18**: p. 11.
51. Makabe, C., et al., *Crack-growth arrest by redirecting crack growth by drilling stop holes and inserting pins into them*. Engineering Failure Analysis, 2009. **16**(1): p. 475-483.
52. Atteya, M., et al. *Crack Arresting With Crack Deflecting Holes in Steel Plates*. in *ASME 2020 39th International Conference on Ocean, Offshore and Arctic Engineering*. 2020.
53. Robert J. Dexter, a.J.M.O., *Manual for Repair and Retrofit of Fatigue Cracks in Steel Bridges*. 2013.
54. Fisher, J., Barthelemy, B., and Mertz, D., *Fatigue behavior of full-scale welded bridge attachments*. 1980, Transportation Research Board.: Washington, D.C.
55. Fu, Y., et al., *Cold expansion technology of connection holes in aircraft structures: A review and prospect*. Chinese Journal of Aeronautics, 2015. **28**(4): p. 961-973.
56. Haagensen, P.J. *The Effect Of Grinding And Peening On The Fatigue Strength Of Welded T-joints*. in *Engineering Sciences*. 1993. WIT Press.
57. K.J. Kirkhope!, R.B., et al., *Weld detail fatigue life improvement techniques. Part 1: review*. Elsevier, 1999. **1**: p. 28.
58. MSL and D.A.F. Dier, *"Assessment of Repair Techniques for ageing or damaged structures" MMS*. 2004: p. 182.
59. MSL, *Strengthening modification and repair of offshore installation*. 1995.

## References

---

60. Institution, T.B.S., *BS 7608:2014+A1:2015 Guide to fatigue design and assessment of steel products*. 2015.
61. Clayton, A.M., *Assessment of UKOSRP crack growth data to investigate the remaining life of offshore structures after inspection*. 1982: London.
62. Ersdal, G., *Assessment of existing offshore structures for life extension*, in *Department of Mechanical and Structural Engineering and Material Science*. 2005, University of Stavanger, Norway.
63. Shipping, L.s.R.o., *Stress concentration factors for simple tubular joints: assessment of existing and development of new parametric formulae*. 1997. p. 106.
64. Efthymiou, M., *Development of SCF formulae and generalised influence functions for use in fatigue analysis.*, in *Recent development in tubular joints technology*. 1988: Surrey, UK.
65. Fjeldstad, A., et al., *Repair Methods for Loadbearing Steel Structures Operating on the Norwegian Continental Shelf*. 2022. p. 306-317.
66. Riise, S., *Experimental assessment of cracked tubular joints repaired with crack-deflecting holes and weld-toe grinding*. 2023. University of Stavanger, Norway
67. Standard Norge (2013) NORSOK N-004: *Design of steel structures, Rev. 3*, February 2013. Standard Norge, Lysaker, Norway
68. Standard Norge (2015), NORSOK N-006 *Assessment of structural integrity for existing offshore load-bearing structures, edition2; April 2015*, Standard Norge, Lysaker, Norway
69. S. A. L. Laham and F. M. Burdekin, *The ultimate strength of cracked tubular K-joints*, Report OTH 497, Health and Safety Executive, UK, 1997
70. F. M. Burdekin, G. J. Yang and J. Cao, *Assessment of fracture strength of cracked tubular joints*, Report OTH 554, Health and Safety Executive, UK, 1998

### Appendix 1 Fatigue testing database of tubular joints

The tables below provide the fatigue testing database collect from multiple resources, where the reference for each resource is provided in the second column. The database base is collected for the following joint parameters.

Total number of joint	<b>358</b>	T Joint	T	282
in Air	345	Non-overlapping K-Joint	NK	34
Seawater	8	Non-overlapping KT-Joint	NKT	3
Seawater + CP	5	Overlapping K-Joint	OK	37
As welded	311	Overlapping KT-Joint	OKT	4
Weld improvement	23	X joint	X	26
Repaired joints	24	Y Joint	Y	7
Constant Amplitude loading	333			
Variable Amplitude loading	25			

Summary of collected fatigue data for tubular joints (in Air, CA, as welded) - 301

Chord wall thickness	Total number of joints	axial loading	IPB loading	OPB loading
3 to 4.5 mm	28	28	0	0
6.3 to 12 mm	104	56	26	22
15.9 to 16 mm	112	68	20	24
20 to 33 mm	45	34	11	0
40 to 44 mm	4	2	2	0
75 to 78 mm	8	2	6	0

Appendices

Serial	Reference	Specimen number	Joint Type	Weld	Load Case	Chord OD (mm)	Chord Wall Thickness (mm)	Chord Length (mm)	Brace OD (mm)	Brace Wall Thickness (mm)	Loading Spectrum	N1	N2	N3	N4	Failure Site	Hot Spot Stress (MPa)	R	Environment
1	UKOSRP I	1/1	T - Joint	As welded	OPB	168.0	6.3		168.0	6.3	CA	1.40E+05	1.20E+05	2.70E+05	5.30E+05	Chord	415	0	Air
2	UKOSRP I	1/2	T - Joint	As welded	OPB	168.0	6.3		168.0	6.3	CA	2.40E+05	9.70E+04	4.00E+05	8.50E+05	Chord	402	0	Air
3	UKOSRP I	1/3	T - Joint	As welded	OPB	168.0	6.3		168.0	6.3	CA	7.60E+05	5.50E+05	1.20E+06	2.30E+06	Chord	281	0	Air
4	UKOSRP I	2/1	T - Joint	As welded	OPB	168.0	6.3		168.0	4.5	CA	9.50E+05	3.80E+05	1.30E+06	1.20E+06	Chord	331	0	Air
5	UKOSRP I	2/2	T - Joint	As welded	OPB	168.0	6.3		168.0	4.5	CA	2.10E+05	6.40E+04	6.00E+05	1.70E+06	Chord	298	0	Air
6	UKOSRP I	2/3	T - Joint	As welded	OPB	168.0	6.3		168.0	4.5	CA	3.10E+05	1.90E+05	4.70E+05	8.80E+05	Chord	368	0	Air
7	UKOSRP I	3/1	T - Joint	As welded	OPB	168.0	6.3		89.0	5.4	CA	1.60E+06	4.00E+05	4.46E+06	9.10E+06	Chord	204	0	Air
8	UKOSRP I	3/2	T - Joint	As welded	OPB	168.0	6.3		89.0	5.4	CA	5.30E+05	6.60E+04	8.60E+05	1.40E+06	Chord	338	0	Air
9	UKOSRP I	3/3	T - Joint	As welded	OPB	168.0	6.3		89.0	5.4	CA	7.50E+05	6.60E+05	5.20E+06	8.40E+06	Chord	273	0	Air
10	UKOSRP I	4/1	T - Joint	As welded	OPB	168.0	6.3		89.0	3.2	CA	2.20E+05	9.90E+04	5.80E+05	1.90E+06	Chord	340	0	Air
11	UKOSRP I	4/2	T - Joint	As welded	OPB	168.0	6.3		89.0	3.2	CA	1.60E+06	3.50E+05	2.10E+06	4.50E+06	Chord	282	0	Air
12	UKOSRP I	4/3	T - Joint	As welded	OPB	168.0	6.3		89.0	3.2	CA	3.20E+06	3.60E+05	3.96E+06	6.50E+06	Chord	321	0	Air
13	UKOSRP I	5/1	T - Joint	As welded	OPB/CEL	168.0	6.3		168.0	6.3	CA	2.40E+05	1.10E+05	7.20E+05	2.00E+06	Chord	316	0	Air
14	UKOSRP I	5/2	T - Joint	As welded	OPB/CEL	168.0	6.3		168.0	6.3	CA	6.60E+05	4.60E+05	1.15E+06	2.00E+06	Chord	351	0	Air
15	UKOSRP I	5/3	T - Joint	As welded	OPB/CEL	168.0	6.3		168.0	6.3	CA	1.70E+05	8.10E+04	3.10E+05	8.20E+05	Chord	395	0	Air
16	UKOSRP I	6/1	OK - Joint	As welded	AX	168.0	6.3		89.0	5.4	CA				8.10E+07	Run out	49.5	0	Air
17	UKOSRP I	7/1	OK - Joint	As welded	OPB	168.0	6.3		89.0	5.4	CA	3.90E+06	1.80E+06	1.20E+07	1.60E+07	Chord	275	0	Air
18	UKOSRP I	7/2	OK - Joint	As welded	OPB	168.0	6.3		89.0	5.4	CA	2.30E+07	6.20E+06	3.40E+07	5.00E+07	Chord	268	0	Air
19	UKOSRP I	9/1	OK - Joint	As welded	OPB	168.0	6.3		89.0	3.2	CA	4.40E+06	2.30E+06	8.70E+06	1.30E+07	Chord	300	0	Air
20	UKOSRP I	9/2	OK - Joint	As welded	OPB	168.0	6.3		89.0	3.2	CA	9.30E+06	2.90E+06	1.80E+07	2.30E+07	Chord	256	0	Air
21	UKOSRP I	10/1	NK - Joint	As welded	AX	168.0	6.3		89.0	5.4	CA	2.40E+07	3.10E+06	2.90E+07	3.50E+07	Chord	202	0	Air
22	UKOSRP I	10/2	NK - Joint	As welded	AX	168.0	6.3		89.0	5.4	CA		2.10E+06		5.80E+06	Brace	266	0	Air
23	UKOSRP I	11 /1	NK - Joint	As welded	OPB	168.0	6.3		89.0	5.4	CA	3.30E+07	3.50E+06	8.30E+07	1.20E+08	Chord	215	0	Air
24	UKOSRP I	11 /2	NK - Joint	As welded	OPB	168.0	6.3		89.0	5.4	CA	2.50E+06	7.20E+05	9.00E+06	1.70E+07	Chord	312	0	Air
25	UKOSRP I	16/1	NKT - Joint	As welded	AX	168.0	6.3		89.0	5.4	CA		6.50E+05	2.60E+06	5.30E+06	Chord	297	0	Air
26	UKOSRP I	17/2	T - Joint	As welded	AX/CEL	168.0	6.3		168.0	6.3	CA				2.00E+08	Run out	182	-1	Air
27	UKOSRP I	17/2 (R)	T - Joint	As welded	AX/CEL	168.0	6.3		168.0	6.3	CA	6.90E+04	3.16E+05	3.24E+05	3.73E+05	Chord	312	-1	Air
28	UKOSRP I	42/2	T - Joint	As welded	AX	914.0	32.0		457.0	8.0	CA	2.81E+06	1.84E+06	4.79E+06	6.35E+06	Chord	94	-1	Air
29	UKOSRP I	37/9	T - Joint	As welded	AX	457.0	16.0		457.0	16.0	CA	2.80E+06	2.50E+06	6.95E+06	8.73E+06	Chord	120	-1	Air
30	UKOSRP I	17/6	T - Joint	As welded	IPB	168.0	6.3		168.0	6.3	CA	1.84E+05	7.15E+05	7.15E+05	9.97E+05	Chord	391	-1	Air
31	UKOSRP I	17/7	T - Joint	As welded	IPB	168.0	6.3		168.0	6.3	CA	1.08E+06	1.78E+06	2.66E+06	5.16E+06	Chord	265	-1	Air
32	UKOSRP I	17/8	T - Joint	As welded	IPB	168.0	6.3		168.0	6.3	CA	3.70E+06	3.70E+06	3.70E+06	6.39E+06	Chord	226	-1	Air
33	UKOSRP I	17/9	T - Joint	As welded	IPB/CEL	168.0	6.3		168.0	6.3	CA	1.01E+06	1.04E+06	1.51E+06	1.55E+06	Chord	400	-1	Air
34	UKOSRP I	17/10	T - Joint	As welded	IPB/CEL	168.0	6.3		168.0	6.3	CA				2.00E+08	Run out	263	-1	Air
35	UKOSRP I	17 /10 (R)	T - Joint	As welded	IPB/CEL	168.0	6.3		168.0	6.3	CA	1.22E+06	1.22E+06	1.46E+06	1.75E+06	Chord	442	-1	Air
36	UKOSRP I	17/11	T - Joint	As welded	IPB/CEL	168.0	6.3		168.0	6.3	CA	1.47E+06	1.47E+06	1.48E+06	1.87E+06	Chord	438	-1	Air
37	UKOSRP I	17/12	T - Joint	As welded	AX/CEL	168.0	6.3		168.0	6.3	CA	4.97E+05	7.44E+05	8.38E+05	1.18E+06	Chord	255	-1	Air
38	UKOSRP I	18/1	T - Joint	As welded	AX/CEL	168.0	6.3		168.0	4.5	CA	2.08E+05	4.98E+05	4.98E+05	5.42E+05	Chord	325	-1	Air
39	UKOSRP I	18/2	T - Joint	As welded	AX/CEL	168.0	6.3		168.0	4.5	CA				2.00E+08	Run out	223	-1	Air
40	UKOSRP I	18/4	T - Joint	As welded	IPB	168.0	6.3		168.0	4.5	CA	7.90E+05	1.33E+06	1.86E+06	1.92E+06	Chord	407	-1	Air

Appendices

Serial	Reference	Specimen number	Joint Type	Weld	Load Case	Chord OD (mm)	Chord Wall Thickness (mm)	Chord Length (mm)	Brace OD (mm)	Brace Wall Thickness (mm)	Loading Spectrum	N1	N2	N3	N4	Failure Site	Hot Spot Stress (MPa)	R	Environment
41	UKOSRP I	18/5	T - Joint	As welded	AX	168.0	6.3		168.0	4.5	CA				2.00E+08	Run out	191	-1	Air
42	UKOSRP I	38/5	T - Joint	As welded	AX	457.0	16.0		457.0	8.8	CA	1.20E+06	1.30E+06	1.98E+06	2.88E+06	Chord	146	-1	Air
43	UKOSRP I	18/6	T - Joint	As welded	OPB	168.0	6.3		168.0	4.5	CA				6.10E+07	Run out	229	-1	Air
44	UKOSRP I	18/6 (R)	T - Joint	As welded	IPB	168.0	6.3		168.0	4.5	CA	1.62E+07	1.63E+07		1.86E+07	Chord	378	-1	Air
45	UKOSRP I	18/7	T - Joint	As welded	AX	168.0	6.3		168.0	4.5	CA	1.73E+07			5.40E+07	Brace	228	-1	Air
46	UKOSRP I	18/8	T - Joint	As welded	AX	168.0	6.3		168.0	4.5	CA				1.48E+08	Run out	162	-1	Air
47	UKOSRP I	17/3	T - Joint	As welded	AX	168.0	6.3		168.0	6.3	CA	2.74E+05	5.20E+05	5.67E+05	5.90E+05	Chord	185	-1	Air
48	UKOSRP I	44/3	T - Joint	As welded	AX	914.0	32.0		228.5	8.0	CA	3.00E+05	4.70E+05	1.20E+06	2.75E+06	Brace	188	-1	Air
49	UKOSRP I	18/10	T - Joint	As welded	IPB	168.0	6.3		168.0	4.5	CA	1.31E+06	1.45E+06	2.11E+06	2.51E+06	Chord	429	-1	Air
50	UKOSRP I	18/11	T - Joint	As welded	AX/CEL	168.0	6.3		168.0	4.5	CA	6.90E+05	9.40E+05	1.00E+06	1.49E+06	Chord	253	-1	Air
51	UKOSRP I	37/5	T - Joint	As welded	AX	457.0	16.0		457.0	16.0	CA	3.50E+05	6.70E+05	1.00E+06	1.50E+06	Chord	190	-1	Air
52	UKOSRP I	18/13	T - Joint	As welded	IPB	168.0	6.3		168.0	4.5	CA	7.00E+04	1.36E+05	2.22E+05	2.65E+05	Chord	660	-1	Air
53	UKOSRP I	18/14	T - Joint	As welded	IPB	168.0	6.3		168.0	4.5	CA	4.44E+05	4.64E+05	7.84E+05	1.10E+06	Chord	497	-1	Air
54	UKOSRP I	17 /1	T - Joint	As welded	AX	168.0	6.3		168.0	6.3	CA	7.98E+05	1.40E+06	1.53E+06	2.03E+06	Chord	245	-1	Air
55	UKOSRP I	18/16	T - Joint	As welded	IPB	168.0	6.3		168.0	4.5	CA	6.03E+07	7.87E+07		8.60E+07	Chord	296	-1	Air
56	UKOSRP I	19/1	T - Joint	As welded	AX/CEL	168.0	6.3		89.0	5.4	CA		4.03E+05	4.21E+05	5.05E+05	Chord	549	-1	Air
57	UKOSRP I	18/15	T - Joint	As welded	AX	168.0	6.3		168.0	4.5	CA	2.10E+05	3.49E+05	4.15E+05	5.43E+05	Chord	259	-1	Air
58	UKOSRP I	19/3	T - Joint	As welded	AX	168.0	6.3		89.0	5.4	CA				2.00E+07	Run out	304	-1	Air
59	UKOSRP I	19/3(R)	T - Joint	As welded	AX	168.0	6.3		89.0	5.4	CA	3.20E+04	6.20E+04	7.76E+04	1.28E+05	Chord	763	-1	Air
60	UKOSRP I	19/4	T - Joint	As welded	AX	168.0	6.3		89.0	5.4	CA		3.80E+05	4.25E+05	7.08E+05	Chord	538	-1	Air
61	UKOSRP I	19/5	T - Joint	As welded	AX/CEL	168.0	6.3		89.0	5.4	CA			9.80E+04	1.30E+05	Chord	912	-1	Air
62	UKOSRP I	19/11	T - Joint	As welded	IPB	168.0	6.3		89.0	5.4	CA	7.50E+05	7.50E+05	8.20E+05	1.07E+06	Chord	355	-1	Air
63	UKOSRP I	19/12	T - Joint	As welded	IPB	168.0	6.3		89.0	5.4	CA	7.70E+05	1.80E+06	1.89E+06	2.53E+06	Chord	265	-1	Air
64	UKOSRP I	19/13	T - Joint	As welded	IPB	168.0	6.3		89.0	5.4	CA		3.30E+05	3.62E+05	4.19E+05	Chord	482	-1	Air
65	UKOSRP I	20/1	T - Joint	As welded	AX/CEL	168.0	6.3		89.0	3.2	CA				2.00E+08	Run out	332	-1	Air
66	UKOSRP I	20/1 (R)	T - Joint	As welded	AX/CEL	168.0	6.3		89.0	3.2	CA	1.10E+06	2.50E+06	2.70E+06	2.90E+06	Chord	487	-1	Air
67	UKOSRP I	20/2	T - Joint	As welded	IPB	168.0	6.3		89.0	3.2	CA				2.00E+08	Run out	350	-1	Air
68	UKOSRP I	20/2 (R)	T - Joint	As welded	IPB	168.0	6.3		89.0	3.2	CA		3.10E+05	2.37E+05	3.93E+05	Chord	487	-1	Air
69	UKOSRP I	20/4	T - Joint	As welded	AX	168.0	6.3		89.0	3.2	CA				2.00E+08	Run out	210	-1	Air
70	UKOSRP I	20/5	T - Joint	As welded	IPB	168.0	6.3		89.0	3.2	CA	2.00E+05	5.00E+05	5.18E+05	8.50E+05	Brace	449	-1	Air
71	UKOSRP I	20/6	T - Joint	As welded	IPB	168.0	6.3		89.0	3.2	CA	8.23E+06	1.00E+07	1.00E+07	1.04E+07	Brace	257	-1	Air
72	UKOSRP I	20/8	T - Joint	As welded	AX/CEL	168.0	6.3		89.0	3.2	CA		3.50E+05	4.50E+05	7.80E+05	Chord	493	-1	Air
73	UKOSRP I	20/11	T - Joint	As welded	AX	168.0	6.3		89.0	3.2	CA				4.00E+06	Chord	489	-1	Air
74	UKOSRP I	21 /1	T - Joint	As welded	OPB	457.0	16.0		457.0	16.0	CA	8.00E+05	3.30E+05	1.10E+06	1.20E+06	Chord	174	0	Air
75	UKOSRP I	21/2	T - Joint	As welded	OPB	457.0	16.0		457.0	16.0	CA	1.90E+05	1.60E+05	6.10E+05	8.10E+05	Chord	267	0	Air
76	UKOSRP I	21 /3	T - Joint	As welded	OPB	457.0	16.0		457.0	16.0	CA	5.70E+06	2.70E+06	7.50E+06	9.70E+06	Chord	132	0	Air
77	UKOSRP I	22/1	T - Joint	As welded	OPB	457.0	16.0		457.0	8.8	CA	2.40E+05	8.80E+04	2.90E+05	3.70E+05	Chord	306	0	Air
78	UKOSRP I	22/2	T - Joint	As welded	OPB	457.0	16.0		457.0	8.8	CA	2.90E+05	2.20E+05	9.50E+05	1.40E+06	Chord	178	0	Air
79	UKOSRP I	22/3	T - Joint	As welded	OPB	457.0	16.0		457.0	8.8	CA	7.70E+05	5.40E+05	3.60E+06	5.89E+06	Chord	131	0	Air

Appendices

Serial	Reference	Specimen number	Joint Type	Weld	Load Case	Chord OD (mm)	Chord Wall Thickness (mm)	Chord Length (mm)	Brace OD (mm)	Brace Wall Thickness (mm)	Loading Spectrum	N1	N2	N3	N4	Failure Site	Hot Spot Stress (MPa)	R	Environment
80	UKOSRP I	23/1	T - Joint	As welded	OPB	457.0	16.0		114.3	6.2	CA	2.40E+06	1.00E+06	5.10E+06	1.50E+07	Chord	166	0	Air
81	UKOSRP I	23/2	T - Joint	As welded	OPB	457.0	16.0		114.3	6.2	CA	1.00E+05	2.70E+04	3.70E+05	6.30E+05	Chord	365	0	Air
82	UKOSRP I	23/3	T - Joint	As welded	OPB	457.0	16.0		114.3	6.2	CA	3.50E+05	1.80E+05	9.00E+05	1.20E+06	Brace	173	0	Air
83	UKOSRP I	24/1	T - Joint	As welded	OPB	457.0	16.0		114.3	4.5	CA	4.80E+05	2.20E+05	2.60E+06	4.50E+06	Chord	187	0	Air
84	UKOSRP I	24/2	T - Joint	As welded	OPB	457.0	16.0		114.3	4.5	CA	3.80E+04	2.80E+04	5.80E+04	8.00E+04	Brace	414	0	Air
85	UKOSRP I	24/3	T - Joint	As welded	OPB	457.0	16.0		114.3	4.5	CA	1.80E+05	6.90E+04	2.40E+05	2.90E+05	Brace	308	0	Air
86	UKOSRP I	25/1	T - Joint	As welded	OPB/CEL	457.0	16.0		457.0	16.0	CA	3.30E+05	5.70E+04	6.70E+05	1.20E+06	Chord	206	0	Air
87	UKOSRP I	25/2	T - Joint	As welded	OPB/CEL	457.0	16.0		457.0	16.0	CA	7.90E+04	3.50E+04	1.80E+05	3.50E+05	Chord	311	0	Air
88	UKOSRP I	25/3	T - Joint	As welded	OPB/CEL	457.0	16.0		457.0	16.0	CA	2.00E+06	8.00E+05	4.05E+06	5.20E+06	Chord	112	0	Air
89	UKOSRP I	26/1	OK - Joint	As welded	AX	457.0	16.0		246.8	8.0	CA				8.20E+07	Run out	80	0	Air
90	UKOSRP I	27/1	OK - Joint	As welded	OPB	457.0	16.0		246.8	8.0	CA	6.70E+05	4.00E+05	2.20E+06	3.80E+06	Chord	370	0	Air
91	UKOSRP I	27/2	OK - Joint	As welded	OPB	457.0	16.0		246.8	8.0	CA	7.80E+06	4.00E+06	4.00E+07	5.30E+07	Chord	166	0	Air
92	UKOSRP I	29/1	OK - Joint	As welded	OPB	457.0	16.0		246.8	12.5	CA	3.00E+06	1.80E+06	1.10E+07	1.80E+07	Chord	271	0	Air
93	UKOSRP I	29/2	OK - Joint	As welded	OPB	457.0	16.0		246.8	12.5	CA	7.10E+05	1.60E+05	1.90E+06	3.20E+06	Chord	322	0	Air
94	UKOSRP I	30/1	NK - Joint	As welded	AX	457.0	16.0		246.8	8.0	CA	7.20E+06	7.30E+06	1.10E+07	1.20E+07	Chord	181	0	Air
95	UKOSRP I	30/2	NK - Joint	As welded	AX	457.0	16.0		246.8	8.0	CA		2.40E+07		4.90E+07	Chord	142	0	Air
96	UKOSRP I	33/1	OKT - Joint	As welded	OPB	457.0	16.0		246.8	8.0	CA	3.10E+06	4.40E+05	1.20E+07	2.10E+07	Chord	193	0	Air
97	UKOSRP I	33/2	OKT - Joint	As welded	OPB	457.0	16.0		246.8	8.0	CA	1.00E+06	3.50E+05	4.60E+06	5.90E+06	Chord	295	0	Air
98	UKOSRP I	35/1	OKT - Joint	As welded	OPB	457.0	16.0		246.8	12.5	CA	3.60E+06	9.40E+05	1.70E+07	2.70E+07	Chord	191	0	Air
99	UKOSRP I	35/2	OKT - Joint	As welded	OPB	457.0	16.0		246.8	12.5	CA	1.00E+06	2.00E+05	3.30E+06	5.90E+06	Chord	282	0	Air
100	UKOSRP I	36/1	NKT - Joint	As welded	AX	457.0	16.0		246.8	8.0	CA	4.20E+06	2.90E+06	6.30E+06	7.30E+06	Chord	194	0	Air
101	UKOSRP I	36/2	NKT - Joint	As welded	AX	457.0	16.0		246.8	8.0	CA	5.20E+06	1.70E+05		9.10E+06	Chord	214	0	Air
102	UKOSRP I	37/1	T - Joint	As welded	IPB	457.0	16.0		457.0	16.0	CA	8.40E+04	1.25E+05	2.90E+05	5.00E+05	Chord	271	-1	Air
103	UKOSRP I	37/3	T - Joint	As welded	AX	457.0	16.0		457.0	16.0	CA	6.00E+04	8.80E+04	1.44E+05	1.53E+05	Chord	322	-1	Air
104	UKOSRP I	18/5 (R)	T - Joint	As welded	AX	168.0	6.3		168.0	4.5	CA	1.16E+06	1.32E+06	1.40E+06	1.63E+06	Chord	324	-1	Air
105	UKOSRP I	18/9	T - Joint	As welded	AX	168.0	6.3		168.0	4.5	CA	2.17E+05	2.18E+05	2.18E+05	2.75E+05	Chord	357	-1	Air
106	UKOSRP I	37/7	T - Joint	As welded	IPB	457.0	16.0		457.0	16.0	CA	2.00E+06	5.00E+06	1.00E+07	1.44E+07	Chord	129	-1	Air
107	UKOSRP I	37/8	T - Joint	As welded	IPB/CEL	457.0	16.0		457.0	16.0	CA	4.50E+05	4.50E+05	1.20E+06	1.53E+06	Chord	271	-1	Air
108	UKOSRP I	17/4	T - Joint	As welded	AX	168.0	6.3		168.0	6.3	CA	7.60E+04	1.45E+05	1.64E+05	2.00E+05	Chord	376	-1	Air
109	UKOSRP I	37/10	T - Joint	As welded	IPB/CEL	457.0	16.0		457.0	16.0	CA	5.00E+05	7.30E+05	3.79E+06	6.18E+06	Chord	183	-1	Air
110	UKOSRP I	37/12	T - Joint	As welded	IPB/CEL	457.0	16.0		457.0	16.0	CA			2.43E+05	3.34E+05	Chord	401	-1	Air
111	UKOSRP I	37/13	T - Joint	As welded	IPB	457.0	16.0		457.0	16.0	CA	3.02E+05	3.37E+05	7.29E+05	1.44E+06	Chord	169	-1	Air
112	UKOSRP I	38/1	T - Joint	As welded	AX/CEL	457.0	16.0		457.0	8.8	CA	5.50E+05	1.00E+06	2.11E+06	3.86E+06	Brace	208	-1	Air
113	UKOSRP I	38/2	T - Joint	As welded	IPB	457.0	16.0		457.0	8.8	CA		2.30E+07		3.00E+07	Brace	170	-1	Air
114	UKOSRP I	38/3	T - Joint	As welded	IPB	457.0	16.0		457.0	8.8	CA		6.00E+05	6.10E+05	1.70E+06	Chord	225	-1	Air
115	UKOSRP I	38/4	T - Joint	As welded	AX	457.0	16.0		457.0	8.8	CA			5.35E+05	6.78E+05	Chord	204	-1	Air
116	UKOSRP I	18/8 (R)	T - Joint	As welded	AX	168.0	6.3		168.0	4.5	CA	2.08E+05	2.53E+05	3.87E+05	4.22E+05	Chord	377	-1	Air
117	UKOSRP I	38.6	T - Joint	As welded	IPB	457.0	16.0		457.0	8.8	CA		1.30E+06	1.80E+06	5.32E+06	Chord	144	-1	Air
118	UKOSRP I	38.7	T - Joint	As welded	AX/CEL	457.0	16.0		457.0	8.8	CA	8.15E+05	7.48E+05	1.11E+06	1.56E+06	Brace	271	-1	Air
119	UKOSRP I	38.8	T - Joint	As welded	AX	457.0	16.0		457.0	8.8	CA	2.27E+05	2.27E+05	3.69E+05	3.91E+05	Chord	269	-1	Air

Appendices

Serial	Reference	Specimen number	Joint Type	Weld	Load Case	Chord OD (mm)	Chord Wall Thickness (mm)	Chord Length (mm)	Brace OD (mm)	Brace Wall Thickness (mm)	Loading Spectrum	N1	N2	N3	N4	Failure Site	Hot Spot Stress (MPa)	R	Environment
120	UKOSRP I	18/12	T - Joint	As welded	AX	168.0	6.3		168.0	4.5	CA	4.60E+04	1.49E+05	2.17E+05	2.36E+05	Chord	417	-1	Air
121	UKOSRP I	39/1	T - Joint	As welded	IPB	457.0	16.0		114.3	6.2	CA		1.60E+06	2.20E+06	3.20E+06	Chord	166	-1	Air
122	UKOSRP I	39/2	T - Joint	As welded	IPB	457.0	16.0		114.3	6.2	CA				3.00E+06	Brace	365	-1	Air
123	UKOSRP I	39/3	T - Joint	As welded	IPB	457.0	16.0		114.3	6.2	CA				2.38E+06	Brace	488	-1	Air
124	UKOSRP I	39/4	T - Joint	As welded	AX	457.0	16.0		114.3	6.2	CA		4.50E+05	1.11E+06	1.57E+06	Brace	266	-1	Air
125	UKOSRP I	39/5	T - Joint	As welded	AX	457.0	16.0		114.3	6.2	CA		6.00E+05	1.34E+06	2.00E+06	Brace	183	-1	Air
126	UKOSRP I	39/6	T - Joint	As welded	AX/CEL	457.0	16.0		114.3	6.2	CA		1.20E+06	1.80E+06	2.28E+06	Chord	179	-1	Air
127	UKOSRP I	39/7	T - Joint	As welded	AX/CEL	457.0	16.0		114.3	6.2	CA	1.87E+05	2.15E+05	3.36E+05	5.47E+05	Brace	254	-1	Air
128	UKOSRP I	40/1	T - Joint	As welded	AX	457.0	16.0		114.3	4.5	CA	1.40E+07	2.15E+07		3.00E+07	Brace	201	-1	Air
129	UKOSRP I	40/2	T - Joint	As welded	IPB	457.0	16.0		114.3	4.5	CA		2.10E+06	3.60E+06	5.33E+06	Chord	315	-1	Air
130	UKOSRP I	40/3	T - Joint	As welded	IPB	457.0	16.0		114.3	4.5	CA				2.00E+08	Run out	230	-1	Air
131	UKOSRP I	40/3 (R)	T - Joint	As welded	IPB	457.0	16.0		114.3	4.5	CA		9.00E+04	9.70E+04	1.10E+05	Brace	691	-1	Air
132	UKOSRP I	40/4	T - Joint	As welded	AX	457.0	16.0		114.3	4.5	CA				1.85E+07	Weld	268	-1	Air
133	UKOSRP I	40/5	T - Joint	As welded	IPB	457.0	16.0		114.3	4.5	CA		1.50E+06	1.70E+06	1.87E+06	Brace	408	-1	Air
134	UKOSRP I	41 /1	T - Joint	As welded	IPB	914.0	32.0		457.0	32.0	CA	2.19E+06		2.10E+07	2.62E+07	Chord	77	-1	Air
135	UKOSRP I	41/2	T - Joint	As welded	AX	914.0	32.0		457.0	32.0	CA				2.00E+08	Run out	112	-1	Air
136	UKOSRP I	41/2 (R)	T - Joint	As welded	AX	914.0	32.0		457.0	32.0	CA	3.00E+05		7.66E+05	8.79E+05	Chord	262	-1	Air
137	UKOSRP I	41 /3	T - Joint	As welded	AX	914.0	32.0		457.0	32.0	CA		3.50E+05	1.40E+06	2.32E+06	Chord	164	-1	Air
138	UKOSRP I	41/4	T - Joint	As welded	IPB	914.0	32.0		457.0	32.0	CA	1.10E+06	1.20E+06	3.46E+06	4.90E+06	Chord	108	-1	Air
139	UKOSRP I	42/1	T - Joint	As welded	IPB	914.0	32.0		457.0	32.0	CA				2.00E+08	Run out	52	-1	Air
140	UKOSRP I	42/1 (R)	T - Joint	As welded	IPB	914.0	32.0		457.0	32.0	CA	1.50E+05	9.00E+04	5.30E+05	9.00E+05	Chord	121	-1	Air
141	UKOSRP I	19/2	T - Joint	As welded	AX	168.0	6.3		89.0	5.4	CA	7.70E+05	1.24E+06	1.72E+06	1.94E+06	Chord	450	-1	Air
142	UKOSRP I	42/3	T - Joint	As welded	AX	914.0	32.0		457.0	8.0	CA	2.50E+06		1.46E+07	1.53E+07	Chord	77	-1	Air
143	UKOSRP I	42/4	T - Joint	As welded	IPB	914.0	32.0		457.0	8.0	CA	1.10E+06	1.20E+06	2.23E+06	3.32E+06	Chord	92	-1	Air
144	UKOSRP I	43/1	T - Joint	As welded	AX	914.0	32.0		228.5	16.0	CA				2.00E+08	Run out	78	-1	Air
145	UKOSRP I	43/1 (R)	T - Joint	As welded	AX	914.0	32.0		228.5	16.0	CA	1.06E+04		2.10E+05	2.40E+05	Chord	294	-1	Air
146	UKOSRP I	43/2	T - Joint	As welded	AX	914.0	32.0		228.5	16.0	CA				2.00E+08	Run out	86	-1	Air
147	UKOSRP I	43/2 (R)	T - Joint	As welded	AX	914.0	32.0		228.5	16.0	CA	7.62E+04		2.40E+06	3.33E+06	Chord	147	-1	Air
148	UKOSRP I	43/3	T - Joint	As welded	IPB	914.0	32.0		228.5	16.0	CA				2.00E+08	Run out	69	-1	Air
149	UKOSRP I	43/3 (R)	T - Joint	As welded	IPB	914.0	32.0		228.5	16.0	CA	1.30E+05	1.40E+05	1.72E+05	2.45E+05	Chord	279	-1	Air
150	UKOSRP I	43/4	T - Joint	As welded	IPB	914.0	32.0		228.5	16.0	CA		2.90E+06	7.50E+06	8.89E+06	Chord	90	-1	Air
151	UKOSRP I	44/1	T - Joint	As welded	IPB	914.0	32.0		228.5	8.0	CA	8.00E+05	9.00E+05	1.16E+06	2.13E+06	Brace	221	-1	Air
152	UKOSRP I	44/2	T - Joint	As welded	IPB	914.0	32.0		228.5	8.0	CA			2.83E+06	7.32E+06	Brace	175	-1	Air
153	UKOSRP I	20/4 (R)	T - Joint	As welded	AX	168.0	6.3		89.0	3.2	CA	4.20E+04	1.80E+05	2.35E+05	3.56E+05	Chord	523	-1	Air
154	UKOSRP I	44/4	T - Joint	As welded	AX	914.0	32.0		228.5	8.0	CA				2.00E+08	Run out	127	-1	Air
155	UKOSRP I	44/4 (R)	T - Joint	As welded	AX	914.0	32.0		228.5	8.0	CA		8.00E+04	1.47E+05	2.30E+05	Brace	380	-1	Air
156	UKOSRP I	45	T - Joint	PWHT	AX	1830.0	75.0		457.5	18.8	CA			1.06E+06	1.25E+06	Brace	168	-1	Air
157	UKOSRP I	46	T - Joint	PWHT	AX	1830.0	75.0		457.5	18.8	CA			4.97E+05	6.60E+05	Brace	233	-1	Air
158	UKOSRP I	47	T - Joint	PWHT	AX	1830.0	75.0		915.0	37.5	CA	2.20E+05	1.90E+05	6.40E+05	7.40E+05	Chord	222	-1	Air
159	UKOSRP I	48	T - Joint	PWHT	AX	1830.0	75.0		915.0	37.5	CA	4.80E+05	5.27E+05	3.21E+06	4.13E+06	Chord	157	-1	Air



Appendices

Serial	Reference	Specimen number	Joint Type	Weld	Load Case	Chord OD (mm)	Chord Wall Thickness (mm)	Chord Length (mm)	Brace OD (mm)	Brace Wall Thickness (mm)	Loading Spectrum	N1	N2	N3	N4	Failure Site	Hot Spot Stress (MPa)	R	Environment	
160	UKOSRP I	49	T - Joint	PWHT	IPB	1830.0	75.0		457.5	18.8	CA		5.30E+04	9.50E+04	1.10E+05	Brace	409	-1	Air	
161	UKOSRP I	50	T - Joint	PWHT	IPB	1830.0	75.0		457.5	18.8	CA				2.00E+08	Run out	100	-1	Air	
162	UKOSRP I	50 (R)	T - Joint	PWHT	IPB	1830.0	75.0		457.5	18.8	CA	1.75E+05	2.17E+05	3.34E+05	3.60E+05	Brace	330	-1	Air	
163	UKOSRP I	51	T - Joint	PWHT	IPB	1830.0	75.0		915.0	37.5	CA		2.60E+04	1.10E+05	1.46E+05	Chord	324	-1	Air	
164	UKOSRP I	52	T - Joint	PWHT	IPB	1830.0	75.0		915.0	37.5	CA				2.00E+08	Run out	102	-1	Air	
165	UKOSRP I	52 (R)	T - Joint	PWHT	IPB	1830.0	75.0		915.0	37.5	CA		1.11E+06	1.35E+06	1.56E+06	Chord	156	-1	Air	
166	UKOSRP I	17/5	T - Joint	As welded	AX	168.0	6.3		168.0	6.3	VA			1.40E+07	2.00E+07	Chord	53.4		Air	
167	UKOSRP I	17/13	T - Joint	As welded	AX	168.0	6.3		168.0	6.3	VA		2.30E+07	4.10E+07	4.70E+07	Chord	38.2		Air	
168	UKOSRP I	17/14	T - Joint	As welded	AX	168.0	6.3		168.0	6.3	VA				2.00E+07	Run out	27.6		Air	
169	UKOSRP I	17/15	T - Joint	As welded	IPB	168.0	6.3		168.0	6.3	VA		4.50E+07	1.23E+08	1.40E+08	Chord	55.7		Air	
170	UKOSRP I	17/16	T - Joint	As welded	IPB	168.0	6.3		168.0	6.3	VA		2.30E+06	2.80E+06	3.62E+06	Chord	88.3		Air	
171	UKOSRP I	17/17	T - Joint	As welded	IPB	168.0	6.3		168.0	6.3	VA		2.50E+07	4.80E+07	6.20E+07	Chord	59.9		Air	
172	UKOSRP I	18/19	T - Joint	As welded	AX	168.0	6.3		168.0	4.5	VA		1.10E+07	1.80E+07	2.20E+07	Chord	54		Air	
173	UKOSRP I	18/20	T - Joint	As welded	AX	168.0	6.3		168.0	4.5	VA		2.60E+07	4.40E+07	4.60E+07	Chord	41.6		Air	
174	UKOSRP I	18/21	T - Joint	As welded	AX	168.0	6.3		168.0	4.5	VA			1.90E+07	2.20E+07	Chord	59.67		Air	
175	UKOSRP I	19/9	T - Joint	As welded	AX	168.0	6.3		89.0	5.4	VA		4.00E+06	1.20E+07	1.40E+07	Chord	105		Air	
176	UKOSRP I	19/10	T - Joint	As welded	AX	168.0	6.3		89.0	5.4	VA		2.90E+07	3.40E+07	4.20E+07	Chord	91.5		Air	
177	UKOSRP I	19/14	T - Joint	As welded	AX	168.0	6.3		89.0	5.4	VA		2.00E+06	9.00E+06	1.50E+07	Chord	78.4		Air	
178	UKOSRP I	20/3	T - Joint	As welded	AX	168.0	6.3		89.0	3.2	VA		5.00E+06	2.10E+07	3.20E+07	Chord	84.6		Air	
179	UKOSRP I	20/7	T - Joint	As welded	AX	168.0	6.3		89.0	3.2	VA			4.70E+07	7.00E+07	Chord	67.16		Air	
180	UKOSRP I	20/9	T - Joint	As welded	AX	168.0	6.3		89.0	3.2	VA		5.00E+06	1.15E+07	1.80E+07	Chord	79.9		Air	
181	UKOSRP I	37/2	T - Joint	As welded	IPB	457.0	16.0		457.0	16.0	VA			1.80E+06	2.60E+06	Chord	83		Air	
182	UKOSRP I	37.4	T - Joint	As welded	IPB	457.0	16.0		457.0	16.0	VA			1.73E+07	1.03E+08	Chord	37.3		Air	
183	UKOSRP I	37/6	T - Joint	As welded	IPB	457.0	16.0		457.0	16.0	VA		6.50E+06	2.40E+07	4.70E+07	Chord	58.1		Air	
184	UKOSRP I	37/11	T - Joint	As welded	IPB	457.0	16.0		457.0	16.0	VA		2.10E+07	2.80E+07	6.00E+07	Chord	45.3		Air	
185	UKOSRP I	39/8	T - Joint	As welded	AX	457.0	16.0		114.3	4.8	VA		9.50E+06	2.40E+07	3.00E+07	Chord	57.3		Air	
186	UKOSRP I	39/9	T - Joint	As welded	AX	457.0	16.0		114.3	4.8	VA		2.00E+06	6.50E+06	9.60E+07	Brace	77.3		Air	
187	UKOSRP I	39/10	T - Joint	As welded	AX	457.0	16.0		114.3	4.8	VA		3.00E+07	1.05E+08	1.11E+08	Brace	53.2		Air	
188	UKOSRP I	39/11	T - Joint	As welded	AX	457.0	16.0		114.3	4.8	VA		5.60E+07	8.50E+07	1.87E+08	Brace	40.4		Air	
189	UKOSRP II	T217		As welded		1830.0	75.0		915.0	37.5	CA			7.60E+04	3.28E+05	3.32E+05	Chord	200	-1	
190	UKOSRP II	T219		As welded		1830.0	75.0		915.0	37.5	CA	1.45E+04	2.00E+04	1.16E+05	1.35E+05		300	-1		
191	UKOSRP II	T218		As welded		1830.0	75.0		915.0	37.5	CA	3.53E+05	4.30E+05	8.80E+05	1.09E+06		150	-1		
192	UKOSRP II	T216		As welded		1830.0	75.0		915.0	37.5	CA		4.30E+05	2.89E+06	3.24E+06		110	-1		
193	UKOSRP II	T210	T - Joint	As welded	AX	914.0	32.0		457.0	16.0	CA	6.00E+05	8.00E+05	1.90E+06	2.25E+06		166			
194	UKOSRP II	T211	T - Joint	As welded	AX	914.0	32.0		457.0	16.0	CA	2.63E+05	4.00E+05	1.05E+06	1.29E+06		200			
195	UKOSRP II	T215	T - Joint	As welded	AX	914.0	32.0		457.0	16.0	CA	1.57E+05	2.23E+05	6.73E+05	7.30E+05		230			
196	UKOSRP II	T204		PWHT		914.0	32.0		457.0	16.0	CA			7.00E+04	2.10E+05	2.78E+05		460		
197	UKOSRP II	T201		PWHT		914.0	32.0		457.0	16.0	CA	1.00E+05	1.40E+05	3.40E+05	4.78E+05		380			
198	UKOSRP II	T203		PWHT		914.0	32.0		457.0	16.0	CA	7.00E+05	9.00E+05	1.50E+06	1.75E+06		300			
199	UKOSRP II	T204		PWHT		914.0	32.0		457.0	16.0	CA	1.27E+06	2.50E+06	6.37E+06	7.78E+06		221			

Appendices

Serial	Reference	Specimen number	Joint Type	Weld	Load Case	Chord OD (mm)	Chord Wall Thickness (mm)	Chord Length (mm)	Brace OD (mm)	Brace Wall Thickness (mm)	Loading Spectrum	N1	N2	N3	N4	Failure Site	Hot Spot Stress (MPa)	R	Environment
200	UKOSRP II	T208		As welded		914.0	32.0		457.0	16.0	CA		8.51E+04	2.93E+05	3.90E+05		230		Seawater + CP
201	UKOSRP II	T209		As welded		914.0	32.0		457.0	16.0	CA		2.87E+05	6.49E+05	1.00E+06		166		Seawater + CP
202	UKOSRP II	G1	NK - Joint	As welded	AX	457.0	16.0		244.0	8.0	CA	1.40E+04	2.05E+04	3.85E+04	7.50E+04	Chord	619	-1	Air
203	UKOSRP II	G2	NK - Joint	As welded	AX	457.0	16.0		244.0	8.0	CA	3.20E+04	7.70E+04	1.41E+05	4.10E+05	Chord	432	-1	Air
204	UKOSRP II	G3	NK - Joint	As welded	AX	457.0	16.0		244.0	8.0	CA	1.18E+05	1.45E+05	3.10E+05	5.75E+05	Chord	368	-1	Air
205	UKOSRP II	LA1-1	OK - Joint	As welded	AX	457.0	16.0		244.0	12.5	CA		1.84E+05	1.84E+05	3.57E+05	Brace	256	-1	Air
206	UKOSRP II	LA1-2	OK - Joint	As welded	AX	457.0	16.0		244.0	12.8	CA	4.30E+05	9.00E+05	9.50E+05	1.01E+06	Brace	203	-1	Air
207	UKOSRP II	LA2-1	OK - Joint	As welded	AX	457.2	16.0		216.3	8.0	CA	3.40E+04	5.90E+04	6.00E+04	9.00E+04	Brace	390	-1	Air
208	UKOSRP II	LA2-2	OK - Joint	As welded	AX	457.2	16.0		216.3	8.0	CA	7.80E+05	1.04E+06		1.24E+06	Brace	276	-1	Air
209	UKOSRP II	LA2-3	OK - Joint	As welded	AX	457.2	16.0		216.3	8.0	CA	8.60E+04	8.66E+04		1.10E+05	Brace	367	-1	Air
210	UKOSRP II	LA2-4	OK - Joint	As welded	AX	457.2	16.0		216.3	8.0	CA		1.12E+06		2.00E+06	Chord	237	-1	Air
211	UKOSRP II	LA3-1	OK - Joint	As welded	AX	457.2	12.0		216.3	8.0	CA	3.80E+04	3.85E+06		6.80E+04	Brace	397	-1	Air
212	UKOSRP II	LA3-2	OK - Joint	As welded	AX	457.2	12.0		216.3	8.0	CA	2.11E+05	3.30E+05	5.60E+05	7.26E+05	Chord	302	-1	Air
213	UKOSRP II	LA4-1	OK - Joint	As welded	AX	457.2	9.0		216.3	8.0	CA	5.30E+04	1.01E+05	1.33E+05	1.61E+05	Chord	405	-1	Air
214	UKOSRP II	LA4-2	OK - Joint	As welded	AX	457.2	9.0		216.3	8.0	CA	2.78E+05	3.03E+05	4.80E+05	7.91E+05	Chord	239	-1	Air
215	UKOSRP II	LB-1	OK - Joint	As welded	AX	457.2	16.0		216.3	8.0	CA		6.20E+04		1.23E+05	Chord	460	-1	Air
216	UKOSRP II	LB-2	OK - Joint	As welded	AX	457.2	16.0		216.3	8.0	CA	1.30E+05			2.96E+05	Brace	279	-1	Air
217	UKOSRP II	K1	OK - Joint	As welded	AX	457.0	16.0		244.0	8.0	CA						396		Air
218	UKOSRP II	K2	OK - Joint	As welded	AX	457.0	16.0		244.0	8.0	CA	3.29E+05	3.53E+05	5.38E+05		Brace	234		Air
219	UKOSRP II	K3	OK - Joint	As welded	AX	457.0	16.0		244.0	8.0	CA	1.76E+05					185		Air
220	UKOSRP II	K4	OK - Joint	As welded	AX	457.0	16.0		244.0	8.0	CA	4.84E+05	5.36E+05	8.58E+05		Brace	286		Air
221	UKOSRP II	K5	OK - Joint	As welded	AX	457.0	16.0		244.0	8.0	CA	3.16E+05	5.44E+05	1.02E+06	1.08E+06	Brace	132		Air
222	UKOSRP II	K6	OK - Joint	As welded	AX	457.0	16.0		244.0	8.0	CA	4.85E+05	7.08E+05	1.68E+06		Brace	204		Air
223	EUR 10309 EN	B1	T - Joint	Ground	AX	914.4	32.0	3900	457.2	16.0	CA	1.13E+05	5.40E+04	2.79E+05	3.20E+05		206	0	Air
224	EUR 10309 EN	B2	T - Joint	Ground	AX	914.4	32.0	3900	457.2	16.0	CA	7.30E+05	5.40E+05	1.41E+06	1.61E+06		152	0	Air
225	EUR 10309 EN	B3	T - Joint	Ground	AX	914.4	32.0	3900	457.2	16.0	CA	8.51E+05	8.83E+05	1.84E+06	2.05E+06		149	0	Air
226	EUR 10309 EN	B4	T - Joint	improved weld shape	AX	914.4	32.0	3900	457.2	16.0	CA	4.50E+05	4.30E+05	1.00E+06	1.10E+06		156	0	Air
227	EUR 10309 EN	B5	T - Joint	improved weld shape	AX	914.4	32.0	3900	457.2	16.0	CA	5.75E+06	5.25E+06	8.20E+06	8.70E+06		93.9	0	Air
228	EUR 10309 EN	B6	T - Joint	As welded	AX	914.4	32.0	3900	457.2	16.0	CA	1.04E+06	7.64E+05	1.97E+06	2.21E+06		81	0	Seawater
229	EUR 10309 EN	B7	T - Joint	Ground	AX	914.4	32.0	3900	457.2	16.0	CA	5.00E+05	3.50E+05	7.42E+05	8.12E+05		124	0	Seawater
230	EUR 10309 EN	B8	T - Joint	Ground	AX	914.4	32.0	3900	457.2	16.0	CA	1.35E+06	7.60E+05	2.16E+06	2.25E+06		82.6	0	Seawater
231	EUR 10309 EN	B9	T - Joint	As welded	AX	914.4	32.0	3900	457.2	16.0	CA						86.7	0	Seawater + CP
232	EUR 10309 EN	B10	T - Joint	Ground	AX	914.4	32.0	3900	457.2	16.0	CA						84.7	0	Seawater + CP
233	Ohtake_1978	C	N - Joint	As welded	AX	762.0	22.5	4350	324.0	18.9	CA		1.21E+04		5.70E+05		258	-1	Air
234	Ohtake_1978	D	N - Joint	As welded	AX	762.0	20.6	4350	273.0	16.7	CA				3.07E+04		785	-1	Air
235	Ohtake_1978	E	N - Joint	As welded	AX	660.0	28.3	4350	273.0	16.7	CA		6.30E+03		7.80E+04		521	-1	Air
236	Ohtake_1978	F	N - Joint	Casted	AX	660.0	28.4	4350	273.0	17.5	CA		9.20E+04		2.38E+05		268	-1	Air
237	Kurobane_1973	K 0-1	NK - Joint	As welded	AX	140.5	3.9		60.9	3.2	CA		5.00E+04		5.58E+04			-1	Air
238	Kurobane_1973	K 0-2	NK - Joint	As welded	AX	140.8	3.9		60.7	3.2	CA		1.96E+06		2.38E+06			-1	Air
239	Kurobane_1973	K 0-3	NK - Joint	As welded	AX	140.3	3.9		60.9	3.2	CA		2.19E+05		4.79E+05			-1	Air

Appendices

Serial	Reference	Specimen number	Joint Type	Weld	Load Case	Chord OD (mm)	Chord Wall Thickness (mm)	Chord Length (mm)	Brace OD (mm)	Brace Wall Thickness (mm)	Loading Spectrum	N1	N2	N3	N4	Failure Site	Hot Spot Stress (MPa)	R	Environment
240	Kurobane_1973	K O-4	NK - Joint	As welded	AX	139.9	4.3		61.0	3.2	CA		1.90E+04		2.46E+04			-1	Air
241	Kurobane_1973	K O-5	NK - Joint	As welded	AX	140.0	4.2		60.9	3.2	CA		1.03E+04		1.75E+05			-1	Air
242	Kurobane_1973	K D76-1	NK - Joint	As welded	AX	140.8	3.9		76.2	3.2	CA		4.29E+06		5.21E+06			-1	Air
243	Kurobane_1973	K D76-2	NK - Joint	As welded	AX	140.8	3.9		76.5	3.2	CA		1.20E+05		2.99E+05			-1	Air
244	Kurobane_1973	K D76-3	NK - Joint	As welded	AX	140.7	3.9		76.3	3.2	CA		5.60E+04		7.91E+04			-1	Air
245	Kurobane_1973	K D76-4	NK - Joint	As welded	AX	139.9	4.4		76.5	3.2	CA		3.90E+03		1.13E+04			-1	Air
246	Kurobane_1973	K D89-1	NK - Joint	As welded	AX	140.0	4.0		89.8	3.2	CA		1.41E+06		1.92E+06			-1	Air
247	Kurobane_1973	K D89-2	NK - Joint	As welded	AX	140.3	3.9		89.5	3.2	CA		3.47E+05		9.24E+05			-1	Air
248	Kurobane_1973	K D89-3	NK - Joint	As welded	AX	140.4	3.9		89.6	3.2	CA		4.52E+04		1.28E+05			-1	Air
249	Kurobane_1973	K D89-4	NK - Joint	As welded	AX	139.8	4.4		89.4	3.2	CA		2.86E+04		5.25E+04			-1	Air
250	Kurobane_1973	K G10-1	NK - Joint	As welded	AX	140.4	4.0		60.9	3.2	CA		7.13E+04		1.07E+05			-1	Air
251	Kurobane_1973	K G10-2	NK - Joint	As welded	AX	140.7	3.9		60.8	3.2	CA		6.98E+06		7.32E+06			-1	Air
252	Kurobane_1973	K G10-3	NK - Joint	As welded	AX	140.4	3.9		60.6	3.2	CA		2.80E+05		4.96E+05			-1	Air
253	Kurobane_1973	K G10-4	NK - Joint	As welded	AX	139.9	4.3		60.8	3.2	CA		3.00E+03		5.80E+03			-1	Air
254	Kurobane_1973	K GMS-1	OK - Joint	As welded	AX	140.3	3.9		60.8	3.2	CA		1.00E+05		1.30E+05			-1	Air
255	Kurobane_1973	K GMS-2	OK - Joint	As welded	AX	140.5	3.9		60.9	3.2	CA		1.74E+05		1.78E+05			-1	Air
256	Kurobane_1973	K GMS-3	OK - Joint	As welded	AX	140.6	3.9		61.0	3.2	CA		1.52E+06		2.96E+06			-1	Air
257	Kurobane_1973	K GMS-4	OK - Joint	As welded	AX	140.0	4.3		60.8	3.2	CA		9.50E+03		1.61E+04			-1	Air
258	Kurobane_1973	K GMS76-1	OK - Joint	As welded	AX	140.0	4.4		76.5	3.2	CA		1.45E+04		2.39E+04			-1	Air
259	Kurobane_1973	K GMS76-2	OK - Joint	As welded	AX	140.0	4.3		76.6	3.2	CA		7.80E+04		1.38E+05			-1	Air
260	Kurobane_1973	K GMS76-3	OK - Joint	As welded	AX	140.0	4.2		76.8	3.2	CA		5.05E+05		1.04E+06			-1	Air
261	Kurobane_1973	K GMS76-4	OK - Joint	As welded	AX	140.0	4.2		76.5	3.2	CA		1.16E+06		5.06E+06			-1	Air
262	Kurobane_1973	K T45-1	NK - Joint	As welded	AX	139.8	4.4		60.8	3.2	CA		9.70E+04		1.33E+05			-1	Air
263	Kurobane_1973	K T45-2	NK - Joint	As welded	AX	139.8	4.4		60.9	3.2	CA		5.51E+05		9.70E+05			-1	Air
264	Kurobane_1973	K T45-3	NK - Joint	As welded	AX	139.8	4.4		60.6	3.2	CA		7.96E+05		1.12E+06			-1	Air
265	Gibstein_1981	32	T - Joint	As welded	AX	914.0	32.0	4570	457.0	16.0	CA	5.00E+04		1.50E+05	1.70E+05	chord	267	0	Air
266	Gibstein_1981	20	T - Joint	As welded	AX	914.0	32.0	4570	457.0	16.0	CA	1.50E+05		4.10E+05	6.80E+05		217	0	Air
267	Gibstein_1981	40	X - Joint	As welded	AX	914.0	32.0	4570	457.0	16.0	CA	9.00E+04		5.00E+05	7.30E+05		198	0	Air
268	Gibstein_1981	32	T - Joint	As welded	AX	914.0	32.0	4570	457.0	16.0	CA	1.90E+05		7.00E+05	8.50E+05	chord	197	0	Air
269	Gibstein_1981	32	T - Joint	As welded	AX	914.0	32.0	4570	457.0	16.0	CA	3.70E+05		9.50E+05	1.30E+06	chord	155	0	Air
270	Gibstein_1981	17	T - Joint	As welded	AX	914.0	32.0	4570	457.0	16.0	CA	1.20E+06		3.70E+06	4.30E+06		82	0	Seawater
271	Gibstein_1981	16	T - Joint	As welded	AX	914.0	32.0	4570	457.0	16.0	CA	2.40E+06		3.90E+06	4.30E+06		82	0	Seawater + CP
272	Gibstein_1981	32	T - Joint	As welded	AX	914.0	32.0	4570	457.0	16.0	CA	1.90E+06		4.10E+06	5.00E+06	chord	94	0	Air
273	Gibstein_1981	21	T - Joint	As welded	AX	914.0	32.0	4570	457.0	16.0	CA	3.30E+06		8.10E+06	1.60E+07		79	0	Air
274	Gibstein_1981	32	T - Joint	As welded	AX	914.0	32.0	4570	457.0	16.0	CA	3.80E+06		1.20E+07	1.40E+07	chord	78	0	Air
275	Gibstein_1981	39	X - Joint	As welded	AX	914.0	32.0	4570	457.0	16.0	CA	5.50E+06		2.00E+07	2.60E+07		75	0	Air
276	Gibstein_1981	2	T - Joint	As welded	AX	508.0	16.0	3300	244.5	10.0	CA			3.00E+04	2.06E+05	chord	438	-1	Air
277	Gibstein_1981	3	T - Joint	As welded	AX	508.0	16.0	3300	244.5	10.0	CA	5.60E+04		7.50E+04	5.80E+05	chord	350	-1	Air
278	Gibstein_1981	10	NK - Joint	As welded	AX	508.0	16.0	3300	305.0	13.5	CA	9.80E+04		1.15E+05	1.49E+06	chord		-1	Air
279	Gibstein_1981	4	T - Joint	As welded	AX	508.0	16.0	3300	244.5	10.0	CA	1.16E+05		1.60E+05	8.66E+05	chord	273	-1	Air

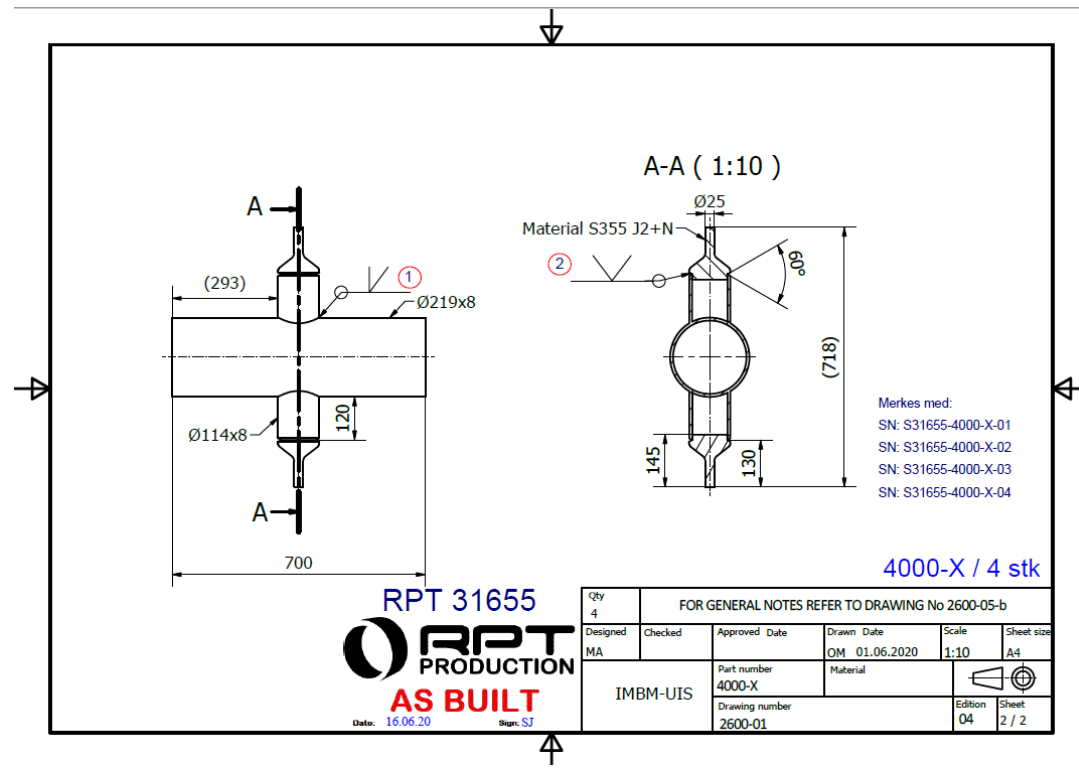
Appendices

Serial	Reference	Specimen number	Joint Type	Weld	Load Case	Chord OD (mm)	Chord Wall Thickness (mm)	Chord Length (mm)	Brace OD (mm)	Brace Wall Thickness (mm)	Loading Spectrum	N1	N2	N3	N4	Failure Site	Hot Spot Stress (MPa)	R	Environment
280	Gibstein_1981	6	T - Joint	As welded	AX	508.0	16.0	3300	244.5	10.0	CA	1.05E+05		2.00E+05	1.07E+06	chord	242	-1	Air
281	Gibstein_1981	7	T - Joint	As welded	AX	508.0	16.0	3300	244.5	10.0	CA	7.50E+04		2.20E+05	5.91E+05	chord		-1	Seawater
282	Gibstein_1981	9	Y - joint	As welded	AX	508.0	16.0	3300	245.0	10.0	CA	2.85E+05		5.00E+05	1.22E+06	chord	210	-1	Air
283	Gibstein_1981	5	T - Joint	As welded	AX	508.0	16.0	3300	244.5	10.0	CA	4.50E+05		6.50E+05	1.60E+06	chord	277	-1	Air
284	Gibstein_1981	8	T - Joint	As welded	AX	508.0	16.0	3300	244.5	10.0	CA	1.94E+06		2.40E+06	3.90E+06	chord		-1	Seawater
285	Gibstein_1981	11	OK - Joint	As welded	AX	508.0	16.0	3300	305.0	13.5	CA	1.90E+06		3.00E+06	4.60E+06	chord		-1	Air
286	Gibstein_1981	1	T - Joint	As welded	AX	508.0	16.0	3300	244.5	10.0	CA					Run out		-1	Air
287	Gibstein_1981	19	T - Joint	As welded	AX	168.0	6.3	840	84.0	3.2	CA	2.00E+04		6.00E+04	7.00E+04		501	0	Air
288	Gibstein_1981	6	T - Joint	As welded	AX	168.0	6.3	840	84.0	3.2	CA	1.00E+04		6.00E+04	7.00E+04	chord	555	0	Air
289	Gibstein_1981	6	T - Joint	As welded	IPB	168.0	6.3	840	84.0	3.2	CA	7.10E+05		3.30E+05	3.70E+05	chord	247	0	Air
290	Gibstein_1981	6	T - Joint	As welded	IPB	168.0	6.3	840	84.0	3.2	CA	4.30E+05		4.70E+05	4.80E+05	chord	278	0	Air
291	Gibstein_1981	22	T - Joint	As welded	AX	168.0	6.3	840	84.0	3.2	CA	1.10E+05		8.00E+05	9.50E+05		267	0	Air
292	Gibstein_1981	6	T - Joint	As welded	IPB	168.0	6.3	840	84.0	3.2	CA	1.53E+06		1.50E+06	1.70E+06	chord	194	0	Air
293	Gibstein_1981	23	T - Joint	As welded	AX	168.0	6.3	840	84.0	3.2	CA	1.70E+06		2.00E+06	2.40E+06		189	0	Air
294	Gibstein_1981	18	T - Joint	As welded	AX	168.0	6.3	840	84.0	3.2	CA	1.20E+06		3.00E+06	3.60E+06		219	0	Air
295	Gibstein_1981	6	T - Joint	As welded	AX	168.0	6.3	840	84.0	3.2	CA	2.90E+06		3.00E+06	3.30E+06	chord	330	0	Air
296	Gibstein_1981	6	T - Joint	As welded	AX	168.0	6.3	840	84.0	3.2	CA	1.00E+07		1.20E+07	1.30E+07	chord	186	0	Air
297	Dijkstra_1981	12	T - Joint	As welded	AX	457.2	15.9	2286	114.3	6.3	CA	3.50E+05		7.00E+05	9.10E+05			-1	Air
298	Dijkstra_1981	11	T - Joint	As welded	AX	457.2	15.9	2286	114.3	6.3	CA	2.00E+06		9.00E+06	1.10E+07			-1	Air
299	Gibstein_1981	16	T - Joint	As welded	AX	457.0	16.0	2285	228.5	6.2	CA	3.50E+05		7.00E+05	9.10E+05	chord	242	-1	Air
300	Gibstein_1981	16	T - Joint	As welded	AX	457.0	16.0	2285	228.5	6.2	CA	2.00E+06		9.00E+06	1.10E+07	chord	123	-1	Air
301	Gibstein_1981	16	T - Joint	As welded	AX	457.0	16.0	2285	228.5	8.0	CA	3.50E+05		6.80E+05	8.20E+05	chord	198	0	Air
302	Gibstein_1981	16	T - Joint	As welded	AX	457.0	16.0	2285	228.5	8.0	CA	3.20E+05		7.60E+05	1.00E+06	chord	198	0	Air
303	Gibstein_1981	16	T - Joint	As welded	AX	457.0	16.0	2285	228.5	8.0	CA	4.40E+05		8.40E+05	1.10E+06	chord	179	0	Air
304	Gibstein_1981	16	T - Joint	As welded	AX	457.0	16.0	2285	228.5	8.0	CA	4.20E+05		1.00E+06	1.30E+06	chord	179	0	Air
305	Gibstein_1981	4	T - Joint	As welded	AX	457.0	16.0	2285	228.5	8.0	CA	1.00E+06		2.20E+06	2.70E+06		106	-1	Seawater
306	Gibstein_1981	10	T - Joint	As welded	AX	457.0	16.0	2285	228.5	8.0	CA	1.00E+06		2.30E+06	2.80E+06		106	0	Seawater
307	Gibstein_1981	16	T - Joint	As welded	AX	457.0	16.0	2285	228.5	8.0	CA	3.60E+06		7.50E+06	8.50E+06	chord	106	0	Air
308	Dijkstra_1981	32 r	X - Joint	As welded	AX	457.2	15.9	2286	457.2	8.7	VA	1.70E+06		2.00E+06	4.00E+06			-1	Air
309	Dijkstra_1981	31 r	X - Joint	As welded	AX	457.2	15.9	2286	457.2	8.7	VA	3.20E+06		6.50E+06	8.40E+06			-1	Air
310	Dijkstra_1981	36	X - Joint	As welded	AX	457.2	15.9	2286	457.2	8.7	CA	2.60E+06		1.00E+07	1.90E+07			-1	Air
311	Gibstein_1981	16	T - Joint	As welded	AX	457.0	16.0	2285	457.0	8.8	CA	1.70E+06		1.00E+06	1.20E+06	brace	192	-1	Air
312	Gibstein_1981	16	T - Joint	As welded	AX	457.0	16.0	2285	457.0	8.8	CA	1.40E+06		2.40E+06	2.90E+06	brace	164	-1	Air
313	Gibstein_1981	16	T - Joint	As welded	AX	457.0	16.0	2285	457.0	8.8	CA	4.50E+06		6.70E+06	8.10E+06	chord	130	-1	Air
314	Gibstein_1981	16	T - Joint	As welded	AX	457.0	16.0	2285	457.0	8.8	CA	5.20E+06		7.80E+06	8.50E+06	chord	125	-1	Air
315	Gibstein_1981	16	T - Joint	As welded	AX	457.0	16.0	2285	457.0	16.0	CA	4.10E+05		6.60E+05	7.90E+05	chord	176	-1	Air
316	Gibstein_1981	16	T - Joint	As welded	AX	457.0	16.0	2285	457.0	16.0	CA	1.10E+06		1.80E+06	2.20E+06	chord	119	-1	Air
317	Gibstein_1981	16	T - Joint	As welded	AX	457.0	16.0	2285	457.0	16.0	CA	3.10E+06		1.60E+07	1.90E+07	chord	81	-1	Air
318	Damilano_1981	1 - I D	Y - joint	As welded		800.0	20.0	2000	368.0	20.0	CA	1.70E+04	2.30E+04	5.00E+04	5.90E+04				Air
319	Damilano_1981	1 - III D	Y - joint	As welded		800.0	20.0	2000	368.0	20.0	CA	1.30E+04	2.30E+04	5.00E+04	5.90E+04				Air

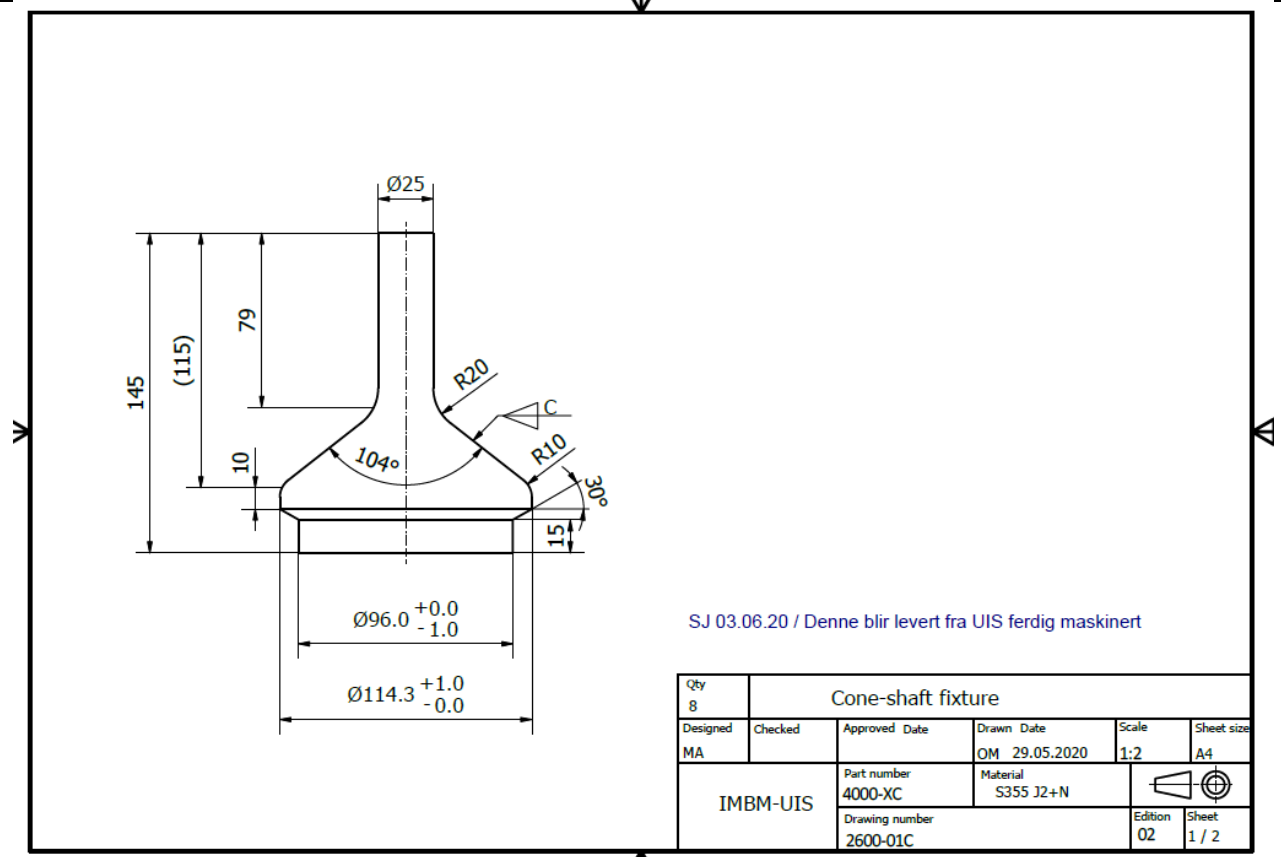
Appendices

Serial	Reference	Specimen number	Joint Type	Weld	Load Case	Chord OD (mm)	Chord Wall Thickness (mm)	Chord Length (mm)	Brace OD (mm)	Brace Wall Thickness (mm)	Loading Spectrum	N1	N2	N3	N4	Failure Site	Hot Spot Stress (MPa)	R	Environment
320	Damilano_1981	2 - II E	Y - joint	As welded		800.0	20.0	2000	368.0	20.0	CA	5.50E+03	7.80E+03	1.70E+04	2.10E+04				Air
321	Damilano_1981	2 - IV C	Y - joint	As welded		800.0	20.0	2000	368.0	20.0	CA	5.50E+03	7.80E+03	1.90E+04	2.10E+04				Air
322	Damilano_1981	5 - IV D	Y - joint	As welded		800.0	20.0	2000	368.0	20.0	CA	6.00E+04	9.00E+04	3.80E+05	7.00E+05				Air
323	Damilano_1981	5 - II C	Y - joint	As welded		800.0	20.0	2000	368.0	20.0	CA	8.50E+04	9.50E+04	5.00E+05	7.00E+05				Air
324	Damilano_1981	FA	X - Joint	As welded	AX	473.0	33.0	2000	341.5	21.5	CA	4.80E+04		4.60E+05	7.50E+05	chord	242	0.1	Air
325	Damilano_1981	FB	X - Joint	As welded	AX	684.0	40.0	2000	340.4	22.4	CA	2.10E+05		4.01E+05	5.80E+05	chord	192	0.1	Air
326	Damilano_1981	FD	X - Joint	As welded	AX	949.0	42.0	2000	342.4	22.4	CA	6.00E+04		3.30E+05	4.40E+05	chord	227	0.1	Air
327	Damilano_1981	FC	X - Joint	As welded	AX	1281.0	78.0	2000	682.0	41.4	CA	2.60E+05		1.14E+06	1.30E+06	chord	111	0.1	Air
328	Damilano_1981	FE	X - Joint	As welded	AX	1280.0	75.0	2000	683.0	40.0	CA	8.00E+04		6.60E+05	9.10E+05	chord	129	0.1	Air
329	Damilano_1981	FA'	X - Joint	As welded	IPB	472.0	22.0	2000	339.8	21.8	CA	5.50E+04	9.10E+04	1.58E+05	1.90E+05	chord	242	0.1	Air
330	Damilano_1981	FB'	X - Joint	As welded	IPB	685.0	40.0	2000	342.5	22.0	CA	1.10E+05	2.60E+05	6.50E+05	7.60E+05	chord	146	0.1	Air
331	Damilano_1981	FD'	X - Joint	As welded	IPB	947.0	44.0	2000	681.8	43.6	CA	1.30E+05	2.05E+05	4.70E+05	6.50E+05	chord	126	0.1	Air
332	Damilano_1981	FC'	X - Joint	As welded	IPB	1275.0	75.0	2000	344.3	22.5	CA	3.00E+04	1.75E+05	6.50E+05	6.60E+05	chord	166	0.1	Air
333	Damilano_1981	FE'	X - Joint	As welded	IPB	1273.0	77.0	2000	687.4	43.9	CA	4.00E+04	8.90E+04	4.60E+05	5.50E+05	chord	126	0.1	Air
334	OTH 89 307	2	X - Joint	As welded	OPB	457.0	16.0	3200	229.0	12.0	CA	2.11E+04		2.47E+05			352.6	0	Air
335	OTH 89 307	1	X - Joint	Repair welded	OPB	457.0	16.0	3200	229.0	12.0	CA	1.63E+04		4.92E+05			235.3	0	Air
336	OTH 89 307	3	T - Joint	Repair welded	OPB	457.0	16.0	3200	229.0	12.0	CA	4.80E+04		3.66E+05			268	0	Air
337	OTH 89 307	13	T - Joint	Repair welded	OPB	457.0	16.0	3200	229.0	12.0	CA	1.74E+05		4.33E+06			164.8	-1	Air
338	OTH 89 307	19	T - Joint	Repair welded	OPB	457.0	16.0	3200	229.0	12.0	CA	3.57E+04		6.79E+05			239	-1	Air
339	OTH 89 307	4	T - Joint	Repair welded	OPB	457.0	16.0	3200	229.0	12.0	CA	2.15E+04		4.14E+05			335.3	-1	Air
340	OTH 89 307	9	T - Joint	Repair welded	OPB	457.0	16.0	3200	229.0	12.0	CA	1.55E+05					179	-1	Air
341	OTH 89 307	20	T - Joint	Repair welded	OPB	457.0	16.0	3200	229.0	12.0	CA	6.22E+04					238.9	-1	Air
342	OTH 89 307	5	T - Joint	Repair welded	OPB	457.0	16.0	3200	229.0	12.0	CA	3.90E+04					376.4	-1	Air
343	OTH 89 307	6	T - Joint	Repair welded + burr ground	OPB	457.0	16.0	3200	229.0	12.0	CA	1.08E+04		3.10E+05			335.5	-1	Air
344	OTH 89 307	15	T - Joint	Repair welded + burr ground	OPB	457.0	16.0	3200	229.0	12.0	CA	2.29E+04		2.23E+05			379	-1	Air
345	OTH 89 307	23	T - Joint	Repair welded + burr ground	OPB	457.0	16.0	3200	229.0	12.0	CA	1.13E+05					236.5	-1	Air
346	OTH 89 307	24	T - Joint	Repair welded + burr ground	OPB	457.0	16.0	3200	229.0	12.0	CA	6.40E+04					318.7	-1	Air
347	OTH 89 307	16	T - Joint	Repair welded + burr ground	OPB	457.0	16.0	3200	229.0	12.0	CA	4.34E+04					375.3	-1	Air
348	OTH 89 307	7	T - Joint	Hole drilling	OPB	457.0	16.0	3200	229.0	12.0	CA	1.99E+04		3.05E+05			350.5	-1	Air
349	OTH 89 307	8	T - Joint	Hole drilling	OPB	457.0	16.0	3200	229.0	12.0	CA	6.65E+04		1.66E+05			353.7	-1	Air
350	OTH 89 307	17	T - Joint	Burr Grinding	OPB	457.0	16.0	3200	229.0	12.0	CA	9.95E+04					209.9	-1	Air
351	OTH 89 307	21	T - Joint	Burr Grinding	OPB	457.0	16.0	3200	229.0	12.0	CA	6.40E+04					226.1	-1	Air
352	OTH 89 307	11	T - Joint	Burr Grinding	OPB	457.0	16.0	3200	229.0	12.0	CA	1.67E+04					333.6	-1	Air
353	OTH 89 307	10	T - Joint	Burr Grinding	OPB	457.0	16.0	3200	229.0	12.0	CA	3.06E+05					176	-1	Air
354	OTH 89 307	18	T - Joint	Burr Grinding	OPB	457.0	16.0	3200	229.0	12.0	CA	4.22E+04					245.7	-1	Air
355	OTH 89 307	12	T - Joint	Burr Grinding	OPB	457.0	16.0	3200	229.0	12.0	CA	2.07E+04					363.2	-1	Air
356	OTH 89 307	14	T - Joint	Burr Grinding	OPB	457.0	16.0	3200	229.0	12.0	CA	2.22E+04					389.5	-1	Air
357	OTH 89 307	22	T - Joint	Burr Grinding	OPB	457.0	16.0	3200	229.0	12.0	CA	1.10E+04					415.7	-1	Air
358	OTH 89 307	25	T - Joint	Burr Grinding	OPB	457.0	16.0	3200	229.0	12.0	CA						277.2	-1	Air

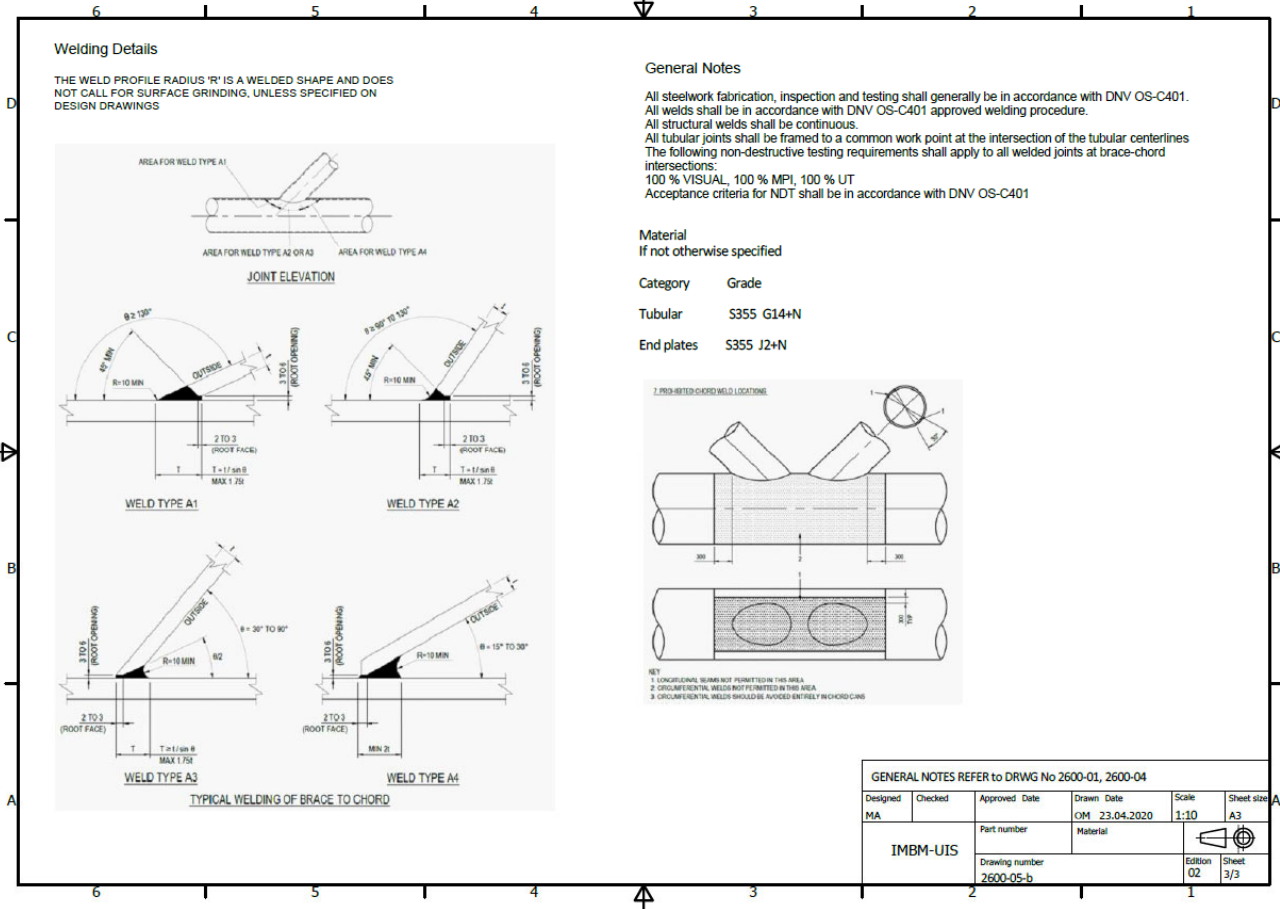
**Appendix 2 Fabrication sheet**



Appendices



## Appendices



GENERAL NOTES REFER TO DRWG No 2600-01, 2600-04					
Designed	Checked	Approved Date	Drawn Date	Scale	Sheet size
MA			OM 23.04.2020	1:10	A3
IMBM-UIS		Part number	Material		
		Drawing number		Edition	Sheet
		2600-05-b		02	3/3



Appendices

WPS Form. acc. to ISO 15609-1

RPT PRODUCTION		WELDING PROCEDURE SPECIFICATION (WPS)		WPS No.: RPT 103-2							
Prod. by: RPT Production as.		Fabricator: RPT Production		Date: 04.11.2019 Rev.: 3							
Project: General		Ref. spec.: Norsok M101, Q00075		Ref. stand: EN-ISO 15614-1							
Location: Orstad		Ref. W/PQR: RPT 25101 rev.0 / RPT 25102 rev.0									
Welding process:	1 141	2 Ar 75% / Co2 25%	3								
Shielding gas types	Argon 99,996%		136								
Purging gas type	Na	l/min									
Gas trailing shoe	Na	l/min									
Weaving yes/no	Yes	Max: 5 mm									
Welding positions	All uphill										
Joint type	BW, FW multi pass										
Joint preparation	Machining / Grinding										
Cleaning method	Solvent degreasing										
Backing	Na										
Back gouging	Yes if required										
Flux designation	Na										
Flux handling	Na										
Tungsten electrode	WC20 / EWLa-2	2,4 mm									
Torch angel	70 - 90 °										
Stand off distance	10 - 15 mm										
Nozzle diameter(s)	12 mm										
Tack welding proc.	8-01-TE-0007										
Identification of parent metal		1 C max:	CE max: 0,44	PCM max:	2 C max:						
CE max:	0,44	PCM max:		CE max:	0,44						
PCM max:		CE max:	0,44	PCM max:							
Part	Name/Grade	Standard	Group	Delivery cond.	Thickness range (mm)	Diameter range (mm)					
1	S355	EN 10025	1.2	Normalized	3 to 50	84 to Plate					
2	S355	EN 10025	1.2	Normalized	3 to 50	84 to Plate					
Identification of filler metal											
Index	Trade name	Classification	Filler handling								
A	Boehler Ni 1-IG	EN ISO 636-A-W3Ni1	8-01-TE-0006								
B	Boehler Ti 60 T-FD SR	ISO T50 5 1 Ni P M21 1 H5	8-01-TE-0006								
C											
Welding parameters				Equipment							
Pass no.	Filler metal	Dia. mm	Welding process	Wire feed speed (m/min)	Current (A) min max	Voltage (V) min max	Current / polarity	Welding speed mm/min min max	Run-out length (mm)	Gas min max	Heat input (kJ/mm)
1	A	2,0	1	-	110 - 150	12 - 14	DC-	40 - 90		16 - 18	1,4 - 2,3
2	B	1,2	2	-	170 - 220	22 - 26	DC+	140 - 250		18 - 20	1,1 - 1,8
Fill	B	1,2	2	-	180 - 220	22 - 28	DC+	140 - 500		18 - 20	0,7 - 2,2
Cap	B	1,2	2	-	170 - 220	22 - 28	DC+	150 - 520		18 - 20	0,7 - 1,8
Heat treatment							Method:				
Preheat min:	50 ° C		Interpass temp.max:	220 ° C		Heat treatment proc.:	Na		Temp.control:	Digital	
Remarks:							Additional info enclosed (yes/no)				
							Date: 04.11.2019 Sign.: <i>[Signature]</i>				
							Approved				
							Date:				

WPS RPT 103-2 rev.3

**Appendix 3 Documentation of cracking events during testing**

Appendix 3 shows the logging of cracking events during testing. The crack length and cycle count reported were based on visual inspection and digital aids like a hand-held microscope and digital image correlator. However, the events and fatigue lives reported in the body of the thesis were based on strain gauge measurements and interpretations which is more reliable than visual inspection.

Appendices

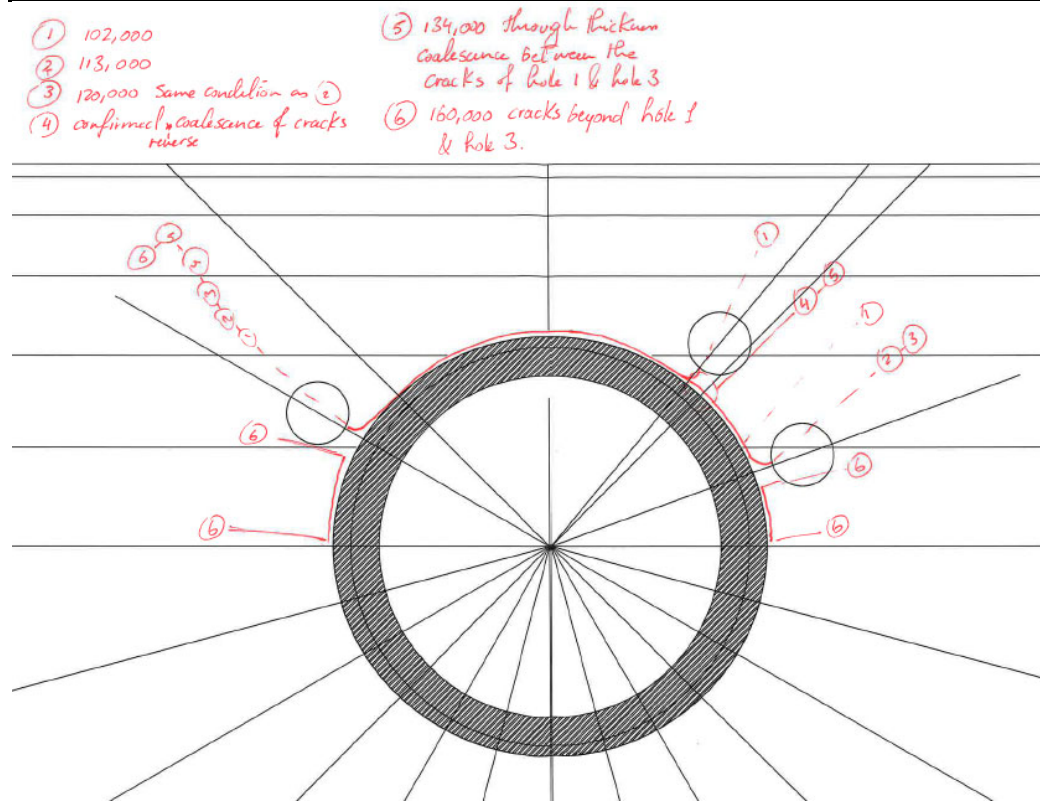


Figure 9-3: Crack propagation sequence as documented during testing.

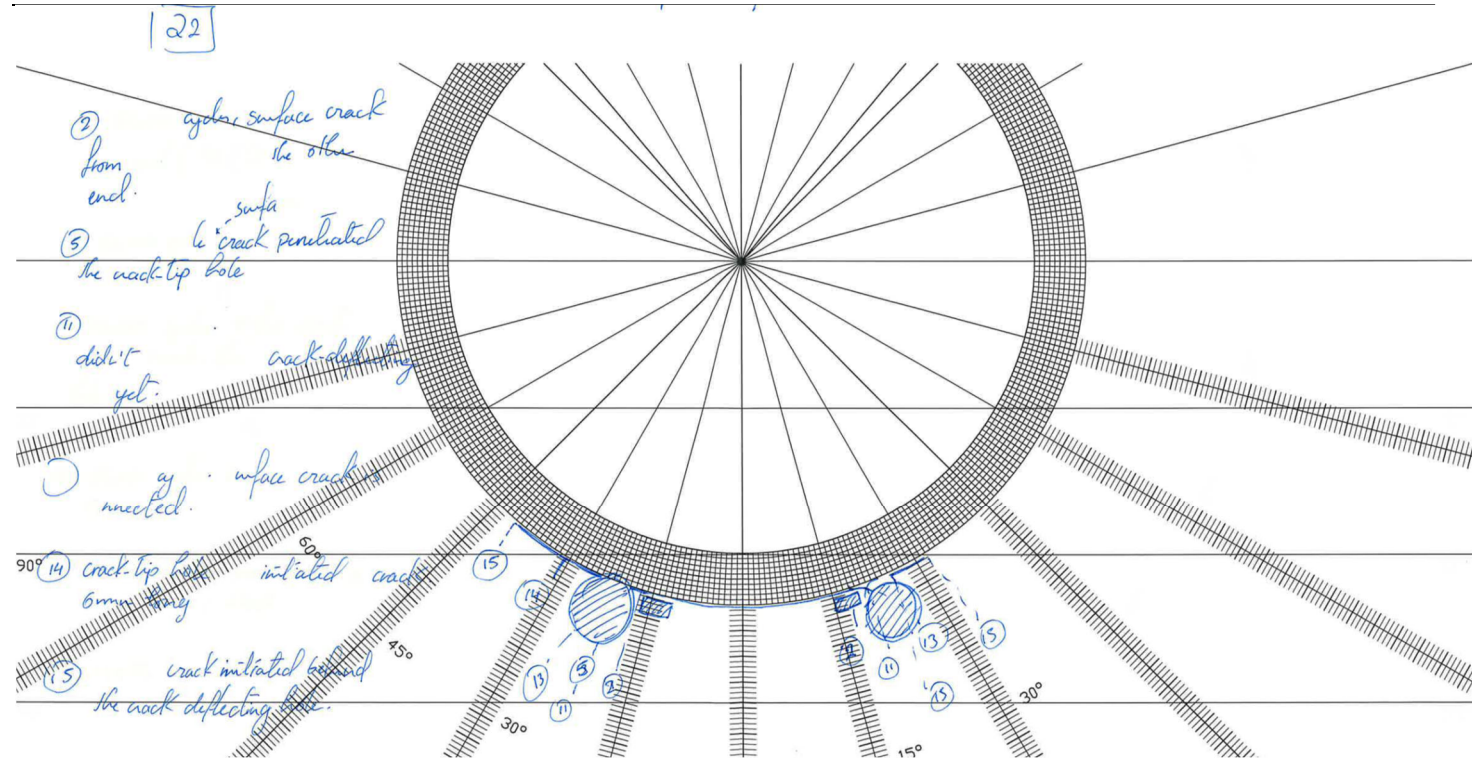


Figure 9-4: Crack propagation sequence, quadrant Q2.

Appendices

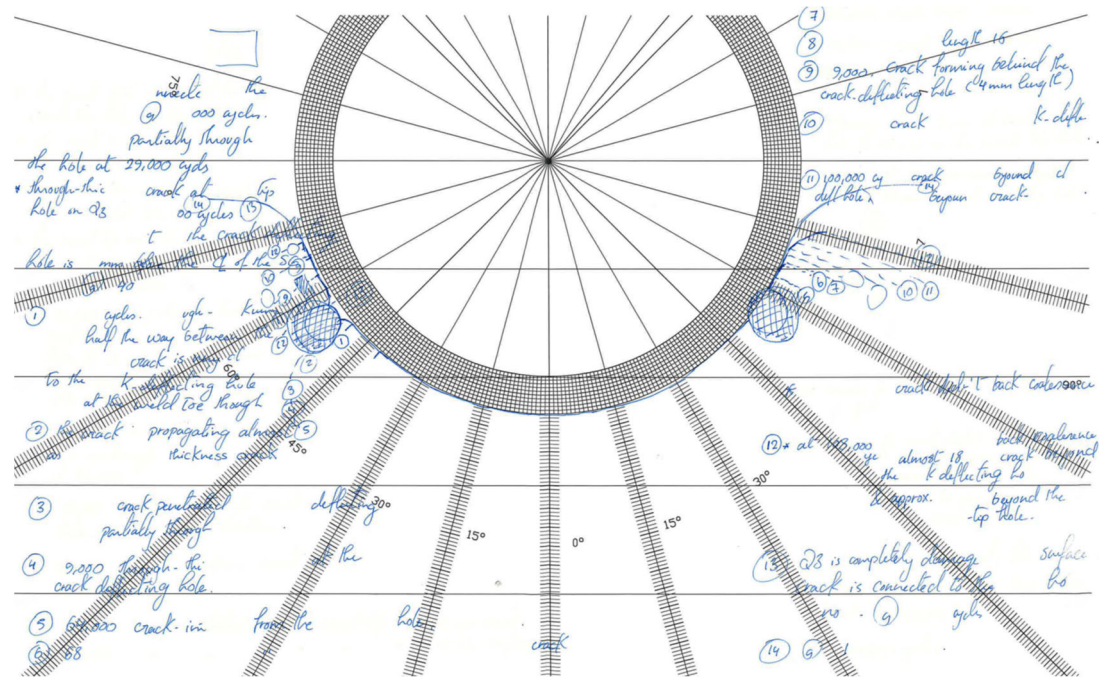


Figure 9-5: Crack propagation sequence, quadrant Q3.



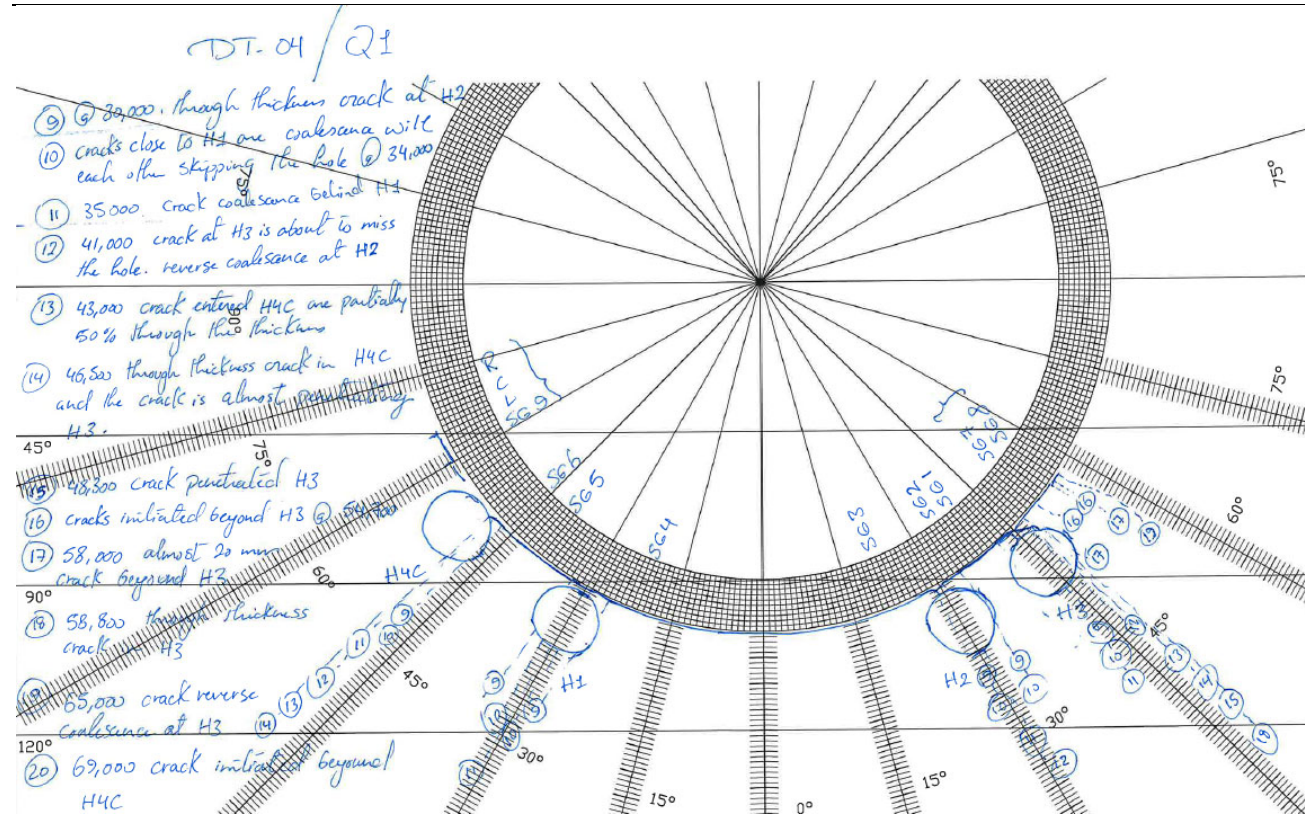


Figure 9-6: Crack propagation sequence, quadrant Q1-a, Specimen DT4

Appendices

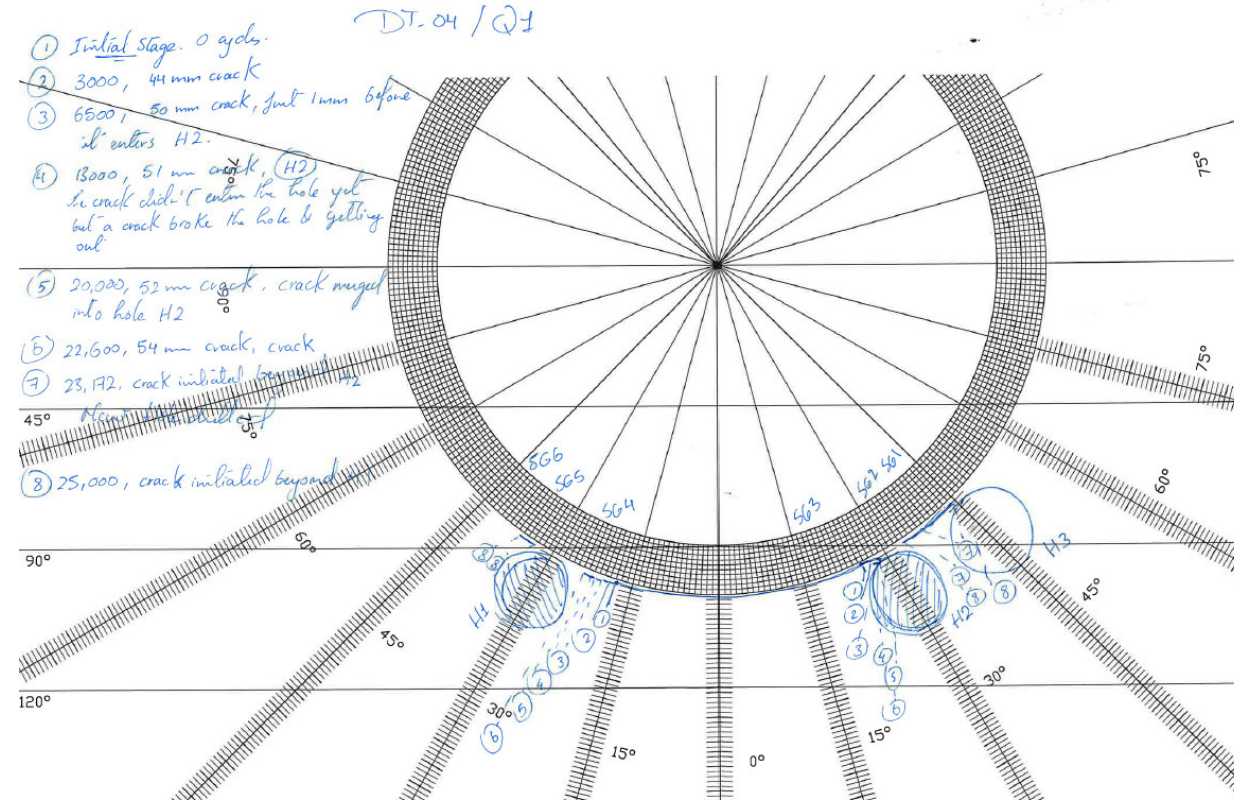


Figure 9-7: Crack propagation sequence, quadrant Q1-b, Specimen DT4

## Appendix 4 Selected tubular joints

The joints provided in the dataset below has:

- R ratio of 0.0 – 0.1,
- In-air environmental condition,
- And axially loaded with constant amplitude.

#	Reference	N3	N4	Hot Spot Stress (MPa)	Estimated through thickness crack length (mm)	RE
1	Gibstein_1981	3.00E+06	3.60E+06	219	63	0.17
2	Gibstein_1981	6.00E+04	7.00E+04	501	63	0.14
3	Gibstein_1981	8.00E+05	9.50E+05	267	63	0.16
4	Gibstein_1981	2.00E+06	2.40E+06	189	63	0.17
5	Gibstein_1981	6.00E+04	7.00E+04	555	63	0.14
6	Gibstein_1981	1.20E+07	1.30E+07	186	63	0.08
7	Gibstein_1981	3.00E+06	3.30E+06	330	63	0.09
8	Gibstein_1981	6.80E+05	8.20E+05	198	159	0.17
9	Gibstein_1981	1.00E+06	1.30E+06	179	159	0.23
10	Gibstein_1981	8.40E+05	1.10E+06	179	159	0.24
11	Gibstein_1981	7.50E+06	8.50E+06	106	159	0.12
12	Gibstein_1981	7.60E+05	1.00E+06	198	159	0.24
13	Gibstein_1981	4.10E+05	6.80E+05	217	317	0.40
14	Gibstein_1981	8.10E+06	1.60E+07	79	317	0.49
15	Gibstein_1981	2.00E+07	2.60E+07	75	317	0.23
16	Gibstein_1981	5.00E+05	7.30E+05	198	317	0.32
17	Gibstein_1981	4.10E+06	5.00E+06	94	317	0.18
18	Gibstein_1981	1.50E+05	1.70E+05	267	317	0.12
19	Gibstein_1981	9.50E+05	1.30E+06	155	317	0.27
20	Gibstein_1981	1.20E+07	1.40E+07	78	317	0.14
21	Gibstein_1981	7.00E+05	8.50E+05	197	317	0.18
22	Dijkstra_1981	60000	63000	462	63	0.05
23	Dijkstra_1981	12000000	13000000	154	63	0.08
24	Dijkstra_1981	3000000	3300000	274	63	0.10



*Appendices*

---

25	Dijkstra_1981	3000000	3600000	180	63	0.20
26	Dijkstra_1981	60000	74000	412	63	0.23
27	Dijkstra_1981	880000	950000	221	63	0.08
28	Dijkstra_1981	2000000	2400000	157	63	0.20
29	Dijkstra_1981	680000	820000	169	159	0.21
30	Dijkstra_1981	1000000	1300000	153	159	0.30
31	Dijkstra_1981	840000	1100000	153	159	0.31
32	Dijkstra_1981	7500000	8500000	90	159	0.13
33	Dijkstra_1981	760000	1000000	169	159	0.32
34	Dijkstra_1981	4.10E+06	5.00E+06	77	317	0.22
35	Dijkstra_1981	1.50E+05	1.70E+05	218	317	0.13
36	Dijkstra_1981	9.50E+05	1.30E+06	127	317	0.37
37	Dijkstra_1981	4.10E+05	6.80E+05	179	317	0.66
38	Damilano_1981	4.60E+05	7.50E+05	242	317	0.63

### **Appendix 5 List of publications**

Publications related to this research work:

- I. State-of-the-art of crack propagation modelling in tubular joints  
Atteya, M., Mikkelsen, O., Lemu, H.G. IOP Conference Series: Materials Science and Engineering, 2019, 700(1), 012035
- II. Crack arresting with crack deflecting holes in steel plates Atteya, M., Mikkelsen, O., Pavlou, D.G., Ersdal, G. Proceedings of the International Conference on Offshore Mechanics and Arctic Engineering - OMAE, 2020, 3, V003T03A026
- III. Experimental and numerical study of the elastic SCF of tubular joints  
Atteya, M., Mikkelsen, O., Wintle, J., Ersdal, G. Materials, 2021, 14(15), 4220